



SCUOLA
NORMALE
SUPERIORE

PhD Thesis, Chemistry

Tesi di Perfezionamento in Chimica

**FUNCTIONAL POLYMERS BY NITROXIDE RADICAL COUPLING
(NRC) REACTION**

Candidate:

Ilaria Domenichelli

Supervisor:

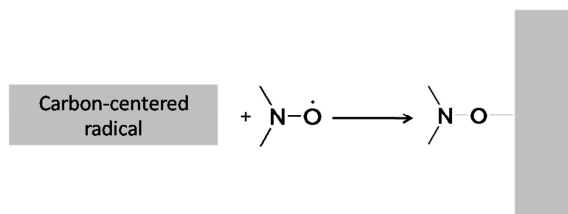
Dr. Elisa Passaglia

Pisa, Academic Year 2015/2016

Synopsis

SYNOPSIS

The Nitroxide Radical Coupling (NRC) reaction (Scheme 1) that occurs between a carbon centered radical and a nitroxide enjoyed considerable success in the recent years owing to some appealing characteristics.



Scheme 1: Nitroxide Radical Coupling (NRC) reaction

The nitroxyl free radicals (or nitroxides) are indeed secondary amine N-oxides that are stable at room temperature and can quickly couple with carbon-centered radicals, such as polymer macroradicals, at close to diffusion-controlled rates ($10^{-9} \text{ L mol}^{-1} \text{ s}^{-1}$)¹. For this particular feature, nitroxides were used as spin-trap to control the extent of crosslinking in the reaction of polyethylene with peroxide^{2, 3} and as probe of polypropylene degradation⁴. In addition the NRC displays characteristics resembling the “click chemistry”¹ approach: it is fast and reliable and easy to implement with high yield; moreover it is an efficient and specific reaction which can be conducted under relatively mild conditions and overall it is compatible with several functional groups and applicable in a modular manner⁵.

The nitroxide radical coupling (NRC) reaction is an excellent tool to add specific functionalities to different polymers by using *ad hoc* synthesized nitroxides that are able to quickly react with the macroradicals formed by H-abstraction from a polymer backbone.

Indeed, the insertion of functional groups (even in low amount) into polymers as polyolefins and polyesters can positively affect important properties such as toughness, adhesion, barrier properties, surface properties (paintability, printability,...), solvent resistance, miscibility with other polymers, and rheological properties⁶ without compromising their fundamental starting features. “Functional” polyolefins can be prepared by the copolymerization of α -olefins with unsaturated monomers bearing polar

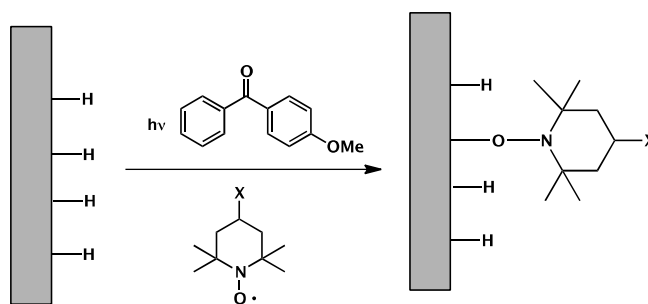
groups, usually with the help of a metal catalyst. However this procedure suffers from the presence of functionalities that can deactivate the catalyst by negatively affecting the process efficiency. Moreover, the classical radical post-polymerization modification of the polymer matrix by using unsaturated monomers does not respond to the requirement of selectivity and does not guarantee the structural preservation of the pristine macromolecular architecture. Indeed, the presence of the propagation and chain transfer steps, increases the amount of free radicals during the functionalization process, causing the occurrence of typical side reactions⁷. Instead by NRC method it is possible to insert selected functionalities by a one-step procedure^{8,9}; the process shows a great compatibility with different functional groups and by modulating the feed ratio, it is possible to achieve a very good control of the grafting degree and of the macromolecular architecture even though the functionalization is carried out in the melt by using peroxide as free radical initiator.

In this scenario, the main objective of this work was to use 2,2,6,6-tetramethylpiperidine-1-oxyl (TEMPO) derivatives as functionalizing agents. In fact, the possibility to synthesize TEMPO derivatives bearing functionalities with specific activity and therefore able to engender properties not inherently owned by basic polymers, can make the NRC approach particularly interesting in both melt and surface radical-initiated functionalization processes.

First, in order to expand the applicability of this functionalization method, the grafting of 2,2,6,6-tetramethylpiperidine-1-oxyl (TEMPO) derivatives bearing new functional groups, the 4-(phenylazo)-benzoyl-2,2,6,6-tetramethylpiperidine-1-oxyl radical (AzO-TEMPO), 4-(2-thienylazo)-benzoyl-2,2,6,6-tetramethylpiperidine-1-oxyl (ThiO-TEMPO) (bearing light-responsive groups or chromophores), and 4-(4,4,5,5,6,6,7,7,8,8,9,9,9-tridecafluorononanoate)-2,2,6,6-tetramethylpiperidine-1-oxyl (Fluo-TEMPO) was carried out in the melt by using peroxide as reaction activator. This was followed by an accurate study of the new properties transferred directly from the nitroxides to the polymer. In particular the photophysical features of the new “functional polymers” bearing covalently grafted azo-aromatic chromophores, were properly investigated to deepen the photoisomerization behavior and mechanism once the chromophore was grafted to polymer backbone.

Furthermore, with the purpose to evaluate the feasibility of NRC reaction to functionalize different polymer matrices, the NRC was applied to bio-polyesters like for example poly(lactic acid) (PLA) and poly(butylene succinate) (PBS) which are becoming increasingly important in view of their thermoplastic processability, thermo-mechanical properties and compostability/biodegradability¹⁰. Both polymers were successfully functionalized with 4-benzoyloxy-2,2,6,6-tetramethylpiperidine-1-oxyl (BzO-TEMPO) and 4-(1-naphthoate)-2,2,6,6-tetramethylpiperidine-1-oxyl (NfO-TEMPO) with good yield and by maintaining their pristine macromolecular structure.

In addition, the NRC was tested to promote the surface functionalization of different polymer substrates with the purpose of imparting new selected properties to film surfaces as wettability or light responsibility. A photografting method was developed by taking advantage of the coupling of TEMPO derivatives with macroradicals generated by H-abstraction through UV irradiation in the presence of a new photoinitiator (Scheme 2). This study allowed even investigating the feasibility of NRC under photografting conditions, to optimize some experimental conditions (e.g. the reagent ratio) and eventually to tailor/modulate the nature of the functional groups to be photografted.

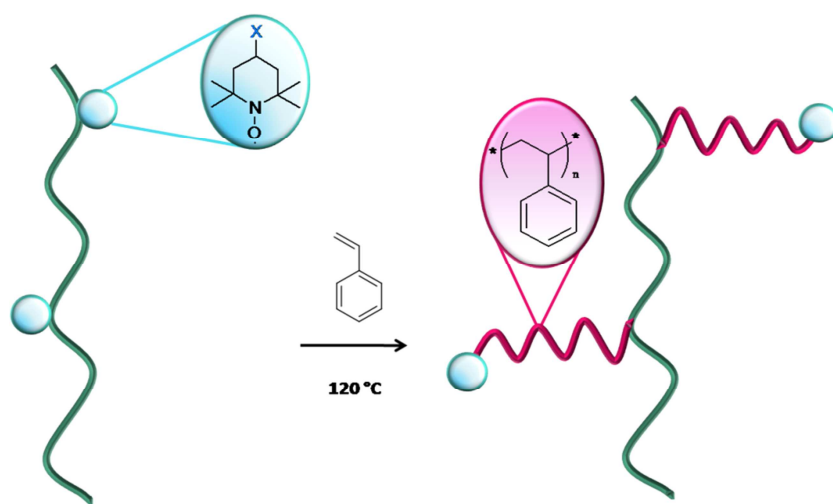


Scheme 2: UV initiated photografting of X-TEMPO derivatives onto a polymer surface.

In the photografting experiments three TEMPO derivatives were used: BzO-TEMPO, NfO-TEMPO and Fluo-TEMPO previously tested in the melt radical grafting. The use of NfO-TEMPO as functionalizing agent, allowed to deeply investigating the different behavior/reactivity of chromophores undergoing to the UV light irradiation, with respect to their grafting reactivity through the melt radical modification⁸.

A careful study about the thermal stability of the >NO-C bond between the nitroxide and the macroradical (generating the alkoxyamine product) by Electron Paramagnetic

Resonance (EPR) spectroscopy supported by Density Functional Theory (DFT)-based calculations was even carried out. The results evidenced and confirmed the reversibility of the coupling reaction between free nitroxide and macroradicals, especially at high temperature and suggested interesting behavior depending on the nature/structure of functionalities brought by TEMPO. This feature is proven to be very useful in controlling the synthesis of polymers with well defined architecture laying foundations for the well-known Nitroxide Mediated Polymerization (NMP)^{1, 11-14}. Accordingly, by exploiting the thermal equilibrium between the alkoxyamine and its free form, the functionalized polyolefins obtained by photografting and by functionalization in the melt were used as macroinitiators in order to grow, in a controlled/living fashion, polystyrene chains from the bulk and surface activated polymers (Scheme 3).



Scheme 3: Schematic representation of the grafting strategy.

A Stefano e alla mia mamma

ACKNOWLEDGMENTS

Firstly, I would like to express my sincere gratitude to Prof. Vincenzo Barone for having given me the chance to take part to the Scuola Normale Superiore PhD program, for his kind availability and helpful discussions during the last three years.

Special mention goes to my supervisor Dr. Elisa Passaglia for the continuous support to my PhD study and related research, for her patience and motivation. Her guidance helped me during all the years of research and during writing this thesis.

Besides my supervisor, I would like to express my special appreciation and thanks to Dr. Francesca Cicogna and Dr. Serena Coiai. for encouraging my research and for allowing me to grow as a research scientist. Their advices have been very precious.

My sincere thanks also go to Dr. Bruno Ameduri who provided me an opportunity to join his team and to learn a lot about polymer synthesis. Without his precious support it would not be possible to conduct part of this research.

I would like to thank the following people for their contribution to this thesis work: Prof. G. Galli, Prof. F. Bellina, Dr. M. Lessi, Dr. E. Martinelli and Dr. S. Taddei (Department of Chemistry and Industrial Chemistry, University of Pisa); Dr. C. Yang and Mr. R. Spiniello (CNR-ICCOM SS Pisa); Dr. A. Raffaelli (CNR-IBF Pisa); Dr. S. Carroccio and Dr. P. Rizzarelli (CNR-IPCB SS Catania); Dr. C. Gambarotti (Department of Chemistry, Materials and Chemical Engineering, Politecnico of Milano); Prof. Nadka Tz. Dintcheva (Department of Civil, Environmental, Aerospace, Materials Engineering, University of Palermo); Prof. G. Filippone (Department of Chemical, Materials and Production Engineering of the University of Naples Federico II).

A special thank goes to Dr. C. Pinzino (CNR ICCOM SS Pisa) who helped me with the acquisition and interpretation of EPR spectra and to Dr. F. Vazart for her invaluable help with the DFT calculations.

I thank all my fellow labmates for the stimulating discussions, and for all the fun we have had in the last three years.

Thanks to my aunt Maura, my uncle Oreste and my cousin Rocco for hosting me during my period in Pisa and for making me feel at home.

Finally, but by no means least, thanks go to mum and Stefano for almost unbelievable support. They are the most important people in my world and I dedicate this thesis to them.

The research activities of the thesis were partially funded by the National Project 'New Polymer Systems with Electric and Optical Functionalities via Nano and Micro Adhesive Dispersion to Produce Materials and Devices for Smart Applications' POLOPTEL 2011-2014, La Fondazione CARIPIA conv. 167/09, and by the Italian Ministry of University and Research (MIUR) under the program FIRB 2010-Futuro inRicerca, Project title: "GREENER-Towards multifunctional, efficient, safe and stable "green" bio-plastics based nanocomposites of technological interest via the immobilization of functionalized nanoparticles and stabilizing molecules(Project cod: RBFR10DCS7).

LIST OF THE PUBLISHED OR SUBMITTED PAPERS

1. I. Domenichelli, S. Coiai, C. Pinzino, S. Taddei, E. Martinelli, F. Cicogna, "Polymer surface modification by photografting of functional nitroxides", Submitted to European Polymer Journal
2. S. Banerjee, I. Domenichelli, B. Ameduri, "Nitroxide-Mediated Alternating Copolymerization of Vinyl Acetate with tert-Butyl-2-trifluoromethacrylate Using a SG1-Based Alkoxyamine", *ACS Macro Lett.* 2016, **5**, 1232–1236
3. F. Cicogna, I. Domenichelli, S. Coiai, F. Bellina, M. Lessi, R. Spiniello, E. Passaglia, "Structural, thermal and photo-physical data of azo-aromatic TEMPO derivatives before and after their grafting to polyolefins" *Data in Brief* 2016, **6**, 562-570
4. F. Cicogna, I. Domenichelli, S. Coiai, F. Bellina, M. Lessi, R. Spiniello, E. Passaglia, "Azo-aromatic functionalized polyethylene by nitroxide radical coupling (NRC) reaction: Preparation and photo-physical properties" *Polymer* 2016, **82**, 366-377
5. I. Domenichelli, S. Coiai, F. Cicogna, C. Pinzino and E. Passaglia, "Towards a better control of the radical functionalization of poly(lactic acid)" *Polym .Int.* 2015; **64**: 631–640
6. F. Cicogna, S. Coiai, P. Rizzarelli, S. Carroccio, C. Gambarotti, I. Domenichelli, C. Yang, N. Tz.Dintcheva, G. Filippone, C. Pinzino and E. Passaglia "Functionalization of aliphatic polyesters by nitroxide radical coupling", *Polym. Chem.*, 2014, **5**, 5656

CONFERENCES I PARTECIPATED WITH ORAL AND POSTER COMMUNICATIONS

European Polymer Federation 2013 Pisa 16-21 June 2013:

FUNCTIONAL POLYOLEFINS RESPONDING TO LIGHT STIMULI F. Cicogna, S. Coiai, I. Domenichelli, F. Bellina, M. Lessi, S. Monti, G. Prampolini, F. Ciardelli, E. Passaglia, Book of abstract P2-41 (Poster)

FUNCTIONALIZED BIO-POLYESTERS BY NITROXIDE RADICAL COUPLING S. Coiai, F. Cicogna, I. Domenichelli, S. Carroccio, C. Gambarotti, N. Tz Dintcheva, G. Filippone, E. Passaglia, Book of abstract O2-74 (Oral Communication)

Modest 2014 Portorož 31st August-4th September 2014:

FUNCTIONALIZED POLY(BUTYLENE SUCCINATE) BY NITROXIDE RADICAL COUPLING S. Coiai, F. Cicogna, C. Yang, I. Domenichelli, C. Pinzino, P. Rizzarelli, S. Carroccio, C. Gambarotti, N. Tz. Dintcheva, G. Filippone, E. Passaglia”, Book of abstract 65 (Oral Communication)

LIGHT RESPONSIVE FUNCTIONAL POLYOLEFINS I. Domenichelli, F. Cicogna, S. Coiai, M. Lessi, F. Bellina, E. Passaglia, Book of abstract P77 (Poster)

European Polymer Federation 2015 Dresden 21-26 June 2015:

SURFACE MODIFICATION OF POLYOLEFINS THROUGH NITROXIDE-MEDIATED PHOTOGRAFTING I. Domenichelli, Z. Zhao, S. Taddei, E. Martinelli, F. Cicogna, S. Coiai, E. Passaglia, Book of abstract SYN-P171 (Poster)

XXII Convegno Italiano Associazione Italiana di Scienze e Tecnologia delle Macromolecole Genova 11-14 September 2016:

MODIFICA SUPERFICIALE DI POLIOLEFINE MEDIANTE PHOTOGRAFTING DI NITROSSIDI FUNZIONALI I. Domenichelli, F. Cicogna, S. Coiai, C. Pinzino, S. Taddei, E. Martinelli, E. Passaglia, Book of abstract: O2.4 (Oral Communication)

AWARDS

Poster prize: LIGHT RESPONSIVE FUNCTIONAL POLYOLEFINS I. Domenichelli, F. Cicogna, S. Coiai, M. Lessi, F. Bellina, E. Passaglia, Book of abstract P77 (Poster), MODEST 2014

List of Acronyms and Abbreviations

LIST OF ACRONYMS AND ABBREVIATIONS USED IN THE TEXT

AA= acrylic acid

ATR-FTIR= Fourier Transform Infrared-Attenuated total Reflectance Spectroscopy

AzO-TEMPO= 4-(phenylazo)-benzoyl-2,2,6,6-tetramethylpiperidine-1-oxyl radical

BFA= butyl 3-(2-furyl)propenoate

BP= benzophenone

BPO= benzoyl peroxide

BuA= butyl acrylate

BzO-TEMPO= 4-benzoyloxy-2,2,6,6-tetramethylpiperidine-1-oxyl

\mathcal{D} = dispersity

DBBA= 3,5-di-tert-butyl-4-hydroxy benzyl acrylate

DCC= N,N'-dicyclohexylcarbodiimide

DCM= dichloromethane

DCP= dicumyl peroxide

DEM= diethyl maleate

DFT= Density Functional Theory

DMAP= 4-dimethylaminopyridine

DMSO-d₆= dimethylsulfoxide-d₆

DSC= Differential Scanning Calorimetry

DTBPIB= Di(tert-butylperoxy-isopropyl)benzene (mixture of isomers)

EA= ethyl acrylate

EOC= random copolymer ethylene/ α -olefin

EPM= ethylene, propylene rubber

EPR= Electron Paramagnetic Resonance

Et₃N= triethylamine

FD= Functionalization degree

FL= 9-fluorenone

Fluo-TEMPO= 4-(4,4,5,5,6,6,7,7,8,8,9,9,9-tridecafluorononanoate)-2,2,6,6-tetramethylpiperidine-1-oxyl

FTIR= Fourier Transform Infrared Spectroscopy

F₅Sty= pentafluoro styrene

GA= glycidyl acrylate

HBF₄= tetrafluoroboric acid

HDPE= high density polyethylene

HO-TEMPO= 4-hydroxy-2,2,6,6-tetramethylpiperidine-1-oxyl

LDPE= low density polyethylene

LLDPE= low linear density polyethylene

MA= methyl acrylate

MAH= maleic anhydride

MeOBP= 4-methoxy benzophenone

M_n= number average molar mass

M_w= weight average molar mass

NaNO₂= sodium nitrite

NfCl= 1-naphtoyl chloride

NfCOOH= 1-naphtoic acid

NfO-TEMPO= 4-(1-naphthoate)-2,2,6,6-tetramethylpiperidine-1-oxyl

NMP= Nitroxide Mediated Polymerization

NMR= Nuclear Magnetic Resonance

NRC= nitroxide radical coupling

NVP= n-vinylpyrrolidone

PAA= poly acrylic acid

PC= polycarbonate

PET= polyethylene terephthalate

PP= polypropylene

PS= polystyrene

PVP= poly-vinylpyrrolidone

RDRP= Reversible Deactivation Radical Polymerization

SEC= Size Exclusion Chromatography

SEBS= styrene-*b*-(ethylene-co-butene)-*b*-styrene)

SS= sodium 4-styrene sulfonate

Sty= styrene

tBuA= *tert*-butyl acrylate

TEMPO= 2,2,6,6-tetramethyl-1-piperidinyloxy

T_g= glass transition temperature

TGA= Thermogravimetric Analysis

THF= tetrahydrofuran

ThiO-TEMPO= 4-(2-thienylazo)-benzoyl-2,2,6,6-tetramethylpiperidine-1-oxyl

XAN= xanthone

VAc= vinyl acetate

VBC= vinylbenzylchloride

VC= vinyl chloride

VLDPE= very low density polyethylene

Table of Contents

TABLE OF CONTENTS

Chapter 1: Introduction	1
1.1: Synthesis of functional polyolefins through (co)polymerization.....	2
1.2: Synthesis of functional polyolefins through Post-polymerization functionalization	2
1.2.1: Functionalization by radical grafting of unsaturated monomers	3
1.3: Macroradicals stabilization by the use of co-agents	10
1.3.1: The use of unsaturated co-agents.....	11
1.3.2: The use of radical-mediating co-agents	17
1.3.2.1: The Nitroxide Radical Coupling (NRC) reaction as a tool to post-polymerization functionalization of polyolefins	20
1.4: Objectives of the work.....	28
Chapter 2: Synthesis of new Functionalized Polyolefins by Nitroxide Radical Coupling Reaction in the melt	31
2.1: Preparation and characterization of AzO-TEMPO, ThiO-TEMPO and Fluo-TEMPO functionalized polyolefins.....	31
2.2: Photo-physical properties of free azo-aromatic TEMPO derivatives.....	43
2.3: Photo-physical properties of HDPE-g-(X-TEMPO) and (EOC)-g-(AzO-TEMPO).....	49
2.4: Conclusions	58
Chapter 3: Synthesis of Functionalized Polyesters by Nitroxide Coupling Reaction in the melt	60
3.1: Preparation and characterization of BzO-TEMPO and NfO-TEMPO functionalized polyesters.....	60
3.2: Fluorescent properties of aliphatic polyesters grafted with NfO-TEMPO.....	73
3.3: Conclusions	75
Chapter 4: Surface Copolymers Modification through Nitroxide-mediated Photografting	77

4.1: Preparation and characterization of functionalized polyolefins	84
4.2: Surface property evaluation	96
4.3: Discussion about the grafting mechanism of X-TEMPO	99
4.4: Discussion about the particular case of NfO-TEMPO	104
4.5: Conclusions	105
Chapter 5: Study of the reversibility of NRC reaction: the stability of alkoxyamine grafted species	107
5.1: Characterization of functionalized polyolefins with Electron Paramagnetic Resonance (EPR) technique	107
5.2: Theoretical study	109
5.2.1: Computational details	111
5.2.2: Computational results	112
5.3: Conclusions	116
Chapter 6: Synthesis of Grafted Polyolefins by Nitroxide-mediated Polymerization.....	117
6.1: Controlled grafting of polystyrene onto polyethylene backbone via “grafting from” technique	117
6.2: Conclusions	134
Chapter 7: Experimental Part	135
7.1: Materials	135
7.2: Synthesis of nitroxides	138
7.2.1: Synthesis of 4-(phenylazo)benzoyl-2,2,6,6-tetramethylpiperidine-1-oxyl radical (AzO-TEMPO)	138
7.2.2: Synthesis of 4-(2-thienylazo)-benzoyl-2,2,6,6-tetramethylpiperidine-1-oxyl radical (ThiO-TEMPO)	138
7.2.3: Synthesis of 2,2,6,6-tetramethylpiperidine-1-oxyl-4-yl 4,4,4,5,5,6,6,7,7,8,8,9,9,9-tridecafluorononanoate (Fluo-TEMPO)	140

7.2.4: Synthesis of 4-(1-naphthoate)-2,2,6,6-tetramethylpiperidine-1-oxyl(NfO-TEMPO).....	141
7.3: Polymers modification through TEMPO derivatives.....	142
7.3.1: Polyolefins melt functionalization procedure	142
7.3.2: Polyesters melt functionalization procedure	143
7.3.3: Polymer photografting	145
7.3.4: Photografting of (LLDPE)-g-(PVP), (LLDPE)-g-(NfO-TEMPO) and (LLDPE)-g-(Fluo-TEMPO) according to the two step mechanism	146
7.4: Radical copolymerization of styrene and styrene derivatives onto the PE-g-X-TEMPO according to the Nitroxide Mediated Polymerization (NMP) technique.....	147
7.5: Characterizations	148
7.5.1: Melting point measure	148
7.5.2: Gas-liquid chromatography	148
7.5.3: Mass spectroscopy	149
7.5.4: Nuclear Magnetic Resonance (NMR)	149
7.5.5: Size Exclusion Chromatography (SEC)	149
7.5.6: Fourier Transform Infrared Spectroscopy (FTIR) and Fourier Transform Infrared-Attenuated total Reflectance Spectroscopy (FTIR-ATR)	150
7.5.7: Thermogravimetric analysis (TGA)	151
7.5.8: Differential Scanning Calorimetry (DSC).....	151
7.5.9: UV-Vis spectra	151
7.5.10: Steady-state fluorescence spectra	153
7.5.11: Photo-activation of AzO-TEMPO, ThiO-TEMPO and functionalized polymers	154
7.5.12: UV light irradiation for photografting technique	154
7.5.13: Electron Paramagnetic Resonance (EPR)	154
7.5.14: Static contact angle	154
7.5.15: Polymer films preparation.....	155
7.5.16: Gel content calculation.....	155
Chapter 8: Conclusions.....	156

Chapter 9: Bibliography..... 157

Introduction

CHAPTER 1

INTRODUCTION

Polyolefins are the class of commodities most widespread throughout the world owing to a series of features, making these polymers particularly performing; among all:

- a) the monomers low price and availability;
- b) the discover and the use of efficient catalytic systems
- c) the broad range of homo or copolymers which can be obtained;
- d) the polymers non-toxicity;
- e) the polymers recyclability;
- f) finally the cheap and environmentally friendly productive process.

Furthermore their noteworthy chemical resistance and the wide range of mechanical properties (ranging from the high stiffness of techno polymers to the typical features of elastomers) guarantee their use in several kind of applications¹⁵, as food packaging, rubbish disposal bags, ultra-high strength fibers and automobile bumpers. By contrast, the presence in the polymer backbone of only sp^3 hybridized carbons and the resulting lack of functional groups do not allow the polyolefins use in applications that require, for example, great coating/adhesion characteristics¹⁶. Nonetheless, the insertion of functional groups (even in low amount), as polar groups, can positively affect important properties such as toughness, adhesion, barrier properties, surface properties (paintability, printability,...), solvent resistance, miscibility with other polymers, and rheological properties⁶ without compromising the fundamental features of polyolefins.

For this reason the polyolefins functionalization has always attracted great interest from chemists. Different methods were discussed in the literature, and in the following paragraphs some of them are described paying particular attention to basic reactions/mechanisms and their role in the achievement of final structure and properties of functionalized products.

1.1: Synthesis of functional polyolefins through (co)polymerization

The direct, random copolymerization of olefins with functionalized monomers could seem the more straightforward method to incorporate functional groups in the polyolefins backbone. It theoretically allows achieving a random sequence of polar groups in the polymer chains and quantitatively controlling their amount by tuning the insertion efficiency during the reaction¹⁷. In particular the direct copolymerization of polar and non-polar vinyl monomers is a good synthetic approach to obtain polymers with adapting properties by playing on the copolymer architecture. Copolymers having different structure can be, in fact, prepared by changing the feed ratio of both monomers by taking into account their insertion efficiency¹⁸. Two main methodologies can be employed: the copolymerization through radical initiators/processes and the use of catalysts. Both the methodologies have some strengths, but also some disadvantages. The direct radical copolymerization of polar and non-polar vinyl monomers presents, indeed, some limitations due to the poor reactivity of the non polar monomer with respect to the functionalized one, that does not guarantee to achieve the polymers structure in a controlled fashion. On the other hand the catalyzed α -olefin/functional monomer copolymerization, usually suffers from metal catalyst deactivation caused by a strong tendency of the catalysts themselves to complex the non-bonded electron pairs on N, O and X (halides) of the polar monomer rather than their double bonds π -electrons. In other words to avoid this phenomenon, a protection of the functional monomers is requested prior to the polymerization.

Detailed analysis of these two synthetic approaches was thoroughly reported in several reviews¹⁷⁻¹⁹.

1.2: Synthesis of functional polyolefins through POST-polymerization functionalization

The post-polymerization functionalization of polyolefins is a process that modifies directly the preformed polymers and can be applied to a wide range of starting polymers, thus

completely overcoming the issues evidenced for the direct copolymerization approaches. The chemical inertness of the polyolefins forced the chemists to use techniques and reagents (generally radicals) whose reactivity towards polymer chains is immediate and quantitative, but, owing to fast reactions, side effects can occur and must be minimized to allow the new materials preserving all the properties of the starting polyolefins. Essentially the process should guarantee the new functionality incorporation¹⁶ avoiding transformation that arouse breaking (degradation) or coupling of the chains (crosslinking), negatively affecting the ultimate physical/chemical properties of the functionalized material. An example of successful process is that of polyolefins with carbenes and nitrenes derivatives (electron deficient carbon and nitrogen species, respectively), which is known to proceed by the concerted insertion of carbenes or nitrenes into the C-H bond of the macromolecular chain²⁰. During this process the radical concentration is very low and this can limit the polymer side reactions; but at the same time the very low stability of the functionalizing agents (even at room temperature) makes difficult the industrial application of these processes.

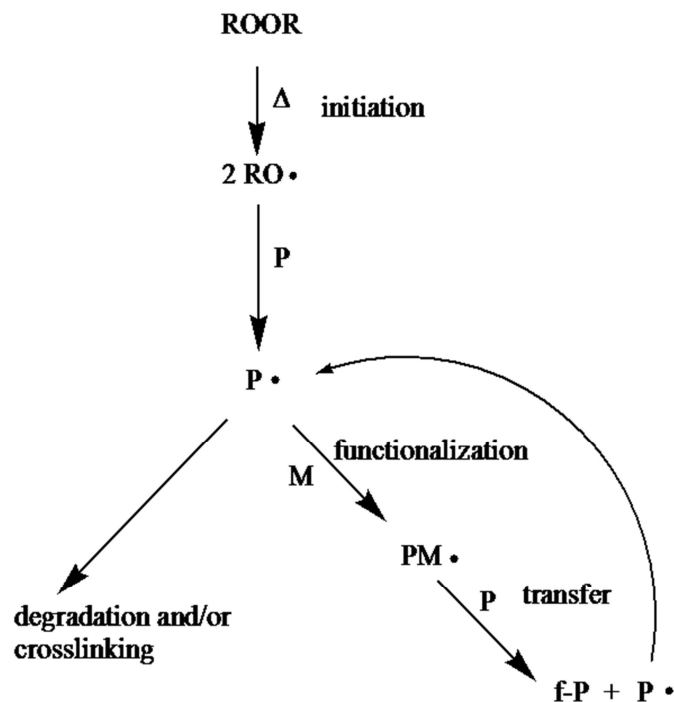
Another kind of post-polymerization modification is constituted by the radical-initiated grafting process of a functional unsaturated monomer onto the polyolefin backbone. This methodology is the most widespread and common functionalization process, industrially used for the production of polymer commodities generally named “compatibilizers” and employed as reactive macromolecular surfactants able to compatibilize blends of immiscible or poorly compatible polymers. Starting from 80'th years²¹⁻²⁵ this process was studied with the aim to insert specific functionalities (generally carboxylic acid and/or anhydride) by keeping under control the side reactions causing the ultimate properties detriment. An overview of the main important studies with particular reference to reactions mechanism are following discussed.

1.2.1: Functionalization by radical grafting of unsaturated monomers

The direct grafting of unsaturated monomers into polyolefins by radical initiators is a process that, as a whole, has a certain degree of complexity from the point of view of the mechanism and it can be discussed in terms of subsequent and parallel reactions (Figure 1.2.1): the *initiation* step that combines the cleavage of initiator (generally a peroxide)

generating the primary radicals, and the formation of macroradicals by H-abstraction from the backbone. Based on their reactivity, the macroradicals can add the unsaturated monomers generating functionalized macroradicals (*propagation or functionalization*) or can evolve by chains scission and/or coupling (*side reactions*). The functionalized macroradicals can further react with the polymer chain by H-abstraction (*transfer*) providing the functionalized product and a new macroradical that can proceed by the same mechanism.

The grafting success is usually measured in terms of *grafting yield* namely the amount of monomer linked to the matrix with respect to the unreacted monomer or consumed by side reactions. The term *functionalization degree* (FD) indicates, instead, the amount of functionalizing agent grafted in the polymer backbone per 100 moles of repeating monomeric units.



ROOR= peroxide
 RO•=primary radical
 P=polyolefin chain
 P•=macroradical
 M=grafting, unsaturated, polar monomer
 PM•=functionalized macroradical
 f-P=functionalized polyolefin

Figure 1.2.1: Scheme of a polyolefin grafting reaction²⁶.

The process generally occurs in the melt and it enjoys of several advantages: short reaction time without solvents, ease products isolation and overall it can be carried out in continuous by using machines (the extruders) having relatively low cost and already industrially used for plastics processing⁷. However these advantages are accompanied by some disadvantages all connected with the chemistry of the process: the need of relatively high temperatures to process the polymer and the use of radical initiators make this methodology not selective. Side reactions, as polymer degradation, crosslinking and monomer homopropagation occur mainly as a consequence of the especial polymer and monomer reactivity and experimental conditions. In order to address these issues, several parameters affecting the process results have to be optimized: in particular monomer type, feed composition (the ratios between all the reagents), processing conditions, time, temperature, mixing machine should be set on the basis of starting polymer features and targeted products. Furthermore, since the polar reagents used to functionalize polyolefins are not very soluble in the hydrophobic reaction medium provided by the molten polyolefins, the grafting reaction occurs mainly at the interface and it is therefore affected by the mixing efficiency and screw/rotor design of the extruder/mixer²⁶.

An accurate analysis of all parameters that significantly influence the mechanism and then the outcome of the functionalization process was widely reported in several reviews^{7, 16, 27}, the aim of this introduction is, instead, to assess in depth the side reactions mechanism and to identify the suitable routes to approach a full control of collateral effects.

As aforementioned, once the macroradical is formed through hydrogen abstraction it can react with vinyl monomers starting the grafting process:



The new formed radical can add a new monomer by increasing the grafted chain length (2) or abstract hydrogen from the polyolefin (transfer) ending with the polyolefin functionalization with a single monomer unit (3):



where:

MM^{\cdot} = macroradical;

$XHC=CHX$ = functional vinyl monomer;

$MM-H$ = polyolefin;

$MM-CHX-CH_2X$ = functionalized polyolefin

The grafting efficiency (E) is defined as the moles of monomer grafted per moles of radicals derived from the initiator⁷, therefore from the reaction (1) it appears clear that each primary radical formed through peroxide decomposition can give no more than one macroradical. For this reason the maximum value of E should be theoretically between 1 and 2 (depending on the peroxide efficiency in providing primary radicals and macroradicals) in the event which all the macroradicals react with the unsaturated monomer. Actually the data reported in Table 1.2.1²⁸ show that the E values are substantially greater than 1 or 2, namely these values are larger of the total amount of primary radicals.

Table 1.2.1: Relative efficiency (E) and functionalization degree (FD) of post-polymerization functionalization runs carried out with different polyolefins* and by using dicumyl peroxide(DCP) as peroxide and diethyl maleate (DEM) as functionalizing monomer at various DCP/DEM molar ratios²⁸.

Runs	DCP/DEM ^a	E ^b	FD % by mol
LLDPE1	0.22/1.80	5	1.0
LLDPE2	0.11/1.80	7	0.7
LLDPE3	0.11/3.60	12	1.2
VLDPE1	0.03/0.50	7	0.2
VLDPE2	0.11/1.80	9	1.0
VLDPE3	0.05/1.80	10	0.5
EPM1	0.22/2.70	9	0.9
EPM2	0.11/1.80	12	1.2
EPM3	0.03/0.50	17	0.5

* LLDPE=low linear density polyethylene, ethylene/propylene + 1-butene units ratio= 6.2; VLDPE= very low density polyethylene, ethylene/propylene + 1-butene units ratio= 10.1; EPM= ethylene-propylene rubber, ethylene/propylene + 1-butene units ratio= 2.3.

a) molar ratio between the peroxide DCP (dicumyl peroxide) and the vinyl monomer DEM (diethyl maleate); b) E= number of grafted DEM units/moles of DCP

This behavior suggests that the transfer reactions (see Figure 1.2.1) play a key role in the mechanism, substantially increasing the number of macroradicals potentially adding the monomer and thus increasing the FD and E values. The E data rises by decreasing the amount of peroxide or for low values of peroxide/monomer ratio. In addition it seems to be depending on the tertiary carbon content (on the polyolefin backbone; see as example samples LLDPE3, VLDPE3, EPM3); it increases by raising the α -olefin content, in agreement with the macroradicals stability and reactivity. Transfer reactions are thus really important in the whole mechanism: they improve the FD values (increasing the E) by maintaining high content of macroradicals during the functionalization process.

On the other part, owing to specific stability of formed macroradicals this inevitably leads to increase the incidence of side reactions with particular reference to crosslinking phenomenon because it increases the concentration of macroradicals and thus the possibility they meet each other.

Collateral reactions, such as chain breaking and crosslinking, are mainly depending on the structure of macroradicals and thus on the nature of the polymer. By comparing the results about the solubility of functionalized products starting from polyethylene (LDPE) and polypropylene (PP) samples it appears evident that while the use of the peroxide leads to the formation of a crosslinked fraction for LDPE, in the case of PP it causes a dramatic abatement of the starting solubility, suggesting a reduction of M_w , as even proved by viscosity measurements (Table 1.2.2). The use of a functionalizing monomer, diethyl maleate (DEM), may control the final solubility of products derived from LDPE, on the basis of peroxide/monomer ratio: by decreasing the R value (it should be lower than 0.09) the functionalized products have the same solubility of the starting polymer. Instead in the case of PP independently of the R ratio the starting solubility is not restored, suggesting that for PP the collateral reactions are difficult to keep under control by simply modulating the feed composition.

Table 1.2.2: Functionalization of LDPE and PP with DEM and MAH in the melt. Reproduced table from ref²⁹.

Runs	DEM* % mol	DCP [§] % mol	R=DCP/DEM mol/mol	Acetone Extracted fraction (%wt)	Toluene Extracted fraction (%wt)	MW _η
E01	0	0	-	0.5	0	-
E02	0	0.11		0.5	42	-
E09	1.8	0.11	0.06	2.8	0	-
E19	1.8	0.22	0.12	1.2	38.1	-
E12	3.6	0.11	0.03	3.1	0	-
E18	3.6	0.17	0.05	2.9	0	-
E16	3.6	0.22	0.06	3.2	0	-
E17	3.6	0.33	0.09	2.0	34.0	-
PP01	-	-	-	-	82.9	370000
PP02	-	0.08	-	-	1.1	100000
PP03	2.44	0.08	30.5	-	1.1	-
PP04	4.88	0.08	61.0	-	1.1	110000
PP05	4.88	0.16	30.5	-	<1	-
PP06	4.88	0.23	21.2	-	<1	-
PP07	1.22	0.08	15.2	-	<1	-
PP08	2.44	0.16	15.2	-	<1	-
PP09	2.44	0.23	11.0	-	<1	-

*DEM= Diethyl maleate, monomer;

[§]DCP= Dicumyl peroxide, initiator

E= LDPE

These results definitely proved that for polyethylene-based polymers it is possible to control the collateral crosslinking extent by playing with the ratio between the peroxide and the monomer concentration owing to the fact that the coupling is a bimolecular reaction whose incidence is then controlled by the macroradical concentration. Conversely the increase of the branched units, such as propylenic units, in the polyolefin backbone generates a remarkable detriment of M_w of functionalized products, due to the formation of less stable tertiary macroradicals undergoing to β -scission reaction not easy to control (Figure 1.2.2).

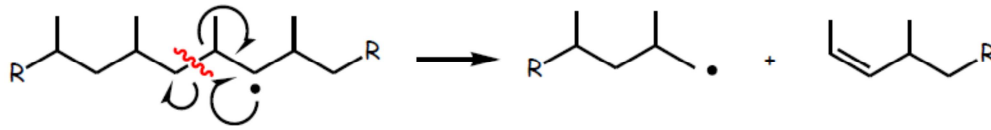


Figure 1.2.2: β-scission reaction mechanism

This polypropylene (PP) structural modification is well documented and it strongly influences the functionalization process by considerably competing with the grafting reaction^{22, 30}. The β-scission process is a monomolecular reaction (Figure 1.2.2) whose extent depends only on the relative stability of the macroradicals and cannot be avoided by tuning the ratio between the reagents (see table 1.2.2). As reported in literature²⁹ and in Table 1.2.2, the increase of the amount of functionalizing monomers in the feed, or the variations in the monomer/peroxide ratio are not able to control the PP degradation.

Moreover, the monomer reactivity towards the formed macroradicals plays a fundamental role in advancing the grafting yield by minimizing side reactions and overall in determining the grafting distribution onto the backbone on the basis of its capability to homopropagate at the processing temperature. Indeed, the functionalizing monomer has to meet different requirements: it has to be soluble in the molten polyolefin, in order to easily diffuse and fast link to the macroradical; its volatility has to be suitable with process temperature; its reactivity towards radical initiator has to be minimized and it shall be directed towards substrate derived radicals and obviously its susceptibility to the homopolymerization has to be controlled. However even if all these features should address the reagent choice, the mostly used unsaturated monomers are generally among maleic anhydride (MAH) and its derivatives or acrylic/methacrylic monomers able to graft functionalities suitable for the final applications (as examples polymers with improved compatibility with technopolymers and/or improved paintability/adhesion performances)³¹⁻³³.

During the last 30 years extensive studies were devoted to keep under control side reactions, with particular reference to crosslinking, chain scission and monomer homopolymerization. As example Moad⁷ by crossing a number of data about the functionalization results reported some experimental variables that may be optimized to maximize the grafting and minimize the side reactions.

Table 1.2.3: Effect of process conditions on side reactions and grafting yields. Reproduced table from ref⁷.

Condition	To minimize			To maximize
	Crosslinking	Chain scission	Homopolymerization	Grafting
Mixing efficiency	Raise	Raise	Raise	Raise
Temperature	Raise	Lower	-	Raise
Pressure	Raise	Lower	Raise	Raise
Monomer conc.	-	Raise	Raise	Raise
Radical conc.	Lower	Lower	Lower	Raise

Obviously this description is really simplified because several parameters are really difficult to optimize by considering that their effects are strongly correlated. The thermal chain scission, for instance, is favored by both a not efficient mixing because of overheating zones formation, and by a very strong mixing which can cause mechanical stresses. Anyway it appears clear the need to avoid the formation of many radical sites for limiting the discussed side reactions; the attempt to improve the grafting yield by increasing the amount of initiator had not success because of the consequent raise of chain breaking and crosslinking. In contrast improving mixing efficiency and thus controlling the local monomer concentration or adding suitable co-agents can improve the grafting yield and decrease the extent of these collateral reactions⁷.

Above all, the main problem of PP based polymers functionalization refers to the β -scission reaction that is due to the formation of not-stabilized tertiary macroradicals, liable to fragmentation, which is not possible to keep under control by modulating the experimental conditions and whose amount is further increased by the transfer reactions. For this reason, it was necessary to find new methodologies to make the PP macroradicals less prone to breaking, and with this aim new chemical reagents were investigated, and particularly the use of several co-agents was developed.

1.3: Macroradicals stabilization by the use of co-agents

Two different classes of co-agents were employed to control the stability of macroradicals and to lead their reactivity towards the desired grafting reaction²⁶:

- ✓ chemicals that are able to quickly react with the macroradicals generating new resonance-stabilized macroradicals: unsaturated co-agents
- ✓ chemicals that are able to decrease the instantaneous concentration of macroradicals through reversible radical reactions: radical-mediating co-agents.

Following the main results about the use of co-agents are described with particular reference to their mechanism in macroradical stabilization.

1.3.1 The use of unsaturated co-agents

The first series of co-agents are chemicals able both to trap the macroradicals and to create, once linked to the polyolefin, new radical sites which are highly reactive towards the monomer⁷. The use of electron-rich monomers as co-agents was a success to improve the grafting and to limit side reactions when electron-deficient monomers are used as functionalizing agents such as MAH or methacrylic acid. One of these co-agents was styrene which showed to be really efficient in the MAH and methacrylic acid grafting onto LDPE and PP backbone.

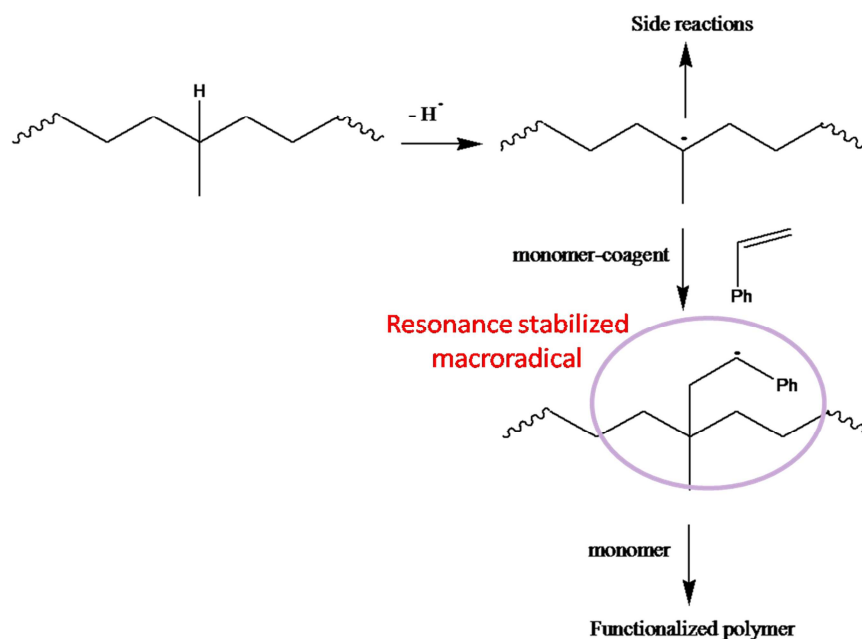


Figure 1.3.1: Polyolefins functionalization by using styrene as monomer-co-agent.

For this system the grafting yield enhancement was attributed to both the formation of resonance stabilized macroradical (Figure 1.3.1) and the generation of a charge transfer complex (CTC) between the electron-rich (styrene) and the electron-poor (MAH) species which is really reactive towards macroradicals⁷, and thus able to provide the functionalized polymer by limiting the side reactions. Other co-agents developed by Al-Malaika^{34, 35}, were based on polyfunctional monomers, especially triacrylate monomers (See for example Figure 1.3.2), they were used to improve the grafting of glycidyl methacrylate or 3,5-di-tert-butyl-4-hydroxy benzyl acrylate (DBBA) onto PP backbone without molecular weight detriment. Thanks to the presence of multiple double bonds, they act as reactive linkers between the functionalizing monomer and the polymer. In other words these co-agents act as chain extenders, by limiting the degradation and allowing achieving a final product having approximately the molecular weight of the pristine polymer. By this way the grafting yield was increased from 10-40%, in absence of the co-agent, to 80-90% in the presence of co-agent (Figure 1.3.2).

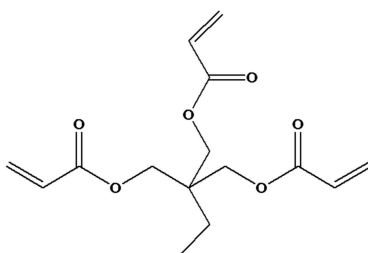


Figure 1.3.2: Trimethyl propane triacrylate

Finally, other chemicals, based on heteroaromatic derivatives, were developed and employed as functionalizing monomers and co-agents for the PP melt functionalization and gave high functionalization degrees without changing the polymer molecular weight and structure^{36, 37}. They are constituted by a heterocyclic ring conjugated with a reactive double bond bearing one electron-withdrawing group. These molecules can quickly react with the PP tertiary radical and, by forming a resonance-stabilized macroradical, they are able to minimize the PP β -scission reaction (Figure 1.3.3).

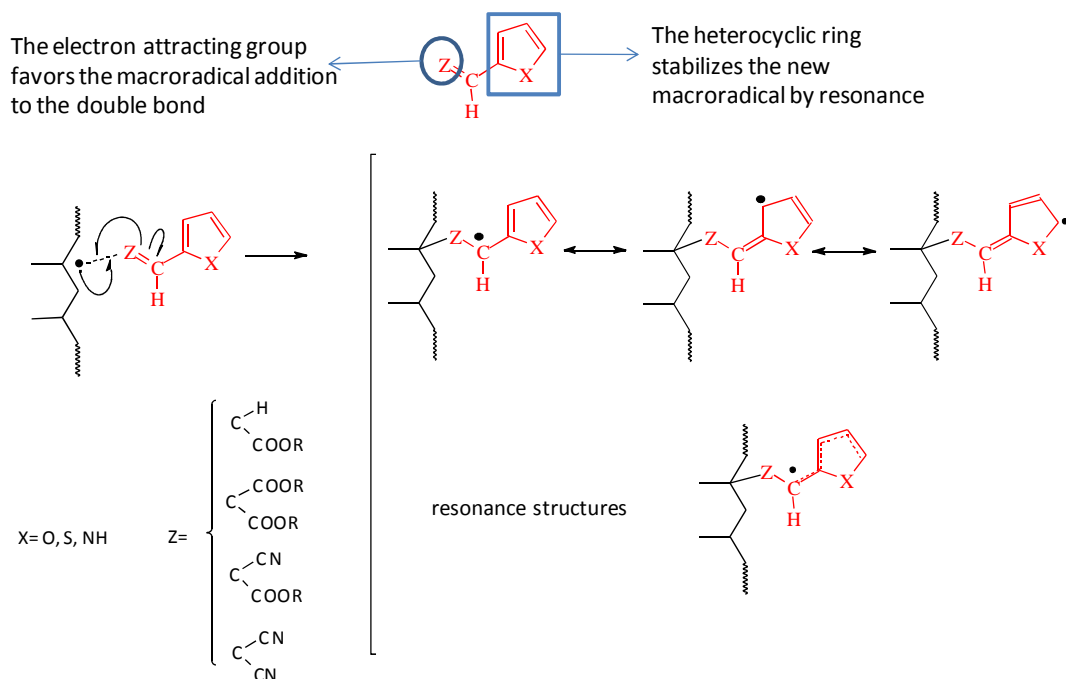


Figure 1.3.3: Structure of heterocyclic co-agents and resonance structures after addition to a PP macroradical²⁶.

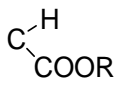
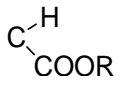
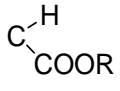
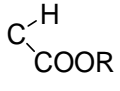
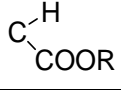
The ability of these co-agents to limit the PP degradation is due to both reactivity of the C=C bond, that is largely determined by the electron density, and stability of the functionalized macroradicals determined by different heteroaromatic rings. From the data reported in literature²⁶ (Table 1.3.1), it is evident how both the electro-withdrawing group and the heterocyclic ring, influence the polymer molecular weight evolution. Wan and co-workers³⁸ investigated the ability of furan, pyrrole and thiophene rings to stabilize the adjacent carbon-centered radical or to differently influence the electron density of the C=C bond. According to theoretical calculations concerning the radical stabilization energy of a methylene radical attached to heterocyclic rings, it appeared evident that furan, thiophene and pyrrole have the same stabilizing delocalization effect of the odd electron into the adjacent π -bond. Thus the different effect of the three co-agents on limiting the degradation of PP chains depends mainly on the change of the electron density of the adjacent C=C bond. The π -electron density of heterocyclic rings, indeed, is strongly dependent on the electro-withdrawing or electro-releasing effect provided by the heteroatom. Considering the electronegativity of heteroatom and the dipole moment of heterocyclic ring, the sequence of the π -electron density is: furan < thiophene < pyrrole.

The PP macroradical is an electron-donor species with nucleophilic character, able to react faster with monomers containing electron-poor double bonds and thus it is more reactive towards furan derivative. Simultaneously, the electronegativity of the substituent

groups ($\begin{matrix} \text{C}-\text{CN} \\ \diagdown \\ \text{COOR} \end{matrix}$, $\begin{matrix} \text{C}-\text{CN} \\ \diagdown \\ \text{CN} \end{matrix}$, $\begin{matrix} \text{C}-\text{H} \\ \diagdown \\ \text{COOR} \end{matrix}$) on the double bond changes the reactivity of the co-agent versus PP macroradicals which react more slowly with electron-rich alkenes but much faster with electron-deficient alkenes. The electronegativity of cyano group, for example, is stronger than that of ester, so cyano is better to impoverish the C=C bond and therefore favors the addition of PP macroradicals. This explains the good control in the M_w obtained for all the samples provided by using the furan derivatives. Furthermore, an increase of the co-agent/primary radical molar ratio, allows improving this effect.

Table 1.3.1: PP functionalized with different kind of co-agents: effect of co-agent structure, reagent, ratio and molecular weight on the efficiency values. Reported table from ref²⁶ (see Figure 1.3.4.).

Sample	X	Y	Co-agent/primary radicals ratio (mol/mol)	Mn (KDa)	Eff ^a
PPa-1	-	-	-	19.43	-
PPa-2	-	-	-	9.61	-
PPa-3	O	$\begin{matrix} \text{C}-\text{CN} \\ \diagdown \\ \text{COOR} \end{matrix}$	10	19.90	n.d.
PPa-4	O	$\begin{matrix} \text{C}-\text{CN} \\ \diagdown \\ \text{CN} \end{matrix}$	10	21.99	n.d.
PPa-5	S	$\begin{matrix} \text{C}-\text{CN} \\ \diagdown \\ \text{COOR} \end{matrix}$	10	14.28	n.d.
PPa-6	S	$\begin{matrix} \text{C}-\text{CN} \\ \diagdown \\ \text{CN} \end{matrix}$	10	16.21	n.d.
PPa-7	NH	$\begin{matrix} \text{C}-\text{CN} \\ \diagdown \\ \text{COOR} \end{matrix}$	10	11.50	n.d.
PPa-8	NH	$\begin{matrix} \text{C}-\text{CN} \\ \diagdown \\ \text{CN} \end{matrix}$	10	15.56	n.d.
PPc-1	-	-	-	310.00	-
PPc-2	-	-	-	124.00	-
PPc-3	O	$\begin{matrix} \text{C}-\text{H} \\ \diagdown \\ \text{COOR} \end{matrix}$	2.8	190.00	2.3

PPc-4	O		12	265.00	2.6
PPc-5	O		23.7	267.00	2.8
PPc-6	S		2.8	164.00	1.9
PPc-7	S		12	211.00	1.8
PPc-8	S		23.7	240.00	2.0

^a Efficiency: molar ratio between the FD and the amount of primary radicals assuming two radicals per peroxide molecule.

As previously discussed, even in this case the grafting efficiency quantifies the ability of the co-agent to undergo hydrogen transfer or disproportionation reactions: low values, that are those generally reached, indicate that the macroradicals formed by the co-agent addition are not able to propagate the functionalization process and any new alkyl macroradicals suitable for β -scission are generated²⁶.

A clear evidence of this behavior for one of the most used co-agent, the butyl 3-(2-furyl)propenoate (BFA), in comparison with MAH can be stated by data reported in Table 1.3.2.

Table 1.3.2: Modification of PP samples with MAH and BFA in the presence of a peroxide³⁷.

Sample	ROOR (%mol)	MAH (%mol)	BFA (%mol)	FD _{MAH} (%mol)	FD _{BFA} (%mol)	MAH (conv%)	BFA (conv%)	Eff.*	M _n 10 ⁻³ (Dalton)	M _w 10 ⁻³ (Dalton)
PP	-	-	-	-	-	-	-	-	56	260
PPMAH4	0.036	0.86	-	0.43	-	50.8	-	6.0	31	81
PPMAH5	0.036	1.71	-	0.49	-	28.7	-	6.8	36	97
PPMAH6	0.036	2.57	-	0.60	-	23.1	-	8.3	29	87
PPBFA3	0.036	-	0.86	-	0.10	-	11.6	1.4	50	244
PPBFA4	0.036	-	1.71	-	0.14	-	8.0	1.9	56	202
PPBFA5	0.036	-	2.57	-	0.19	-	7.4	1.6	56	226

By keeping constant the molar concentration of the different reagents, in the case of functionalization runs carried out with MAH the efficiency values are always >1 confirming the occurrence of the H-transfer reaction from the PP–MAH' macroradicals to

PP chains. This phenomenon leads to a sharply drop of molecular weight caused by the β -scission reactions, for all the used reagents ratios. On the contrary, the efficiency values obtained by using BFA, result to be ca. 1 underlying the lack of transfer reactions and consequently a greater control of polymer molecular weight, very close to that of pristine polymer for all the reagents concentration. However the functionalization degrees are generally low, because the new formed PP-BFA \cdot macroradical is stabilized by resonance and shows a lower tendency, compared to PP-MAH \cdot , to give H-abstraction (Figure 1.3.4). This make the macroradical more likely involved in coupling or in disproportionation reactions.

The increase of grafting level can be reached by raising the amount of primary radicals and, on the basis of peculiar BFA reactivity by keeping them in stoichiometric ratio with BFA.

Furthermore, when BFA and MAH are used jointly, the best results in terms of functionalization degree and M_w conservation are achieved by working under stoichiometric conditions among all the reagents (Figure 1.3.5). This approach ensures to preserve the polymer molecular weight and to reach at the same time good conversion level of both the monomers up to FD of 1.6 mol%. The optimal ratio BFA/primary radicals equal to 1 acts in the degradation/branching competition favoring the latter one and limiting considerably or totally the effect of the β -scission³⁷.

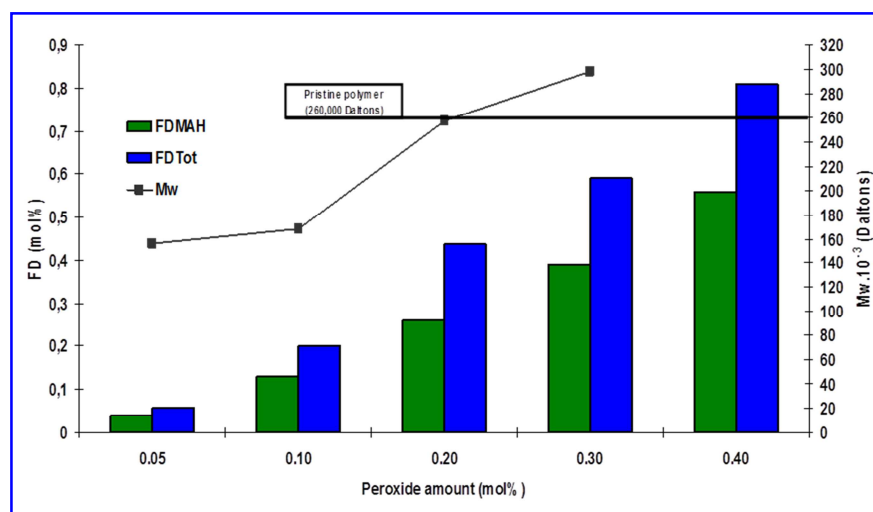


Figure 1.3.4: Dependence of FD and M_w on peroxide concentration for samples prepared under stoichiometric conditions. Reported figure from ref³⁷.

1.3.2. The use of radical-mediating co-agents

The latter series of co-agents are generally chemicals able to decrease the instantaneous concentration of free active radicals through reversible radical reactions during the functionalization of polyolefins. This was demonstrated to be a powerful method to control both degradation/crosslinking side reactions and the homopolymerization of the functional monomer. Several kinds of these co-agents, as alkylthiuram disulfide³⁹, dithiocarbamate^{40, 41}, *N*-bromosuccinimide (NBS)⁴² and nitroxides among which 2,2,6,6-tetramethyl-1-piperidinyloxy (TEMPO)^{42, 43} derivatives were used. All of them are suitable in limiting the β -scission reaction of polypropylene macroradicals by promoting the reversible radical addition between PP macroradicals and mediating radicals generated by addition of these co-agents (Figure 1.3.6)²⁶.

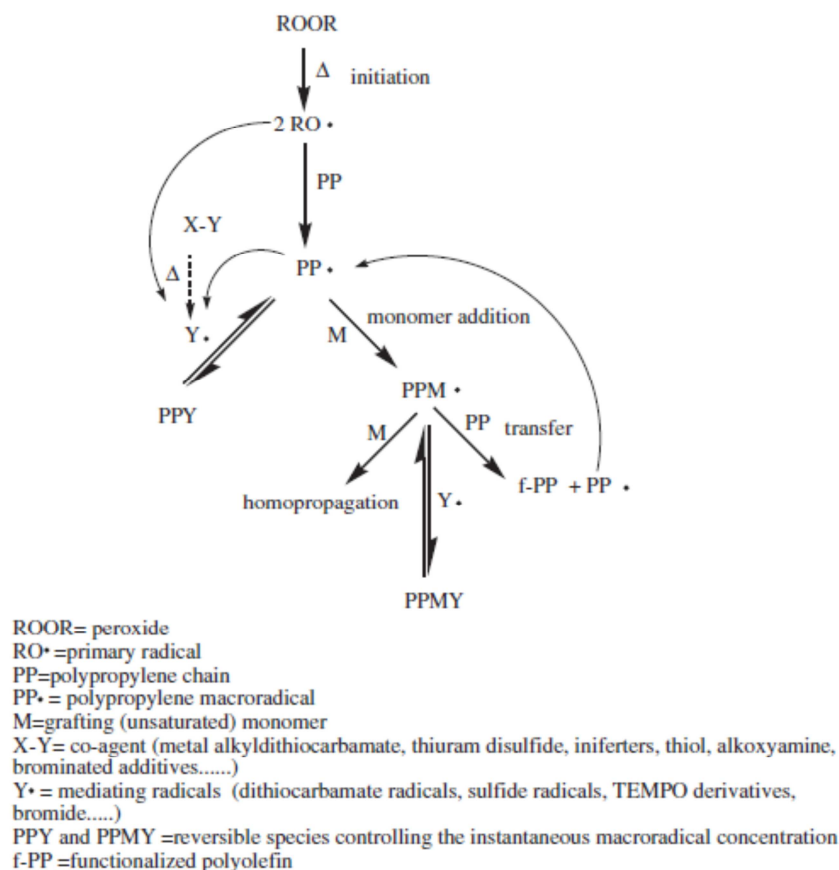


Figure 1.3.5: Simplified reaction mechanisms and possible structures of macroradicals during PP radical functionalization in the presence of a mediating radical co-agent. Reported figure from ref²⁶.

The simplified scheme, above reported (Figure 1.3.5), just describes the radical functionalization of PP (but it can be extended to all the polyolefins) in the presence of these mediating radical co-agents and it is based on the reaction between the co-agents and the active free radicals (carbon-centred and alkoxy species). On the one hand the active free radicals (i.e. the primary radicals generated by peroxide scission) are converted, *in situ*, into mediating radical which are not able anymore to attack the polymeric backbone, but act as weaker initiator of functional monomer homopropagation. This translates into a decrease of the instantaneous concentration of radical species with a noteworthy control of the side reactions. On the other hand, the mediating radicals can react with PP \cdot , PPM \cdot or with radical which are derived from the monomer homopolymerization. All these reactions are reversible, this means that the PP macroradical lifetime is significantly prolonged increasing the functionalization probability²⁶.

As example the PP functionalization with maleic anhydride (MA in this example) in presence of NBS, allows achieving a modified PP with markedly enhanced grafting level and a certain control of molecular weight⁴⁴ (Figure 1.3.6).

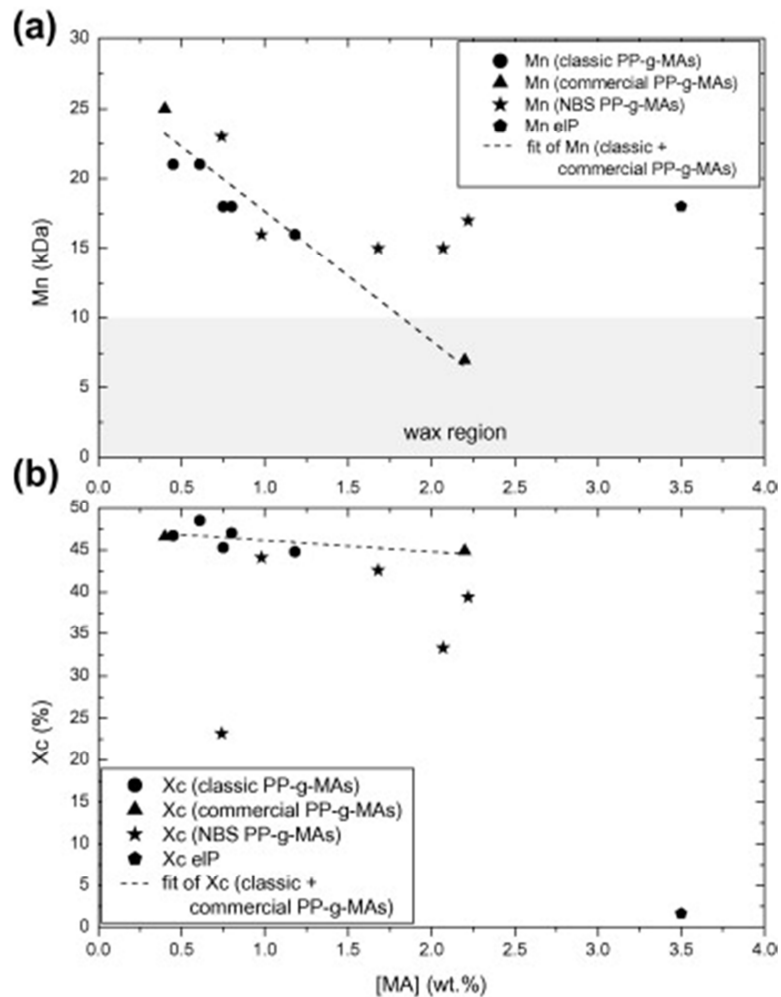


Figure 1.3.6: Evolution of (a) the number average molar mass (M_n) and of (b) the crystallization degree (X_c) of the PP-g-MAs with the grafting level ($[MA]$). Classic PP-g-MAs are samples prepared via functionalization reaction without addition of NBS; commercial PP-g-MAs are supplied by Chemtura and Clariant; NBS PP-g-MAs are PP-g-MAs prepared with the addition of NBS. eIP are highly functionalized elastomeric PP-g-MA prepared using NBS as mediating co-agent⁴⁴.

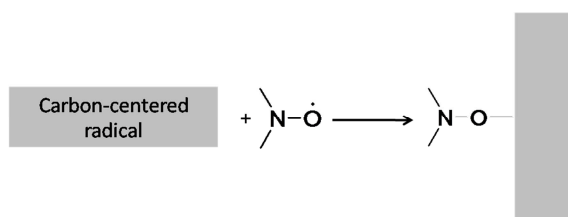
The above reported graph (Figure 1.3.6) correlates some NBS PP-g-MAs (functionalized PP by adding a low amount of NBS) characteristics, with those of classic PP-g-MAs (functionalized PP in absence of NBS).

Specifically the evolution of the average number molecular weight (M_n) and the crystallization degree (X_c) of PP-g-MAs with their grafting level ($[MA]$) is highlighted. For classic and commercial PP it appears clear the M_n decrease with the $[MA]$ raise, thus suggesting the β -scission side reactions occurrence. Conversely the addition of small amount of NBS (NBS PP-g-MAs and eIP) allows reaching higher grafting level (up to 2–3 times higher than classic PP-g-MAs) while partially avoiding M_n falling into the wax region

($M_n < 10$ kDa). Anyway the amount of added NBS has to be adapted with the MA and peroxide amounts to maintain the crystallinity of the NBS PP-*g*-MAs comparable to that of the commercial PP-*g*-MAs.

1.3.3: The Nitroxide Radical Coupling (NRC) reaction as a tool to post-polymerization functionalization of polyolefins

Among the radical mediating co-agents the nitroxides play a special role that deserves a specific attention regarding their structure and reactivity. The nitroxyl free radicals (or nitroxides) have a particular chemical structure, characterized by the lack of hydrogen atoms linked to the carbon atoms in α -position with respect the NO group, which guarantees the stability of the compound as radical species⁹. Furthermore they can quickly couple with carbon-centered radical species, such as macroradicals, giving rise to the well known Nitroxide Radical Coupling (NRC) reaction.



Scheme 1.3.1: Nitroxide Radical Coupling (NRC) reaction

For this particular feature, the nitroxides were used as spin-trap to control the extent of crosslinking in the reaction of polyethylene with peroxide^{2,3}. Several applications, indeed, require specific properties belonging to crosslinked polyolefins such as: resistance to high temperature deformation, high flow resistance, good impact property (toughness), abrasion resistance, environmental stress crack resistance, solvent (chemical) resistance and good tensile properties. Polyolefins are, thus, treated with organic peroxides in order to achieve a crosslinked material. In the case of polyethylene, to obtain a material with homogeneous features, it is necessary to avoid a premature crosslinking during the initial mixing of the reagents/chemicals². For this purpose the TEMPO derivatives were used as additives to trap the early forming radicals from the peroxide increasing the scorch time. Interestingly, by analyzing the obtained product with ¹³C-NMR, the authors² noticed that,

TEMPO molecules, used as additive to control the crosslinking process, were grafted to the polymer backbone and were present in different locations of the hydrocarbon substrate confirming the occurrence of NRC reaction (Scheme 1.3.1).

Micallef et al⁴ synthesized nitroxides bearing covalently linked fluorophore, that were employed as probes of the polypropylene degradation. The obtained results demonstrated that the NRC and the use of profluorescent nitroxide are powerful tools to investigate the polymer degradation, especially during the induction period where most analytical techniques are unable to detect any change in the polymer. Furthermore at temperature close to 150 °C, namely when the polypropylene is instable and tends to quickly degrade, the probe acts as a retarder of thermo-oxidative degradation, by significantly increasing the nitroxide-doped polypropylene lifetime via TEMPO coupling with the macroradical. This confirms once again that NRC reaction is able to provide functionalized PP⁴.

Based on this evidence a new method to functionalize polyethylene^{8,9} by means of NRC reaction was developed: the quick reaction between functionalized TEMPO derivatives and the macroradicals formed by primary radical, could address the whole functionalization procedure towards a stoichiometric process, completely avoiding any side reactions. 4-hydroxy-2,2,6,6-tetramethylpiperidine-1-oxyl (HO-TEMPO), 4-benzoyloxy-2,2,6,6-tetramethylpiperidine-1-oxyl (BzO-TEMPO)⁹ and 4-(1-naphthoate)-2,2,6,6-tetramethylpiperidine-1-oxyl (NfO-TEMPO)⁸, which are TEMPO derivatives bearing a hydroxyl group, an aromatic group and a naphthalene group respectively, were used to achieve a functional polyethylene based material. The functionalization runs were carried out in the melt by tuning the temperature and the ratios of the reagents.

The grafting success was clearly proved by UV-Vis (Figure 1.3.7), ¹H-NMR and FTIR spectroscopy (Figure 1.3.8). In particular the last two spectroscopies allowed the evaluation of the FD, which ranged between 0.1 and 0.2 mol%, by providing appropriate calibration curves.

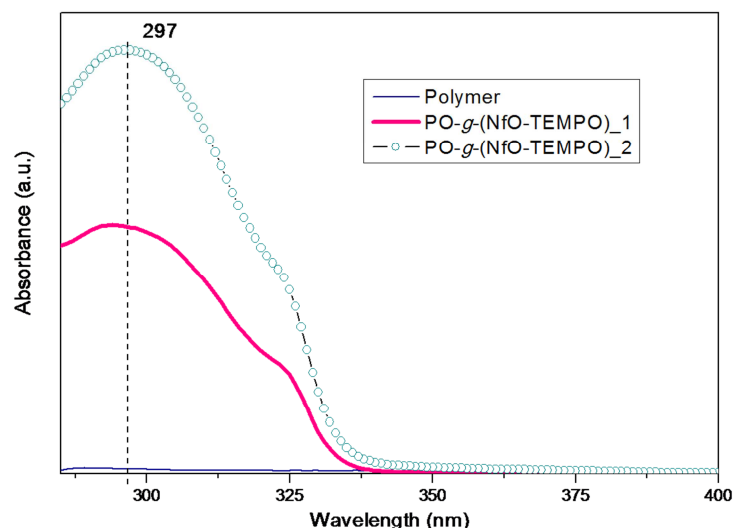


Figure 1.3.7: UV-Vis absorption spectra of PO-*g*-(NfO-TEMPO)₁ and PO-*g*-(NfO-TEMPO)₂. Figure reported from ref⁸.

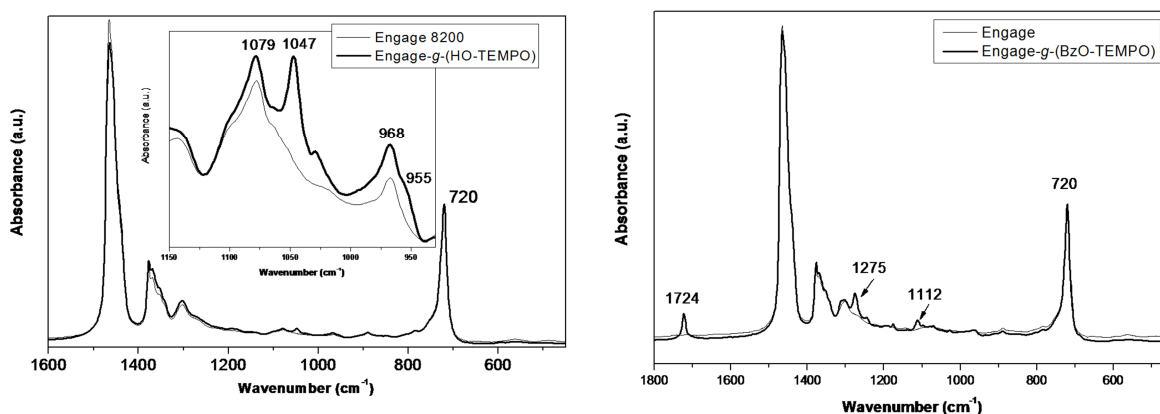


Figure 1.3.8: Superimposition of the FT-IR spectra of pristine Engage and of Engage-*g*-HO-TEMPO or Engage-*g*-BzO-TEMPO samples. Figures reported from ref⁹.

Precisely, the UV-Vis spectra (Figure 1.3.7) highlighted the presence of an absorption band centred at 297 nm belonging to the naphthalene sub-unit, on the other hand FTIR spectra (Figure 1.3.8) showed bands attributable to the HO-TEMPO or BzO-TEMPO group, thus both proving the occurrence of the grafting reaction.

Interestingly the insertion of functional groups into polyolefin backbone via NRC, did not lead to collateral effects caused by side reactions, both M_n and M_w were indeed very similar to those of the starting polymer. Furthermore the torque values did not show any

increase in contrast to the pure polymer treated with the only peroxide (an example is reported in the Figure 1.3.9)⁹.

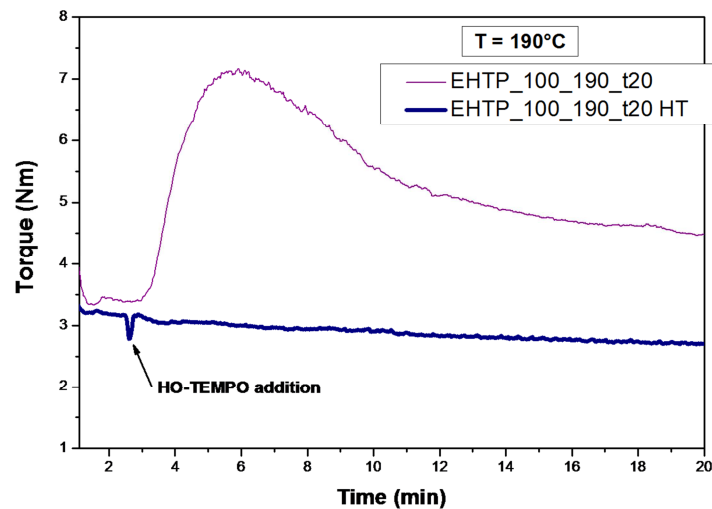


Figure 1.3.9: Comparison between the torque curves of the run EHTP_100_190_t20 (pure polymer treated with only peroxide) and EHTP_100_190_t20 HT (polymer treated with peroxide and HO-TEMPO). Figure reported from ref⁹.

Finally the NRC reaction permitted to achieve functional polymers, by transfer of the features typical of the nitroxides functional groups, directly from the functionalizing agents to the polymer itself.

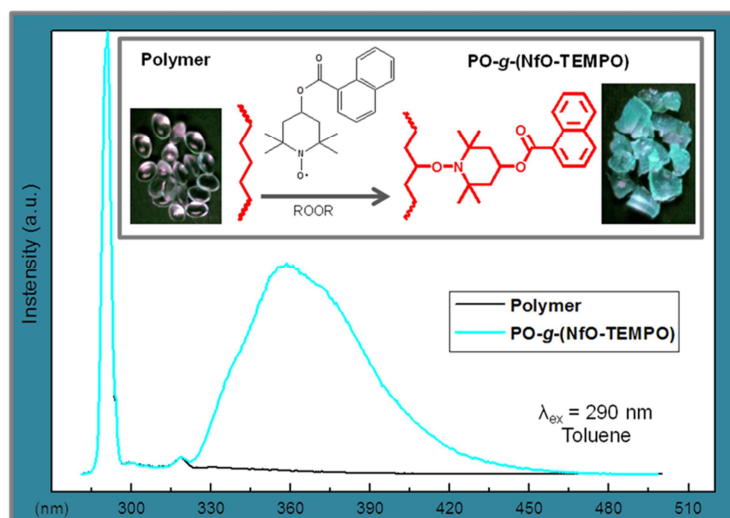


Figure 1.3.10: Comparison between the emission spectrum of the pristine polymer (black line) and the polymer after functionalization with NfO-TEMPO (light blue line) and digital images of pure polymer and PO-g-(NfO-TEMPO) under excitation with a long-range UV lamp ($\lambda = 254$ nm)⁸.

The fluorescence emission spectrum of PO-g-NfO-TEMPO (Figure 1.3.10) not only provided clear evidence of the grafting of NfO-TEMPO, but also revealed a fully restored fluorophore emission, thus obtaining a fluorescent polymer.

In addition Electron Paramagnetic Resonance (EPR) was used to deepen insight into the grafting mechanism and the >NO-C bond stability. A mixture composed of the polymer, peroxide and NfO-TEMPO, in the same molar concentrations used for the functionalization reactions, was heated inside the cavity of the EPR instrument and EPR spectra were recorded at regular intervals of temperature.

The comparison of the initial EPR spectrum with the spectrum recorded at 200 °C (Figure 1.3.11) clearly highlighted a decrease of the signal area by confirming the role as trapping agents played by the NfO-TEMPO towards the macroradicals created during the functionalization run⁸.

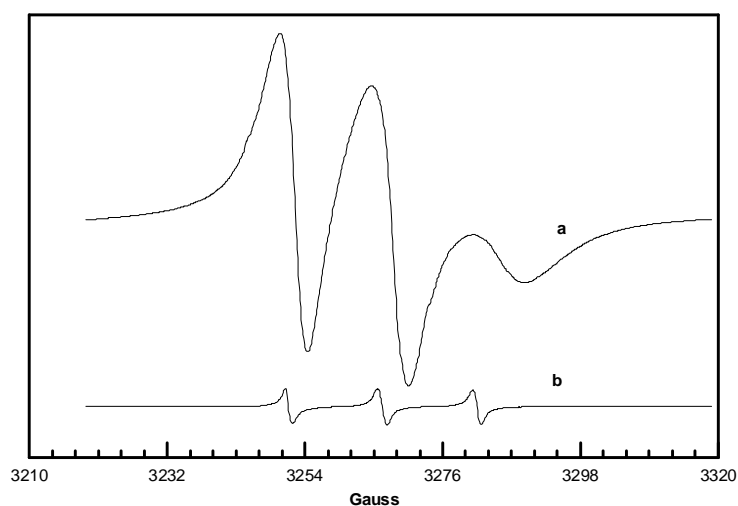


Figure 1.3.11: EPR spectra of the mixture polymer, peroxide and nitroxide recorded at 25°C (a) and 200°C (b). Figure reported from ref⁸.

The evolution of the signal area decrease with the raise of the temperature, is well underlined in Figure 1.3.12. Moreover no variation of the amount of free radicals was observed during the cooling of the sample to room temperature, suggesting that the covalent bond between nitroxide and macroradical was stable at least in this experimental conditions.

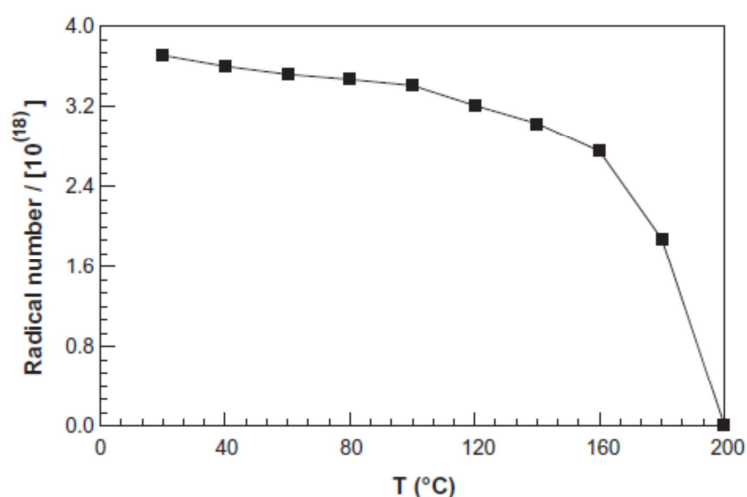


Figure 1.3.12: Radical number of NfO-TEMPO molecules as a function of the EPR cavity temperature⁸.

These evidences were in line with the hypothesized grafting mechanism, namely the reaction between nitroxides and macroradicals gave rise to covalent bonds causing the

progressive decreasing of the free TEMPO radicals in the analyzed mixture. In other words by means of EPR spectroscopy, the mechanism which involves the complete inhibition of crosslinking was validated⁸.

Having regard to the above, it appears clear the ability of the NRC reaction to create functional polymer by a one-step procedure. Furthermore the NRC reaction shows a great compatibility with different functional groups and, by modulating the feed ratio, it is possible to achieve a very good control of the grafting degree and the macromolecular architecture, even though the functionalization is carried out in the melt using peroxide as free radical initiator.

In addition, the NRC displays characteristics resembling to the “click chemistry”^{1, 45} approach: it is fast, reliable and easy to implement with high yield, it is an efficient and specific reaction which can be conducted under relatively mild conditions and overall it is compatible with several functional groups and applicable in a modular manner⁵. These features ensured the NRC as a powerful tool for synthesis of polymers with well defined architecture as for instance linear or not linear polymers and copolymers (Figures 1.3.13 and 1.3.14) or star-shape copolymers (Figure 1.3.15)^{1, 46}.

For better describing these approaches that purpose in Figure 1.3.13 is reported a scheme concerning the synthesis of an ABC triblock copolymer via an one-pot method obtained by combination of NRC reaction with other “click chemistry” in a simple way because of the tolerance of these coupling reactions. Specifically in this synthesis the heterofunctional alkyne-polystyrene bromine (alkyne-PS-Br), poly(ethylene oxide)-TEMPO (PEO-TEMPO) or poly(ϵ -caprolactone)-TEMPO (PCL-TEMPO), and poly(*tert*-butyl acrylate)azide (PtBA-N₃) were used as precursors. Click reaction between azide end group of PtBA-N₃ and alkyne functional group of alkyne-PS-Br was carried out jointly with the NRC reaction between TEMPO end group of PEO-TEMPO or PLC-TEMPO and bromine functional group of alkyne-PS-Br, with high efficiency. The final triblock copolymers, PtBA-b-PS-b-PEO or PtBA-b-PS-b-PCL were indeed obtained with controlled molecular weight and low dispersity⁴⁶.

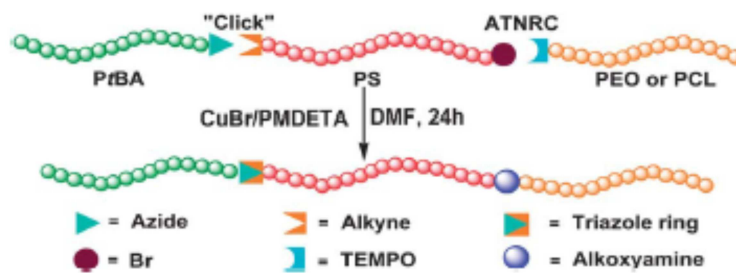


Figure 1.3.13: One-pot synthesis of ABC triblock copolymers of PtBA-b-PS-b-PEO by combination of NRC reaction with CuACC chemistry⁴⁶.

The use of NRC reaction can be extended also to the synthesis of graft copolymer. In fact in Figure 1.3.14 is showed the mechanism used to obtain the graft copolymer poly(4-glycidyloxy-2,2,6,6-tetramethylpiperidin-1-oxyl-co-ethylene oxide) [poly(GTEMPO-co-EO)]-g-PS by means of NRC reaction between the multi-pendant TEMPO groups belonging to the linear precursor poly(GTEMPO-co-EO) and PS-Br with a bromide end group in CuBr/N,N,N',N'',N''-Pentamethyldiethylenetriamine (PMDETA) system. The obtained data underlined an efficiency of NRC reaction for the graft copolymers in the range of 90.2–95.9%.

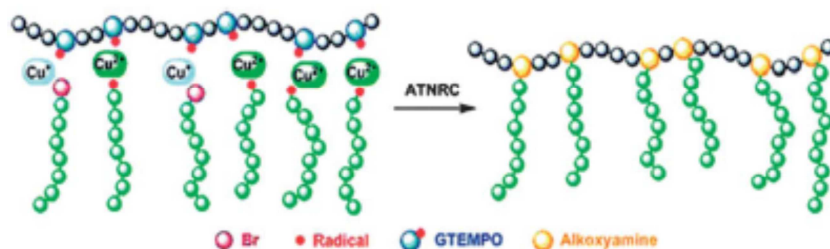


Figure 1.3.14: The illustration of graft [Poly(GTEMPO-co-EO)-g-PS] by NRC reaction⁴⁶.

Furthermore the NRC reaction was used in order to achieve star shape polymer, whose synthesis among all polymers with well defined structure, has always presented a challenge for chemists. The synthesis of a star shape copolymer, bearing PS-b-PEO as arm chains and hyperbranched polyglycerol (HPG) as core, was carried out by combining the Atom Transfer Radical Polymerization (ATRP) mechanism with the NRC reaction (Figure 1.3.15). The results highlighted a coupling efficiency of the NRC reaction truly satisfactory (90%) despite the high density of coupling sites on HPG⁴⁶.

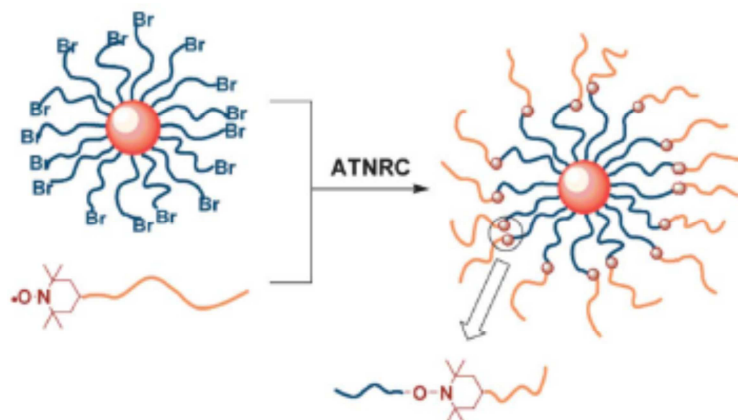


Figure 1.3.15: The synthetic illustration of HPG-g-(PS-b-PEO) $_n$ by ATRP mechanism and NRC reaction⁴⁶.

Another interesting feature of NRC is the reversibility of the coupling reaction between free nitroxide and macroradicals, especially at high temperature. By taking advantage from this reversibility, the exchange of chemical functionality on macromolecules is possible, indeed chain-end groups can be substituted with a variety of functional nitroxide derivatives (Figure 1.3.9)^{1, 46}.

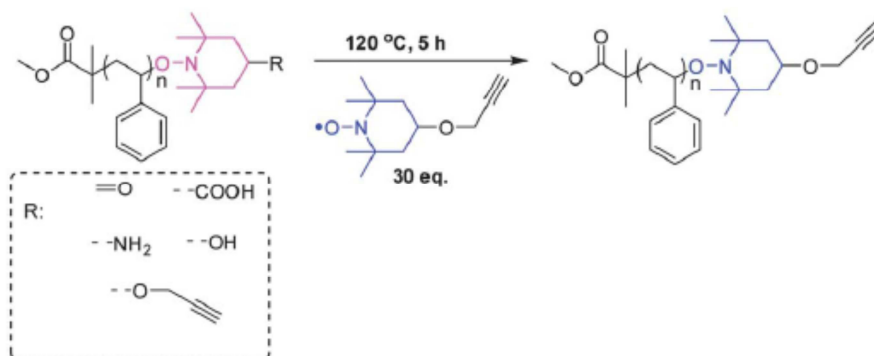


Figure 1.3.16: Terminal functionalization via nitroxide radical exchange reaction¹.

1.4: Objectives of the work

By considering the state-of-art on functionalization processes and the recent results concerning in particular the NRC approach, during this PhD thesis, an in-depth study about the possibility to apply this reaction to different polymers with the aim to insert specific functional groups in the melt or onto the surface, was investigated.

Specifically, first to expand the study of the functionalization in the molten state, the grafting of 4-(phenylazo)-benzoyl-2,2,6,6-tetramethylpiperidine-1-oxyl radical (AzO-TEMPO), 4-(2-thienylazo)-benzoyl-2,2,6,6-tetramethylpiperidine-1-oxyl (ThiO-TEMPO) (bearing light-responsive groups or chromophores) and 4-(4,4,5,5,6,6,7,7,8,8,9,9,9-tridecafluorononanoate)-2,2,6,6-tetramethylpiperidine-1-oxyl (Fluo-TEMPO) (bearing fluorinated alkyl chain) onto a random copolymer ethylene/ α -olefin (EOC) and onto the high density polyethylene (HDPE), was carried out by means of a peroxide as reaction activator. The functionalized polymers were characterized by infrared analysis (FTIR) and thermogravimetric analysis (TGA), with the aim to evaluate the grafting occurrence, whereas functionalization degree was calculated by FTIR spectroscopy.

This was followed by an accurate study of the new properties transferred directly from the nitroxides to the polymer. In particular the photophysical features of both the free nitroxides and of new “functional polymers” bearing covalently grafted azo-aromatic chromophores, were properly investigated by means of UV-Vis at different wavelengths. Finally, water contact angle measurements were used to confirm the photo-isomerization effects onto wettability changes of the surface of these materials.

Furthermore, with the purpose to evaluate the feasibility of NRC reaction to functionalize different polymer matrices, 4-benzoyloxy-2,2,6,6-tetramethylpiperidine-1-oxyl (BzO-TEMPO) and 4-(1-naphthoate)-2,2,6,6-tetramethylpiperidine-1-oxyl (NfO-TEMPO) were successfully grafted on bio-polyesters, namely poly lactic acid (PLA) and poly butylen succinate (PBS). The grafting was confirmed by fluorescence spectroscopy; the functionalization degree was estimated by UV-Vis and $^1\text{H-NMR}$ spectroscopy; whereas the preservation of molecular weight distribution was evidenced by SEC analysis. Moreover, by combining theoretical calculations with experimental evidence collected by the EPR analysis of a functionalized PBS sample and by $^1\text{H-NMR}$ spectroscopy a possible grafting site on the PBS chain was identified.

In addition the NCR was tested to promote the surface functionalization of a linear low density polyethylene (LLDPE) and a styrene-b-(ethylene-co-butene)-b-styrene (SEBS) block copolymer. A photografting method was developed by taking advantage of the coupling of TEMPO derivatives with macroradicals generated by H-abstraction through UV irradiation in the presence of a new photoinitiator. During this experiment BzO-TEMPO, NfO-TEMPO, and Fluo-TEMPO were used as functionalizing agents. The samples

were analyzed by infrared analysis (FTIR and ATR-FTIR), electron paramagnetic resonance (EPR), and TGA. The fluorescence emission spectroscopy was used to investigate the optical properties of the NfO-TEMPO surface functionalized films, while the static contact angle measurements were used to evaluate the wettability features of the polymer surface modified with Fluo-TEMPO.

In addition a careful study about the thermal stability of the >NO-C bond between the nitroxide and the macroradical (generating the alkoxyamine product) by EPR spectroscopy and by Density Functional Theory (DFT) calculations was carried out. In particular these investigations were aimed at trying to thoroughly understand if an electronic effect of the substituting groups of TEMPO derivatives can influence the bond dissociation enthalpy of the >NO-C bond.

Finally by exploiting the thermal equilibrium between the alkoxyamine and its free form, the functionalized polyolefins obtained by photografting and by functionalization in the melt were used as macroinitiators in order to grow, in a controlled/living fashion, polystyrene chains from the bulk and surface activated polymers.

The grafting success was evaluated by infrared analysis (ATR-FTIR), TGA, and differential scanning calorimetry (DSC) analysis.

Results and Discussion

CHAPTER 2

SYNTHESIS OF NEW FUNCTIONALIZED POLYOLEFINS BY NITROXIDE RADICAL COUPLING REACTION IN THE MELT

2.1: Preparation and characterization of AzO-TEMPO, ThiO-TEMPO and Fluo-TEMPO functionalized polyolefins.

The 4-(phenylazo)-benzoyl-2,2,6,6-tetramethylpiperidine-1-oxyl radical (AzO-TEMPO), 4-(2-thienylazo)-benzoyl-2,2,6,6-tetramethylpiperidine-1-oxyl (ThiO-TEMPO) and 4-(4,4,5,5,6,6,7,7,8,8,9,9,9-tridecafluorononanoate)-2,2,6,6-tetramethylpiperidine-1-oxyl (Fluo-TEMPO) were chosen as functional TEMPO derivatives to graft onto a random copolymer ethylene/ α -olefin (EOC) and onto the high density polyethylene (HDPE), in the melt by using a peroxide as radical initiator. Fluo-TEMPO was grafted onto the EOC copolymer, whereas ThiO-TEMPO was used to functionalize the HDPE and finally with AzO-TEMPO both the polyolefins were modified. These TEMPO derivatives were synthesized *ad hoc* precisely with the purpose to provide the polyolefins with new and never investigated functional groups. In particular, greater emphasis will be given to the photo physical properties of the azo-aromatic TEMPO derivatives both in solution and grafted onto the polyolefins.

The synthesis of AzO-TEMPO was realized by modifying a procedure already reported in literature⁴⁷, whereas the ThiO-TEMPO (see Experimental Part, Scheme 7.2.2.1, Chapter 7) was obtained by esterification of the (E)-4-(thiophen-2-yl diazenyl)-benzoic acid (**2** in Experimental Part, Scheme 7.2.2.1, Chapter 7) prepared from 4-carboxybenzenediazonium tetrafluoroborate (**1** in Experimental Part, Scheme 7.2.2.1, Chapter 7) and 2-thienylmagnesium bromide, according to the procedure reported by Moylan, McNelis and coworkers⁴⁸. Finally the synthesis of Fluo-TEMPO was carried out according to a conventional Steglich esterification reaction, using the fluorinated carboxylic acid in the presence of N,N'-dicyclohexylcarbodiimide (DCC) and a catalytic

amount of 4-dimethylaminopyridine (DMAP) (see Experimental Part, Scheme 7.2.3.1, Chapter 7).

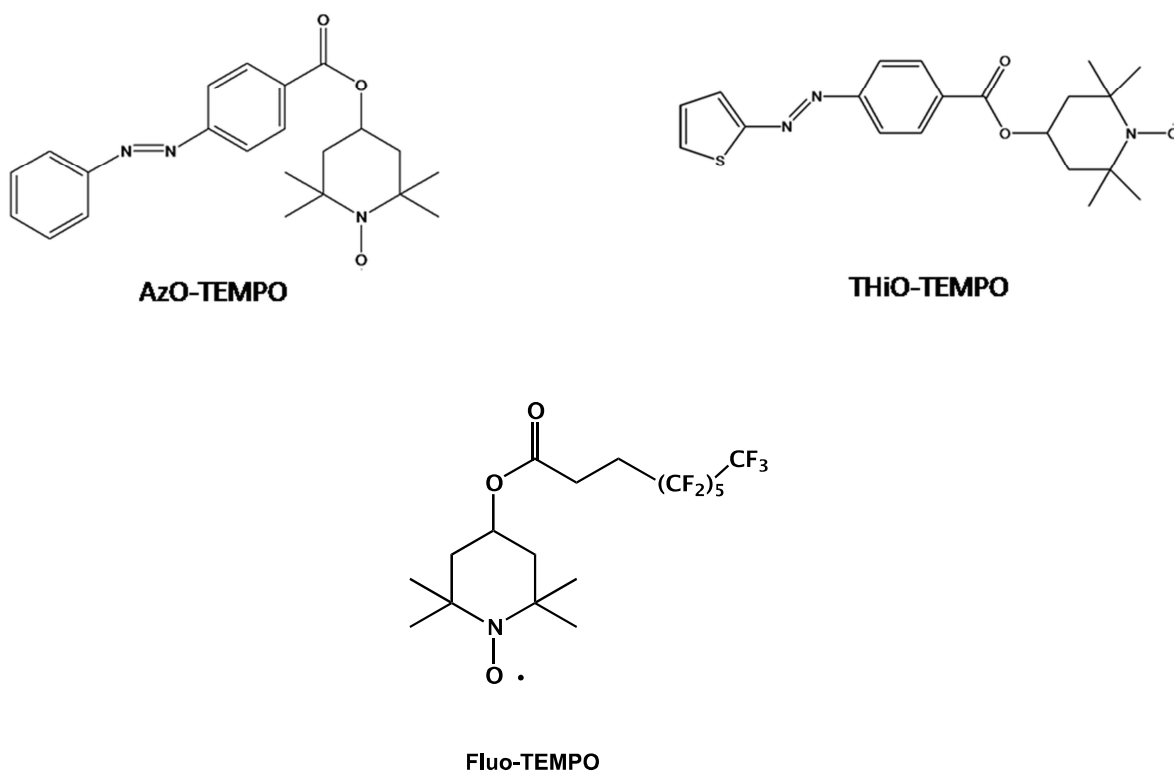
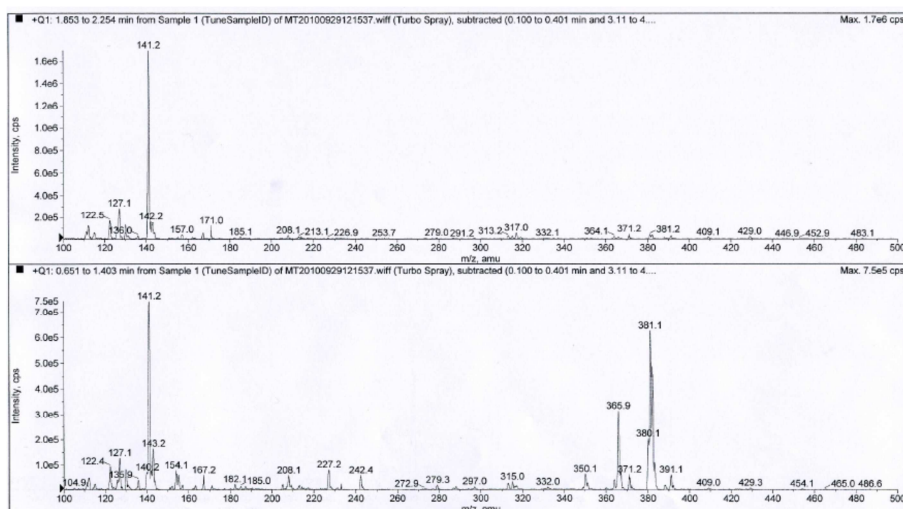


Figure 2.1.1: Chemical structure of AzO-TEMPO, ThiO-TEMPO and Fluo-TEMPO.

ThiO-TEMPO and Fluo-TEMPO were prepared in a frame of collaboration activities with research groups working at the Department of Chemistry and Industrial Chemistry of Pisa University. The three TEMPO derivatives were purified by column chromatography, and then characterized by HPLC-MS analysis (Figure 2.1.2) and by FT-IR spectroscopy both confirming their molecular structure.

A



B

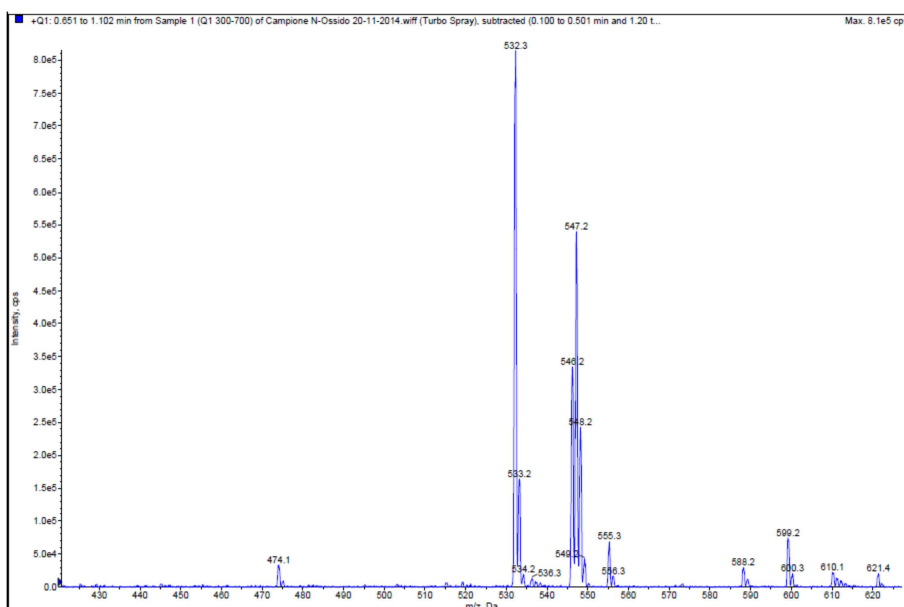


Figure 2.1.2: HPLC-MS chromatogram of: **A** AzO-TEMPO m/z: 381 [M + 1], 380 [M] and **B** Fluo-TEMPO m/z: 547 [M+1], 532 [M-14]; the ThiO-TEMPO HPLC-MS chromatogram is not available, anyway the m/z: 386 [M] was found.

The HPLC-MS chromatograms of nitroxides underlined mass peaks at m/z: 380 and 381 corresponding to AzO-TEMPO [M] and [M+1] respectively (Figure 2.1.2A), 547 belonging to Fluo-TEMPO [M+1] (Figure 2.1.2B) and 386 which is characteristic to ThiO-TEMPO [M] (unfortunately the spectrum is not available).

The infrared spectra of azo-aromatic TEMPO derivatives showed a band at 1715 cm^{-1} due to the carbonyl stretching and a band at 3055 cm^{-1} , in the case of AzO-TEMPO, and at

3077 cm^{-1} , in the case of ThiO-TEMPO, attributable to the C-H stretching of the benzene and of the thiophene, respectively. Both spectra showed also a very weak band at about 1410 cm^{-1} that can be attributed to the asymmetric stretching of the diazo group⁴⁹ (Figure 2.1.3).

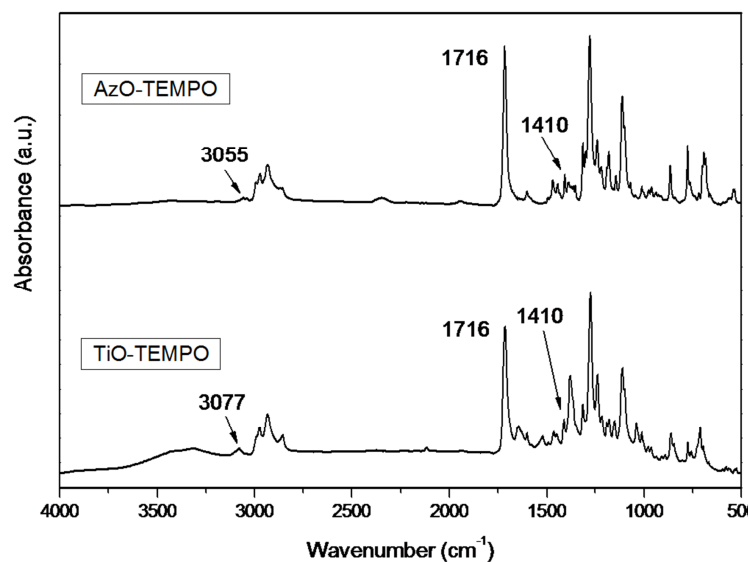


Figure 2.1.3: FT-IR spectrum of AzO-TEMPO and ThiO-TEMPO collected from KBr

Concerning the Fluo-TEMPO, the infrared spectrum (Figure 2.1.4) clearly showed a band at 1731 cm^{-1} corresponding to the carbonyl stretching, furthermore the intense absorptions in the wide range $1400\text{-}984\text{ cm}^{-1}$ proved the presence of fluorinated alkyl functionalities $-(\text{CF}_2)_n\text{CF}_3$.

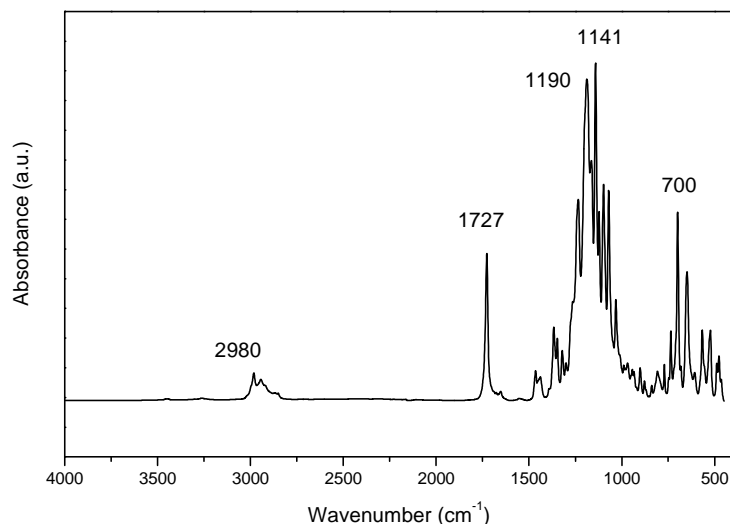


Figure 2.1.4: FT-IR spectrum of Fluo-TEMPO collected from KBr

Thermograms of TEMPO derivatives showed a single degradation step in the case of AzO-TEMPO ($T_{\text{onset}}=270^{\circ}\text{C}$) and a gradual weight loss between 100 and 240 $^{\circ}\text{C}$ followed by the main degradation step ($T_{\text{onset}}=248^{\circ}\text{C}$) in the case of ThiO-TEMPO (Figure 2.1.5). The initial weight loss was attributed to the volatilization of some side products or reagent residues derived from the synthesis of ThiO-TEMPO (see Chapter 7, section 7.2.2) and in a very limited extent to the volatilization/degradation of the nitroxide as supported by EPR measurements collected after treating the nitroxide at 190 $^{\circ}\text{C}$ for 10 min (Figure 2.1.6).

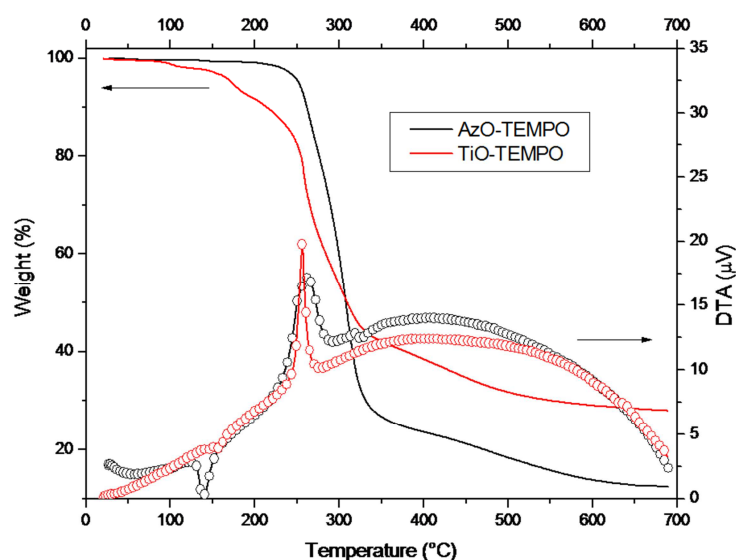


Figure 2.1.5: Thermogram and DTA signal of AzO-TEMPO and ThiO-TEMPO under nitrogen from 30 $^{\circ}\text{C}$ to 700 $^{\circ}\text{C}$, heating rate 10 $^{\circ}\text{C}/\text{min}$.

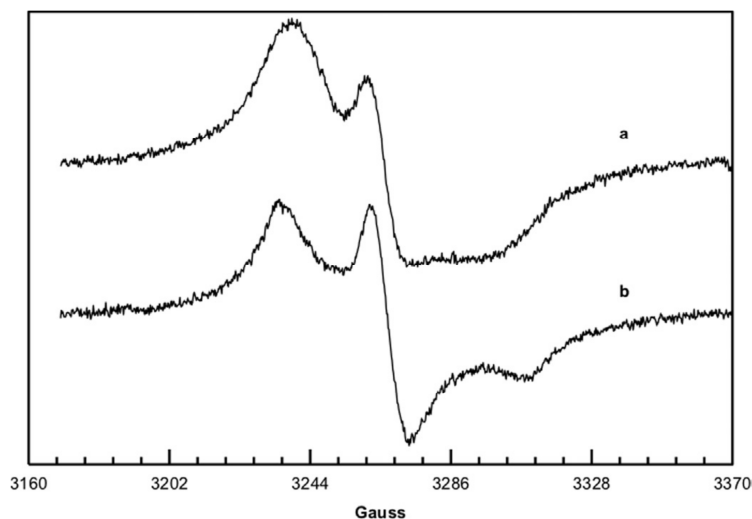


Figure 2.1.6: EPR spectrum of ThiO-TEMPO mixed with silica gel registered at room temperature before (a) and after heating at 190°C for 10 min (b).

In the case of Fluo-TEMPO (Figure 2.1.7) the main degradation step at about $T_{\text{onset}}=200^{\circ}\text{C}$ was observed. DTA curve showed a peak attributed to the melting (at about 50°C).

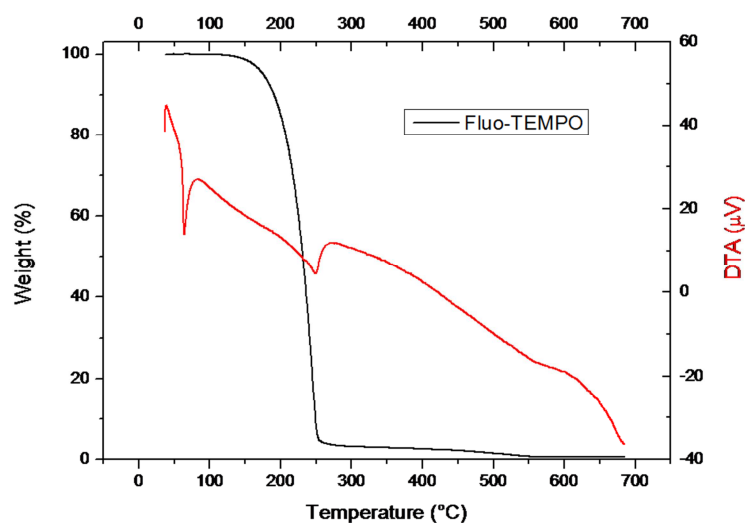


Figure 2.1.7: Thermogram and DTA signal of Fluo-TEMPO under nitrogen from 30°C to 700°C, heating rate 10°C/min.

Functionalized polyolefin with X-TEMPO, were obtained by free radical grafting post-reactor modification. Reactions were carried out in the melt, at 170 °C and 190°C for EOC and HDPE respectively, in a discontinuous mechanical mixer and they were initiated by di(tert-butylperoxy-iso-propyl)benzene.

The torque value, recorded during runs, was almost constant, only a very low difference between the initial and final torque was present (an example is showed in Figure 2.1.8),

by suggesting a very good control of side reactions such as crosslinking or degradation of the polymer matrix^{8,9}, which was usually observed in the post-reactor modification of polyolefins with unsaturated monomers.

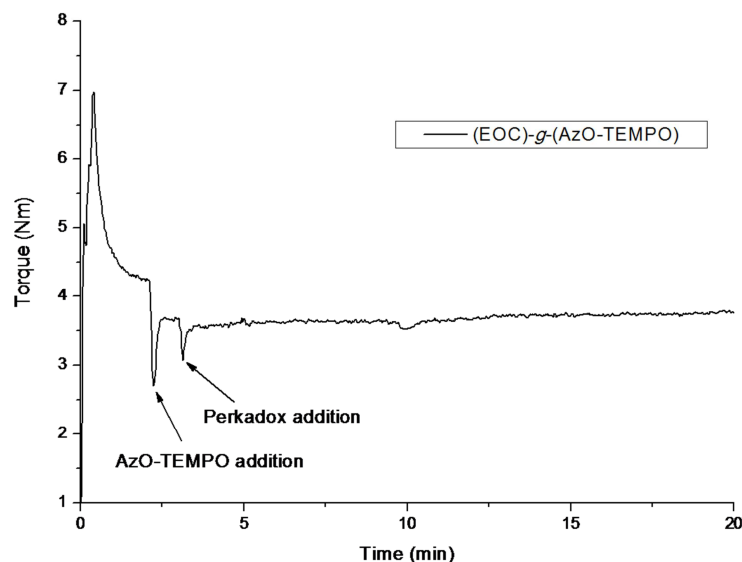


Figure 2.1.8: Torque curve of the run (EOC)-g-(AzO-TEMPO)

Crude samples were extracted with boiling acetone for 16 h in order to remove all low molecular weight compounds (reagents and by-products), then analyzed by FT-IR with the aim to evaluate the grafting occurrence and to determine the functionalization degree (FD). Infrared spectra of functionalized HDPE and EOC, confirmed the grafting of the TEMPO derivatives (Figures 2.1.9, 2.1.10 and 2.1.11). The spectra belonging to the samples bearing AzO- and ThiO-TEMPO, evidenced the presence of a band at 1722 cm^{-1} due to the carbonyl stretching of the grafted functionalities; as the same the normalized spectra of EOC modified with Fluo-TEMPO evidenced the band at 1736 cm^{-1} , which may be associated to the carbonyl stretching of the ester group, and the presence of C-F vibrations stretching in the range between 1400 and 1000 cm^{-1} .

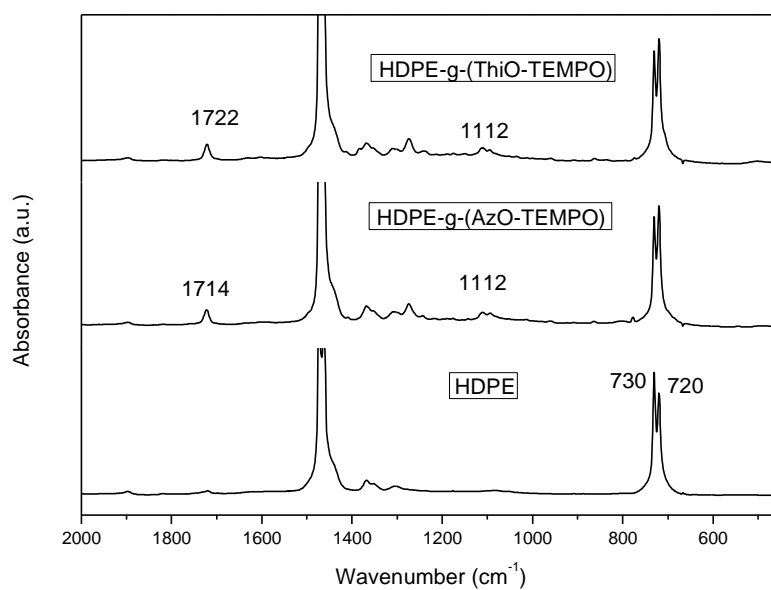


Figure 2.1.9: FT-IR spectra of HDPE, HDPE-g-(AzO-TEMPO) and HDPE-g-(ThiO-TEMPO).

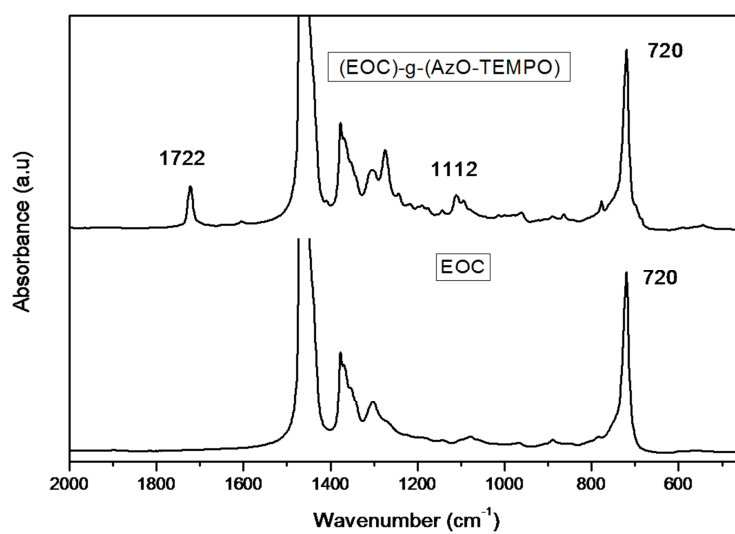


Figure 2.1.10: FT-IR spectra of (EOC)-g-(AzO-TEMPO).

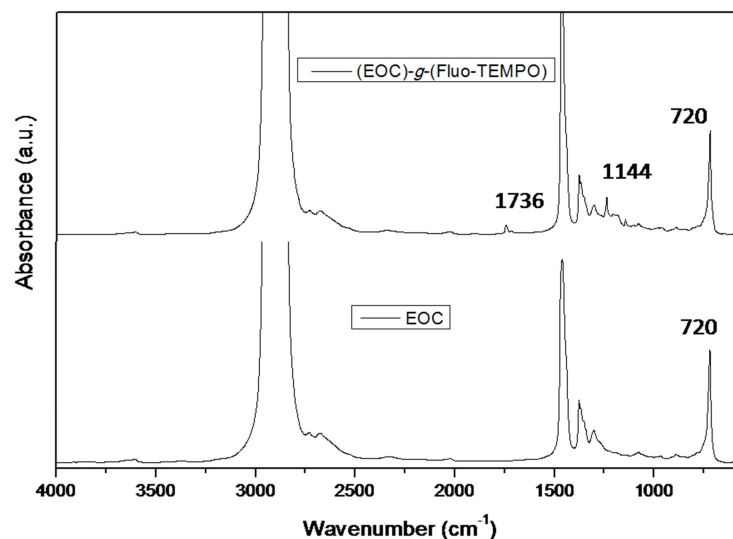


Figure 2.1.11: FT-IR spectra of EOC, (EOC)-g-(Fluo-TEMPO)

From the FT-IR spectra of functionalized HDPE samples, and by using the data of a calibration curve which was previously reported by our research group⁹, it was possible to roughly evaluate the functionalization degree (FD) of the HDPE-g-(X-TEMPO) samples which was about 0.1 mol% for both TEMPO derivatives. In the case of (EOC)-g-(AzO-TEMPO), by using the same calibration curve, a FD value of about 0.18 mol% was calculated reflecting the different feed conditions used to modify the two polymers (Table 2.1.1). On the basis of the FD values and by considering the number average molecular weight of the pristine polymer (see Experimental Part, Table 7.1.2 in Chapter 7), it was possible to state that about 1 functional group per each HDPE polymer chain and about 2-3 functional groups per each EOC chain were grafted. These low FDs and the random arrangement of the functional groups onto the polymer chain, allowed excluding the interactions between chromophores. For this reason, the trans-cis-trans photo- and thermal-isomerization of chromophores grafted to the polyolefins were studied and compared to those characteristics of the free TEMPO derivatives.

To evaluate the FD of (EOC)-g-(Fluo-TEMPO) sample, a calibration curve was, instead, prepared *ad hoc*. The curve was obtained by recording FTIR spectra of mixtures (at known composition) of copolymer and nitroxide. The ratio between the area of the Fluo-TEMPO diagnostic band (1145 cm⁻¹ corresponding to the -CF₃ stretching) and of the band at 720cm⁻¹ (methylene rocking of polyethylene) used as internal reference, was plotted

versus the amount of the nitroxide simulating the grafted species. The linear fitting of the data allowed the preparation of the calibration curves (Figure 2.1.12) used to evaluate the FD of functionalized EOC. The FD value obtained by following the calibration curve, for the (EOC)-g-(Fluo-TEMPO) sample was 0.08%.

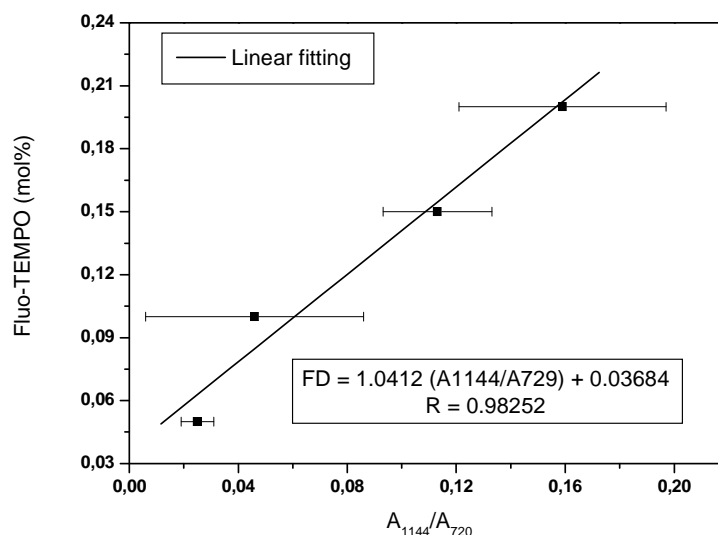


Figure 2.1.12: Calibration curves for (EOC)-g-(Fluo-TEMPO) sample. The reported error was evaluated by considering the FD values of three determinations.

To check the thermal stability of the functionalized polymers and to state if at high temperature a homolytic bond cleavage of the >N-O-C bond can cause the leaching of the grafted TEMPO from the polymer matrix, the samples were analyzed by TGA under nitrogen flow. Thermograms of functionalized polymers evidenced a first weight loss (about 1 wt% for the samples bearing AzO and ThiO-TEMPO and 1.6 wt% for the sample bearing Fluo-TEMPO) starting at about 270°C in the case of the samples functionalized with the azo-aromatic TEMPO derivatives and at about 247°C in the case of (EOC)-g-(Fluo-TEMPO) (Figure 2.1.13). This first degradation step was followed by the main degradation step of the polymer matrix at about 485°C, for HDPE, and at about 470°C, for EOC (Figure 2.1.13).

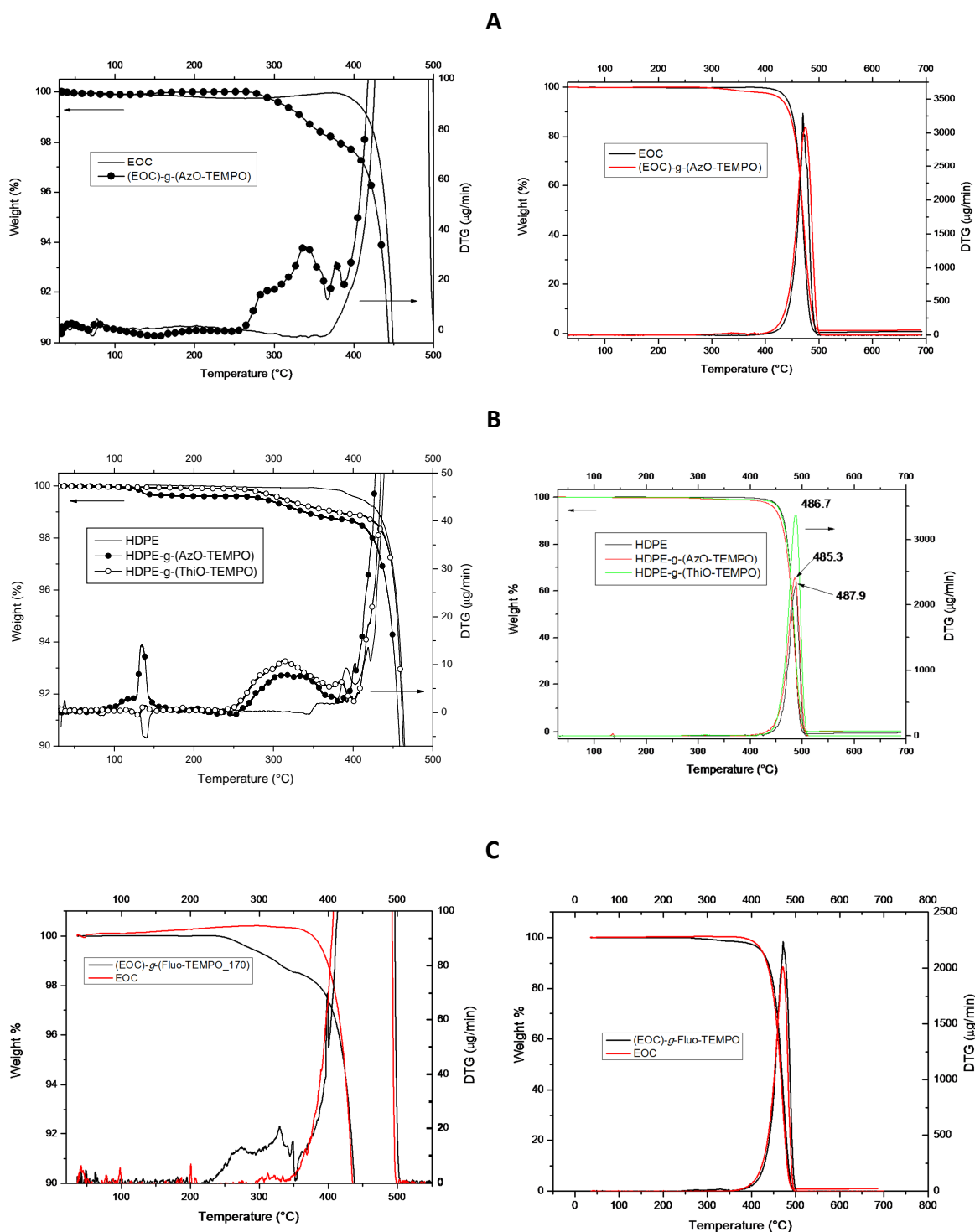


Figure 2.1.13: TGA thermograms and their first derivative of **A:** EOC before and after functionalization with AzO-TEMPO, **B:** HDPE before and after functionalization with AzO-TEMPO or ThiO-TEMPO and **C:** EOC before and after functionalization with FluO-TEMPO. The analyses are carried out under nitrogen flow.

Both temperatures are very close to the degradation temperature of the two pristine polymers thus suggesting that the functionalization process did not alter the thermal degradation mechanism of the matrix. As far as the first weight loss, it can be due to the bond cleavage between the grafted TEMPO moiety and the macroradical. In fact the balance among the bonded and free form of the nitroxides, at high temperature was shifted towards the radical form. The percentage of this weight loss roughly corresponds to the FD evaluated by FT-IR analysis (Table 2.1.1) confirming the attribution of this TGA step to the detachment of TEMPO moieties.

Table 2.1.1: Radical functionalization of polyolefins: feed composition, functionalization degree (FD) and thermal properties

Sample name	Feed composition		Functionalization Degree ¹		Thermal properties	
	X-TEMPO ²	Peroxide	FD _{FT-IR} ³	FD _{TGA} ⁴	T _{5%} ⁵	T _{max} ⁶
	(mol%)	(mol%)	(mol%)	(mol%)	(°C)	(°C)
EOC ⁷	-	-	-	-	440	470
HDPE ⁷	-	-	-	-	456	488
(EOC)-g-(AzO-TEMPO)	0.28	0.09	0.18	0.20	430	475
HDPE-g-(AzO-TEMPO)	0.14	0.04	0.12	0.09	447	486
HDPE-g-(ThiO-TEMPO)	0.14	0.04	0.11	0.08	455	487
(EOC)-g-(Fluo-TEMPO)	0.17	0.057	0.08	0.11	422	472

¹Functionalization Degree (FD): moles of the grafted functional groups with respect to 100 moles of monomer repeating units. ²X-TEMPO: functional TEMPO derivative. ³FD evaluated by FT-IR analysis. ⁴FD evaluated by TGA analysis under nitrogen. ⁵Temperature corresponding to 5% weight loss. ⁶Maximum degradation temperature. ⁷EOC and HDPE starting polymers.

2.2: Photo-physical properties of free azo-aromatic TEMPO derivatives

The UV-Vis spectra of both the TEMPO derivatives compared with that one of azobenzene, all obtained from diluted acetonitrile solutions, are shown in Figure 2.2.1. They revealed that the AzO-TEMPO main absorption band at 323 nm (π - π^* transition) is red shifted of about 10 nm and shows a higher extinction molar coefficient (ϵ) respect on the azobenzene same band⁴⁷. The other two bands of AzO-TEMPO at 224 nm (σ - σ^* transition)⁵⁰ and 446 nm (n - π^* transition) maintain the same position of those of azobenzene. The main absorption band of ThiO-TEMPO is even more red shifted (about 53 nm) with respect to that of azobenzene because of the presence of the electron donating thiophene ring (substituent of the N=N bond) that makes ThiO-TEMPO classifiable as “aminoazo-benzene” type chromophores. This kind of molecules have the main π - π^* transition moved to a lower energy, so closely to the n - π^* transition to cause their partial overlapping. For that reason the band at 446 nm (n - π^* transition) in the spectrum of ThiO-TEMPO looks like a long tail of the main absorption band⁵¹.

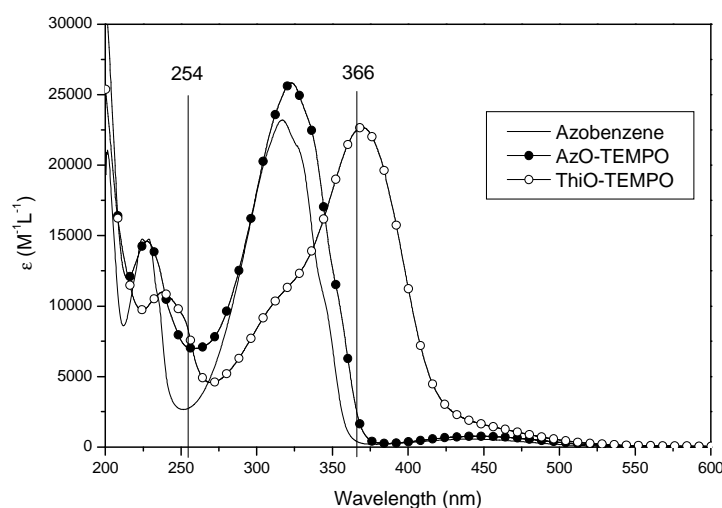


Figure 2.2.1: UV-Vis absorption spectra of azobenzene, AzO-TEMPO and ThiO-TEMPO in acetonitrile.

The irradiation of the azobenzene and TEMPO derivatives solutions at 366 nm caused the photo-isomerization of all compounds from the *trans* isomer to a new Photo Stationary State (PSS₃₆₆) rich in the *cis* isomer (Figure 2.2.2 and Figure 2.2.3). In all cases isosbestic points were detected (two in the case of azobenzene and AzO-TEMPO and three in the

case of ThiO-TEMPO) confirming that the isomerization involves two species that are in equilibrium between each other.

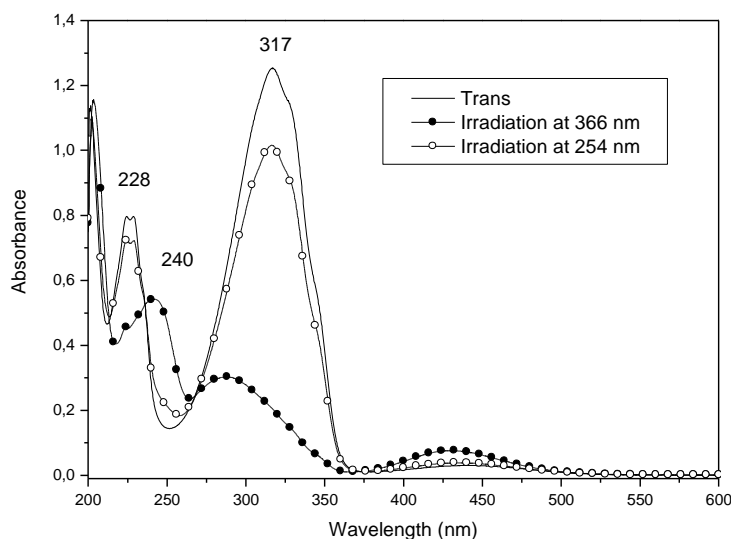


Figure 2.2.2: Absorption spectra of azobenzene before and after irradiation at 366 nm and 254 nm

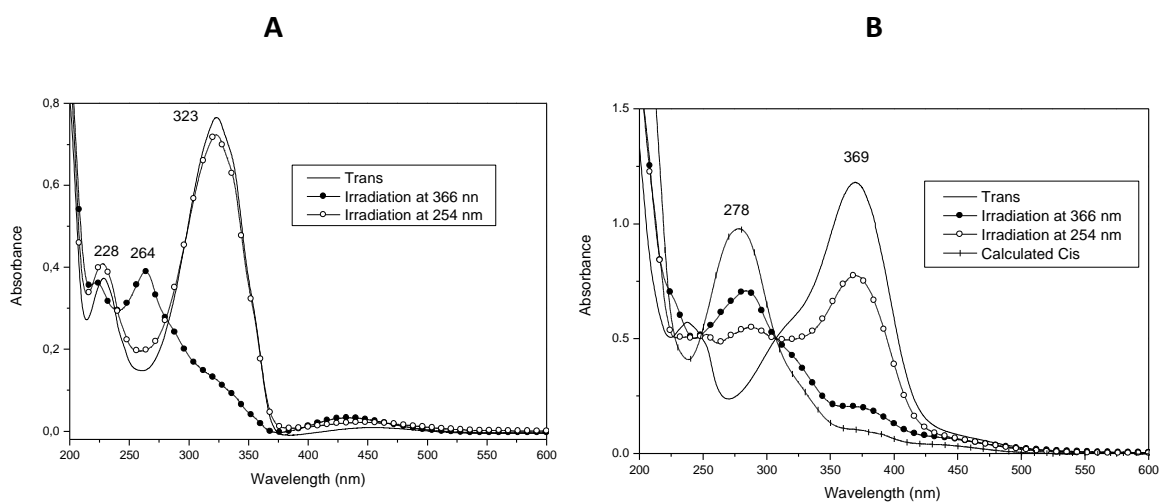


Figure 2.2.3: Absorption spectra of **A:** AzO-TEMPO and **B:** ThiO-TEMPO in acetonitrile solution before and after irradiation at 366 nm and 254 nm, respectively.

When the AzO-TEMPO solution was hit by the UV-rays at 366 nm the band at 320 nm, belonging to the *trans* isomer, decreased while the band at around 460 nm, belonging to the *cis* isomer, increased⁴⁷ (Figure 2.2.4). The reaching of the new photo stationary states (PSS₃₆₆) occurred in about 35 min of irradiation and were mainly composed of the pure *cis* isomer⁵². Concerning the ThiO-TEMPO solution, its irradiation with the same lamp

generated the decrease of the band at 369 nm and the increase of a band at 284 nm (Figure 2.2.4).

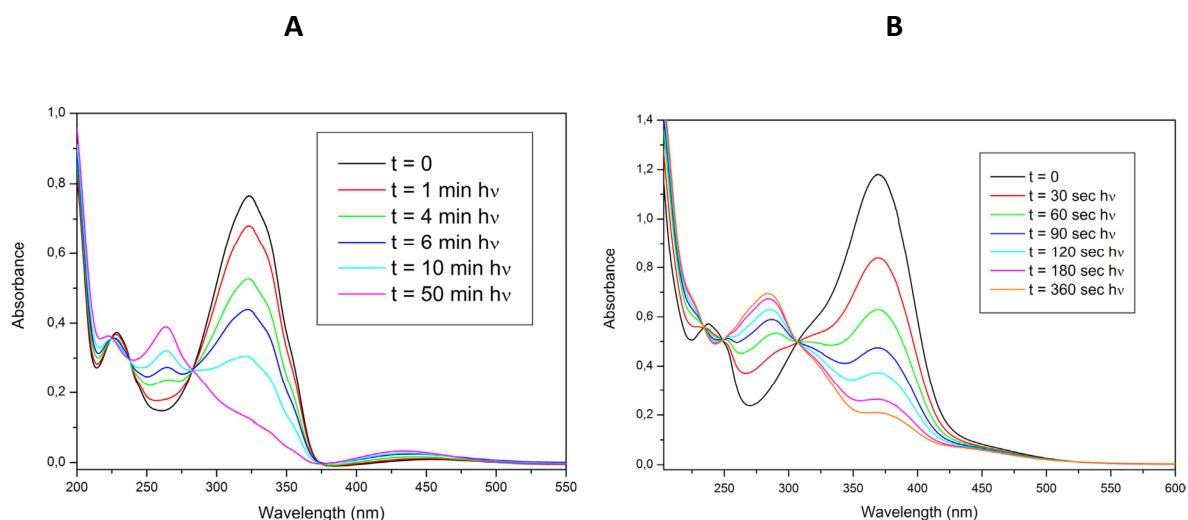


Figure 2.2.4: Absorption spectra of: **A:** AzO-TEMPO (acetonitrile solution) and **B:** ThiO-TEMPO (acetonitrile solution) collected after different irradiation times during irradiation at 366 nm.

As shown in the picture above the increase of the ThiO-TEMPO band at 440 nm is not evident, but rather, it seems to undergo a decrease during irradiation, actually the reduction of the main band at 369 nm can screen and partially compensate the expected increase of the less intense band at 440 nm. In this case, the PSS_{366} was reached in about 6 min of irradiation. The faster isomerization of ThiO-TEMPO with respect to that of AzO-TEMPO can be imputed to the higher molar extinction coefficient of ThiO-TEMPO at the irradiation wavelength rather than to a different photo-isomerization efficiency of the two chromophores.

The back *cis-trans* isomerization of azobenzene derivatives can be obtained thermally or by irradiation with opportune wavelength light. Usually the azobenzene photoisomerization is accomplished under visible light because in this region the molar extinction coefficient of the *cis* isomer is higher respect that of the *trans* isomer⁵¹, whereas in the UV region, the difference between the molar extinction coefficient of the *cis* and *trans* isomers is lower. Only at about 240 nm the *cis* isomer of azobenzene absorbs more than the *trans* isomer. Anyway, the presence of substituents onto the

benzene ring of azobenzene derivatives can shift the absorption maxima both of the *cis* and *trans* isomer thus, in some cases, the *cis* isomer can absorb more than the *trans* isomer both in the visible and in the UV region. In these cases, the *cis-trans* photo-isomerization can be promoted by irradiation with visible or UV light⁵³⁻⁵⁵. Regarding the AzO-TEMPO, its *cis* isomer absorbs more than the *trans* species both in the visible region and in the UV between 240 and 280 nm, whereas, the *cis* isomer of ThiO-TEMPO has a higher extinction coefficient only in the UV region between 250 and 300 nm. In the light of this, to photo-isomerize the *cis* isomer of AzO-TEMPO both the visible or the UV light can be used, whereas, in the case of ThiO-TEMPO only UV irradiation can be efficient. In order to verify this hypothesis, irradiation at 254 nm was carried out. As hypothesized, the irradiation of the *cis* isomer of AzO-TEMPO with a 254 nm emitting lamp completely restored the *trans* isomer in 35 min. The same conversion was observed also in the case of azobenzene showing that its *cis* isomer can be photo-isomerized by irradiation in the UV region. Irradiation of both *cis* and *trans* ThiO-TEMPO with the same lamp gave a new PSS₂₅₄ (Figure 2.2.3) having a spectral pattern that appears as a combination of the spectrum of the *trans* and *cis* isomers.

This result was confirmed by the TLC analysis of the irradiated solution that evidenced the presence of two products. To evaluate the composition of this PSS₂₅₄, the absorption spectrum of the pure *cis* isomer of ThiO-TEMPO would be necessary, however by considering that the separation of the two isomers was not possible neither by column chromatography nor by other techniques, the spectrum of the *cis* isomer of ThiO-TEMPO was esteemed on the basis of the Fischer method⁵⁶. To apply this method two requirements are necessary: first, upon irradiation of a sample by two different wavelengths, two PSS having different composition have to be reached; second, the *trans-cis* system has to be sufficiently thermally and photo-chemically stable to make possible the establishment of true photo-stationary states. It is also necessary to make the assumption that the ratio between the quantum yields for the *trans-cis* and *cis-trans* isomerization are constant, independently on the irradiation wavelength. In the case of ThiO-TEMPO the first two requirements are fulfilled, whereas for the last assumption there is not possibility to evaluate the quantum yield at different wavelengths and it was assumed that this hypothesis is also valid.

Application of the Fischer method to the two PSSs, obtained upon irradiation of ThiO-TEMPO solution with 254 nm and 366 nm lamps, allowed to extrapolate the spectrum of the *cis* isomer (Figure 2.2.3) and to esteem the composition of the mixture at PSSs (Table 2.2.2). To account for the different compositions at PSSs, it is necessary to consider that the *trans-cis* isomerization is both a photo-chemically and thermally reversible process. Both processes are interconnected and depend on the nature of azobenzene derivatives. Particularly, the rate of the photochemical process depends on the quantum yield of the *cis-trans* isomerization and on the extinction coefficients of each isomer at the irradiation wavelength; whereas, the thermal reversibility is mainly related to the nature of substituent on the azobenzene and to the isomerization medium. In the case of ThiO-TEMPO, irradiation at 254 nm gives a mixture of the two isomers because this wavelength is quite near to one isosbestic point of this molecule (Figure 2.2.3). At this wavelength the extinction coefficient of the *cis* and *trans* isomer is similar, therefore both the isomers are absorbing during irradiation and an equilibrium composition is obtained. A rough evaluation of the quantum yield for the *trans-cis* isomerization of AzO-TEMPO and ThiO-TEMPO upon irradiation at 366 nm was carried out by considering the equation and the method reported in literature by Gauglitz⁵⁷ and Rau⁵⁸. To evaluate the incident irradiation intensity, the photo-isomerization of azobenzene was used as actinometer⁵⁹. Quantum yields obtained by this method for both AzO-TEMPO and ThiO-TEMPO were quite low being about 0.05, but they are in agreement with the value reported in the literature for AzO-TEMPO⁴⁷.

Thermal back-isomerization from *cis* to *trans* isomer was observed for both X-TEMPO derivatives, but the process is quite slow especially in the case of AzO-TEMPO that regained only about 35% of *trans* form in 24 hs. Faster back isomerization is observed in the case of *cis* ThiO-TEMPO that needs about 6 hs to recover 90% of *trans* isomer. The rate of the back thermal isomerization depends on the mechanism of the process. It can occur either by inversion of a nitrogen center or via rotation where the latter seems to be favored for derivatives with strong dipole moment⁵⁰, even if a combination of the two mechanisms cannot be excluded. The presence of a polar substituent on the phenyl ring, generally, accelerates the isomerization rate by increasing the dipole moment of the molecule and by lowering the activation barrier of the thermal relaxation. This effect can be responsible for the faster thermal isomerization detected in the case of ThiO-TEMPO

that has the thiophene ring, an electron donor group, substituted to N=N bond⁵⁰. Exposition of *cis* isomers of both TEMPO derivatives to natural light (laboratory light) gives two new PSSs containing about 92% *trans* isomer in the case of AzO-TEMPO and 40% of *trans* isomer in the case of ThiO-TEMPO.

Finally, more irradiation cycles were repeated both in the case of AzO-TEMPO and ThiO-TEMPO giving in all cases the same composition and the same conversion as a demonstration of the fact that *trans-cis-trans* isomerization is completely reversible and the process is repeatable.

In the underlying table all the spectral parameters are reported.

Table 2.2.2: UV-Vis absorption and photo-physical properties of *trans* azobenzene, AzO-TEMPO and ThiO-TEMPO in solution (CH₃CN)

Sample	λ_{\max} (nm)	ϵ_{\max} (M ⁻¹ cm ⁻¹)	PSS ₃₆₆ ¹ (min)	Composition at PSS ₃₆₆	Dark cis-trans ² h (% trans)	PSS ₂₅₄ ³ (min)	Composition at PSS ₂₅₄
	226	14500					
Azobenzene	316	23000	35	100% Cis	16 h (8.5%) ⁴	35	n.d.
	446	550					
	228	14100					
AzO-TEMPO	323	25500	35	100% Cis	24h (10%)	35	0% Cis
	446	266					
	237	11260					
ThiO-TEMPO	369	23200	6	91% Cis	6h (80%)	20	38% Cis

¹Irradiation time necessary to reach the Photo Stationary State under 366 nm emitting lamp(PSS₃₆₆).²Time after which the tabulated composition is regained during thermal cis-trans back-isomerization.³Irradiation time necessary to reach the Photo Stationary State under 254 nm emitting lamp(PSS₂₅₄). All samples were irradiated from the cis rich form.⁴5x10⁻⁵M in THF⁵⁰

2.3: Photo-physical properties of HDPE-g-(X-TEMPO) and (EOC)-g-(AzO-TEMPO)

The photo-physical properties of X-TEMPO functionalized polyolefins were evaluated by recording UV spectra of polymer films before and after irradiation with an opportune wavelength lamp. The absorption spectra of the X-TEMPO grafted to the polyolefins are quite similar to the spectra recorded for the free chromophores in solution, suggesting that they are molecularly dispersed in the matrices (Figure 2.3.1).

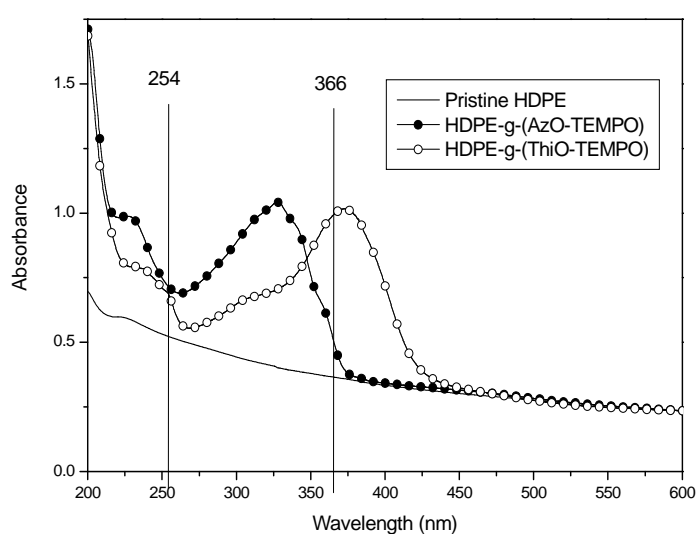


Figure 2.3.1: Superimposition of UV-Vis absorption spectra of pristine HDPE, HDPE-g-(AzO-TEMPO) and HDPE-g-(ThiO-TEMPO).

The UV spectrum of AzO-TEMPO grafted to HDPE or to EOC highlights a partially resolved vibrational structure of the main absorption band that is more evident in the spectra of functional polyolefins than in the spectrum of AzO-TEMPO recorded in solution (Figure 2.2.4). The presence of a low resolved vibrational structure is described in the literature also for azobenzene solutions⁵¹. Interestingly, a higher vibrational resolution was observed in the UV spectrum of azobenzene embedded in polyethylene films or in solution cooled to 77 K⁶⁰. Therefore, the fact that in the spectra of AzO-TEMPO recorded in solution, the vibrational structure is less evident than in the spectra recorded from polymers, may reveal that AzO-TEMPO grafted to the polymer matrices is organized in a rigid environment. The comparison between the free and grafted TEMPO derivatives

evidenced also that the grafted chromophores exhibited the *trans-cis-trans* isomerization processes already observed for the free TEMPO derivatives, suggesting that the photo- and thermal-isomerization in the polymer matrix proceeded without side reactions (Figures 2.2.4; 2.3.2 and 2.3.3).

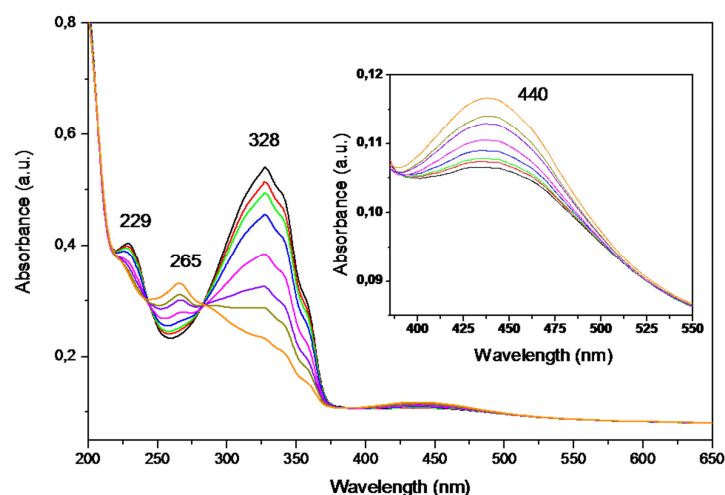


Figure 2.3.2: Absorption spectra of (EOC)-g-(AzO-TEMPO) collected after different irradiation times during irradiation at 366 nm

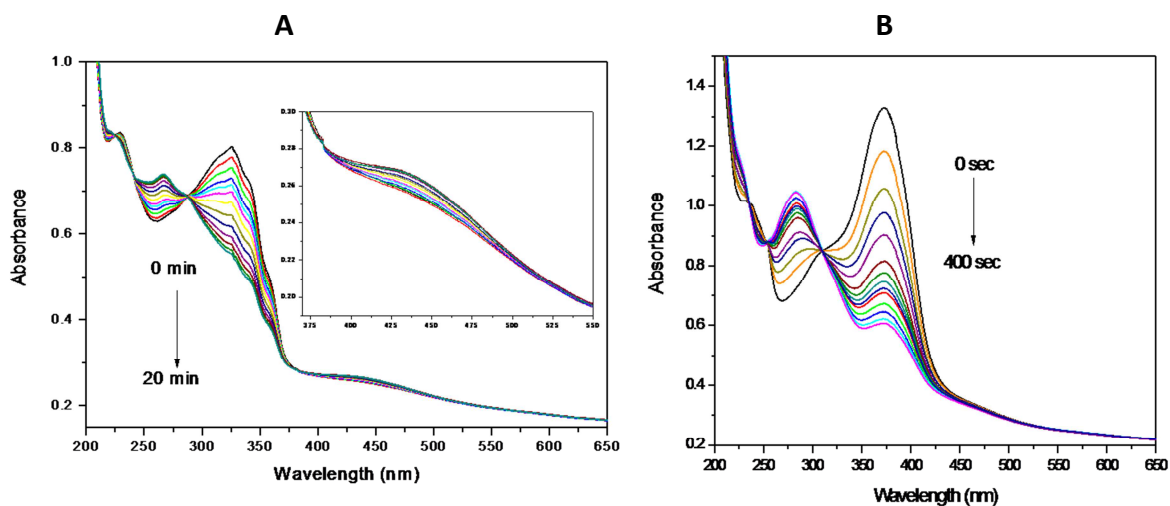


Figure 2.3.3: Absorption spectra of **A:** (HDPE)-g-(AzO-TEMPO) and **B:** (HDPE)-g-(ThiO-TEMPO) collected after different irradiation times during irradiation at 366 nm

Anyway, some differences, especially in terms of isomerization efficiency and isomerization kinetics, between chromophores free in solution or embedded, after grafting, in the polymer matrix were detected. In particular, the degree of photoisomerization (R) at PSS₃₆₆ or at PSS₂₅₄ (Table 2.3.1), evaluated from the relation:

$$R = [(A_0 - A_\infty)/A_0] * 100$$

where:

- A_0 is the absorbance before the irradiation,
- A_∞ is the absorbance at PSS at the same wavelength⁶¹,

revealed that the process is less effective when the TEMPO derivatives are grafted to the polymer than when they are free in solution.

Table 2.3.1: Degree of photo-isomerization $R = [(A_0 - A_\infty)/A_0] \times 100$ at PSS reached upon irradiation at 366 nm (PSS₃₆₆) at 254 nm (PSS₂₅₄)

Sample	R at PSS ₃₆₆	R at PSS ₂₅₄ *
AzO-TEMPO (CH ₃ CN solution)	82	-
ThiO-TEMPO (CH ₃ CN solution)	83	34
(EOC)-g-(AzO-TEMPO)	57	-
HDPE-g-(AzO-TEMPO)	60	-
HDPE-g-(ThiO-TEMPO)	64	20

* The PSS was reached upon irradiation of the film having the absorption spectrum typical of the *trans* isomer of grafted ThiO-TEMPO

For example R is about 60% for X-TEMPO grafted to polymer chains, and analyzed as polymer films, whereas it is about 80% when the molecules are irradiated in solution. Evidently, the presence of the polymer network affects the isomerization of the azo-moiety and only a fraction of the grafted molecules can effectively be isomerized. These deviations of the final conversions from that obtained in solution could be due to the restriction of the mobility of chromophores in polymer solids and to the heterogeneous distribution of local free-volume at the isomerization sites.

The time necessary to reach the PSSs under irradiation is longer for the TEMPO derivatives grafted to the polymer matrix than for the free chromophores in acetonitrile solution. This effect can be well evidenced by reporting the absorbance variation as a function of the irradiation time (Figures 2.3.4 and 2.3.5).

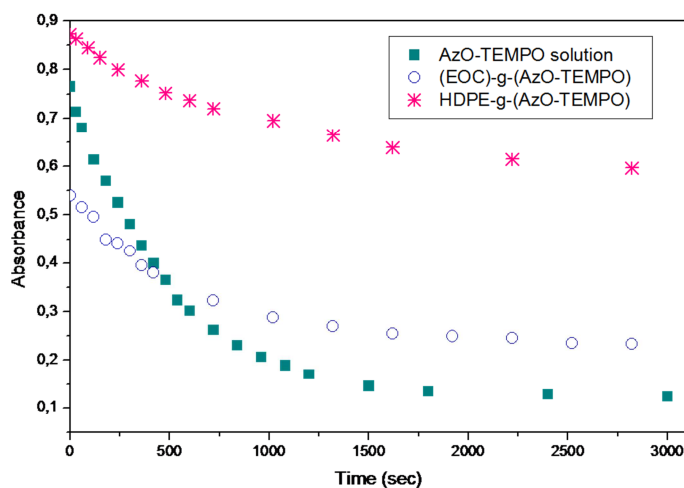


Figure 2.3.4: Absorbance vs. irradiation time at 366 nm for A) AzO-TEMPO in acetonitrile solution, (EOC)-g-(AzO-TEMPO) and HDPE-g-(AzO-TEMPO)

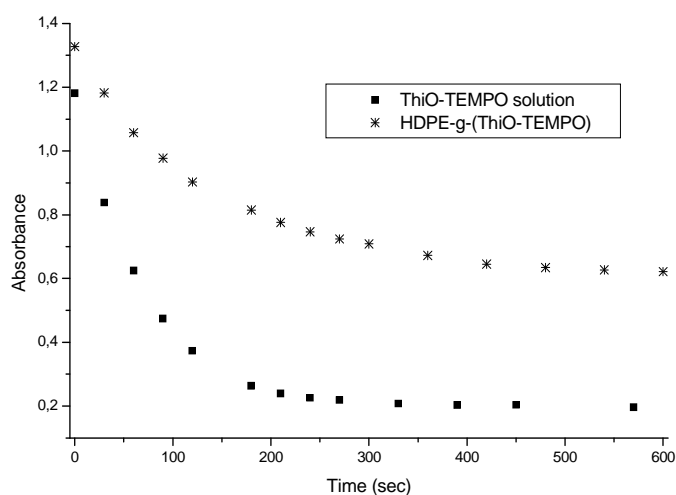


Figure 2.3.5: Absorbance vs. irradiation time at 366 nm for ThiO-TEMPO in acetonitrile solution and HDPE-g-(ThiO-TEMPO)

The comparison of the curves, even considering the different starting absorbance, clearly shows that the isomerization of the free molecules in solution is faster and gives a larger degree of photo-isomerization. The absorbance data collected during the irradiation can be used to evaluate the kinetics of the *trans-cis* photo-isomerization process and, as a first approximation, kinetic data can be fitted by a first order kinetic law (Equation (1)):

$$\ln[(A_0 - A_\infty)/(A_0 - A_t)] = kt \quad (1)$$

where:

- A_0 , A_t and A_∞ are the absorbance values before irradiation, at time t of irradiation and at PSS, respectively,
- $k = I_0(\epsilon_t\phi_{tc} - \epsilon_c\phi_{ct})\ln 10 + k_{ct}$

where:

- I_0 is the incident irradiation intensity,
- ϵ_t and ϵ_c are the molar extinction coefficient of the *trans* and *cis* form at the irradiation wavelength, respectively;
- ϕ_{tc} and ϕ_{ct} are the isomerization quantum yields of the *trans-cis* and *cis-trans* photoisomerization;
- k_{ct} is the rate constant for the thermal *cis-trans* isomerization.

It is necessary to underline that the photoisomerization of an azo-aromatic compound is a very complex process since it involves many different aspects that it is difficult to consider. The process is not only a pure photochemically reversible process, but it involves a thermal conversion that can play a significant role⁶². Equation (1) was used as a tool to easily compare the experimental results reported in Figures 2.3.4 and 2.3.5. By applying Equation (1), higher rate constants were obtained for the *trans-cis* isomerization of both X-TEMPO molecules in solution than for the same chromophores grafted to the polymers (Figure. 2.3.6 and 2.3.7, and Table 2.3.2).

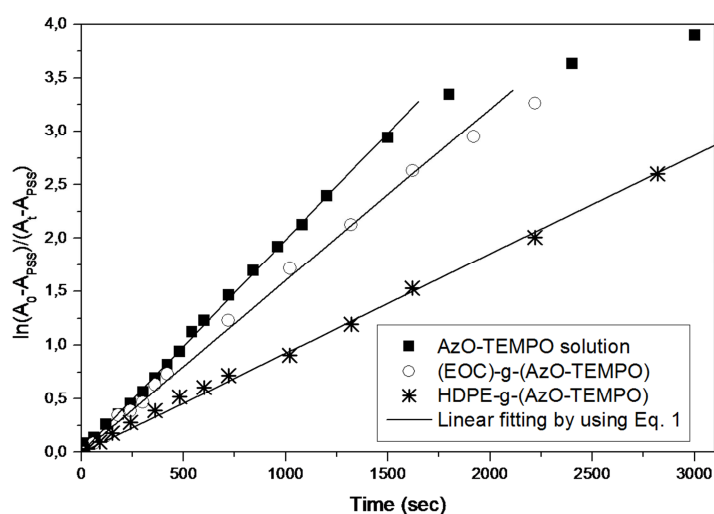


Figure 2.3.6: First order kinetic plots of data for the *trans-cis* isomerization of AzO-TEMPO in acetonitrile solution and grafted to HDPE or EOC

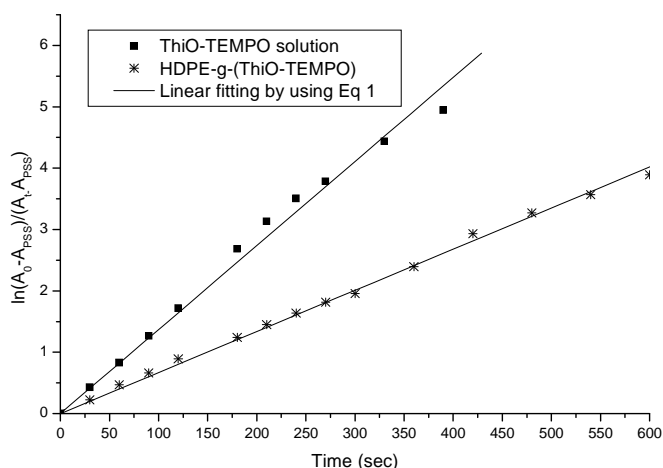


Figure 2.3.7: First order kinetic plots of data for the trans-cis isomerization of ThiO-TEMPO in acetonitrile solution and grafted to HDPE

Table 2.3.2: Kinetic parameters for the trans-cis isomerization of AzO-TEMPO and ThiO-TEMPO in solution or grafted to HDPE or EOC and crystallinity of EOC and HDPE samples.

Sample	k (sec^{-1})	Crystallinity (%) ¹
AzO-TEMPO solution	$2.0 \times 10^{-3} \pm 9 \times 10^{-6}$	-
(EOC)-g-(AzO-TEMPO)	$1.6 \times 10^{-3} \pm 2 \times 10^{-5}$	13.3 ²
HDPE-g-(AzO-TEMPO)	$9.0 \times 10^{-4} \pm 9 \times 10^{-6}$	65.0 ³
ThiO-TEMPO solution	$1.4 \times 10^{-2} \pm 3 \times 10^{-4}$	-
HDPE-g-(ThiO-TEMPO)	$6.7 \times 10^{-3} \pm 5 \times 10^{-5}$	63.2 ³

¹Evaluated by DSC analysis considering that the melting enthalpy of polyethylene 100 % crystalline is 290 J/g, ²Evaluated on the first heating scan⁶³. The crystallinity of pristine EOC was about 15%, ³ Evaluated on the second heating scan. The crystallinity of pristine HDPE was about 70%

Furthermore, from the Figure 2.3.6 is possible to deduce that the photoisomerization of AzO-TEMPO grafted into HDPE is slower respect when it is grafted onto EOC copolymer. To explain this different behavior is necessary to consider that the *trans-cis* isomerization of azo-aromatic derivatives is accompanied by the rearrangement of the hindered

azobenzene moiety. For example, in the case of azobenzene, the distance between the para carbon atoms of the aromatic rings goes from 0.90 nm (*trans*) to 0.55 nm (*cis*)⁶⁴. Keeping in mind these considerations is easy to understand that to allow this physical transformation of the chromophores, a change of the conformation of the polymer chains is necessary to accommodate the *cis* isomer. The polymers that are more flexible are able to adapt more rapidly to the size and shape of the *cis* isomer upon its formation from the *trans* form. If the polymer chain rearrangement occurs on the time scale associated with the photo-isomerization of the chromophores, the process occurs faster. On the contrary, those polymers that are more rigid and have small free volumes, hinder the isomerization and slow down the *trans-cis* isomerization process. The reverse is true for the back thermal isomerization process; indeed, those polymers that are more flexible are also able to adapt more rapidly to the size and shape of the *cis* isomer, as a consequence the thermal back isomerization to the *trans* form is slower because of the greater stabilization of the *cis* isomer. In a rigid media, the polymer chains change their conformation slowly than the isomerization process; as a consequence the *cis* isomer is, for longer time, surrounded by a polymer conformation that resembles the template shape of the *trans* isomer rather than that of the *cis* form. In these conditions, the *cis* isomer quickly re-isomerizes to the *trans* form⁶⁵. On the basis of these considerations, two aspects have to be considered to compare the isomerization rate between different media: first the mobility of the polymer matrix or generally of a solution, and second the free volume distribution. With regard to the isomerization of AzO-TEMPO grafted to EOC or HDPE, the data reported in Table 2.3.2 suggest that the process is faster in EOC than in HDPE. Evidently, the EOC chains can more easily change their conformation with respect to HDPE probably because the EOC chains are more flexible and/or the free volume of HDPE is smaller. Both contributes can be related to the crystallinity of the two matrices; indeed the crystalline phase of a polymer is rigid and also the interfacial region between the amorphous and crystalline phase is considered to be stiffer than the flexible amorphous phase. As a consequence, a polymer that is characterized by a higher crystallinity is also more rigid⁶⁵⁻⁶⁷ or less flexible, than a less crystalline matrix. Therefore, with the aim to relate the isomerization kinetics observed for the functionalized polymers, with the crystallinity of the matrix, all prepared samples were analyzed by DSC (Table 2.3.2, Figures 2.3.8 and 2.3.9).

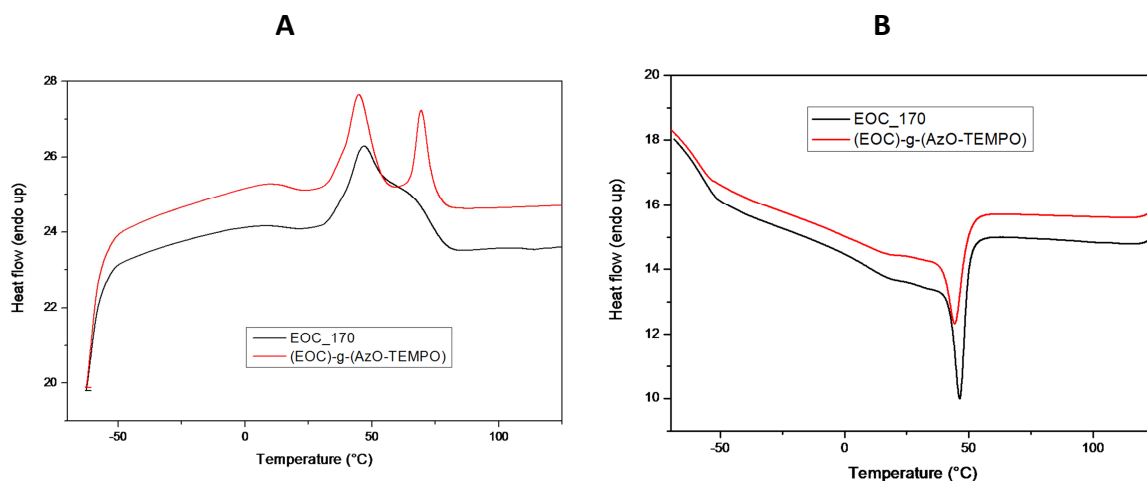


Figure 2.3.8: DSC curves of EOC mixed in brabender at 170°C and of EOC functionalized with AzO-TEMPO (A) first heating scan and (B) cooling (10°C/min) under nitrogen.

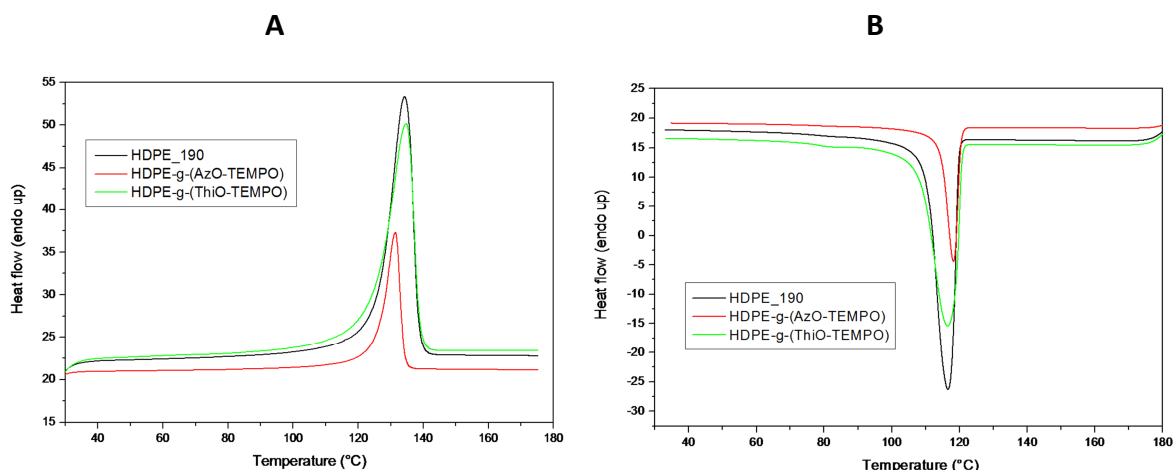


Figure 2.3.9: DSC curves of HDPE mixed in brabender at 190°C and HDPE functionalized with AzO-TEMPO and ThiO-TEMPO, second heating and cooling (10°C/min) under nitrogen.

The analysis evidenced that EOC has a lower crystallinity than HDPE and that after grafting of the TEMPO derivatives, it further decreases⁶⁸. Moreover, both X-TEMPO moieties were expected to be localized in the amorphous region, or at least at the interfacial region between the amorphous and the crystalline fraction of EOC or HDPE because the functional groups are too sterically hindered to enter in the crystalline region of the polymer^{65, 69}. The more rigid and crystalline HDPE environment has the role to disfavor and to slow down the formation of the less kinetically stable and more hindered *cis* isomer, whereas when the chromophores are grafted to the less rigid matrix (EOC) the effect is less evident. On the basis of these considerations, the slower formation of the *cis*

isomer embedded in the more rigid polymer matrix can be attributed to the fact that the molecules experienced a more strained conformation accounting for a general slowing down of the process^{65, 66}. The thermal back-isomerization from *cis* to *trans* isomer was observed for all our samples; in the case of HDPE-g-(ThiO-TEMPO) 5/6 hs are necessary to recover about 80% of the starting absorbance, whereas in the case of HDPE-g-(AzO-TEMPO) the same conversion requires about 30 h. This comparison confirms that, as occurred in solution, ThiO-TEMPO isomerizes quickly than AzO-TEMPO, also when it is grafted and embedded in a polymer matrix. Comparison between the thermal back isomerization of AzO-TEMPO grafted to HDPE or EOC evidenced that the process is slower in EOC (60% of the *trans* form of AzO-TEMPO grafted to EOC is recovered in 30 hs from the *cis* form) confirming that the less rigid matrix allows for the formation, upon irradiation, of a less strained *cis* isomer that slowly rearranges to the more thermodynamically stable *trans* isomer. Finally, the water contact angle on the surface of the pristine polymers and of the functionalized polymer was determined before and after photo-isomerization from the *trans* to the *cis* rich PSS₃₆₆. The aim is to highlight the change of the surface wettability caused by the isomerization of the azo-aromatic group⁷⁰. Results (Table 2.3.3) evidenced that the radical functionalization of the matrix does not change the wettability of the polymer matrix whereas, after isomerization, a small decrease of the contact angle values is observed. This behavior is in agreement with the fact that the *trans* isomer has no dipole moment, whereas the dipole moment of the non planar *cis* isomer is $3D$ ⁶⁴. The differences between the values reported in the Table 2.3.3 are small, but significant if related to the functionalization degree. Finally, the more polar ThiO-TEMPO seems to cause a larger effect than AzO-TEMPO confirming the potential usefulness of this group and of the NRC reaction for the preparation of smart polyolefins.

Table 2.3.3: Water contact angle of pristine polymers and functionalized polymers recorded before and after irradiation at 366 nm.

Sample	Contact angle (°)	Contact angle (°)after irradiation at 366 nm
HDPE	99.1±2.2	-
EOC	98.2±2.1	-
HDPE-g-(AzO-TEMPO)	96.7±1.1	93.3±1.5
HDPE-g-(ThiO-TEMPO)	98.3±2.6	94.8±2.1
(EOC)-g-(AzO-TEMPO)	97.8±0.8	95.1±1.7

2.4: Conclusions

TEMPO derivatives bearing covalently linked azo-type chromophores or a fluorocarbon chain were prepared and successfully grafted to HDPE or EOC, by free radical post reactor modification initiated by peroxide. The grafting occurrence was definitely demonstrated by TGA and FTIR spectroscopy, in particular the latter allowed the evaluation of the FD by means of appropriate calibration curves. Furthermore results reported here evidenced that UV-Vis absorption spectra, recorded from film of functionalized materials with azo-type chromophores, show the same trend of the spectra of the two functionalizing agents in solution, confirming that the photo-physical properties of the chromophores are preserved when they are grafted to the polymer. At the same time the presence of fluorine in the sample grafted with TEMPO bearing fluorocarbon chain was undoubtedly evidenced by FTIR measurements.

In particular the photophysical properties of the two azo-aromatic derivatives, both as a free radical and grafted moieties, were deeply investigated. They showed different extinction molar coefficient, even after grafting, most probably associable to the nature of the aromatic ring substituted to the N=N double bond. The quantum yields obtained for both AzO-TEMPO and ThiO-TEMPO were quite low being about 0.05, however they are in agreement with the value reported in the literature.

In terms of isomerization kinetics and isomerization efficiency some differences between the free and grafted chromophores were observed, attributable to the matrix effect and particularly to the polymer crystallinity. Polymers having higher crystallinity are more rigid and enable with more difficult a rearrangement of the azo-aromatic moiety although the functional groups were likely localized in the amorphous region, or at least at the interfacial region between amorphous and crystalline phase. The isomerization of the azo-aromatic moiety is strongly dependent on the conformational mobility of the chromophore and of the polymer chains, therefore the process can be hindered by a less flexible matrix as occurred in the case of HDPE. Interestingly, the surface of the functionalized polymers showed a change in the wettability properties after isomerization of the chromophores thus highlighting the dipole moment appearance passing from the planar *trans* isomer to the not planar *cis* isomer.

CHAPTER 3

SYNTHESIS OF FUNCTIONALIZED POLYESTERS BY NITROXIDE

COUPLING REACTION IN THE MELT

3.1: Preparation and characterization of BzO-TEMPO and NfO-TEMPO functionalized polyesters

The NRC feasibility was further tested by applying the TEMPO derivatives grafting process to polyester-based materials like poly(butylene succinate) (PBS) and poly(lactic acid) (PLA). These biodegradable aliphatic polyesters are becoming increasingly important given that they have thermoplastic processability and thermo-mechanical properties¹⁰. However, their versatility and successful use as commodity plastics is limited, as is the exploitation in biomedical, electronic and optical sectors. The lack of reactive functionalities limits the use of biodegradable aliphatic polyesters in a series of demanding applications, where the precise control and placement of functionality is critical. Modification by radical grafting is an interesting and more convenient post-polymerization modification strategy for preparing side-chain functionalized polyesters, following a well-known approach used for preparing functionalized polyolefins^{7, 27, 71}. In the case of biodegradable aliphatic polyesters, the peroxide modification, the radical grafting of maleic anhydride (MAH), and the preparation and use of polyester-graft-MAH were reported⁷²⁻⁷⁴. The reactivity of polyesters versus peroxide radicals was exploited in order to increase the polymer melt viscosity by branching and/or crosslinking⁷⁵⁻⁷⁸. Highly branched PLA and PBS were obtained by treating the molten polymers in an extruder or batch mixer with peroxides via a coupling reaction between macroradicals. The radical grafting of MAH on PBS, PLA, and copolyesters was also investigated. Carlson et al and Mani et al⁷⁹⁻⁸¹ firstly reported the preparation of MAH functionalized biodegradable polyesters by reactive extrusion and their use as interfacial adhesion promoters in blends and composites. This reaction was further investigated by modulating the MAH/peroxide

ratio⁸². The grafting yield increased if the amount of peroxide was increased, but with a decrease in the extent of polymer crosslinking. In addition, Signori et al.⁸³ proposed the functionalization of PBSA with MAH in combination with cinnamate-like coagents to increase the grafting yield, following a method previously described for polyolefins^{36, 71, 84}. One of the main drawbacks of this approach is the difficulty in pinpointing the covalent grafting of MAH moieties both qualitatively and quantitatively. Indeed, infrared spectroscopy, which is generally used to show stretching vibrations associated with the functional groups, is not very suitable in this case because of the overlap between the C=O stretching signal of the covalent grafted moieties with the C=O stretching signal of the polyester chains. The functionalization degree is generally calculated by laborious acid-base titrations, and the low quantity of grafted groups that is generally achieved and the possible degradation of polymer chains by hydrolysis do not make this approach very reliable. Moreover, the radical functionalization method is affected by poor control and lack of selectivity. Consequently, a procedure providing excellent control of macroradical formation versus grafting of functional molecules, together with sensitive analytical techniques, is highly desirable. In this context the radical functionalization of MAH in the presence of suitable co-agent able to control side reactions can be approached⁸⁵, but the radical coupling reaction between a macroradical formed on the polymer backbone by H-abstraction and a functional nitroxide can be considered a very interesting tool to graft specific functionalities onto polymer chains.

With this aim 4-benzoyloxy-2,2,6,6-tetramethylpiperidine-1-oxyl (BzO-TEMPO), and 4-(1-naphthoate)-2,2,6,6-tetramethylpiperidine-1-oxyl (NfO-TEMPO) (Figure 3.1.1) were used.

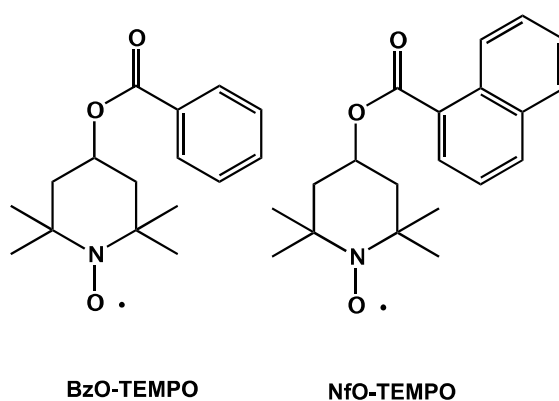


Figure 3.1.1: Structure of 4-benzoyloxy-2,2,6,6-tetramethylpiperidine-1-oxyl (BzO-TEMPO) and 4-(1-naphthoate)-2,2,6,6-tetramethylpiperidine-1-oxyl (NfO-TEMPO).

Both nitroxides were already used in grafting polyolefins with good results in terms of grafting yield and macromolecular weight control^{8,9}. In particular (NfO-TEMPO) is a pro-fluorescent nitroxide whose fluorescence is restored after formation of alkoxyamine (and thus after the grafting) providing a really performing tool in assessing the NRC reaction.

PBS and PLA were grafted in the melt in an internal batch mixer (BrabenderPlastograph OHG47055), by using respectively benzoyl peroxide (BPO) and di(tert-butylperoxyisopropyl)benzene (mixture of isomers) (DTBPIB) chosen on the basis of the polymers processing temperature (120°C in case of PBS and 180°C in case of PLA) and different amounts of nitroxide as reported in the Table 3.1.1. The collected samples were characterized in terms of molecular weight evolution (by SEC measurements) while the FD was determined by UV spectroscopy by getting ready calibration curves using PBS/BzO-TEMPO and PBS/NfO-TEMPO CHCl₃ solutions at known compositions (Figures 3.1.2 and 3.1.3). Further confirmations about the grafting levels were obtained by NMR spectroscopy

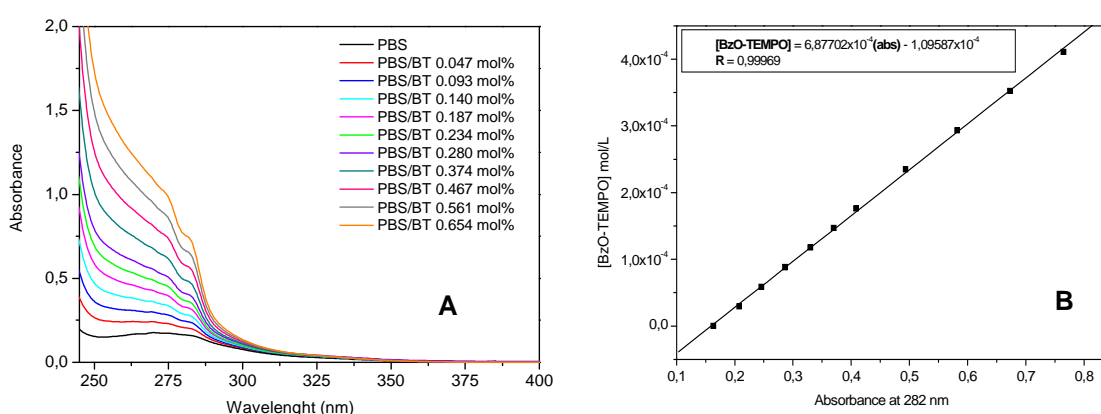


Figure 3.1.2: A UV-Vis spectra of PBS/BzO-TEMPO calibration solutions and B UV-Vis calibration curve at 282 nm

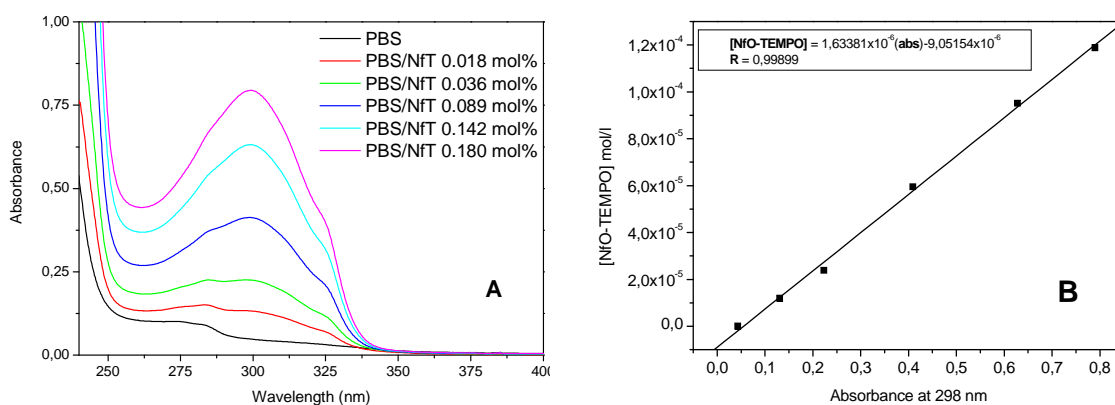


Figure 3.1.3: **A** UV-Vis spectra of PBS/NfO-TEMPO calibration solutions and **B** UV-Vis calibration curve at 298 nm

Table 3.1.1: PBS and PLA radical functionalization: feed composition, molecular weight, functionalization degree.

Sample name	Feed composition		Functionalization degree ^a		Molecular weight and distribution		
	Peroxide (mol%)	f-TEMPO ^b (mol%)	FD _{UVc} (mol%)	FD _{NMRd} (mol%)	M _n (D)	M _w (D)	M _w /M _n
PBS ^e	-	-	-	-	17700	42180	2.38
PBS-120	-	-	-	-	16900	42700	2.53
PBS-BPO-120	1	-	-	-	n.d. ^f	n.d. ^f	n.d. ^f
PBS-BT1-BPO-120	1	0.5	0.15	n.d.	15630	35100	2.24
PBS-BT2-BPO-120	1	1	0.24	0.24	15060	34410	2.28
PBS-NfT1-BPO-120	1	0.5	0.26	n.d.	15130	33860	2.24
PBS-NfT2-BPO-120	1	1	0.30	0.29	16980	39910	2.35
PLA	-	-	-	-	111460	199340	1.79
PLA-180	-	-	-	-	108750	184730	1.70
PLA-DTBPIB-180	0.5	-	-	-	n.d. ^f	n.d. ^f	n.d. ^f
PLA-NfT2-DTBPIB-180	0.5	1	0.04	0.04	69290	168070	2.43
PLA-BT-DTBPIB-180	0.125	1.5	0.025	n.d.	97000	159000	1.6

^aThe functionalization degree represents the moles of the grafted functional groups per 100 moles of monomeric units.

^bf-TEMPO: functional TEMPO derivative. ^cDetermined by the UV-Vis calibration curve. ^dDetermined by ¹H-NMR analysis.

^ePBS pristine polymer extracted with boiling MeOH for 15 hrs. ^fNot determined because the sample is partially insoluble in CHCl₃

Initially PBS was treated at 120°C without adding any reagents (PBS-120, blank sample) and then its reactivity versus BPO radicals was investigated by treating the molten

polymer with 1 mol% of BPO (PBS-BPO-120) (Figure 3.1.4). This amount of peroxide is enough to induce a concentration of macroradicals that promotes the formation of 60-80% gel content.

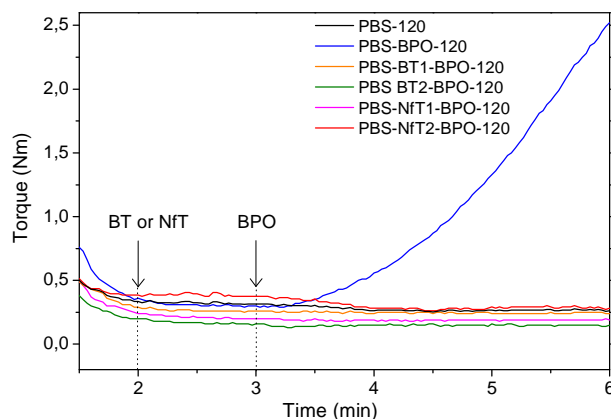


Figure 3.1.4: Torque curves of PBS-120, PBS-BPO-120, PBS-g-(BzO-TEMPO), and PBS-g-(NfO-TEMPO) samples.

After the peroxide was added, an immediate increase in the torque was observed, which indicates an increase in the melt viscosity during the run. This effect is due to the coupling reaction between PBS macroradicals, which are formed by hydrogen abstraction from polymer chains. Indeed, PBS-BPO-120 is only partially soluble in CHCl_3 , thus confirming that branching/crosslinking occurred during the treatment of PBS with the peroxide. Nonetheless, this undesired reaction needs to be controlled during the modification in order to obtain a functionalized material in which the initial structure of the polymer is preserved. Two different concentrations of both functional nitroxides were chosen: 1 mol%, corresponding to the maximum number of peroxide radicals that can be produced during the run (considering that each run was carried out for a time corresponding to the half-life time of the peroxide); 0.5 mol%, that is half of the peroxide concentration. The latter corresponds to the concentration of primary radicals considering that generally only 50% of primary radicals are active in the H-abstraction, the rest being lost by β -scission reaction. While the PBS reaction with BPO demonstrated an appreciable increase in the torque, no increase in the torque was observed for the four-functionalization runs. Importantly, this effect is consistent with a suppression of the coupling reaction between PBS macroradicals, as previously observed during the functionalization of polyolefins⁸.

⁹(see Chapter2). The SEC analysis of the purified samples (completely soluble in CHCl_3) indicated a slight decrease in both M_n and M_w if compared with PBS-120 and pristine PBS, probably due to some limited degradation (Table 3.1.1). However, in the case of PBS-NfT2-BPO-120, prepared using the highest amount of NfO-TEMPO, the molecular weight values were very close to those of PBS-120.

Proof of the PBS functionalization was obtained by UV-Vis analysis of purified samples (residues to methanol extraction, to avoid non reacting functionalizing agents and byproducts). Besides confirming the successful functionalization, UV-Vis spectroscopy led to the quantitative determination of the moles of the grafted functionalities. The characteristic absorptions of BzO-TEMPO centered at 275 and 282 nm (enlargement in Figure 3.1.5) and due to the π - π^* transition of the aromatic ring were observed in the spectra of the functionalized samples (Figure3.1.5.a). Similarly, in the case of PBS-g-(NfO-TEMPO) samples, the UV-Vis spectra (Figure 3.1.5.b) showed an absorption band centered at 298 nm, which is characteristic of the π - π^* transition of the aromatic moiety of NfO-TEMPO (enlargement in Figure3.1.5b)⁸.

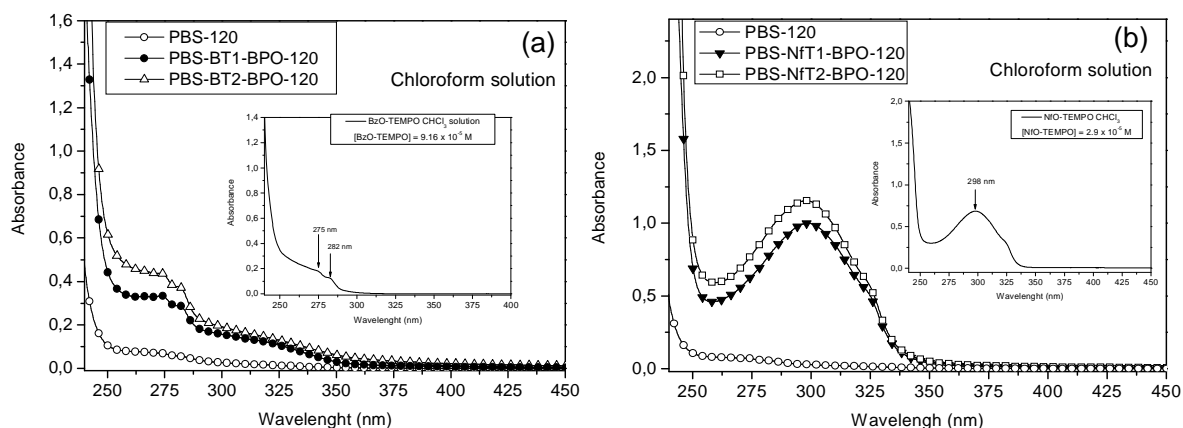


Figure 3.1.5: UV-Vis absorption spectra of PBS-g-(BzO-TEMPO) (a) and PBS-g-(NfO-TEMPO) samples (b). The insets show the spectra of BzO-TEMPO and NfO-TEMPO.

The functional grafted groups were evaluated by determining the functionalization degree (FD= moles of grafted functional groups per 100 moles of monomeric units) using two calibration curves based on standard solutions at known concentrations of PBS and BzO-TEMPO or NfO-TEMPO (Figure 3.1.2 e 3.1.3). The resulting linear correlations were used to quantify the chromophore concentration in the functionalized PBS samples from

solutions of a known polymer concentration (assuming similar extinction coefficients of grafted and free chromophores), and the FD was determined accordingly (Table 3.1.1). Although rather low, the FDs are of the same order of magnitude as the values reported in the literature with regard to the functionalization of polyesters with MAH and peroxide, which range between 0.4 and 1.5 wt%^{73, 82, 86}. Indeed, the highest FD obtained with NfO-TEMPO corresponds to 0.6 wt%, but the amount of functionalizing agent used is notably lower (i.e. 0.8-1.9 wt% NfO-TEMPO versus 3-8 wt% MAH) and the conversion ranges between 33-50% rather than 15-30% for MAH grafting. This suggests an enhanced yield for the nitroxide radical coupling functionalization methodology. In addition, in the case of PBS the moles of grafted moieties per 100 moles of monomeric units are comparable to those obtained with polyethylene using the same functionalization method^{8, 9}. Although a direct comparison is not fully appropriate because the reaction temperature and the peroxide adopted were different, in the case of PBS the amount of nitroxide used to obtain the functionalization by controlling the final molecular weight of the polymer was three times lower than that used with polyethylene. This may be due to a better control of macroradical side reactions in polyesters compared to polyolefins, which suggests that the nitroxide radical coupling reaction is a well-performing functionalization method for this kind of polymer too.

The FD of the two PBS-g-(BzO-TEMPO) samples increased with the BzO-TEMPO concentration keeping the peroxide moles constant. In contrast, in the PBS-g-(NfO-TEMPO) samples, the FD values were similar (around 0.3 mol%) irrespectively of the NfO-TEMPO concentration in the feed. The data seem to indicate that the NfO-TEMPO is more likely than BzO-TEMPO to graft to PBS: FD values were higher, and for the highest FD, the molecular weight of the polymer was closer to the pure PBS. This different behavior may be due to a different reactivity of the functional TEMPO molecules, depending mainly on their solubility/dispersibility in the molten polymer.

To corroborate the outcomes of the UV-Vis procedure, the FD values of PBS-BT2-BPO-120 and PBS-NfT2-BPO-120 were determined by ¹H-NMR spectroscopy (Table 3.1.1). In order to get a complete attribution of polymer signals, the ¹H-NMR spectrum of the purified PBS-120 sample was acquired first. The signals observed in this spectrum are in agreement with the previously reported analysis of Bionolle 1001⁸⁷ (Figure 3.1.6). Besides the typical PBS signals, the spectra of the functionalized samples (Figures 3.1.6b and

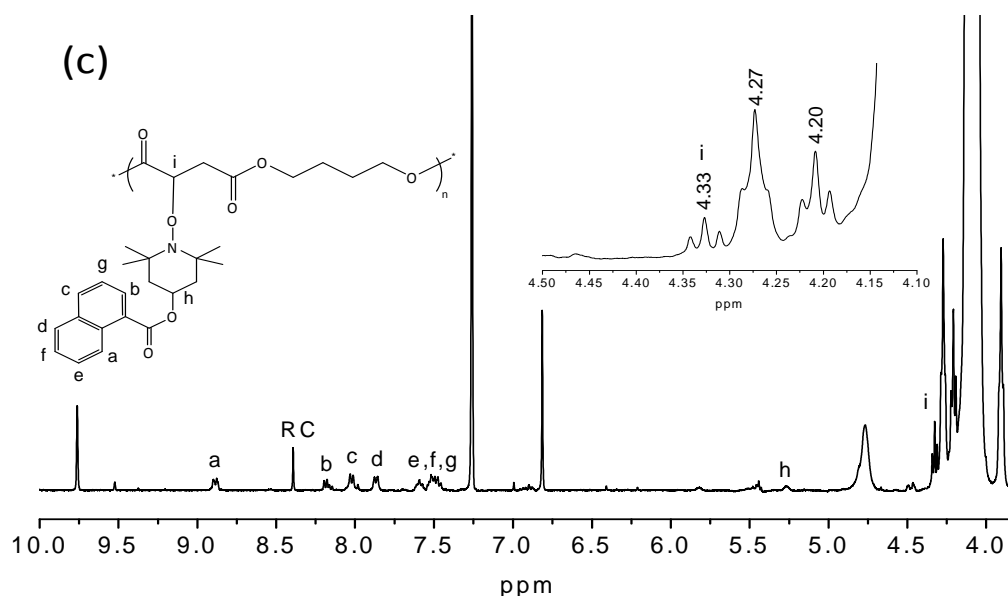


Figure 3.1.6: ^1H -NMR spectra of PBS-120 (a), PBS-BT2-BPO-120 (b), and PBS-NfT2-BPO-120 (c)

The ^1H -NMR spectrum of PBS-BT2-BPO-120 shows three signals (Ha, Hb, Hc) in the 7-8 ppm range due to the aromatic protons (see molecule structure in Figure 3.1.6b for attributions). For the quantitative determination of the grafted groups, a known amount of a reference compound (1,4-dinitrobenzene, RC) was dissolved in a deuterated chloroform solution of the functionalized polymer at a known concentration^{8, 9}. A comparison between the area of the peak of the RC protons at 8.39 ppm with those of the aromatic protons of the grafted BzO-TEMPO unit enabled the FD_{NMR} to be evaluated (Table 3.1.1). Similarly, in the case of PBS-NfT2-BPO, the ^1H -NMR spectrum (Figure 3.1.5c) showed five multiplet signals (Ha-Hg) in the 8.9-7.4 ppm range, which are all due to protons of the naphthalene ring. Note that the FD values collected by UV calibration and NMR determination (Table 3.1.1) are in a very good agreement, thus underlining that the UV-Vis methodology, through the use of appropriate calibration curves, can be successfully used to quantitatively evaluate the FD of PBS samples functionalized with BzO-TEMPO and NfO-TEMPO. We attributed the signal at 9.76 ppm in the spectra of the functionalized samples to the formation of aldehyde groups⁸⁷ probably deriving from a partial thermo-oxidative degradation of the polymer which occurs during the functionalization process.

Interestingly, by comparing the spectrum of PBS-120 (Figure 3.1.6a) and the spectra of functionalized samples (Figures 3.1.6b and 6c), a triplet at about 4.3 ppm emerges in the

spectra of functionalized samples. On the basis of the chemical shift and multiplicity, this signal can be attributed to a methine proton in the alpha position compared to the carbonyl group of the succinic acid unit of PBS substituted by the functional TEMPO moiety (Hi, Figures 3.1.6b and 3.1.6c). The presence of this signal supports the mechanism of grafting previously reported, which proposes the insertion of the functional moieties onto the dicarboxylic acid units of the polyester^{73, 86}.

In order to provide direct evidence of the grafting site, an EPR study was carried out on a functionalized PBS sample to tentatively intercept the EPR signals of PBS macroradicals formed by the homolytic cleavage of the -C-ON< bond induced by the temperature increase. Purified PBS-BT2-BPO-120 was heated in the EPR cavity and spectra were registered at different temperatures. At the beginning of the experiment (at 40°C), the spectrum exhibited a weak asymmetric three-line signal due to free BzO-TEMPO entrapped in the rigid polymer phase, whose presence is due to the equilibrium between grafted and ungrafted species⁸. By gradually increasing the temperature, the nitroxide signal became similar to the signal of a nitroxide radical that is free to rotate (Figure 3.1.7), the integrated area at 100°C corresponding to a 3.67×10^{15} spin. A further increase in the temperature up to 155°C produced an increase in the EPR signal due to the TEMPO radicals, thus suggesting that the homolytic cleavage of the nitroxide-PBS bond had occurred. The integrated area of this signal after 5 minutes at this temperature corresponds to a 1.28×10^{16} spin, which is about 10% of the FD of this sample.

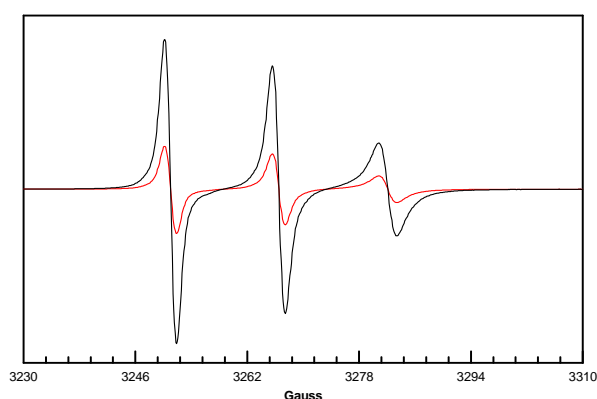


Figure 3.1.7: EPR spectrum of PBS-BT2-BPO-120 registered at 373K (red line) and at 428K after 5 min at this temperature (black line).

Interestingly, in addition to the main three-line signal due to the nitroxide radical, with a nitrogen isotropic hyperfine splitting constant (A_N) of 15.3 G and a carbon (^{13}C isotope) isotropic hyperfine splitting constant (A_C) of 6.8 G, the EPR spectrum collected at 155°C also revealed a very weak signal (labeled as “b” in Figure 3.1.8) with a proton splitting constant of 21 G.

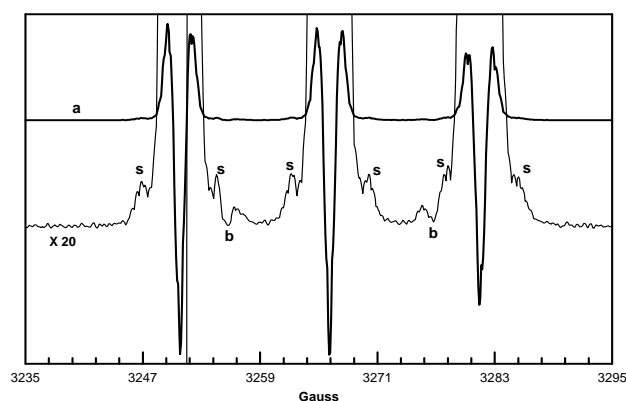


Figure 3.1.8: EPR spectrum (second derivative) of PBS-BT2-BPO-120 registered at 155°C “a” is the signal of detached BzO-TEMPO radicals; “s” signals are due to ^{13}C satellites, $g_{\text{iso}} = 2.00472$; “b” is the signal of PBS macroradicals formed by detachment at high temperature of the grafted f-TEMPO, $g_{\text{iso}} = 2.00492$.

This signal, which is partially covered by the strong nitroxide signal, indicates the formation of a carbon-centered radical coupled with one alpha proton, which can be attributed to the PBS macroradical likely generated by the detachment of the nitroxide. The intensity of this signal could be very low because of the very high reactivity of carbon-centered radicals, which at high temperatures can give rise to recombination reactions even with the free nitroxide.

The PLA functionalization was tested using BzO-TEMPO and NfO-TEMPO as a functional molecules, in order to easily prove the grafting thanks to the UV-Vis or to the emission from the functionalized product. The peroxide addition again caused a marked increase in the torque values (Figure 3.1.9) plus the formation of a CHCl_3 insoluble material due to coupling reactions between PLA macroradicals, as reported in the literature⁷⁹.

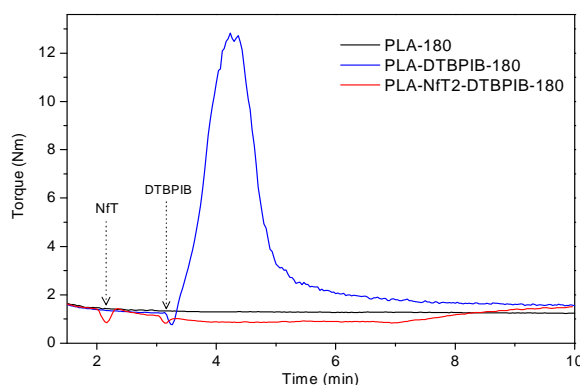


Figure 3.1.9: Torque curves of PLA-180, PLA-DTBPIP-180, and PLA-NfT2-DTBPIP-180.

The functionalization run PLA-NfT2-DTBPIP-180 did not show the same torque increment, which is probably due to the coupling between PLA macroradicals and NfO-TEMPO giving the desired functionalized product. The same trend was evidenced also in the case of the functionalization run PLA-BT-DTBPIP-180. However, the SEC analysis carried out after purification of the sample showed a partial decrease in both M_n and M_w and an increase in the dispersity (Table 3.1.1). Accordingly, although the coupling reaction between PLA macroradicals was suppressed, a degradation effect was found. Given that coupling is a bimolecular reaction, the macroradicals concentration was probably reduced, thus inhibiting coupling between macroradicals, though some of them were likely involved in degradation probably by a β -scission reaction^{79, 88}. The UV-Vis analysis of the purified PLA-NfT2-DTBPIP-180 sample (Figures 3.1.10) revealed an absorption band centered at 299 nm which confirms the presence of the grafted chromophore (naphtoic group). Analogously, in the case of PLA-g-(BzO-TEMPO) sample (Figure 3.1.11) the UV-Vis spectra showed an absorption band at about 280nm which is typical of the BzO-TEMPO chromophore.

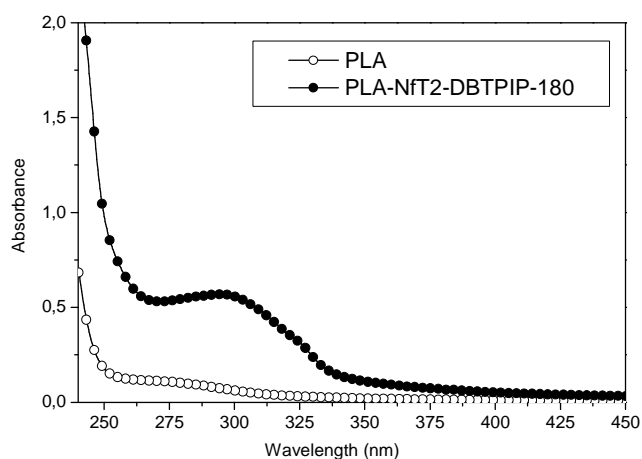


Figure 3.1.10: UV-VIS spectrum of PLA-NfT2-DBTPIP-180 sample

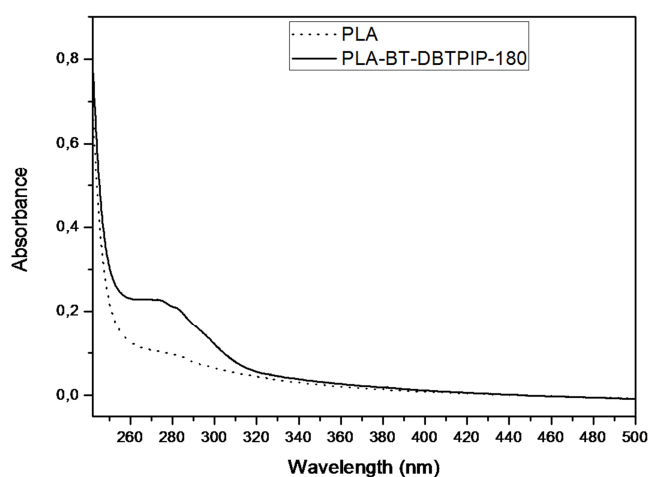


Figure 3.1.11: UV-VIS spectrum of PLA-BT-DBTPIP-180 sample

To roughly estimate the FDs, the absorbance of the bands at 298 nm and at 280 nm were plotted versus the PBS/NfO-TEMPO and the PBS/BzO-TEMPO calibration curves previously reported (Figure 3.1.3). Very low FDs were found, in the case of PLA-g-(NfO-TEMPO) was calculated a FD equal to 0.04 mol%, which was confirmed by $^1\text{H-NMR}$ analysis (Table 3.1.1), whereas in the case of PLA-g-(BzO-TEMPO) the evaluated FD was 0.025 mol%. However it is necessary to consider that in this last case, the used peroxide amount was half of that employed during the functionalization run PLA-NfT2-DBTPIP-180. As reported in the literature, the PLA macroradical is generated by H-abstraction at the

tertiary carbon atom, which is thus likely to be the grafting site of the functional nitroxide^{72, 89, 90}.

3.2: Fluorescent properties of aliphatic polyesters grafted with NfO-TEMPO

In a previous work on polyethylene radical functionalization with NfO-TEMPO⁸, it was shown that the fluorescence emission spectrum of NfO-TEMPO was characterized by a very low emission intensity, whereas in the case of the methoxy-derivative of NfO-TEMPO (which can be considered as a model compound of the grafted TEMPO), the maximum emission position and its intensity was very close to that of 1-naphthoic acid. In agreement with the literature, molecules containing a nitroxide tethered to a fluorophore show dramatically reduced fluorescence due to intramolecular quenching of the fluorophore excited singlet state⁹¹⁻⁹³. In contrast, the free radical trapping of the nitroxide moiety yields a diamagnetic alkoxyamine and restores the emission from the fluorophore. Because of this behavior, if the pro-fluorescent nitroxide is grafted to the backbone of PBS, a fluorescence emission for the functionalized polymer is expected. Fluorescent emission spectra of PBS, PBS-NfT1-BPO and PBS-NfT2-BPO were thus collected from polymer films (Figure 3.2.1). The spectra of the two functionalized samples showed a large emission band centered at 365 nm, as similarly observed for polyethylene-g-(NfO-TEMPO)⁸, thus confirming once again that grafting had been successful. The difference observed in the emission intensity of the samples reflects the FD values of PBS-NfT1-BPO-120 and PBS-NfT2-BPO-120.

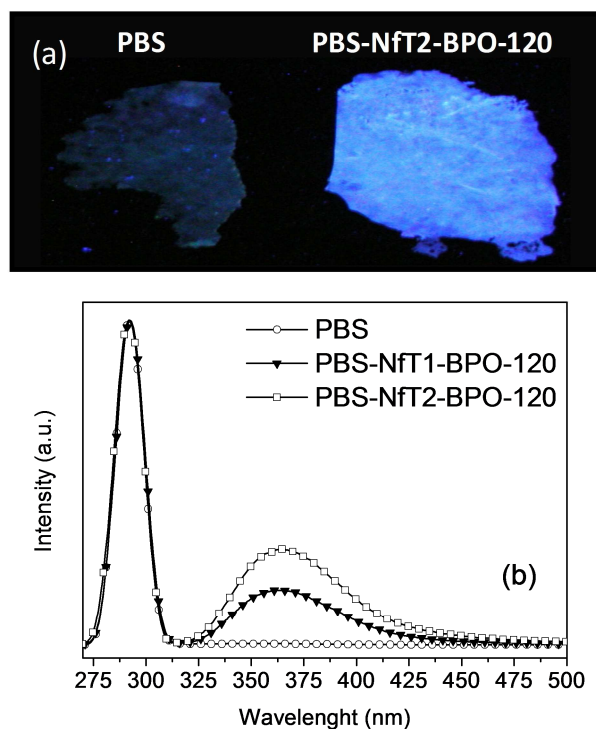


Figure 3.2.1: Digital images of PBS and PBS-Nft2-BPO-120 under excitation with a long-range UV lamp ($\lambda = 254$ nm) (a), and fluorescence emission spectra ($\lambda_{\text{exc}} = 290$ nm) of PBS, PBS-Nft1-BPO-120, and PBS-Nft2-BPO-120 film (b). The spectra are normalized with respect to the scattering intensity.

Similarly to PBS-g-(NfO-TEMPO) samples, a fluorescent PLA sample was obtained, in which the optical properties were transferred from the chromophore to the polymer. The fluorescence emission spectrum of the PLA-Nft2-DTBPIB-180 film (Figure 3.2.2) showed a weak but visible band centered at 360 nm, similar to the one observed in the analogous functionalized PBS samples. The low emission intensity is in agreement with the low FD of this sample.

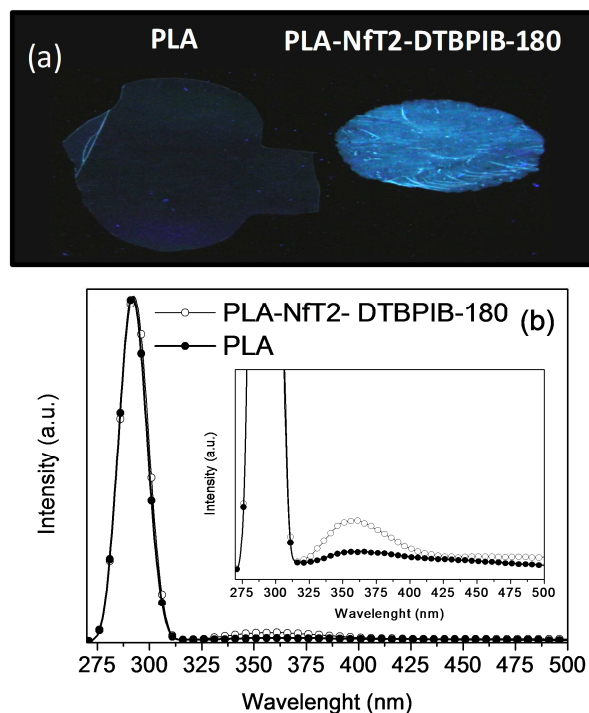


Figure 3.2.2: Digital images of PLA and PLA-Nft2-DTBPIB-180 under excitation with a long-range UV lamp ($\lambda = 254$ nm) (a) and fluorescence emission spectra ($\lambda_{exc} = 290$ nm) of PLA, PLA-Nft2-DTBPIB-180 film (b). The spectra are normalized with respect to the scattering intensity.

This thus demonstrates the possibility to simply transfer the optical properties of the chromophore to the biodegradable polymer using a post-polymerization method. From these results it appears that low functionalization degrees are sufficient to give fluorescence, which is a property not observed in the pure material. This is indeed the main objective of a post-polymerization functionalization reaction: to impart new properties without changing the original characteristics of the polymer.

3.3: Conclusions

The NRC reaction with TEMPO bearing aromatic moieties (BzO- and NfO-TEMPO) was employed to functionalize new polymer substrates differing from polyolefins and belonging to the biopolyesters class, namely PBS and PLA. The grafting was clearly proved by UV-Vis and $^1\text{H-NMR}$ spectroscopy that also allowed the evaluation of the FD, which ranged between 0.15 and 0.30 mol% in agreement with values obtained even by conventional grafting procedures, highlighting the feasibility and versatility of NRC

approach. The SEC data indicated that the grafted polyesters molecular weight is close to that of the pristine polymers, thus suggesting even for such polymer substrate the NRC ability to limit the radical-induced crosslinking/branching.

Additionally, by combining EPR analysis and $^1\text{H-NMR}$ spectroscopy, it was demonstrated that the grafting site of PBS derives from the hydrogen abstraction from one of the two CH_2 groups of the succinic acid unit.

Finally the fluorescence emission spectra of both PBS and PLA samples functionalized with NfO-TEMPO not only provided a clear evidence of the grafting, but also revealed a fully restored fluorophore emission, generating with this method fluorescent polyesters.

The NRC reaction is thus be suitable in providing a convenient and versatile route for introducing different functional groups on biodegradable aliphatic polyesters using a range of functional TEMPO derivatives. It is particularly attractive considering the ever-increasing demand for specific functionalized polyesters to replace commodity plastics in several applications such as films for packaging. It also provides a tool in polymer tailoring as demonstrated by the fluorescent feature exhibited by the functionalized polyesters. Such a fluorescent feature could be exploited to develop sensors or anti-counterfeit packaging. The polyesters carrying integral fluorescent moieties could also be exploited to design fluorescent biodegradable and biocompatible polymers for biomedical applications⁹⁴.

CHAPTER 4

SURFACE COPOLYMERS MODIFICATION THROUGH NITROXIDE-MEDIATED PHOTOGRAFTING

The properties and the microstructures of the surface of a polymer material are particularly important because all physical and chemical interactions between the material and the environment take place at this interface⁹⁵. For this reason, the modification of the polymer surface properties is often requested for applications where the bulk properties have not to be changed, but the pristine surface appears to be inadequate for specific applications. Different examples were reported in the literature that take advantage of a modification process confined only to the surface a polymer matrix. For some applications requiring high adhesive interactions like for example coating, painting, printing, or in the active packaging sector for metal chelation^{96,97}, or in the preparation of separation membranes⁹⁸, polar groups were confined to surfaces. Meanwhile, for some other uses like for example in biomedical applications or in the anti fouling field, it is of particular importance to have a super hydrophobic surface and that could be obtained by the surface modification of different polymer matrices⁹⁹⁻¹⁰¹. A methodology that enjoyed considerable success is the photografting technique that can be used to modify the surface without altering the bulk properties of the polymer matrix. This procedure is based on surface grafting reactions initiated by ultraviolet irradiation in the presence of a photoinitiator. The photoinitiator, once activated by UV radiation, is able to abstract a hydrogen atom from the polymer surface. The macroradical, thereby generated, can react with vinyl monomers allowing the grafting of a single molecule or of a polymer chain¹⁰². Compared with other techniques like for example plasma or corona treatment, the photografting method shows several advantages as:

- ✓ easy industrialization,
- ✓ low cost of processing,

to control the grafting efficiency. Yang and Ranby¹⁰⁴ evaluated several kinds of monomers, which are able to undergo to surface photografting polymerization. By comparing different acrylates, as acrylic acid (AA), methyl acrylate (MA), butyl acrylate (BuA) and glycidyl acrylate (GA), they noticed that AA shows the highest photopolymerization efficiency and its grafting efficiency is between 60% and 80%, while MA and BuA have the highest grafting efficiency. The GA grafting efficiency gradually increases with the reaction time. These differences may be attributed to the distinct affinity of the monomer for:

- I. the macroradical,
- II. the semipinacol free radical

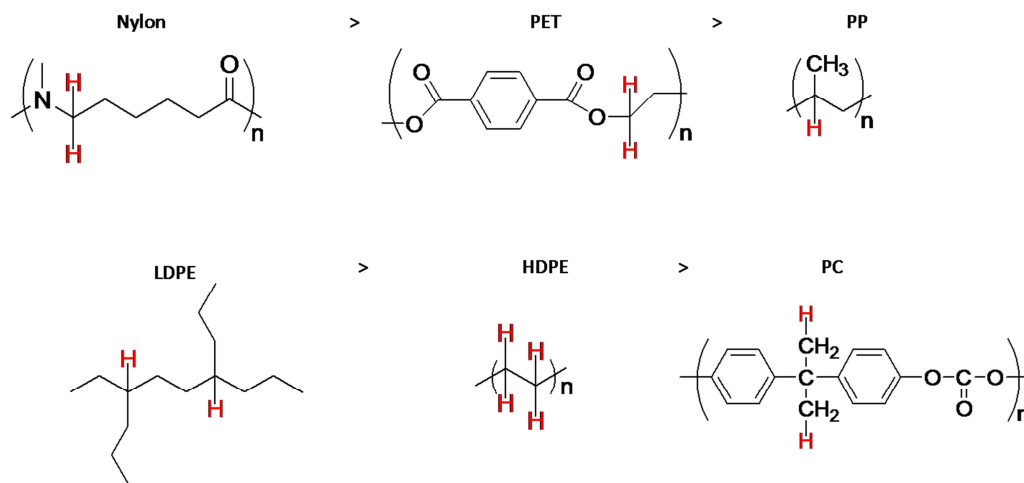
which have increasing polarity in this order.

This may explain why AA, the more polar monomer, is attracted to the semipinacol free radical, while the others acrylate monomers are less polar and thus more prone to react with the macroradical. Instead, a comparison between vinyl acetate (VAc) and ethyl acrylate (EA), reveals a big difference: the grafting amount calculated for VAc was 2.6 %, while for EA was 60.8 %¹⁰⁵. This deviation is due to the fact that VAc acts as an electro-donating monomer, little prone to react with free radicals, conversely EA is strongly reactive toward free radicals. For this reason the lost of EA in side reactions is minimal and thus the percentage of grafting is higher, conversely, being less reactive to radicals, VAc is consumed by side reactions. Another factor characterizing the monomer grafting efficiency is the steric hindrance. For instance, the comparison between different substituted acrylamides¹⁰⁵ evidenced that the presence of cumbersome groups makes difficult the approach of the monomer to the substrate and reduces the grafting efficiency. Finally, it is often reported that the grafting efficiency increases with the monomer concentration up to a certain limit and then starts to decrease with further increase of monomer. This happens because the increase of the monomer concentration favors its homopolymerization rather than the grafting¹⁰⁶.

✓ **Substrate nature**

Ranby and Yang¹⁰⁴ investigated the effect of the substrate nature on the grafting efficiency by testing several polymer matrices for the AA photografting in the presence of

BP. The reactivity order in the photografting reaction observed by the authors was reported in Figure 4.2.



The red drawn hydrogen atoms indicate the hydrogen atoms that most likely will be abstracted to form a macroradical

Figure 4.2: Decreasing pathway of the grafting efficiency of different polymer substrates. Figure reported from ref¹⁰⁴.

The reason of this reactivity order was related to the different reactivity of the C-H bond of these polymers. Nylon and PET have electro-donor atoms (N and O respectively), directly linked to the C-H bond, which gives an activating effect to the formation of the macroradical. PP tertiary hydrogen atoms are easy to abstract because the so formed tertiary radicals are relatively more stable than other carbon centered radicals. Since LDPE contains some tertiary hydrogen in the branching point, its reactivity is higher than that of HDPE that has only secondary hydrogen. Finally polycarbonate (PC) contains only primary hydrogen in the methyl later group that is difficult to abstract by the excited BP and thus shows the lowest reactivity. Besides the chemical composition, the polymer crystallinity is another important variable to control the grafting occurrence. A decrease in the crystallinity of the matrix leads to a grafting improvement because the reactants can easily diffuse to reach the active site in the amorphous phase¹⁰⁵. Finally the substrate has to be transparent to the UV radiation.

✓ Solvent effect

The choice of solvent depends on several factors such as the monomer solubility, its capability to swell the substrate, the generation of free radicals derived from solvent, etc. First of all, the solvent has to efficiently swell the substrate to favor the monomer and photoinitiator diffusion inside the matrix.

Furthermore, the efficiency of grafting in solution depends on the competitive reaction of macroradicals ($P\cdot$) with monomer (1) or solvent (2) and this occurs especially when the photografting is carried out by using alcohols:



where $P\cdot$ represents the macroradical and M is the monomer.

When reaction (1) prevails, the desired grafting is reached otherwise the monomer homopolymerization is favored.

✓ Photoinitiator concentration

Yang and Ranby¹⁰⁴ evaluated the grafting efficiency of AA on LDPE by using three different initiators: BP, 9-fluorenone (FL), and xanthone (Xan) and evaluated also as their concentration affects the grafting efficiency. They noticed that by increasing the BP concentration the grafting efficiency does not show significant changes, conversely in the case of FL the higher is the concentration, the less is the grafting efficiency. Finally Xan shows an intermediate effect, namely the grafting efficiency decreases with a high photoinitiator concentration, but in a more limited extent than FL (Figure 4.3).

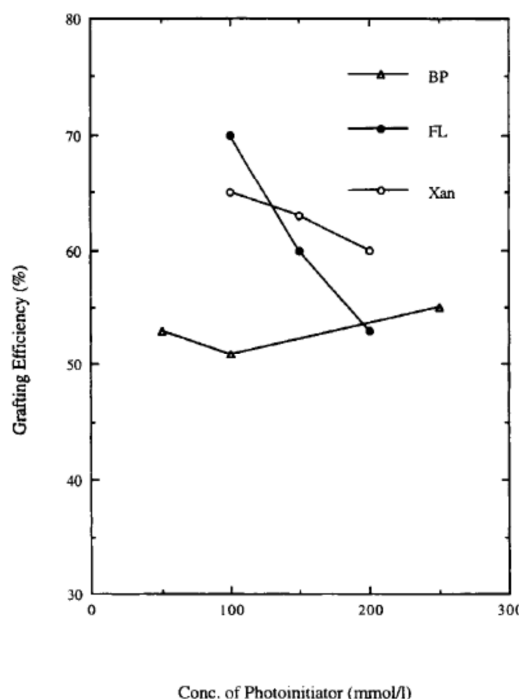


Figure 4.3: Effect of photoinitiators concentration on the grafting efficiency¹⁰⁴.

The authors attributed these results to a screening effect of the system due to the UV absorption properties of both the photoinitiator and the monomer being the BP the photoinitiator that shows the least screening effect, and FL the photoinitiator that has the largest screening effect; and Xan evidences an intermediate behavior.

✓ Temperature

Generally the grafting increases with temperature. Several interpretations were proposed to explain this observation, one of them was that a faster monomer diffusion process in the polymer substrate is achieved by increasing the temperature. Another one was that by increasing the temperature the thermal decomposition rate of initiator becomes higher as well as the initiator efficiency in producing free radicals on the pristine polymer. As results an increase in the polymer macroradicals concentration, and thus an enhance in the graft polymerization¹⁰⁵ was observed. A really interesting conclusion was that the maximum grafting is achieved for a temperature near the glass transition temperature (T_g) of the polymer; for temperatures below the T_g , the generated surface radicals cannot react, owing to the reduced monomer diffusion and limited chain flexibility, whereas for T

significantly above T_g , the number of radicals available for grafting decreases and thus the combination of monomer radicals results in lower grafting amount.

A technical upgrading of this methodology to increase the grafting efficiency and to limit some side reactions (like for example the homopolymerization of the monomer), was proposed by Bowman¹⁰⁷ and Castell^{108,109}. A sequential grafting by separating the whole process in two steps was discussed. The first step sees, in absence of monomers, the coupling between the semipinacol radical, derived from BP, and macroradicals, promoted by UV irradiation. In the second step monomer solutions are added to the activated substrate and graft polymerization is initiated by UV irradiation. Castell called the result of the first step “surface initiator” and he observed that this activated surface is stable and can be stored for further usage. This “surface initiator” can react with an acrylic acid, initiating the polymerization under the presence of UV light. In this way the formation of homopolymer is reduced because there is no free BP on the polymer surface or in the monomer solutions and semipinacol is not able to abstract a hydrogen atom from the monomer to start its homopolymerization (Figure 4.4).

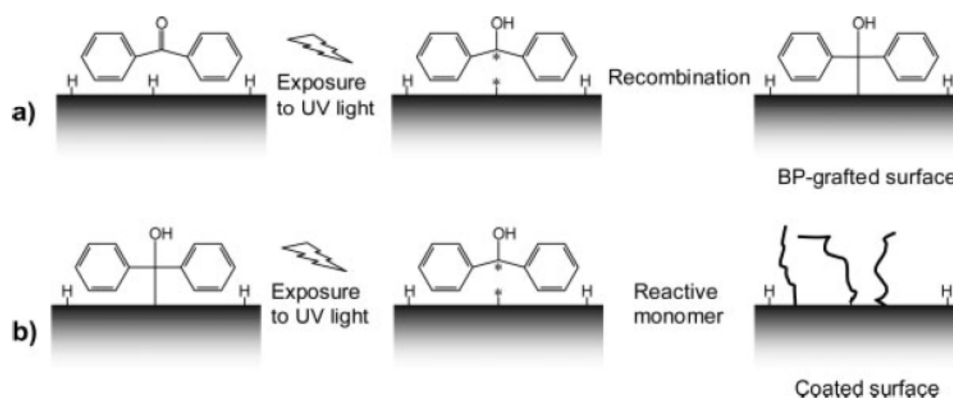


Figure 4.4: Modification of PP surface using a two-step grafting method¹⁰⁸.

In this study, in the place of the vinyl monomers usually employed to modify various polymer surfaces, the UV initiated photografting of functional TEMPO derivatives is proposed as a possible alternative. Indeed, from the data discussed in the previous chapters it is evident that the coupling reaction between macroradicals and TEMPO derivatives (NRC reaction) is a powerful tool to functionalize polyolefin and polyesters

that allows transferring the functional properties characteristic of the TEMPO radicals to the polymer matrix. The process described in the previous chapters is carried out in the melt and the formation of macroradicals is promoted by peroxide. In the following paragraph, macroradicals are generated by a photoinitiator under UV radiation and the coupling reaction between TEMPO derivatives and so formed macroradical is described. Finally, a discussion about the possible mechanism of this process is reported.

4.1: Preparation and characterization of functionalized polyolefins

The functionalization of linear low density polyethylene (LLDPE) and styrene-*b*-(ethylene-*c*o-*b*utene)-*b*-styrene) (SEBS) block copolymer films, was obtained through UV induced photografting reactions initiated by 4-methoxybenzophenone (MeOBP), which was selected as photoinitiator because it has the same reactivity as the more common benzophenone, but it shows lower toxicity^{109, 110}. Furthermore it is also less volatile than BP avoiding leaching issues sometime discussed in the literature as a possible cause of reduced efficiency of BP especially at high temperature¹¹¹. Finally the presence of the methoxy group can increase the compatibility and miscibility of the photoinitiator to the polymer matrix. As functional TEMPO derivatives, BzO-TEMPO, NfO-TEMPO (See Chapter 3) and Fluo-TEMPO (See Chapter 2) (Figure 4.1.1) were used.

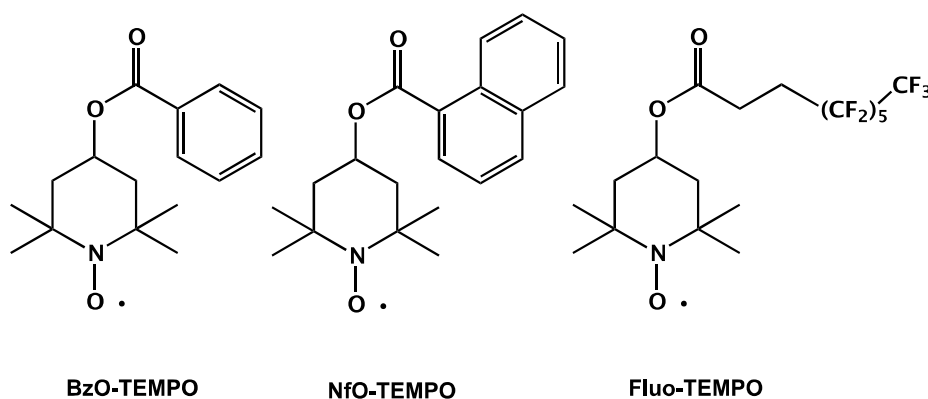


Figure 4.1.1: Structure of 4-benzoyloxy-2,2,6,6-tetramethylpiperidine-1-oxyl (BzO-TEMPO), 4-(1-naphthoate)-2,2,6,6-tetramethylpiperidine-1-oxyl (NfO-TEMPO) and 4-(4,4,5,5,6,6,7,7,8,8,9,9,9-tridecafluorononanoate)-2,2,6,6-tetramethylpiperidine-1-oxyl (Fluo-TEMPO).

As regards the matrix, these two polymers were selected because they have low crystallinity, which, in agreement with literature data¹⁰⁵, seems to be an important factor to favor a higher grafting yield.

The samples were prepared by spraying an acetone solution of X-TEMPO and MeOBP over the polymer surface followed by irradiation of the dried films (Method A). Alternatively, to modify LLDPE, another methodology was used. The TEMPO derivatives and MeOBP were mixed with the polymer in the melt, and then films of this pre-reactive mixture were irradiated (Method B). In this case, a more homogeneous dispersion of reagents can be obtained avoiding the use of the solvent that can interfere with the photografting process, allowing in any case the modification of the polymer surface properties. In order to check the presence of the functionalizing group belonging to the TEMPO derivatives, onto the polymer surface, the LLDPE functionalized samples were analyzed by ATR-FTIR spectroscopy and the analyses were carried out onto both the film surfaces. The spectra of the samples obtained by method A showed the simultaneous grafting of X-TEMPO and semipinacol derived from MeOBP (Table 4.1.1, Figure 4.1.2 and Figure 4.1.3) whereas no signals were detected on the non-irradiated side. The presence of multiple or large bands in the carbonyl region are probably due to some surface oxidation products.

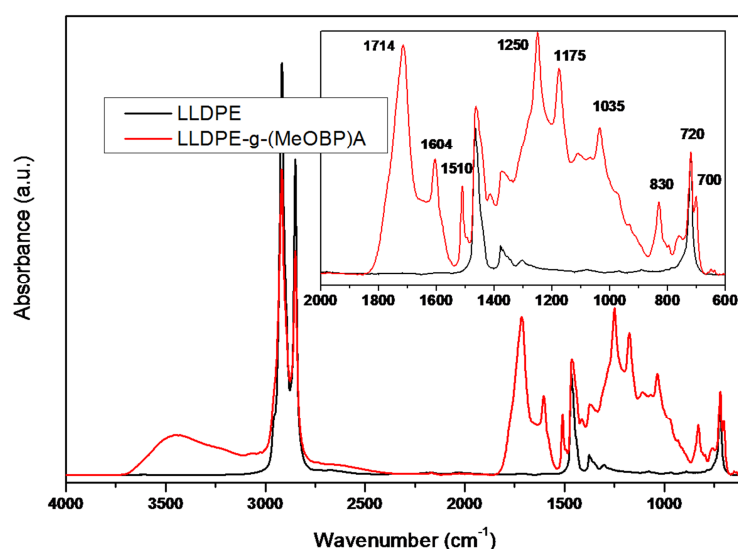


Figure 4.1.2: ATR-FTIR spectra of LLDPE and LLDPE-g-(MeOBP)A

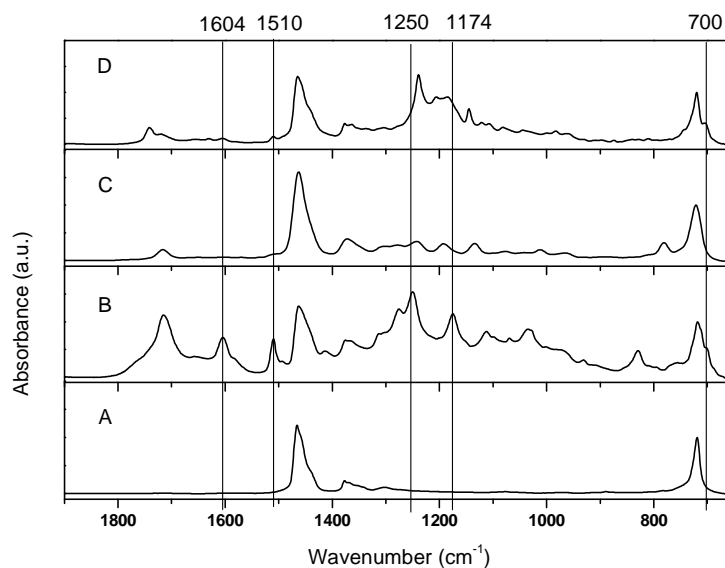


Figure 4.1.3: ATR-FTIR spectra of functionalized LLDPE samples obtained by method A compared with the spectrum of pristine LLDPE: A) LLDPE, B) LLDPE-g-(BzO-TEMPO)A, C) LLDPE-g-(NfO-TEMPO)A and D) LLDPE-g-(Fluo-TEMPO)A. All the spectra were normalized to the band at 720 cm^{-1} (methylene rocking of LLDPE). The showed frequencies (black lines) correspond to the characteristic bands of the grafted semipinacol derived from MeOBP (Figure 4.1.2).

Table 4.1.1: Typical frequency of grafted X-TEMPO and semipinacol

X-TEMPO	Frequency (cm^{-1})	Assignment
BzO-TEMPO ⁹	1724	C=O stretching
	1275	C-O stretching of C(=O)-O
	1112	C-O stretching of the bond that links the ester group to the piperidine ring
NfO-TEMPO ⁸	1717	C=O stretching
	1133	C-O stretching
	781	C-H out of plane bending of naphthalene
Fluo-TEMPO ^a	1743	C=O stretching
	1240	CF ₂ stretching
	1145	CF ₃ stretching
Semipinacol ¹⁰⁸	1510 and 1604	C=C stretching of the aromatic
	1250	C-O-C asymmetric stretching of MeO
	1174	C-O stretching
	700	out of plane bending of phenyl ring

^a Figure 2.1.4 in Chapter 2

The behavior reported for LLDPE was found also in the SEBS ATR-FTIR spectra. Indeed it was possible to note the contemporary grafting of functionalizing nitroxides (only NfO-TEMPO and Fluo-TEMPO were used with SEBS) and semipinacol. Concerning the non irradiated side, no evidences of grafting were observed (Figure 4.1.4).

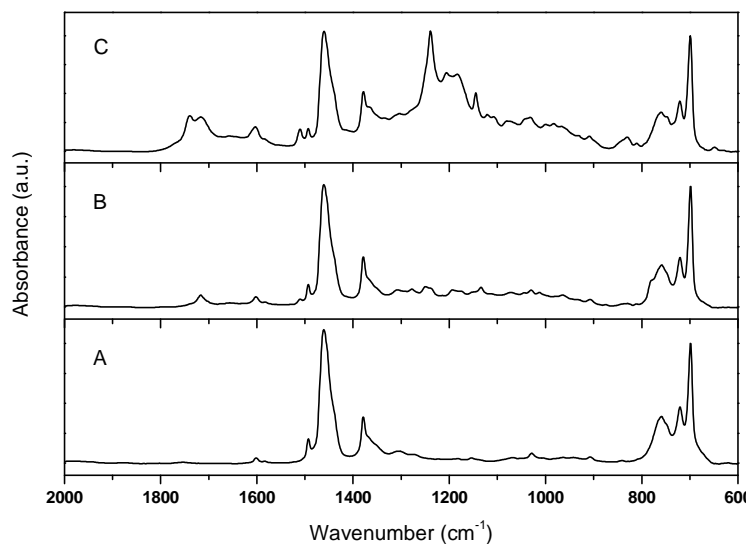


Figure 4.1.4: ATR-FTIR spectra of A) SEBS; B) SEBS-g-(NfO-TEMPO); C) SEBS-g-(Fluo-TEMPO). The spectra were normalized to the band at 700 cm⁻¹ (the C-C stretching of the SEBS aromatic ring).

As regards instead, the samples obtained through method B, the ATR spectra show the bands characteristic of the X-TEMPO grafting while the semipinacol bands appeared to be less intense (Figure 4.1.5).

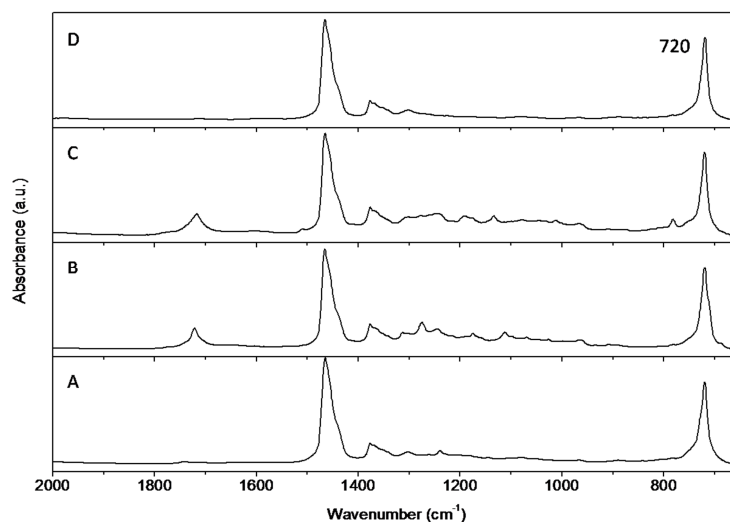


Figure 4.1.5: ATR-FTIR spectra of functionalized LLDPE samples obtained by method B compared with the spectrum of pristine LLDPE: A) LLDPE, B) LLDPE-g-(BzO-TEMPO)B, C) LLDPE-g-(NfO-TEMPO)B and D) LLDPE-g-(Fluo-TEMPO)B. All spectra were normalized to the band at 720 cm^{-1} (methylene rocking of LLDPE)

Furthermore spectra collected from both sides of films showed bands characteristic of the grafting of X-TEMPO although they have a low intensity especially on the non-irradiated side (an example is showed in the Figure 4.1.6). Lower evidences of surface oxidation were observed in all these samples.

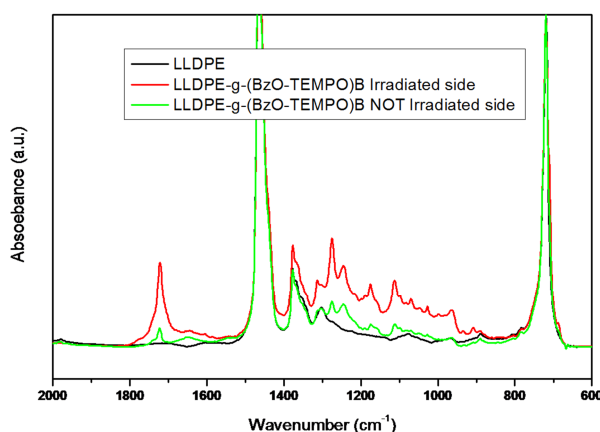


Figure 4.1.6: ATR-FTIR spectra of LLDPE, LLDPE-g-(BzO-TEMPO)B collected from the irradiated and not irradiated side of the film.

This behavior suggests the occurrence of a bulk photografting process. In agreement with this observation, UV-Vis investigation of LLDPE film evidenced that the UV radiation can

penetrate through the film thickness being the absorbance of the film about 0.4 in all the UV range (Figure 4.1.7).

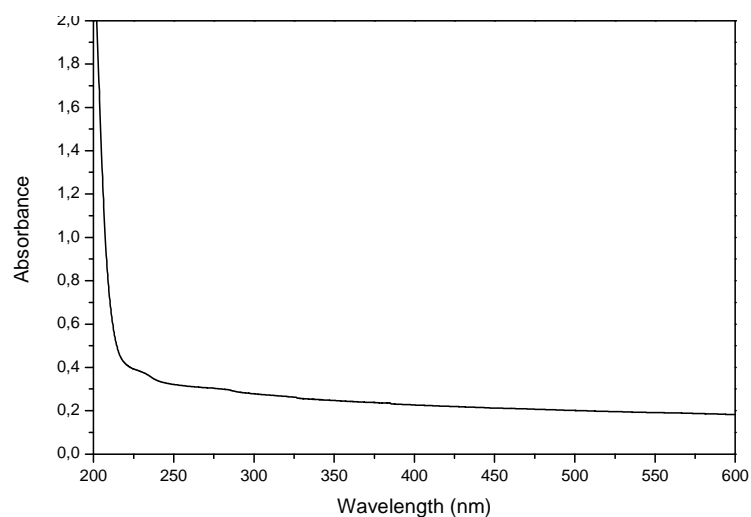


Figure 4.1.7: UV-Vis spectrum of LLDPE film

To better characterize the functionalized films, transmission FT-IR spectra of these samples were recorded. The data confirmed the grafting of X-TEMPO (Table 4.1.1) and, in the case of the samples obtained by method A also of the semipinacol (Figures 4.1.8 and 4.1.9). A FT-IR spectra comparison between (LLDPE)-g-(BzO-TEMPO) prepared by means of method A and method B is showed in Figure 4.1.10.

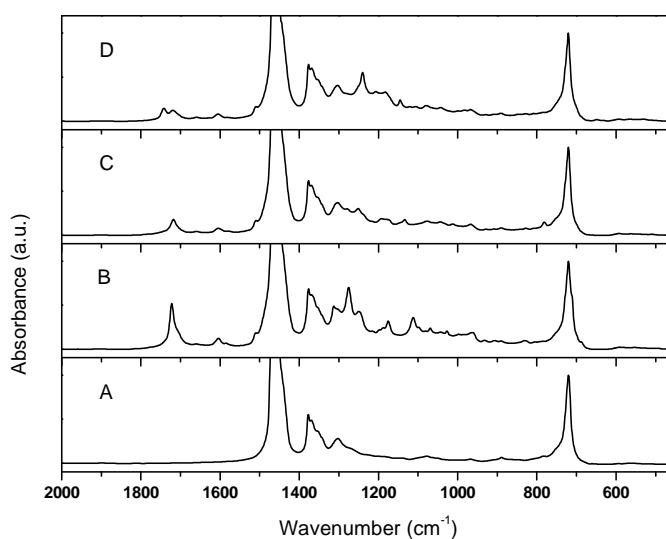


Figure 4.1.8: FT-IR spectra of samples prepared by method A: A) LLDPE; B) LLDPE-g-(BzO-TEMPO)A; C) LLDPE-g-(NfO-TEMPO)A and D) LLDPE-g-(Fluo-TEMPO)A

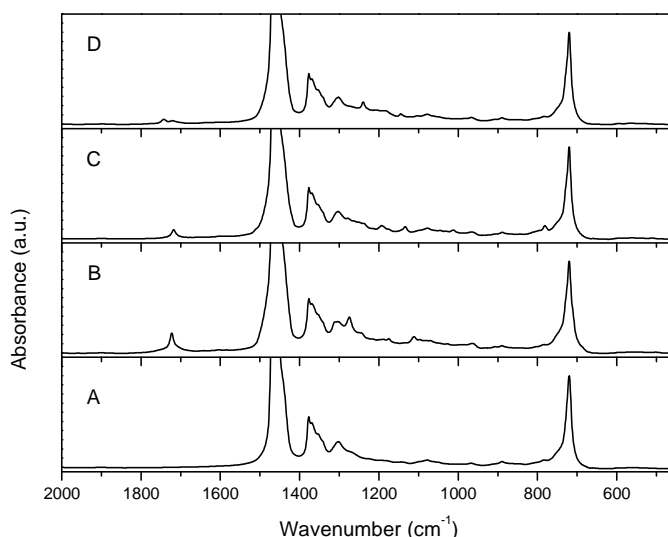


Figure 4.1.9: FT-IR spectra of samples prepared by method B: A) LLDPE; B) LLDPE-g-(BzO-TEMPO)B; C) LLDPE-g-(NfO-TEMPO)B and D) LLDPE-g-(Fluo-TEMPO)B.

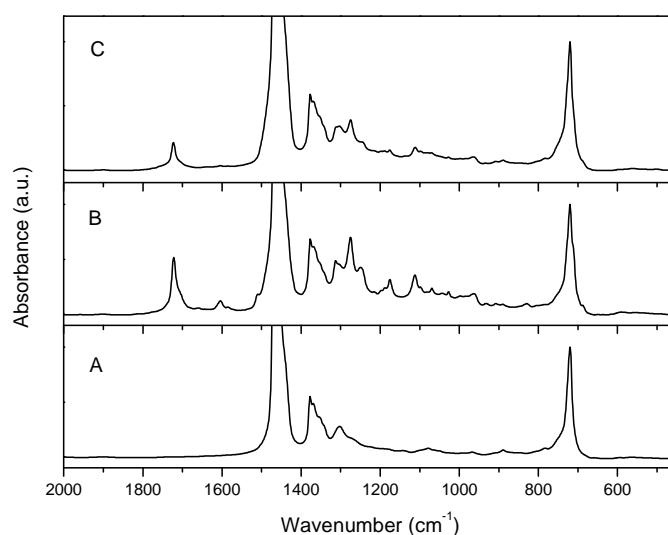


Figure 4.1.10: FT-IR spectra of A) LLDPE; B) LLDPE-g-(BzO-TEMPO)A; C) LLDPE-g-(BzO-TEMPO)B

Another interesting result from the ATR-FTIR versus FT-IR analysis is that the spectra of the samples functionalized with NfO-TEMPO show a lower degree of oxidation of the polymer surface with respect to those of the samples grafted with BzO-TEMPO and Fluo-TEMPO. This particular behavior of NfO-TEMPO will be discussed later.

In the case of samples obtained by method A, the amount of the grafted X-TEMPO was determined gravimetrically by weighting the samples before and after the photografting and the purification steps (Table 4.1.2). Generally, a weight increase of about 2-3 wt% was detected in agreement with the data reported in the literature for the photo-assisted

grafting of BP, a molecule that cannot propagate similarly to X-TEMPO derivatives¹¹². However, due to the competitive grafting of X-TEMPO and semipinacol, it is not possible to evaluate the amount of grafted X-TEMPO alone.

Table 4.1.2: Weight increase of the functionalized samples obtained by method A

Sample	Weight increase ^a (%)
LLDPE-g-(MeOBP)A ^b	0.6
LLDPE-g-(BzO-TEMPO)A	3.7
LLDPE-g-(NfO-TEMPO)A	2.1
LLDPE-g-(Fluo-TEMPO)A	2.5
SEBS-g-(NfO-TEMPO)A	1.6
SEBS-g-(Fluo-TEMPO)A	2.5

^aThe weight increase was determined after the surface photografting and the purification of the samples. ^b In this case 1/3 of MeOBP was used relative to that used in the other runs.

In the case of the samples obtained by method B the amount of photo-grafted species was estimated by FT-IR spectroscopy using *ad hoc* prepared calibration curves (⁹, Figure 2.1.12 in Chapter 2 and Figure 4.1.12) (Table 4.1.3). For these samples the conversion is quite high, considering the amount of grafted X-TEMPO with respect to its amount in the feed (see Experimental Part, Chapter 7, section 7.3.3).

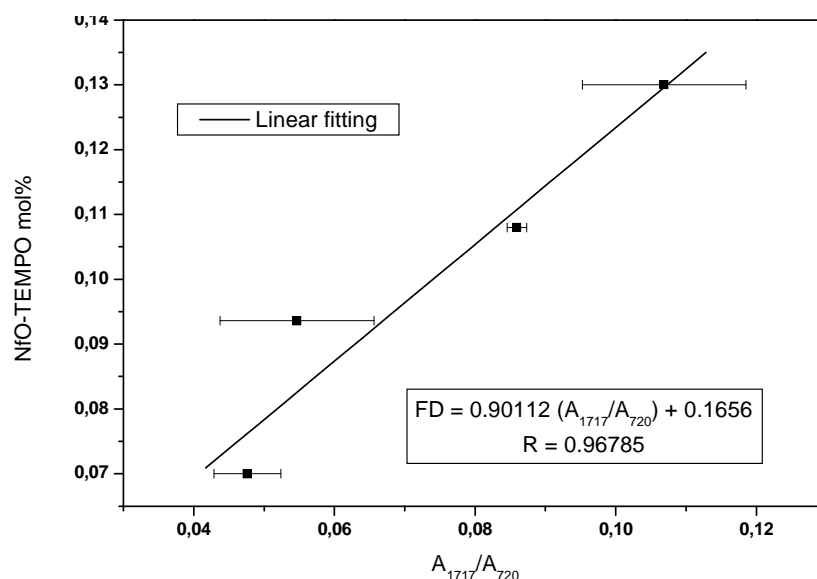


Figure 4.1.12: Calibration curve used to evaluate the functionalization degree of LLDPE-g-(NfO-TEMPO)B

Table 4.1.3: Functionalization degree (FD) and X-TEMPO conversion for the samples obtained by method B.

Sample	FD _{FT-IR}	Conversion ^a (%)
	(mol%) [wt%]	
LLDPE-g-(BzO-TEMPO)B	0.08 [0.56]	27
LLDPE-g-(NfO-TEMPO)B	0.12 [1.00]	40
LLDPE-g-(Fluo-TEMPO)B	0.06 [0.83]	40

^a Amount of grafted X-TEMPO with respect to its quantity in the feed

LLDPE functionalized samples were extracted with boiling toluene in order to state if some modification of the polymer matrix occurred during photografting (Table 4.1.4). Indeed the radical functionalization of polyethylene is usually accompanied by side reactions, typically chain extension and/or cross-linking, that, in the melt can be controlled by modulating the feed conditions²⁶. However, the literature reports the occurrence of photo-crosslinking of polyethylene assisted by photoinitiators and this can be a side process of the photografting of X-TEMPO^{111, 113}.

Table 4.1.4: Percentage of toluene insoluble fraction for the LLDPE functionalized samples

Samples	Toluene insoluble fraction (%)
LLDPE ^a	0
LLDPE-g-(MeOBP)A ^b	72.3
LLDPE-g-(BzO-TEMPO)A	84.5
LLDPE-g-(NfO-TEMPO)A	83.0
LLDPE-g-(Fluo-TEMPO)A	75.0
LLDPE-g-(MeOBP)B	66.0
LLDPE-g-(BzO-TEMPO)B	62.6
LLDPE-g-(NfO-TEMPO)B	23.0
LLDPE-g-(Fluo-TEMPO)B ^c	30.0

^aFilm of LLDPE irradiated in the absence of reagents. ^bThe amount of MeOBP used for the preparation of this sample is 1/3 of that used for the other surface functionalized samples. ^cThe amount of reagents used to obtain this sample is 1/2 of that used for the other samples.

Independently of the method used to functionalize the films, and the type of X-TEMPO, a quite high toluene insoluble fraction was collected in all cases, apart for the blank LLDPE film that was irradiated in the absence of reagents and that resulted completely soluble (Table 4.1.4). Considering the ability of X-TEMPO to react with carbon centered radicals and control the side reactions usually occurring during the radical functionalization of polyolefins and polyesters in the melt^{8,9} (see Chapter 2 and 3), it is expected that the presence of X-TEMPO can partially limit the formation of an insoluble fraction. However, from the data reported in Table 4.1.4, this control seems to occur only in part in the B samples and among the samples of this series it appears more evident when NfO-TEMPO was used.

To further highlight the formation of the covalent bond between the polymer and the X-TEMPO, and to confirm the amount of the grafted species, TGA analyses of all the samples obtained by method A were carried out. Indeed, the >NO-R bond of alkoxyamines is thermally reversible and by heating the equilibrium between the bonded and the free form can be shifted towards the free radicals⁸. As underlined in the previous Chapters, thermograms of LLDPE samples functionalized with X-TEMPO show a two steps degradation profile. The first step was attributed to the detaching of X-TEMPO and the

weight loss associated to this step was related to the amount of the grafted functionality. All LLDPE films obtained by photografting showed the same behavior (Figure 4.1.12B, C and D), the weight loss and the onset temperature associated with the first step were reported in Table 4.1.5. The onset temperature associated with this step is different for all the samples and seems to be dependent on the nature of X-TEMPO. The TGA analysis of the SEBS functionalized samples compared with the thermogram of the pristine polymer, showed similar results to that reported for the LLDPE functionalized samples (Figure 4.1.12A, Table 4.1.5).

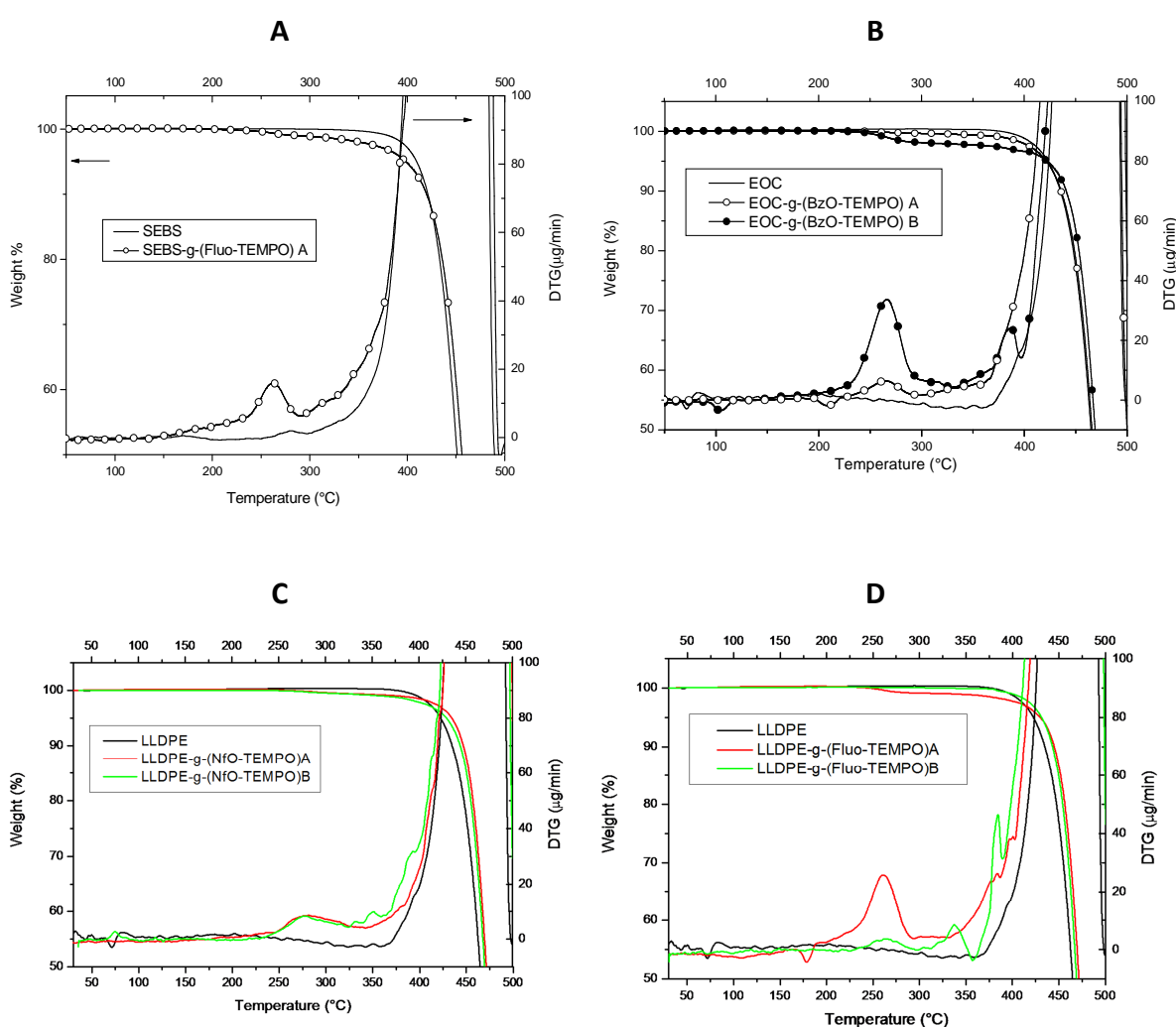


Figure 4.1.12: TGA thermograms and their first derivative of SEBS before and after the treatment with Fluo-TEMPO (A) and LLDPE before and after functionalization with BzO-TEMPO(B), NfO-TEMPO (C) and Fluo-TEMPO (D).

Table 4.1.5: TGA data of the first weight loss of LLDPE and SEBS functionalized samples^a

Sample	T _{onset} first step ^b (°C)	Weight loss ^c (%)
LLDPE-g-(MeOBP)A ^d	-	-
LLDPE-g-(BzO-TEMPO)A	244	2.5±0.3
LLDPE-g-(NfO-TEMPO)A	240	1.2±0.2
LLDPE-g-(Fluo-TEMPO)A	223	1.5±0.2
LLDPE-g-(MeOBP)B ^d	-	-
LLDPE-g-(BzO-TEMPO)B	248	1.0±0.2
LLDPE-g-(NfO-TEMPO)B	250	1.0±0.1
LLDPE-g-(Fluo-TEMPO)B	234	1.2±0.2
SEBS-g-(NfO-TEMPO)A	251	1.3±0.3
SEBS-g-(Fluo-TEMPO)A	219	2.1±0.2

^aThe analysis were carried out under nitrogen flow from 30 to 700°C (heating rate 10°C/min)

^bT_{onset} corresponding to the first weight loss

^cWeight loss percentage associated to the first step

^dFor this sample only the polymer degradation step was detected at 471° C

The agreement between the TGA data and the weight increase determined gravimetrically (compare Tables 4.1.2 and 4.1.5) is quite good. Differences between the two values can be attributed to the fact that during the TGA analysis only the detaching of X-TEMPO was observed, indeed in the case of LLDPE-g-(MeOBP)A or B, where semipinacol derived from MeOBP was grafted onto the LLDPE film, only the degradation of the polymer matrix was detected. From the data reported in Table 4.1.5, it can be observed that a comparable amount of grafted X-TEMPO can be obtained by method A or B, but in the case of method A a larger quantity of reagents is necessary to obtain the grafting (see Experimental Part, Chapter 7, section 7.3.3), moreover the simultaneous grafting of the semipinacol and also a larger extent of the surface oxidation were observed.

From the data discussed so far, it is quite evident that the more homogeneous distribution of the reagents inside the polymer matrix obtained by method B can favor the control of some side processes like for example the grafting of the semipinacol and partially the chain extension reaction, reducing the insoluble toluene fraction as well as the extent of surface oxidation. The method B allows also a higher efficiency of the photografting process as evidenced by TGA analysis. However, the deposition of the

reagents onto the surface by method A probably is the troublesome point of the whole process. Indeed, acetone solutions were sprayed on the sample surface by an airbrush, but the control of the extent of surface coverage is limited by the procedure itself that is not completely reproducible. Moreover, both X-TEMPO and MeOBP are microcrystalline powders that retain their microcrystallinity even after evaporation of the acetone from the polymer surface. The presence of crystallites can reduce the incident radiation efficiency by light scattering causing a reduction of the grafting degree¹¹¹. Moreover, acetone can help the grafting process, but it can only partially swell the polymer^{95, 114}. The reagents are thus expected to be confined on the first layers of the films as confirmed by the fact that the ATR-FTIR spectra collected from the non-irradiated side of the film prepared by method A showed no signals of grafted X-TEMPO. Finally, it cannot be excluded that a possible low affinity of the reagents for the matrix and/or their evaporation due to the air circulation during irradiation, especially in the samples prepared by method A, can influence the photografting efficiency.

4.2: Surface property evaluation

The aim of this study is the surface modification of polymers through photografting of X-TEMPO derivatives and from the results so far discussed it is evident that different functional groups were successfully photo-grafted onto different types of polymer surfaces. To account for the unique feature given to the polymer by the grafted functional groups, specific analyses were carried out. In particular, the films functionalized with NfO-TEMPO were analyzed by fluorescence emission spectroscopy, whereas in the case of the films functionalized with Fluo-TEMPO measurements of the contact angle were performed to evaluate the hydrophobicity and lipophobicity of the modified surfaces.

The fluorescence emission spectra collected from LLDPE-g-(NfO-TEMPO)A, LLDPE-g-(NfO-TEMPO)B and SEBS-g-(NfO-TEMPO)A are reported in Figure 4.2.1.

The emission spectrum of LLDPE-g-(NfO-TEMPO)A shows a large band at about 430 nm, whereas a more complex spectral pattern with a maximum at about 380 nm and a shoulder at about 430 nm, can be observed in the case of LLDPE-g-(NfO-TEMPO)B. The emission maximum of these spectra evidences a noteworthy red shift with respect to the

emission spectrum collected in the case of a similar sample functionalized in the melt by using a peroxide⁸. Probably the development of some highly conjugated fluorescent products via the formation of an excimer can cause this shift¹¹⁵. Such interactions can be more feasible in the sample obtained by method A where the chromophores were mainly confined on the surface, than in the sample B where the nitroxide radicals were dispersed throughout the whole film thickness and the conjugation between the chromophores is less probable. Accordingly, the emission spectrum of B sample shows two overlapping bands: one centered at about 380 nm, the typical emission of the single naphthalene group, and the second at about 430 nm probably due to the excimer emission. Although a rigorous quantum efficiency evaluation was not carried out, it can be observed that the fluorescence intensity was very low for all the samples, and effectively lower than that recorded for the sample obtained in the melt⁸ containing about the same amount of NfO-TEMPO. The same behavior was noticed also for the SEBS-g-(NfO-TEMPO); in this case the spectrum showed a large band, with low emission intensity, centered at about 430nm.

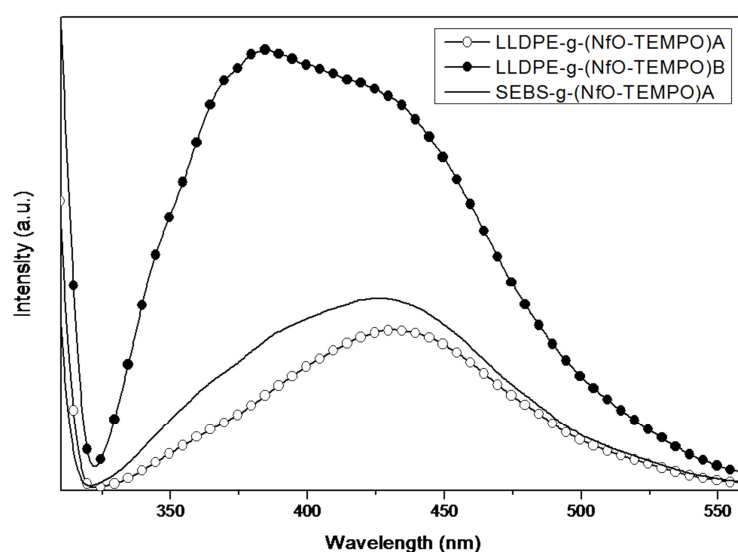


Figure 4.2.1: Fluorescence emission spectra of LLDPE-g-(NfO-TEMPO)A, LLDPE-g-(NfO-TEMPO)B and SEBS-g-(NfO-TEMPO)A. λ_{exc} : 300nm

In order to evaluate the wettability properties of the films functionalized with Fluo-TEMPO, static contact angle measurements were carried out using water and *n*-hexadecane as probing liquids. Data of the Fluo-TEMPO modified films are collected in Table 4.2.1 and compared with those of the non-functionalized films.

Table 4.2.1: Contact angles for the films of LLDPE-g-(Fluo-TEMPO), SEBS-g-(Fluo-TEMPO) and the corresponding pristine copolymers.

Film	$\theta_w^{a)}$	$\theta_h^{a)}$
	(°)	(°)
LLDPE	96 ± 2	31 ± 1
LLDPE-g-(Fluo-TEMPO)A	98 ± 2	40 ± 2
LLDPE-g-(Fluo-TEMPO)B	96 ± 2	49 ± 1
SEBS	96 ± 1	36 ± 2
SEBS-g-(Fluo-TEMPO)A	98 ± 2	38 ± 1

^(a) Measured with water and *n*-hexadecane.

The values of θ with water and *n*-hexadecane are conventionally regarded as estimations of hydrophobicity ($\theta_w > \sim 90^\circ$) and lipophobicity ($\theta_h > \sim 60^\circ$), respectively. According to this criterion both the Fluo-TEMPO functionalized and non-functionalized films are hydrophobic ($\theta_w = 96\text{--}98^\circ$) and poorly lipophobic (31–49°). The inclusion of the Fluo-TEMPO functions appears to especially affect the lipophobic character of the modified films, being θ_h generally larger than that of the pristine copolymers. However, this trend was more significant for LLDPE-based films, for which θ_h increases of 9–18°. Such an increase, although not so high, was surprising if one considers the relatively low functionalization degree typical of the present samples (e.g. 0.12 mol% for LLDPE-g-(Fluo-TEMPO)B). Measurements of liquid–solid contact angles are commonly used to evaluate solid surface tension γ_s . However, the correlation between θ and γ is still a controversial question and none of the different approaches proposed are generally accepted^{116–118}. Accordingly, we followed the additive-component method of the surface tension of Owens, Wendt, and Kaelble^{119–122}. The surface tension values γ_s calculated for the Fluo-TEMPO modified copolymers and the pristine polyolefin films are collected in Table 4.2.2. Consistently with their hydrophobic nature, all the films display relatively low surface tensions (24–26 mN m⁻¹). Moreover, in agreement with the contact angle values discussed above, films functionalized with Fluo-TEMPO generally show a lower surface tension than the corresponding pristine films, even though this trend is more evident for the LLDPE-based samples (e.g. γ_s passed from 25.7 mN m⁻¹ for LLDPE-g-(Fluo-TEMPO)B to

21.8 mN m⁻¹ for LLDPE). In any case, the largely predominant contribution to γ_s is the dispersion component γ_s^d , being γ_s^p 1.7–2.9 mN m⁻¹, typical of an apolar surface.

A decrease in surface tension of the functionalized copolymer films suggests that the fluorinated chains of the Fluo-TEMPO moieties are preferentially located at the polymer-air interface, as a result of their low surface energy. This finding supports the hypothesis that a surface modification of the pristine polyolefins has occurred.

Table 4.2.2: Surface tensions for the films of LLDPE-*g*-(Fluo-TEMPO), SEBS-*g*-(Fluo-TEMPO) and the corresponding pristine copolymers.

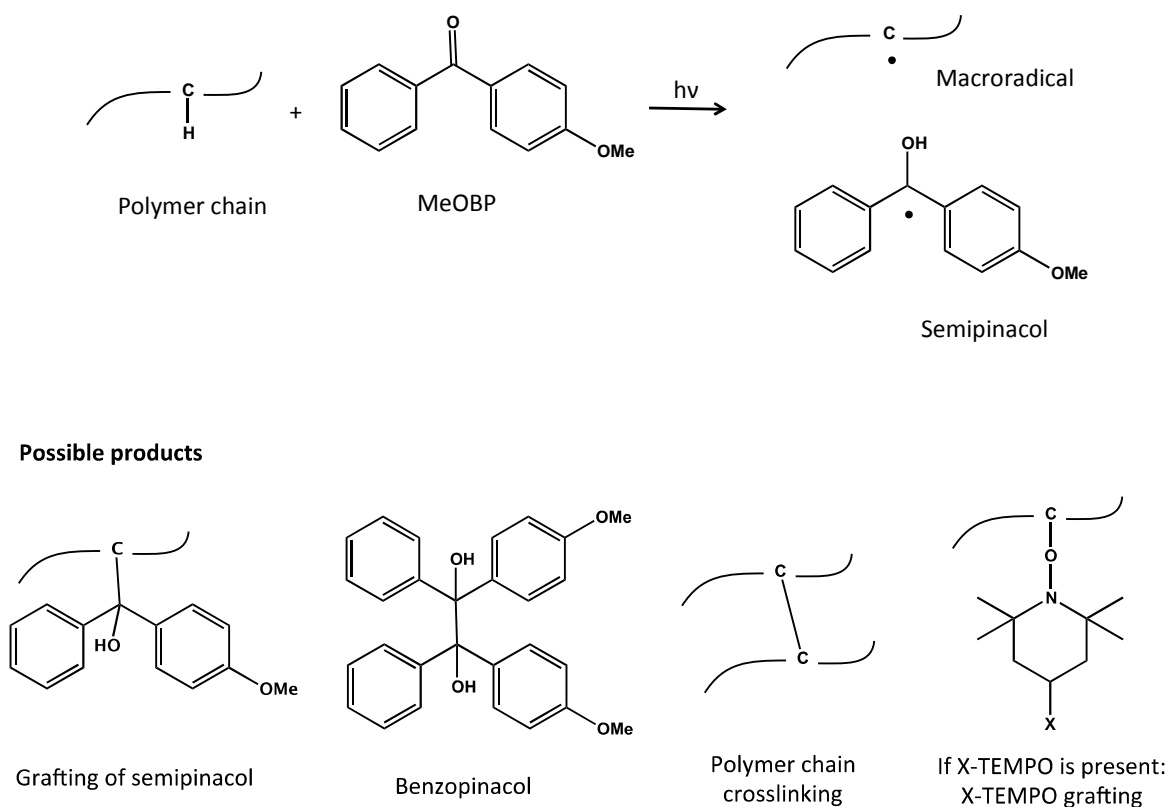
Film	$\gamma_s^{d(a)}$ (mN m ⁻¹)	$\gamma_s^{p(a)}$ (mN m ⁻¹)	$\gamma_s^{(a)}$ (mN m ⁻¹)
LLDPE	23.8	1.9	25.7
LLDPE- <i>g</i> -(Fluo-TEMPO)A	21.5	1.9	23.4
LLDPE- <i>g</i> -(Fluo-TEMPO)B	18.9	2.9	21.8
SEBS	22.6	2.1	24.7
SEBS- <i>g</i> -(Fluo-TEMPO)A	22.1	1.7	23.8

^(a)Calculated with the Owens–Wendt–Kaelble method: γ_s^d dispersion component, γ_s^p polar component.

4.3: Discussion about the grafting mechanism of X-TEMPO

As previously discussed, BP or its derivatives in their excited triplet state can abstract a hydrogen atom from the polymer backbone generating a macroradical and a ketyl radical (or semipinacol). The radical species derived from the photoinitiator (semipinacol) is rather unreactive towards H-atom abstraction, but it can dimerize to benzopinacol or combine with other radicals, e.g. P•, P-M• or P(-M)_nM• (where P• is the starting macroradical and P-M• or P(-M)_nM• are the growing polymer chains) thus giving termination reaction^{123, 124}. Macroradicals are the reactive species and can start the vinyl

monomer polymerization or can crosslink if the reaction is carried out in the absence of other reagents^{95, 111}. If X-TEMPO free radicals are added during the reaction, they can react with macroradicals by coupling. From this description, it is evident that the photografting of X-TEMPO to the polymer matrix is really a complex process involving different competing reactions (Scheme 4.3.1).



Scheme 4.3.1: Formation of macroradicals and semipinacol by UV-irradiation and possible products deriving from the reactions of macroradicals, semipinacol and X-TEMPO.

Probably, beyond the described processes, some other reactions and factors can influence the photografting of X-TEMPO. For example, under UV irradiation and in the presence of oxygen, polyolefins can be photo-oxidized generating new functional groups that can further react under UV irradiation¹²⁵. Besides, also the solubility, the affinity and the hindrance of X-TEMPO with respect to the polymer matrix can influence its diffusion inside the polymer. From the discussed results, it seems that the simultaneous grafting of the semipinacol and X-TEMPO occurs especially in the case of samples prepared by method A whereas the more homogeneous dispersion of the reagents by applying the method B seems to be useful to limit a few of the possible reactions such as the grafting

of semipinacol, partially the oxidation of the matrix and the polymer chain extension. Probably, as reported in literature^{109, 124}, a double steps mechanism, where the first step is the grafting of MeOBP followed by the polymerization of vinyl monomers under UV light, can be effective also in the case of X-TEMPO. In this case the second step is the grafting of X-TEMPO in place of vinyl monomers polymerization. Some explorative runs of the two steps method were carried out with the aim to state the feasibility of this procedure also in the case of the grafting of X-TEMPO.

For these experiments, to limit the surface photo-oxidation, a procedure already reported in literature^{103, 124} was applied. By this method the photoinitiator solution was deposited between two polymer films and then the obtained double layer was treated under UV light. The comparison between ATR-FTIR spectra of the pristine polymer and of the (LLDPE)-g-(MeOBP)_E sample obtained by this method, shows that the bands characteristic of the grafting of semipinacol were present and that although some photo-oxidation bands are still present, they show a low intensity. This suggests that by this procedure the photo-oxidation was not completely avoided but at least limited (Figure 4.3.1).

After the first step completion, static water contact angle measurements were carried out. They showed a decrease from $96^\circ \pm 2$ to $89^\circ \pm 2$ of the water contact angle pointing out the presence of hydrophilic groups on the surface originated from the grafted semipinacol¹⁰⁹.

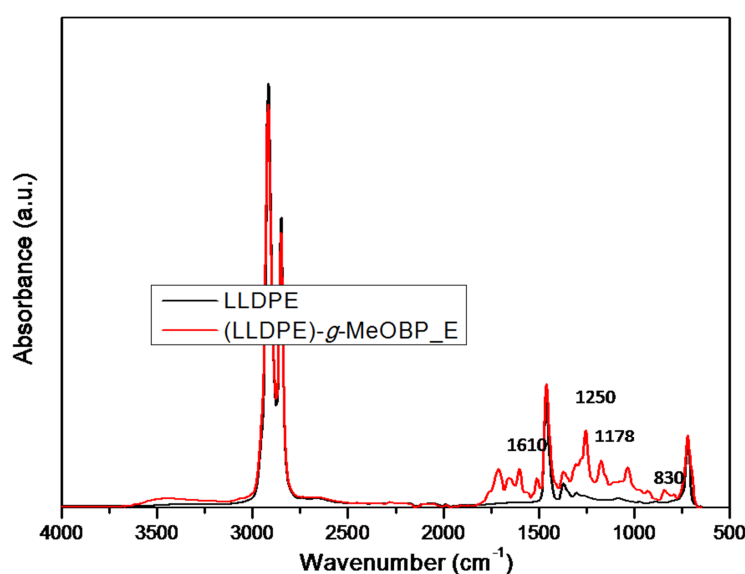


Figure 4.3.1: Superposition of the ATR-IR spectra of pristine LLDPE (black line) and UV-treated LLDPE films in the presence of MeOBP between two polyethylene films (red line).

To prove the second step of the photografting mechanism, the NVP monomer was deposited between two LLDPE films, previously functionalized with the photoinitiator, and irradiated under UV light, ((LLDPE)-g-(PVP)). The same procedure was also conducted on a pristine polymer film not previously activated with MeOBP, ((LLDPE)/(NVP)). To demonstrate the photopolymerization of N-vinylpyrrolidone onto MeOBP functionalized polymer surface, the ATR-IR spectra of these samples, ((LLDPE)-g-(PVP) and ((LLDPE)/(NVP)), were analyzed and compared with that of the pure LLDPE (Figure 4.3.2).

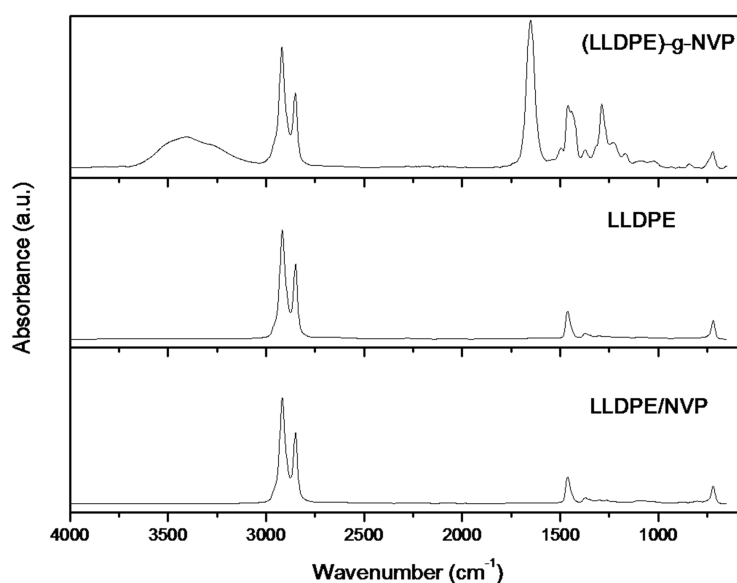


Figure 4.3.2: ATR-IR spectra of pristine polymer, ((LLDPE)-g-(PVP) and ((LLDPE)_NVP.

ATR-FTIR spectrum of the sample ((LLDPE)-g-(PVP) shows a band at 1660 cm^{-1} assigned to a superimposition of the stretching of C-O and of C-N characteristic of polyvinylpyrrolidone (PVP)^{124, 126}. Furthermore the static contact angle measurements, carried out by using water as wetting liquid, highlighted that the contact angle value decreases from $96^\circ \pm 2$ to $70^\circ \pm 2$ when PVP was grafted, in agreement with the data reported in literature¹²⁴. Conversely, the ATR-FTIR spectrum of ((LLDPE)/NVP after purification presented no significant differences with the pure copolymer and no appreciable change was evidenced in the contact angle measures. These results demonstrated that the bond between the semipinacol and the macroradical generated during the first step, can be re-activated under UV irradiation and, if the second step is carried out in the presence of a vinyl monomer, its photo-polymerization can start from the polymer surface.

The two-step photografting mechanism was investigated also using the TEMPO derivatives, precisely Fluo-TEMPO and NfO-TEMPO, in place of NVP. The samples were obtained by following the aforementioned “sandwich” procedure and the ATR-IR and fluorescence analysis were carried out. The comparison between the infrared spectrum of the MeOBP functionalized LLDPE and that of the sample obtained after the Fluo-TEMPO photografting by the two-step method ((LLDPE)_g(Fluo-TEMPO)), showed the presence of a very weak band at about 1244 cm⁻¹. The enlargement and the superimposition with the (LLDPE)_g(Fluo-TEMPO)_B ATR-IR spectrum, reported in Figure 4.3.3, allowed attributing this band to the C-F stretching. This may be a clear clue of the grafted nitroxide presence onto the polymer surface.

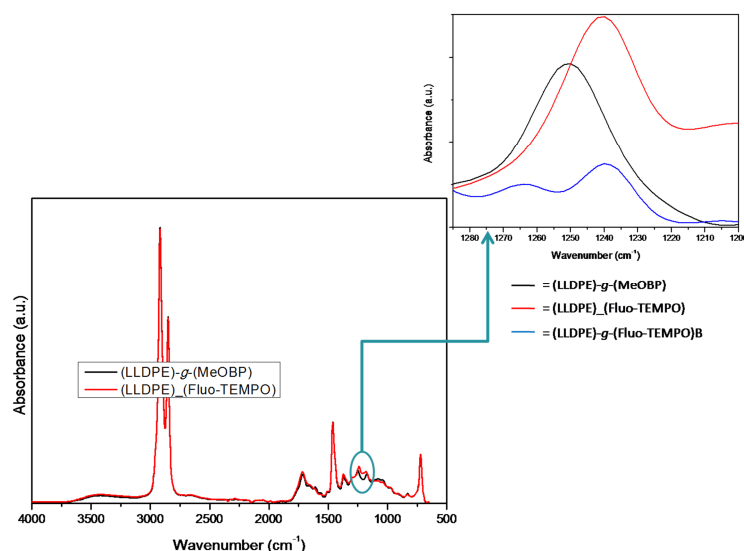


Figure 4.3.3: ATR-IR spectra of LLDPE functionalized with only photoinitiator (black line) and the same sample after the nitroxide addition (LLDPE_gFluo-TEMPO). In the enlargement the compared spectra belonging to LLDPE functionalized with only photoinitiator (black line) and the same sample after the nitroxide addition (LLDPE_gFluo-TEMPO) (red line) and the LLDPE film functionalized in bulk with Fluo-TEMPO (LLDPE)_g(Fluo-TEMPO)_B (blue line).

Regarding the sample obtained by the two-step method and using NfO-TEMPO as functionalizing nitroxide, the fluorescence analysis underlined an emission band centered at 367 nm and therefore very similar to the emission spectrum collected in the case of a sample functionalized in the melt (Figure 4.3.4). This result may be attributed to the lack

of π -stacking between the NfO-TEMPO naphthalene rings because of the low amount of grafted functionalities, which were found to be well separated onto the polymer surface.

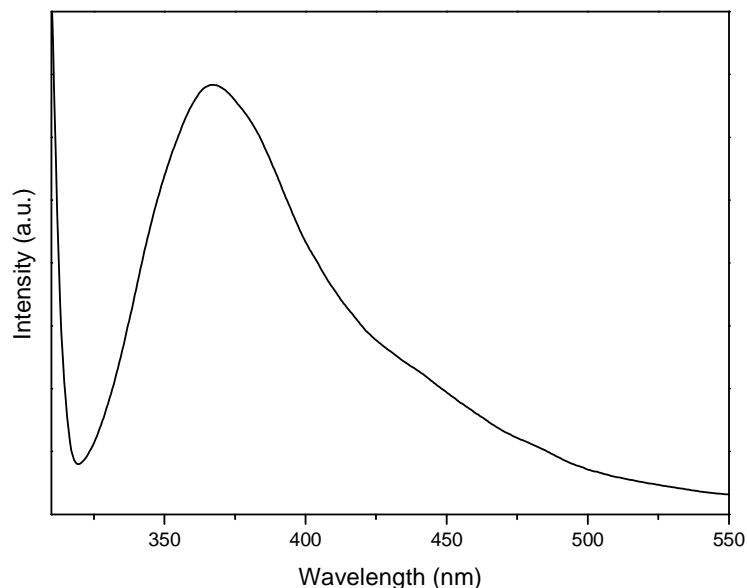


Figure 4.3.4: Fluorescence analysis of the LLDPE film treated with NfO-TEMPO during the second step of the photografting mechanism.

Taking everything into account and according to published data^{107, 109}, the first step of the mechanism allowed to create a “surface initiators” that can be further re-activated under UV irradiation : in the second step functional nitroxides can be successfully grafted onto the polymer surface.

4.4: Discussion about the particular case of NfO-TEMPO

The photografting of NfO-TEMPO deserves a special discussion, indeed all the samples containing this functional group showed a particular behavior with respect to the other X-TEMPO grafted polymers. For example the ATR-FTIR spectra of LLDPE-g-(NfO-TEMPO), contrary to all other X-TEMPO functionalized LLDPE samples, did not show bands attributable to the photo-oxidation. Meantime, the insoluble toluene fraction of the bulk functionalized LLDPE is quite limited with respect to the other samples. Moreover, the fluorescence emission is red shifted with respect to that observed in the case of samples functionalized in the melt in the presence of peroxide⁸ and has a lower intensity. All these

behaviors could be associated with some specific features of the naphthalene moiety. Indeed naphthalene is reported to be a quencher of the benzophenone triplet excited state by an energy transfer mechanism¹²⁷. By this mechanism, the naphthalene is excited to its triplet state and excited benzophenone comes back to the ground state, as consequence it is no more able to abstract hydrogen atom from the polymer. Probably the H-abstraction and the triplet excited state quenching of BP are strongly competing processes that can influence the final results of the reaction giving mainly grafting or cross-linking. It is also reported that a naphthoyl group bonded to 2,2,6,6-tetramethyl piperidin-4-ol can protect high density polyethylene (HDPE) and polypropylene (PP) from thermal and photo-oxidation process and that the simultaneous presence on the same molecule of the naphthoyl moiety and of the hindered amine has a synergic effect in the protection of both polyolefins¹¹⁵. The authors hypothesized a mechanism where the molecules containing the naphthoyl group bonded to the hindered amine decomposed under UV radiation producing naphthalene radicals. These radicals can scavenge the oxygen to form aromatic peroxy radicals¹¹⁵ and other non-emitting species. By this mechanism it can be explained both the protection towards oxidation observed during the NfO-TEMPO photografting as well as the decrease and the red shift of the emission spectra of NfO-TEMPO photo-grafted to LLDPE and to SEBS. Indeed, the naphthoyl group reacts preferentially with oxygen preventing the oxidation of the polymer, meanwhile the naphthalene ring fragments formed during photolysis can recombine giving highly conjugated species, whose emission spectrum was shifted towards red whit respect to that of naphthalene.

4.5: Conclusions

Since the formation of a covalent bond between the functional TEMPO derivatives and macroradicals is a good method to functionalize polyolefins and polyesters in the melt by using a peroxide, the NRC reaction was here accomplished to covalently immobilize some specific functionalities onto polymer surfaces according to the photografting technique. In this case two methods were proposed to modify the surface properties of two polymers (LLDPE and SEBS) through the photografting of BzO-TEMPO, NfO-TEMPO and

Fluo-TEMPO. Both methods allowed the surface modification, although the method B, where a pre-reactive mixture was prepared by melt mixing the reagents before photografting, seems to guarantee better results in terms of grafting efficiency and control of side reactions (chain extension/crosslinking) and oxidation. Fluorescence emission spectroscopy and contact angle measurements allowed stating that by photografting of X-TEMPO derivatives it is possible to transfer the peculiar properties of the functional groups present onto the TEMPO moiety to the polymer surface. However the fluorescence emission study evidenced the NfO-TEMPO photografting occurrence, although a particular interaction between the excited naphthoyl group and the photoinitiator under photografting conditions was considered as responsible of the relatively low grafting of this functional X-TEMPO. Finally the success of the two step photografting mechanism was demonstrated: in particular the first step allows creating "surface initiators" that can be further re-activated under UV irradiation whereas the second step can be a possible alternative to graft functional nitroxides onto the polymer surface.

CHAPTER 5

STUDY OF REVERSIBILITY OF NRC REACTION: THE STABILITY OF THE ALKOXYAMINE GRAFTED SPECIES

5.1: Characterization of functionalized polyolefins with Electron Paramagnetic Resonance (EPR) technique

As outlined in the previous Chapter, the onset temperature associated with the first degradation step, recorded by TGA analysis, is different for all the samples and seems to be dependent on the nature of X functionality of X-TEMPO derivative (Table 5.1.1).

Table 5.1.1: Detaching T recorded by TGA analysis

Sample	T _{onset} first step ^b (°C)
LLDPE-g-(BzO-TEMPO)	244
LLDPE-g-(NfO-TEMPO)	240
LLDPE-g-(Fluo-TEMPO)	223
LLDPE-g-(HO-TEMPO)*	233

^bT_{onset} corresponding to the first weight loss recorded by TGA analysis

*This is a LLDPE sample prepared by grafting of 4-hydroxy-2,2,6,6-tetramethylpiperidine-1-oxyl (HO-TEMPO) in the melt by means of the use of a peroxide⁹.

Further evidences of the differences in the detaching temperature of X-TEMPO were obtained by Electron Paramagnetic Resonance (EPR) analysis. Even if the samples were purified before the analysis, all samples show an initial EPR spectrum (Figure 5.1.1a) due to a low fraction of free nitroxide probably deriving from the equilibrium between the free and bond form of the macroalkoxyamine. This spectrum evolved, on heating, in the spectrum recorded at 180 °C (Figure 5.1.1b). The increase of the signal area confirms the homolytic bond cleavage of the >NO-R bond, whereas the increased symmetry of the

signal is an evidence of the larger mobility of the free nitroxide in the melt matrix owing to polymer bond cleavage.

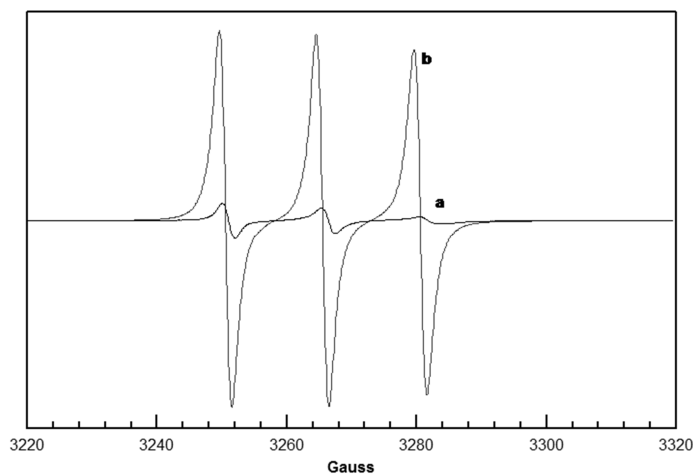
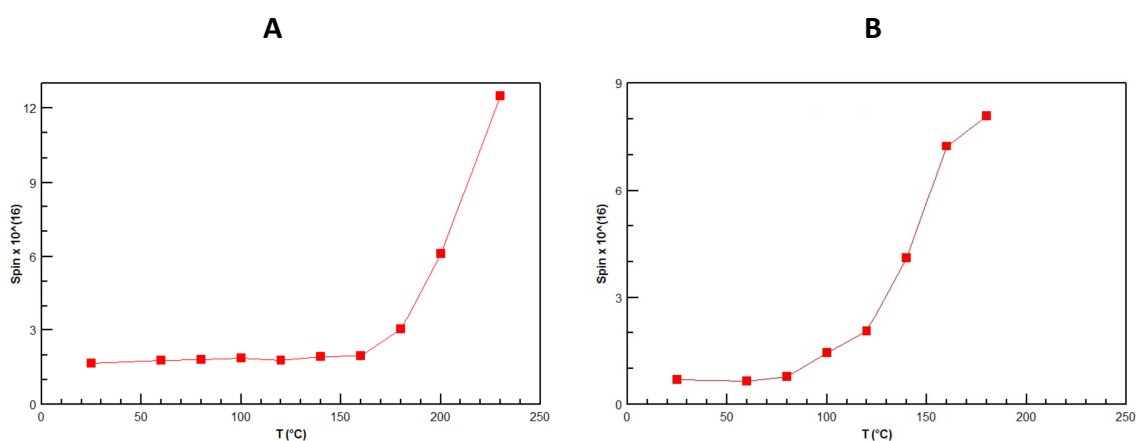


Figure 5.1.1. EPR spectra of LLDPE-g-(Fluo-TEMPO) at 60°C (a) and at 180°C (b).

By reporting the spin number as a function of temperature, it was observed that, in agreement with TGA data, the detaching of X-TEMPO, evidenced by an increase of the spin number, is depending on the nature of X (Figure 5.1.2).



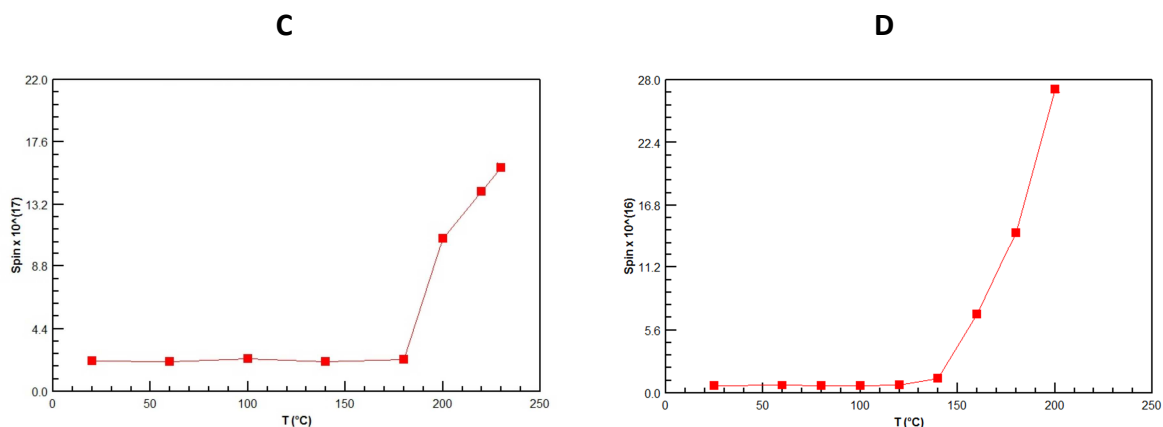


Figure 5.1.2: Spins number vs. temperature of **A:** LLDPE-g-(NfO-TEMPO), **B:** LLDPE-g-(Fluo-TEMPO), **C:** LLDPE-g-(BzO-TEMPO) and **D:** LLDPE-g-(HO-TEMPO).

In particular aromatic moieties seems to stabilize the >NO-R bond, whereas the less stable alkoxyamine is generated by grafting the Fluo-TEMPO. The entropy factor could have the main role in determining the differences in the detaching temperature of X-TEMPO from the polymer chains. The entropy of the system can be influenced by many factors, including the temperature increase and the polymer environment surrounding the X-TEMPO as well as the nature of X and its affinity to the polymer matrix or its steric hindrance but it is difficult to correlate all these parameters with the observed differences.

In order to thoroughly understand if an electronic effect of the X group of X-TEMPO can influence the bond dissociation enthalpy of the >NO-R bond, Density Functional Theory (DFT) calculations were carried out.

5.2: Theoretical study

The main objective of most quantum chemical approaches is the (approximate) solution of the time-independent, non-relativistic Schrödinger equation:

$$\hat{H} \psi_i(\vec{x}_1, \vec{x}_2, \dots, \vec{x}_N, \vec{R}_1, \vec{R}_2, \dots, \vec{R}_M) = E_i \psi_i(\vec{x}_1, \vec{x}_2, \dots, \vec{x}_N, \vec{R}_1, \vec{R}_2, \dots, \vec{R}_M)$$

where \hat{H} is the Hamilton operator for a molecular system consisting of M nuclei and N electrons in the absence of magnetic or electric fields.

$\psi_i(\vec{x}_1, \vec{x}_2, \dots, \vec{x}_N, \vec{R}_1, \vec{R}_2, \dots, \vec{R}_M)$ stands for the wave function of the i^{th} state of the system, which depends on the $3N$ spatial coordinates (\vec{r}_i) and the N spin coordinates (s_i) of the electrons, which are collectively termed (\vec{x}_i) and the $3M$ spatial coordinates of the nuclei, (\vec{R}_i).

Finally, E_i is the numerical value of the energy of the state described by ψ_i ¹²⁸.

The wave function ψ_i contains all information that can possibly be known about a quantum system, therefore solving the Schrödinger equation one can predict the behavior of any electronic system. Unfortunately, because of the presence of too many degrees of freedom, analytical solutions of the Schrödinger equation are possible only for a very few simple systems. In order to solve this problem it is necessary to involve some approximations¹²⁹. One of the earliest approximations was formulated in 1928 by Hartree, who considered the many-electron wave function as a product of single-particle functions. However this simplification cannot be accepted as a model wave function for fermions because it assigns a particular one-electron function to a particular electron and hence violates the fact that electrons are indistinguishable^{128, 129}. In 1930 Fock incorporated the Fermi statistic in this model, approximating the N -electron wave function by an *antisymmetrized* product (Slater determinant) of N one-electron wave functions $\chi_i(\vec{x}_i)$. However, replacing the true N -electron wave function by a single Slater determinant represents a drastic approximation, indeed it does not take in account Coulomb correlation, leading to a total electronic energy different from the exact solution of the non-relativistic Schrödinger equation.

The turning point was when Thomas in 1927 and Fermi in 1928 assumed that the motions of the electrons are not correlated and that the corresponding kinetic energy can be described by a local approximation based on the results for free electrons. In this way the energy is completely given in terms of the electron density¹²⁹. Although this approach appears rather inaccurate for most applications, it laid the foundation for the development of the Density Functional Theory (DFT). DFT was born in 1964 when a paper by Hohenberg and Kohn appeared in the Physical Review. The Hohenberg-Kohn theorem, asserts that all ground-state properties of a many-electron system are determined by the electron density which is a function of the three spatial coordinates¹³⁰. In this way it is possible to reduce the number of variables from $3N$ variables (the

coordinates of all N atoms in the system) characteristic of a many-body electronic wave function to only three variables. This makes calculations involving the electron density faster than calculations with wave functions. In fact, density functional theory makes possible to study systems with hundreds and even thousands of atoms¹²⁸. Furthermore in DFT, the total ground state energy of a many-electron system is a functional of the density; therefore by knowing the electron density functional, it is possible to calculate the total energy of the system.

5.2.1: Computational details

All calculations were performed with the Gaussian suite of programs¹³¹. The computations were carried out with the hybrid B3LYP functional¹³²⁻¹³⁵, in conjunction with the m-aug-cc-pVTZ basis set^{136, 137}, where d functions on hydrogens were removed. Semiempirical dispersion contributions were also included into DFT computations by means of the D3 model of Grimme, leading to B3LYP-D3 functional^{138, 139}. Full geometry optimizations were performed for all compounds (see Figure 5.2.2.1) checking the nature of the obtained structures by diagonalizing their Hessians.

5.2.2: Computational results

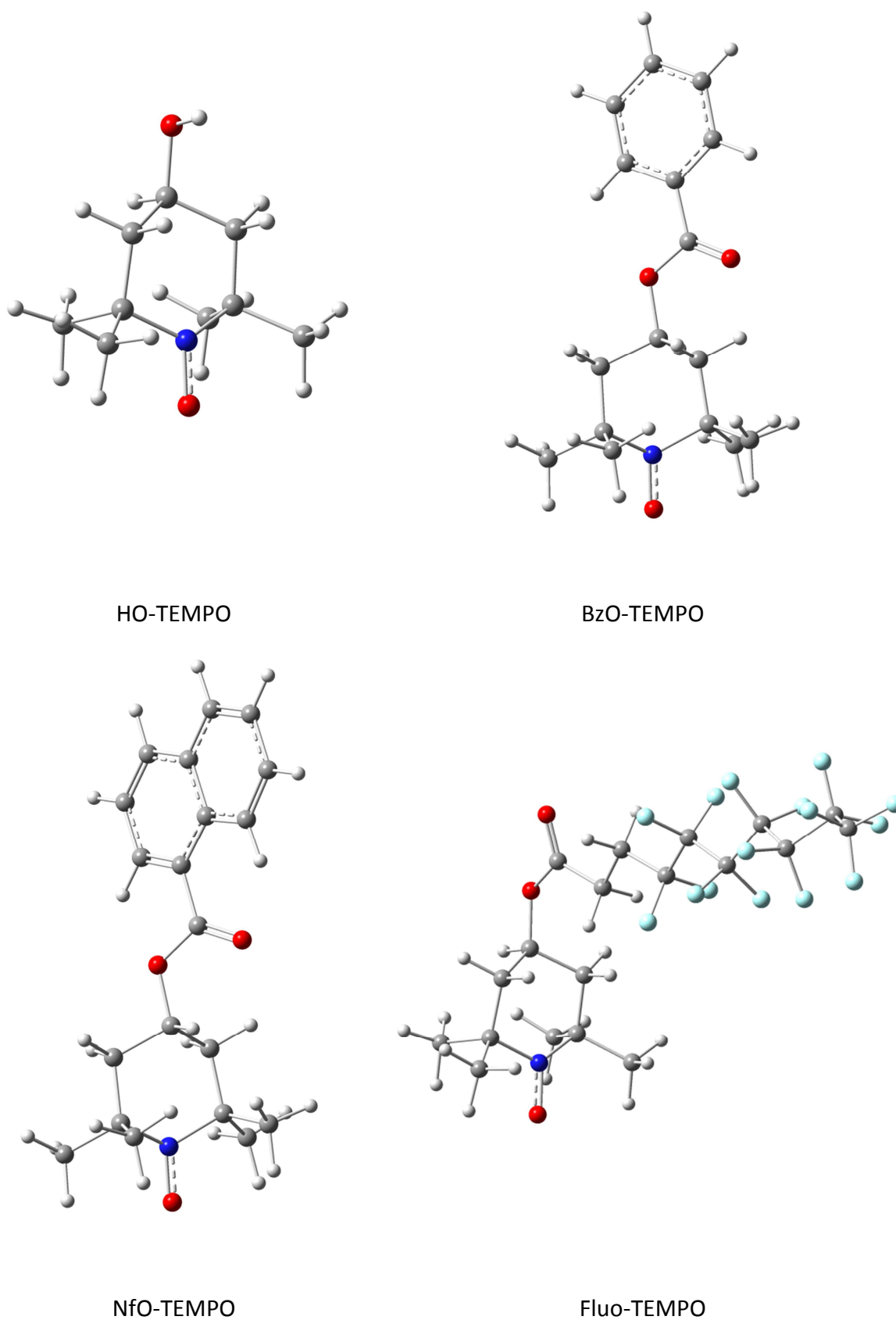


Figure 5.2.2.1: Optimized geometries of HO-TEMPO, BzO-TEMPO, NfO-TEMPO and Fluo-TEMPO

Considering that the polymer, which is functionalized with the TEMPO derivatives, is a linear low density polyethylene, it was possible to simulate it as a basic alkyl radical. In order to figure out the right number of carbon atoms to include in this radical, some tests were run based on HO-TEMPO, which is the smallest investigated compound and therefore the one that requires the less time for calculations. These tests consisted in calculating the energy difference between the alkoxyamine and the sum of the free radicals using alkyl radicals of different lengths: pentyl, heptyl, nonyl and undecyl radicals (see Table 5.2.2.1).

Table 5.2.2.1: Energy differences between the HO-TEMPO based alkoxyamines and the sum of HO-TEMPO and the corresponding alkyl radicals

	Energy difference(kcal/mol)	ΔE^a (kcal/mol)
pentyl radical	42.22637475	
heptyl radical	42.68054549	0.454170741
nonyl radical	42.98865647	0.308110979
undecyl radical	43.08758461	0.098928143

^a: evolution of the energy difference with the lengthening of the chain

One can see first from data reported in Table 5.2.2.1 that the energy difference becomes higher when the carbon atoms number of the alkyl radicals increases. However the evolution of this difference becomes lower by lengthening the chain, starting from 0.45 kcal/mol (pentyl to heptyl radicals), to 0.09 kcal/mol (nonyl to undecyl radicals). Considering this slight evolution between nonyl and undecyl radicals and in order to save some computational time, the polymer was simulated as a nonyl radical for this study.

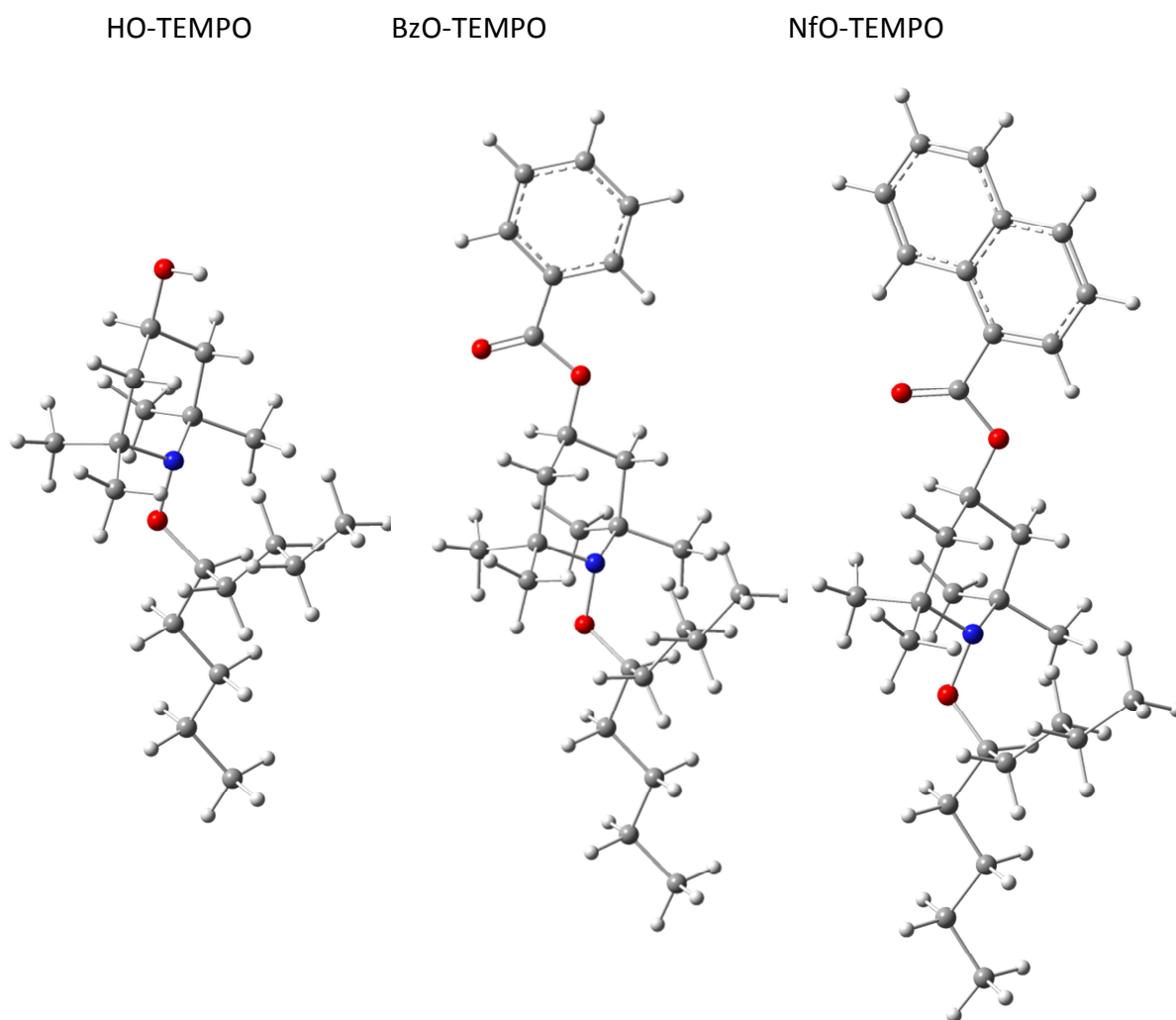


Figure 5.2.2.2: Optimized geometries of HO-TEMPO-*g*-nonane, BzO-TEMPO-*g*-nonane and NfO-TEMPO-*g*-nonane

As shown on Figures 5.2.2.2 and 5.2.2.3, the nonyl moiety presents the same orientation in the optimized geometries of all the four investigated compounds, which allows comparing their energies.

Table 5.2.2.2: Energy differences between alkoxyamines and the sum of the corresponding nitroxides and nonyl radical

Sample	Calculated Energy difference (kcal/mol)	Experimental T detaching ^a (° C)
nonane- <i>g</i> -HO-TEMPO	42.98865647	140
nonane- <i>g</i> -BzO-TEMPO	43.10999423	160
nonane- <i>g</i> -NfO-TEMPO	43.10311296	170
nonane- <i>g</i> -Fluo-TEMPO	44.69535582	110

^a: T detaching recorded by EPR analysis, roughly evaluated as intercept of tangents to curves reported in Figure 5.1.2

In Table 5.2.2.2, the energy differences between alkoxyamines and the sum of the corresponding nitroxides and nonyl radical is depicted. It is evident that the calculated energy differences are in a good agreement with the experimental detaching temperatures measured by EPR for all the nitroxides, besides the Fluo-TEMPO. Indeed, detaching nonane-g-HO-TEMPO was found to require a lower temperature than detaching nonane-g-BzO-TEMPO and nonane-g-NfO-TEMPO (140 °C vs 160-170°C). In the same time the energy difference between the nonane-g-HO-TEMPO and the free HO-TEMPO and nonyl radicals was also found lower than that between nonane-g-BzO-TEMPO and nonane-g-NfO-TEMPO and their free forms. This suggests that breaking the C-O bond in nonane-g-BzO-TEMPO and in nonane-g-NfO-TEMPO requires a similar energy, and a higher one than breaking the C-O bond in nonane-g-HO-TEMPO. In the case of nonane-g-Fluo-TEMPO the results do not follow the right trend. The model using the nonyl radical to simulate the polymer chain is not efficient for this compound (Figure 5.2.2.3), by considering that the fluorocarbon chain should interact with the polymer. However, the nonyl radical is not long enough to exhibit these interactions and the simulation of a polymer chain with higher carbons on backbone would have necessitated a huge computational cost.

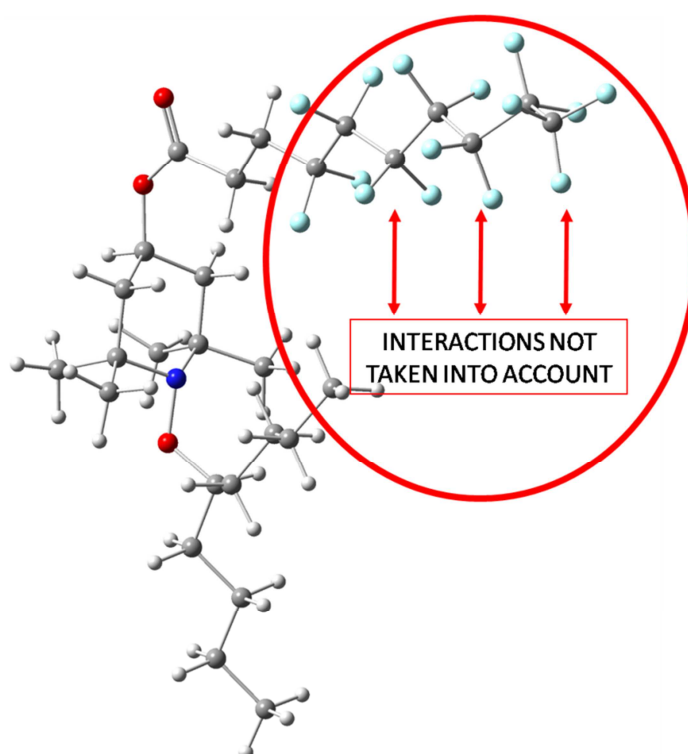


Figure 5.2.2.3: Optimized geometry of Fluo-TEMPO-g-nonane

5.3: Conclusions

The stability of the alkoxyamines $>\text{NO-C}$ bond was here investigated by means of EPR measurements and DFT calculations. Through EPR different detaching temperatures depending on the X-TEMPO substituting group, were measured. This allowed establishing a thermal stability ranking where Fluo-TEMPO appears to be the less stable, followed by HO-TEMPO, and then BzO-TEMPO and NfO-TEMPO which showed similar stability. These experimental data were in good agreement with the DFT energy calculations for all the nitroxides, besides the Fluo-TEMPO. Indeed in this case the employed model to simulate the polymer chain was not efficient to exhibit the interactions between the fluorocarbon chain and the polymer matrix which affect the alkoxyamine stability. On the other hand it was not possible to use a most appropriate model because that would need a huge computational cost. However thanks to these accurate characterizations, an electronic effect of the TEMPO derivative functional group, which influences the bond dissociation enthalpy, was demonstrated

CHAPTER 6

SYNTHESIS OF GRAFTED POLYOLEFINS BY NITROXIDE MEDIATED POLYMERIZATION.

6.1: Controlled grafting of polystyrene onto polyethylene backbone via “grafting from” technique

The objectives of this study is to attempt the functionalization of polyolefins with different TEMPO derivatives here used as “macroinitiators” for the synthesis of polyolefin-*g*-polystyrene graft copolymers via “grafting from” technique using styrene or styrene derivatives as (co)monomers. Generally the grafted chains introduction onto the surface of polymeric substrates can be performed according to three different strategies:

- ✓ “*Grafting to*” approach refers to preformed polymers bearing end-functional groups that can react with suitable functionalities, belonging to the polymer matrix, by means of a covalent bond, by generating a stable tethered polymer brush. A drawback of this method is that only a little amount of macromolecular chains can be immobilized onto the polymer surface. In fact the chains have to diffuse through the existing polymer to reach the specific functional groups, but this turns out to be hard because of the steric repulsion of the polymer chains, that generates a low grafting density¹⁴⁰. In addition another limitation is caused by the creation of impurities of non-grafted polymer chains with the polymer grafted surface which are complicated to eliminate¹⁴¹.
- ✓ “*Grafting through*” approach is based on macromonomers polymerization. The macromolecules are indeed functionalized with polymerizable groups which enable to copolymerize the macromonomers with monomers of a lower molecular weight. In this way a comb-shaped structure can be created with high grafting density of macromolecules¹⁴¹.

- ✓ “*Grafting from*” approach makes use of active species, immobilized onto the polymer surface, to initiate the polymerization of monomers from the surface toward the bulk phase, circumventing the diffusion problem of the “*grafting to*” method¹⁴⁰. Furthermore this procedure allows achieving higher grafting density than the “*grafting to*” method, because in this case there are relatively small molecules, the monomers, that have to reach the surface bound initiator site¹⁴¹.

Specifically in this study the macroalkoxyamines employed as matrices were constituted by polyethylenes as substrates and AzO-TEMPO, ThiO-TEMPO and Fluo-TEMPO as functionalizing agents (see Figure 2.1.1 in Chapter 2). In particular (HDPE)-*g*-(AzO-TEMPO), (HDPE)-*g*-(ThiO-TEMPO) and (EOC)-*g*-(AzO-TEMPO) were obtained through free radical grafting via a post-reactor modification strategy (see Chapter 2, section 2.1), while (LLDPE)-*g*-(Fluo-TEMPO)A and (LLDPE)-*g*-(Fluo-TEMPO)B were prepared through the photografting technique (see Chapter 4, section 4.1). Contrary to all the other methodologies described in literature for the synthesis of this kind of macroalkoxyamines¹⁴²⁻¹⁴⁶, the nitroxides radical coupling reactions, as already described in Chapter 2 and 4, enables to insert specific/complex functionalities by a one step methodology. The process shows, indeed, a great compatibility with different functional groups, allowing the easy and rapid synthesis of the macroinitiators without using metal catalyst.

As regards the polystyrene grafting reaction, it was carried out by taking advantage from the presence of TEMPO, in order to obtain a “Reversible Deactivation Radical Polymerization (RDRP)” according to the scheme reported in Figure 6.1.1 and in agreement with literature on the “*grafting from*” TEMPO functionalized polymers/surfaces¹⁴²⁻¹⁴⁶.

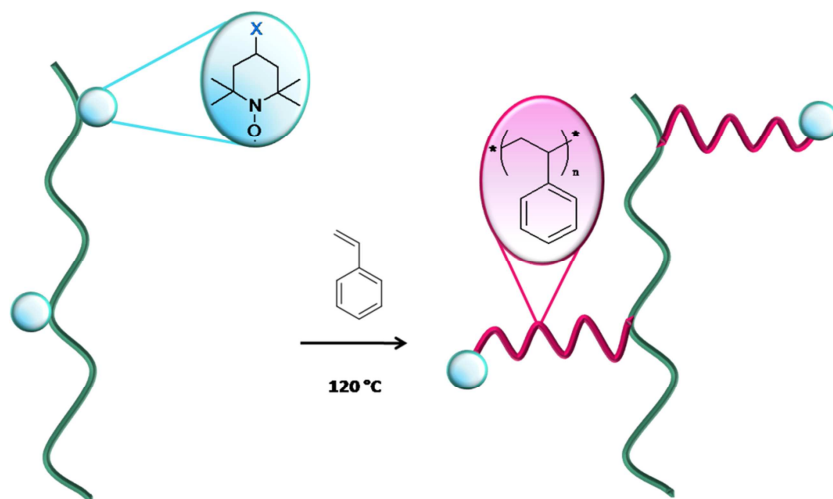


Figure 6.1.1: Schematic representation of the grafting strategy¹⁴²⁻¹⁴⁶.

The establishment of a thermal equilibrium between a (macro)alkoxyamine (dormant) and its free (active) form, is well documented and it constitutes the basis for the Nitroxide Mediated Polymerization (NMP). NMP is, indeed, characterized by a reversible coupling reaction between an alkyl (macro)radical and a nitroxide, acting as controlling agent, to yield a (macro)alkoxyamine as the predominant species. Upon the temperature increasing, the O-C bond between the nitroxide and the alkyl radical, undergoes a homolytic cleavage producing the growing propagating radicals and the nitroxide¹⁴⁷ (Figure 6.1.2).

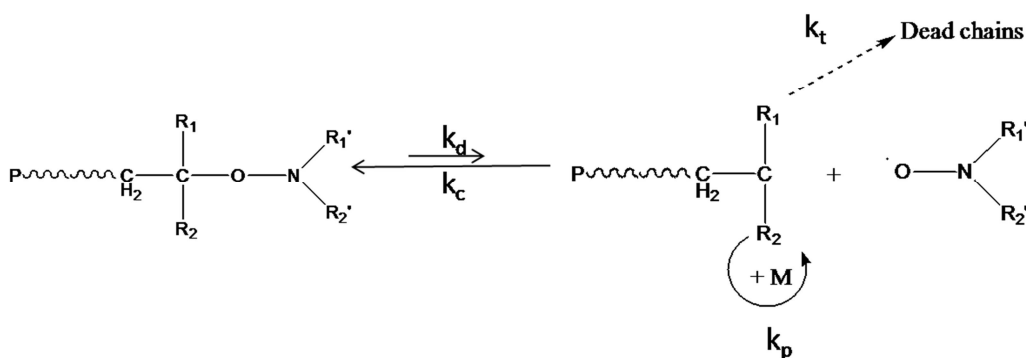


Figure 6.1.2: Reversible activation/deactivation involving the alkoxyamine species

The equilibrium is an exclusively thermal process where neither catalyst nor bimolecular exchange are required. For this reason the polymerization kinetics is governed by both this activation-deactivation equilibrium and the persistent radical effect¹⁴⁷. Furthermore, the O-C bond dissociation energy is strongly dependent on: (a) structure of the nitroxide

and (b) stability of the formed alkyl radical¹⁴⁸. Thus, the choice of the monomer and the nitroxide plays a pivotal role to allow a controlled propagation leading to RDRP.

In 1993, motivated by the awareness that the nitroxides can trap the free radicals, by forming an adduct having a weak bond and, thus, successfully decrease the polymerization rate¹⁴, Georges¹¹ was the first scientist to use a nitroxide in a free radical polymerization. By employing 2,2,6,6-tetramethyl-1-piperidinyloxy (TEMPO) as a controlling agent, benzoyl peroxide (BPO) as initiator and styrene (Sty) as monomer at 123°C, he could obtain polystyrene (PS) with controlled molecular weight and a narrow dispersity (\bar{D} = 1.27). Georges noted the small dispersity was obtained early in the reaction, evidencing that the polymeric chains were initiated all in the same time and the \bar{D} remained narrow during the entire duration of the polymerization, as proof of a pseudo living/controlled process. A further evidence of the controlled behavior of the free radical polymerization was given by the linear increase of the molecular weight with monomer conversion, maintaining narrow \bar{D} . These results opened the way of RDRP by using TEMPO as a controlling agent. The period since the Georges' first experiment was followed by a great number of significant developments in the NMP technique, which largely demonstrated the ability of TEMPO to control the (co)polymerization of Sty or styrene derivatives^{12, 13, 149-153}.

In this scenario, the aim of this study is to investigate the possibility to grow, in a controlled fashion, PS or polystyrene derivatives brushes from the polyolefins backbone. Depending on the technique used to obtain the macroinitiators, two different methodologies were adopted to grow polymer chains: (HDPE)-*g*-(AzO-TEMPO), (HDPE)-*g*-(ThiO-TEMPO) and (EOC)-*g*-(AzO-TEMPO) graft copolymers were dissolved in trichlorobenzene and then mixed with the Sty monomer at 120 °C for 48 h (Method 1). (LLDPE)-*g*-(Fluo-TEMPO)A and (LLDPE)-*g*-(Fluo-TEMPO)B, were dipped in the Sty monomer (liquid) and the embedded films were heated up to 120 °C for 72 h (Method 2). After the polymerization runs, all the samples were cleaned by extraction with chloroform or acetone (see Experimental Part, Chapter 7, section 7.4), with the aim to eliminate the ungrafted PS. In addition the (EOC)-*g*-(AzO-TEMPO) was chosen as matrix to graft, according to the method 1, copolymer brushes constituted by styrene and some styrene derivatives as: pentafluorostyrene (F₅Sty), 4-vinylbenzylchloride (VBC) and sodium 4-styrene sulfonate (SS) (Table 6.1.1). The choice of F₅Sty as comonomer is due to its

particular surface properties conferred to it by the presence of fluorine atoms, which also have the advantage to be easily detected through ^{19}F -NMR spectroscopy¹⁵⁴. Regarding the VBC, it is selected for the presence of $-\text{CH}_2\text{Cl}$ functionality that can be easily substituted with different functional groups by endowing modified materials with specific properties owing to the functional groups^{155, 156}. Finally, the last choice fell on SS thanks to the presence of a sulfonate group which may allow the creation of an amphiphilic material^{149, 157}, as well as protonic exchange (e.g. fuel cell membranes).

Table 6.1.1: Experimental conditions for the radical (co)polymerization of functionalized polyolefins with styrene and styrene derivatives.

Sample	monomer A	monomer B	[monomer]/ [X-TEMPO]	T (°C)	Time (h)
(EOC)- <i>g</i> -(AzO-TEMPO)_PS ^a	Sty	-	180	120	48
(HDPE)- <i>g</i> -(AzO-TEMPO)_PS ^a	Sty	-	180	120	48
(HDPE)- <i>g</i> -(ThiO-TEMPO)_PS ^a	Sty	-	180	120	48
(EOC)- <i>g</i> -(AzO-TEMPO)_PS- <i>co</i> -PF ₅ Sty ^a	Sty	F ₅ Sty	360*	120	48
(EOC)- <i>g</i> -(AzO-TEMPO)_PS- <i>co</i> -PSS ^a	Sty	SS	360*	120	48
(EOC)- <i>g</i> -(AzO-TEMPO)_PS- <i>co</i> -PVBC ^a	Sty	VBC	360*	120	48
(LLDPE)- <i>g</i> -(FluO-TEMPO)A_PS ^b	Sty	-	6900	120	72
(LLDPE)- <i>g</i> -(FluO-TEMPO)B_PS ^b	Sty	-	6900	120	72

Conditions ^a: Solvent used = 1,2,4-trichlorobenzene 10 mL; ^b: Bulk reaction, *: [Sty]/[Sty derivatives]= 1/1

To evaluate the grafting occurrence, the ATR-FTIR spectra of the macroalkoxyamines before and after polymerization of styrene or styrene derivatives, were compared and the attributions suggested by considering the possible structure of the grafted samples. All the spectra were normalized with respect to the band at 720 cm^{-1} attributed to the CH_2 rocking absorption of polyethylene.

Concerning the products obtained according to method 1, no bands ascribable to the comonomers grafting were observed (Figure 6.1.3) with the exception of products labeled (EOC)-*g*-(AzO-TEMPO)_PS and (EOC)-*g*-(AzO-TEMPO)_PS-*co*-PSS graft copolymers.

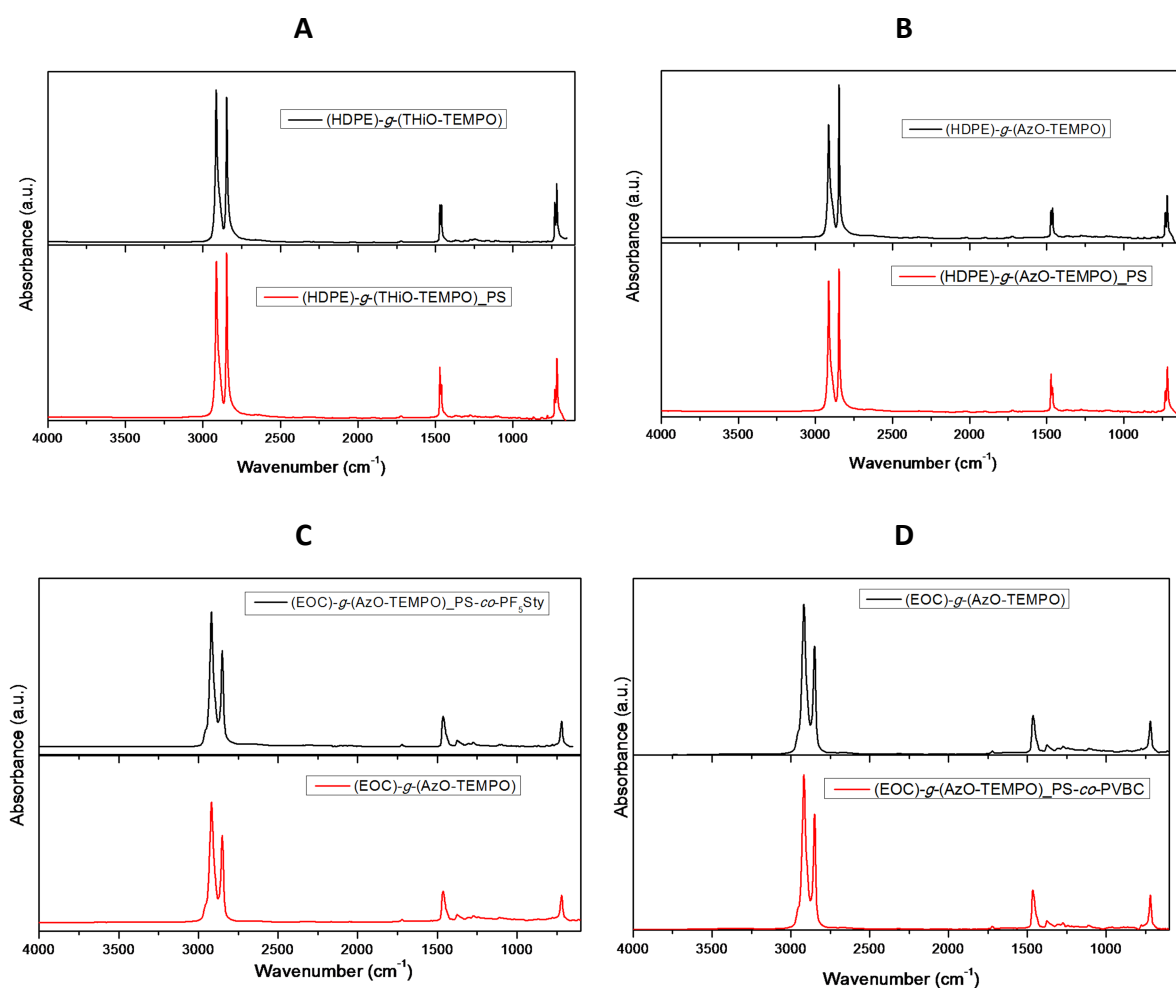


Figure 6.1.3: ATR-FTIR spectra of **A:** (HDPE)-*g*-(THiO-TEMPO) (black line) and (HDPE)-*g*-(THiO-TEMPO)_{PS} (red line), **B:** (HDPE)-*g*-(AzO-TEMPO) (black line) and (HDPE)-*g*-(AzO-TEMPO)_{PS} (red line), **C:** (EOC)-*g*-(AzO-TEMPO) (red line), (EOC)-*g*-(AzO-TEMPO)_{PS-co-PF₅Sty} (black line) and **D:** ATR-FTIR spectra of the (EOC)-*g*-(AzO-TEMPO) (black line), (EOC)-*g*-(AzO-TEMPO)_{PS-co-PVBC} (red line).

Indeed, spectrum of (EOC)-*g*-(AzO-TEMPO)_{PS} sample showed the presence of a band centered at 699 cm^{-1} which may be attributed to the out-of-plane bending of the CH groups in the polystyrene aromatic ring (Figure 6.1.4).

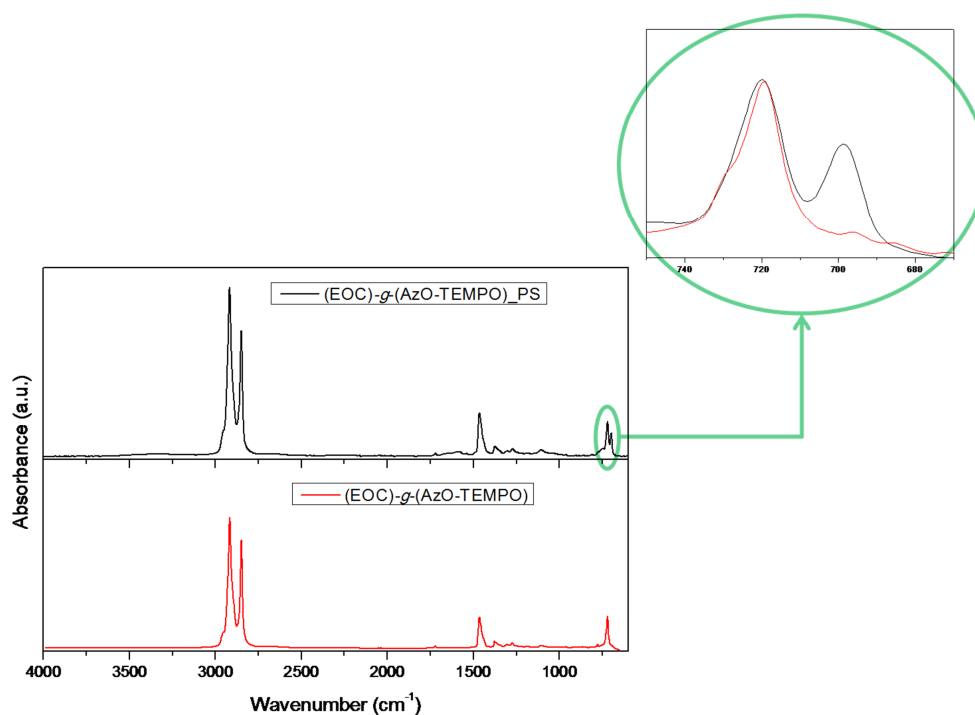


Figure 6.1.4: ATR-FTIR spectra of the (EOC)-g-(AzO-TEMPO) (red line), (EOC)-g-(AzO-TEMPO)_PS (black line).

Furthermore, in the (EOC)-g-(AzO-TEMPO)_PS-co-PSS ATR-FTIR spectrum, a weak band at around 1040 cm^{-1} that may be related to the SO_3 group symmetric vibration^{158, 159}, suggested the grafting of Sty and SS even if with really low yield (Figure 6.1.5).

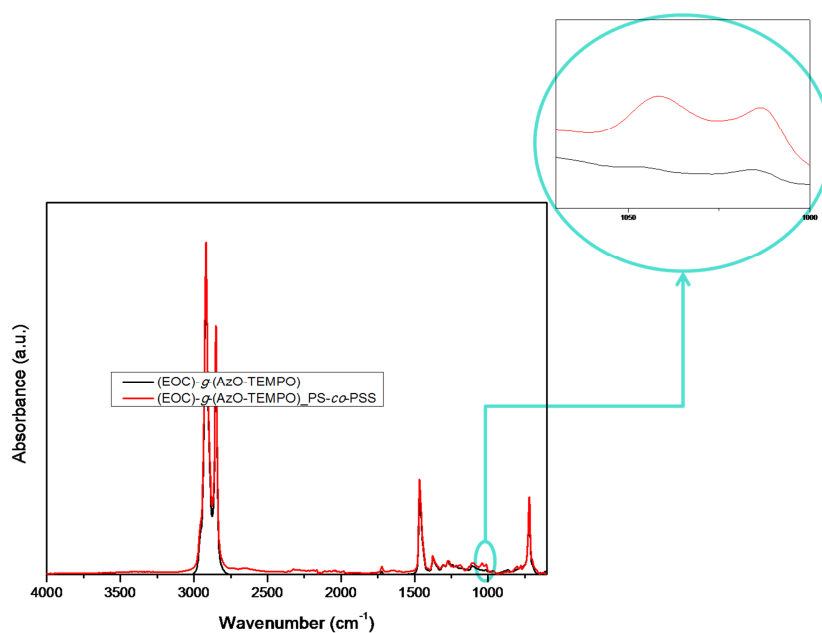


Figure 6.1.5: ATR-FTIR spectra of the (EOC)-g-(AzO-TEMPO) (black line), (EOC)-g-(AzO-TEMPO)_PS-co-PSS (red line).

Therefore on the basis of these preliminary evidences it seems clear that by using the method 1 and macroinitiators derived from possible cleavage of grafted AzO and ThiO-TEMPO, the grafting of Sty or styrene derivatives via copolymerization occurs with very low yield. On the contrary, the ATR-FTIR spectra of the samples obtained according to the method 2 and by using samples derived from Fluo-TEMPO insertion definitely revealed the presence of diagnostic bands of Sty grafting: in particular the signals at 699 and 756 cm^{-1} owing to the out-of-plane bending of the CH groups of the PS aromatic ring, the band at 1493 cm^{-1} attributed to the stretching vibrations of the carbons in the PS aromatic ring, and finally the band at around 1600 cm^{-1} related to the PS aromatic stretching bond were highlighted suggesting even a good covering of films surface (Figure 6.1.6).

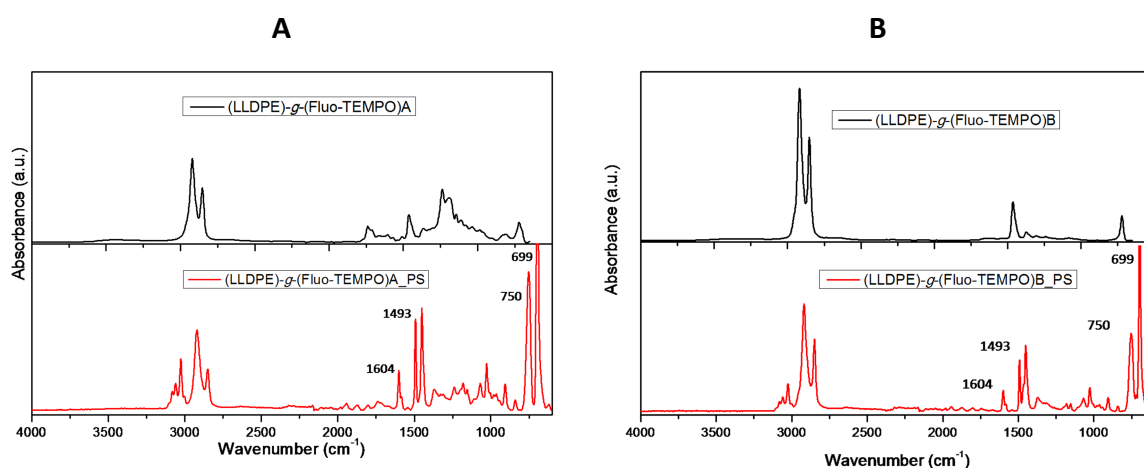


Figure 6.1.6: ATR-FTIR spectra of **A:** (LLDPE)-*g*-(Fluo-TEMPO)A (black line) and (LLDPE)-*g*-(Fluo-TEMPO)A_PS (red line) and **B:** (LLDPE)-*g*-(Fluo-TEMPO)B (black line) and (LLDPE)-*g*-(Fluo-TEMPO)B_PS (red line).

The apparently low grafting yield for the samples derived from method 1, could be due to the use of solvent, which generates a reduction in the polymerization rate and significantly decreases the monomer conversion of TEMPO mediated radical polymerization systems¹⁵⁰. Moreover, in these runs the amount of the monomer was significantly smaller than the quantity used in the method 2 ([Sty]/[TEMPO]= 180 vs [Sty]/[TEMPO]= 6900).

However, the thermal stability of grafted alkoxyamine is a key parameter that plays a fundamental role in these copolymerization reactions. It was showed that the homolytic

cleavage of -C-ON< bond, necessary to initiate the copolymerization reaction, occurs at relatively low temperatures for the moieties derived from Fluo-TEMPO grafting (as provided by EPR, see Chapter 5, section 5.1). They are indeed closer to the reaction temperature (employed for the *grafting from* approach) than those of the other alkoxyamines, justifying the apparent higher yield for (LLDPE)-*g*-(Fluo-TEMPO) samples. Conversely the high thermal stability of grafted AzO and ThiO-TEMPO derivatives (as proved by TGA, see chapter 2, section 2.1.) probably reduces the availability and the amount of species able to initiate the Sty polymerization, with detriment in copolymer grafting yield.

However, in order to investigate the PS chain grafting occurrence more deeply, further characterizations were carried out. First of all, efforts were made to evaluate the content of the grafted PS via gravimetric measurements, namely by weighting the samples before and after the graft copolymerization, but without adequate results. Indeed, regarding the samples prepared through method 1, a negligible weight increase in PS-grafted samples compared with the matrix, made impossible a proper grafting evaluation, whereas for the samples synthesized according to the method 2, the problem was their partial solubility in chloroform during the purification steps (via centrifugation). Anyway the samples were analyzed by TGA under nitrogen flow starting from room temperature up to 600°C at 10 °C/min to tentatively evidencing degradation steps attributable to the different polymer species.

The thermograms of the samples obtained according to the method 1 (Figure 6.1.7) compared to polyethylene starting materials and a PS sample obtained by free radical polymerization, highlighted a behavior similar to that of the starting polyolefins, even if the degradation of the grafted copolymers occurred at lower temperature^{160, 161}. This may be attributed to the breaking of bonds between the polyolefin matrix and the PS brushes; however, the degradation profiles are really similar and, as evidenced by DTG curves, only one step can be detected (Figure 6.1.8). In this condition, it seems that the degradation of the aromatic part in the copolymerized samples is merged with the degradation of the aliphatic polymer backbone and consequently the weight loss due to the styrene moiety cannot be distinguished¹⁶¹. For this reason, it was not possible to calculate a weight lost percentage correlated to the amount of polystyrene grafting.

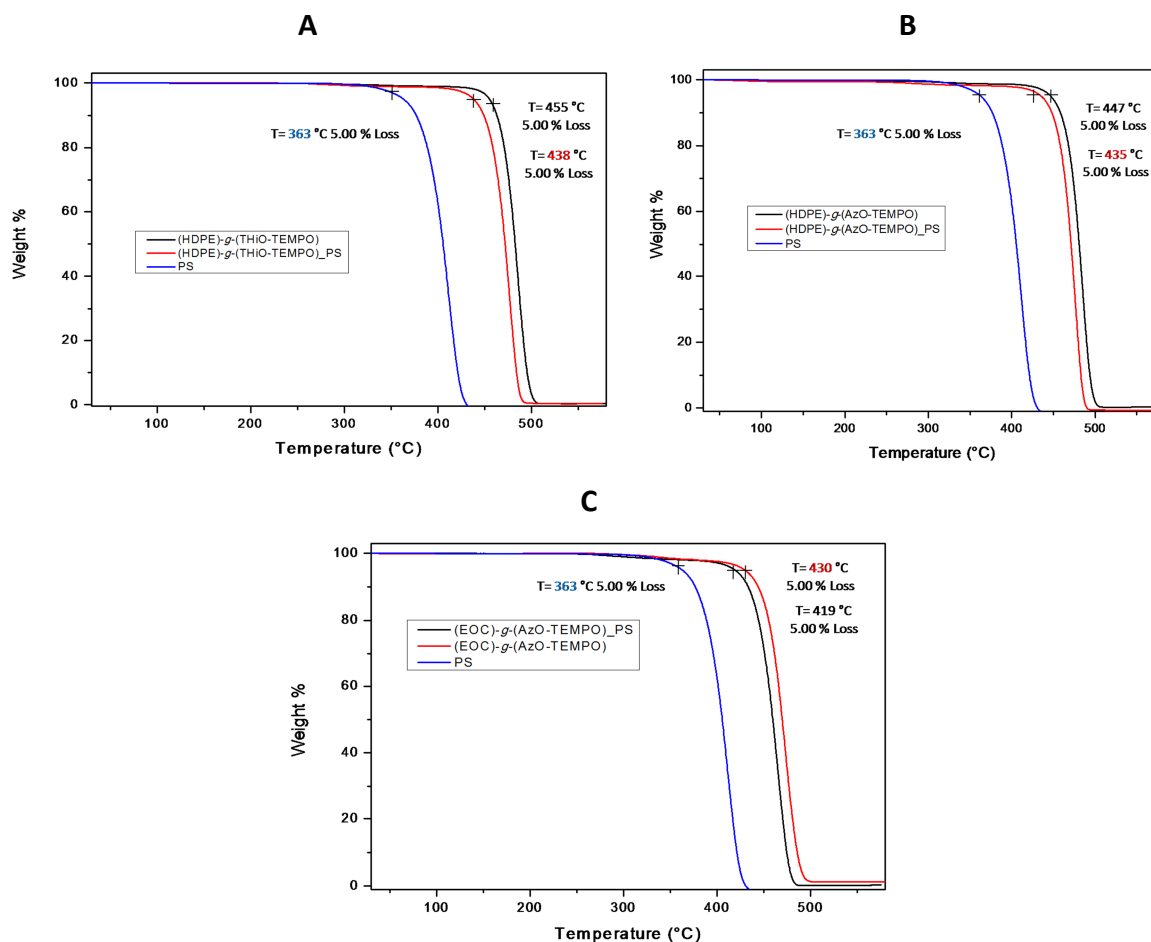


Figure 6.1.7: TGA thermograms of the functionalized HDPE and EOC samples before (black line) and after (red line) the treatment with styrene and the free polystyrene (blue line). The analysis carried out under nitrogen flow.

The DTG curves (Figure 6.1.8) highlighted a difference in the maximum degradation temperature between the starting material and the sample copolymerized with PS of about 10°C; by underlining the decrease of thermostability due to the PS grafting¹⁶².

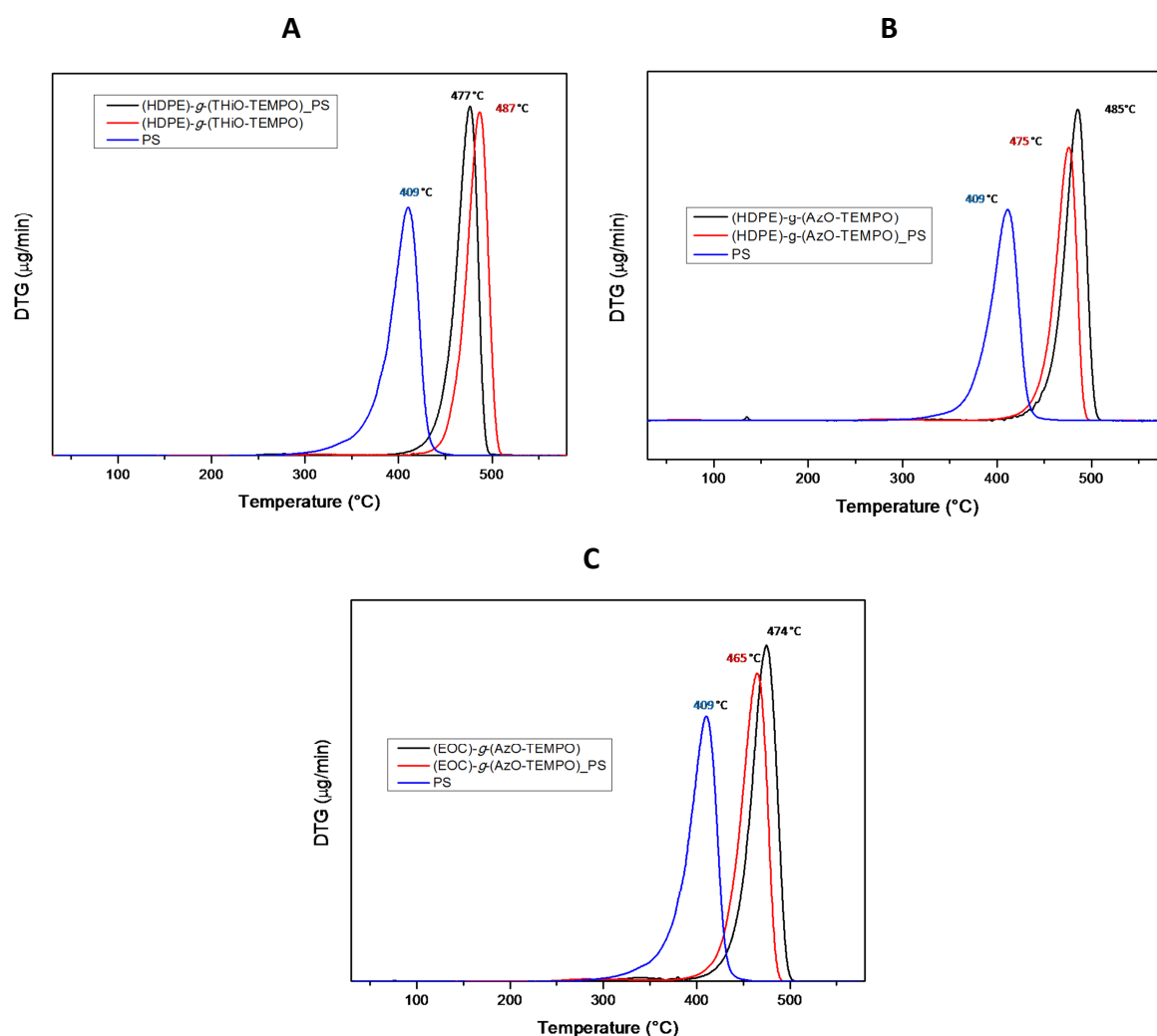


Figure 6.1.8: DTG thermograms of: **A:** ThiO-TEMPO functionalized HDPE macroinitiators (red line), ThiO-TEMPO functionalized HDPE copolymerized with styrene (black line) and free PS (blue line), **B:** AzO-TEMPO functionalized HDPE macroinitiators (black line), AzO-TEMPO functionalized HDPE copolymerized with styrene (red line) and free PS (blue line), **C:** AzO-TEMPO functionalized EOC macroinitiators (black line), AzO-TEMPO functionalized EOC copolymerized with styrene (red line) and free PS (blue line). The analysis carried out under nitrogen flow.

The samples treated with the styrene derivatives as the comonomer underlined a behavior similar to those of the samples grafted with only Sty (Figure 6.1.9).

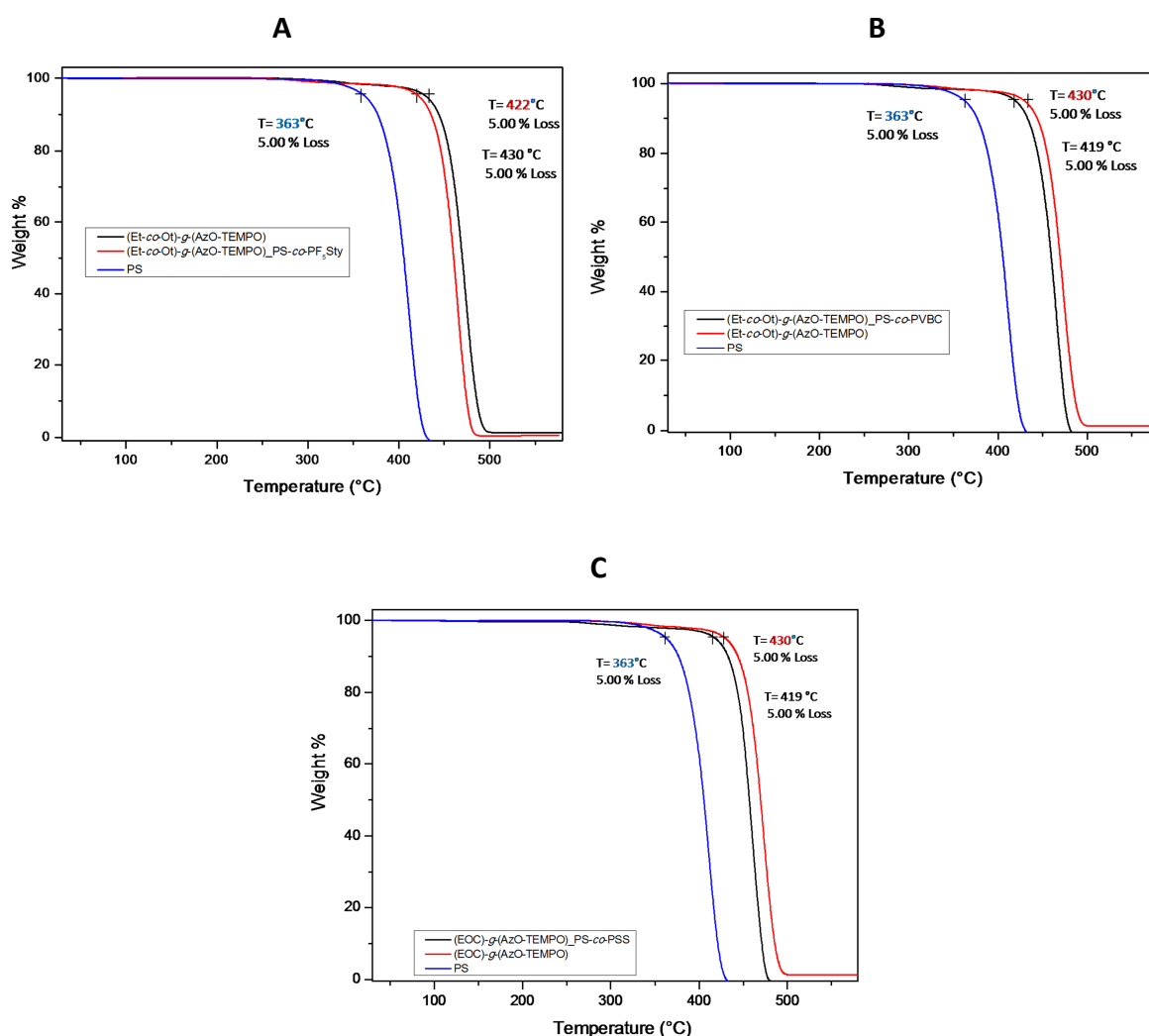


Figure 6.1.9: TGA thermograms of **A:** the (EOC)-g-(AzO-TEMPO) (black line), (EOC)-g-(AzO-TEMPO)_PS-co-PF₃Sty (red line) and pristine polystyrene (blue line), **B:** the (EOC)-g-(AzO-TEMPO) (red line), (EOC)-g-(AzO-TEMPO)_PS-co-PVBC (black line) and pristine polystyrene (blue line) and **C:** the (EOC)-g-(AzO-TEMPO) (red line), (EOC)-g-(AzO-TEMPO)_PS-co-PSS (black line) and pristine polystyrene (blue line). The analysis carried out under nitrogen flow.

In particular, the (EOC)-g-(AzO-TEMPO)_PS-co-PSS thermogram (Figure 6.1.10) evidenced a first degradation step starting at around 100°C which may be attributed to the loss of free and hydrogen bonded water and adsorbed gas molecules due to the presence of highly hydrophilic sulfonic acid groups¹⁶¹. While the second step could represent the cleavage of the brushes bond with the backbone even though, also in this case, the degradation of the polystyrene chains is merged with the degradation of the polyethylene and consequently Sty moiety degradation cannot be distinguished from the matrix¹⁶¹.

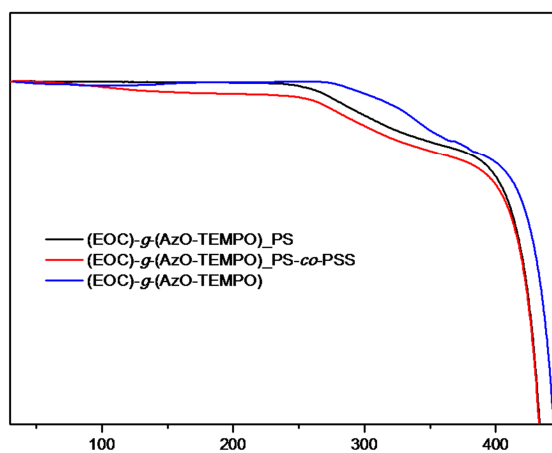
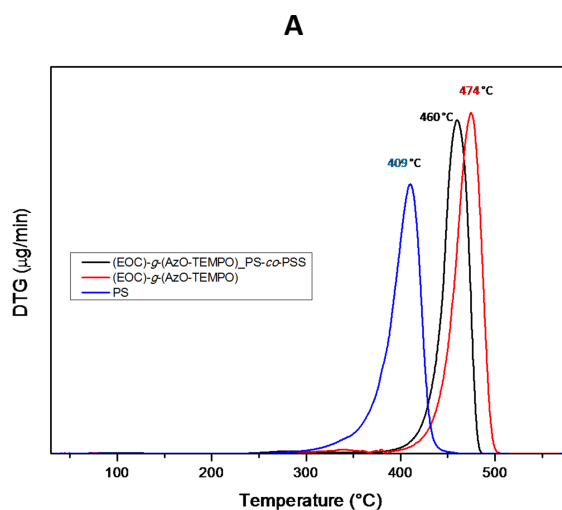


Figure 6.1.10: TGA thermograms of the (EOC)-*g*-(AzO-TEMPO) (blue line), (EOC)-*g*-(AzO-TEMPO)_PS-co-PSS (red line) and (EOC)-*g*-(AzO-TEMPO)_PS (black line). The analysis carried out under nitrogen flow.

The DTG thermograms confirmed the maximum degradation temperature decrease, by stating the copolymer grafting occurrence (Figure 6.1.11).



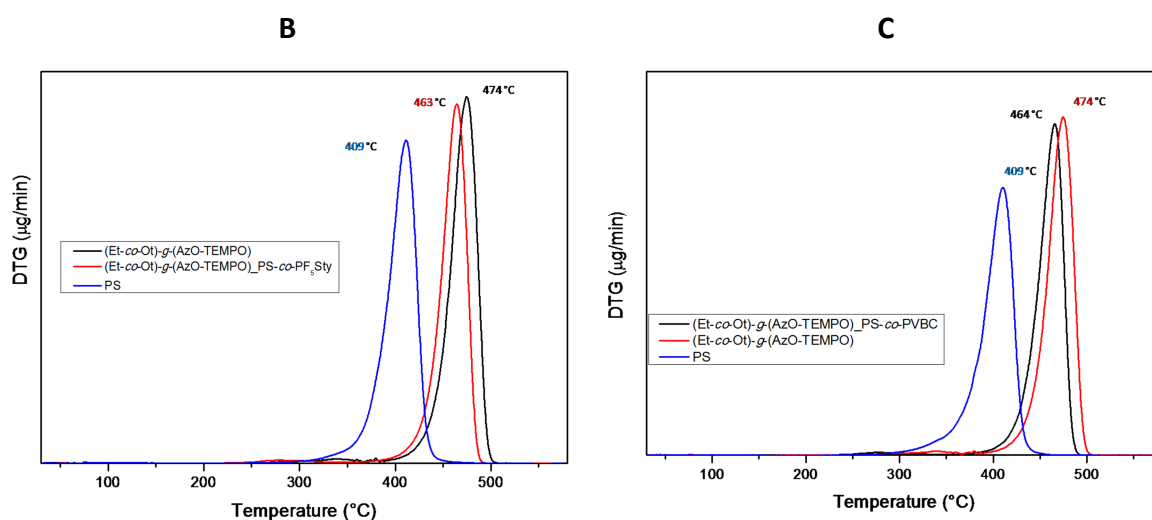


Figure 6.1.11: DTG thermograms of **A:** AzO-TEMPO functionalized EOC macroinitiators (red line), AzO-TEMPO functionalized EOC copolymerized with styrene and sodium 4-styrene sulfonate (black line) and free PS (blue line), **B:** AzO-TEMPO functionalized EOC macroinitiators (black line), AzO-TEMPO functionalized EOC copolymerized with styrene and pentafluoro styrene (red line) and free PS (blue line) and **C:** AzO-TEMPO functionalized EOC macroinitiators (red line), AzO-TEMPO functionalized EOC copolymerized with styrene and vinylbenzyl chloride (black line) and free PS (blue line). The analysis carried out under nitrogen flow.

As regards the samples obtained by method 2 namely polyethylene samples grafted with Fluo-TEMPO, the thermograms of the copolymers, compared with the curves collected for the matrices, showed significant difference in terms of thermal stability: in both cases the copolymers provided by *grafting from* approach evidenced a shift in the temperature (at maximum rate of degradation, DTG curves) of about 50 °C toward the temperature characteristic of PS. Moreover a bimodal peak suggesting the presence of copolymer fractions having thermal stability depending on their composition, likely meaning different LLDPE/polystyrene ratios, can be noticed, even if also in this case the evaluation of the amount of grafted PS chains is not possible. (Figures 6.1.12, 6.1.13, and 6.1.14).

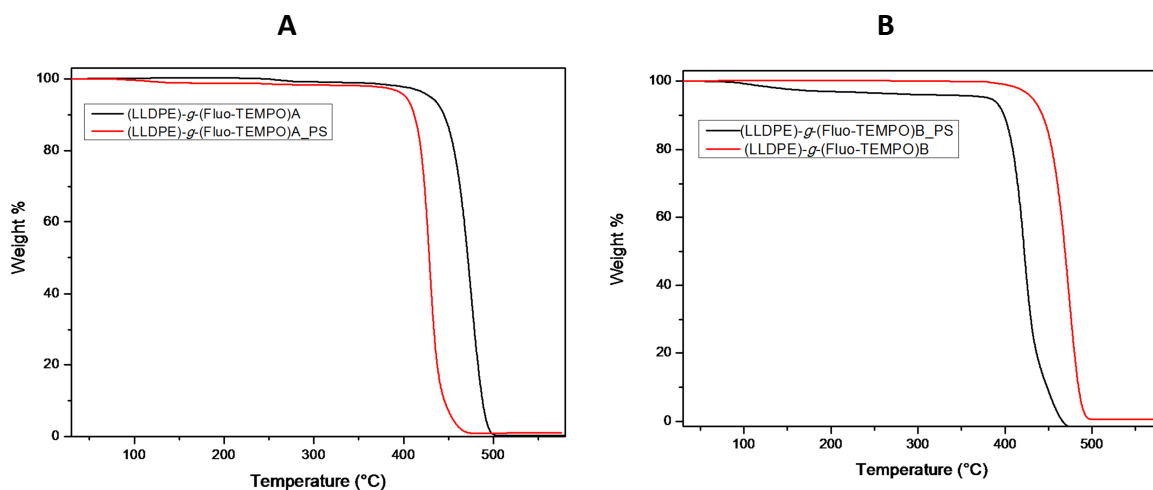


Figure 6.1.12: TGA thermograms of **A:** (LLDPE)-*g*-(Fluo-TEMPO)A_{PS} (black line) and the (LLDPE)-*g*-(Fluo-TEMPO)A (red line) and **B:** (LLDPE)-*g*-(Fluo-TEMPO)B_{PS} (black line) and the (LLDPE)-*g*-(Fluo-TEMPO)B (red line). The analysis carried out under nitrogen flow.

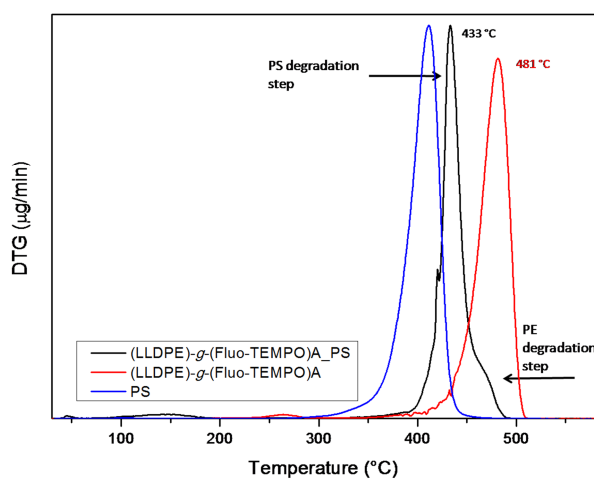


Figure 6.1.13: DTG curves of (LLDPE)-*g*-(Fluo-TEMPO)A (red line), (LLDPE)-*g*-(Fluo-TEMPO)A_{PS} (black line) and PS (blue line). The analysis carried out under nitrogen flow.

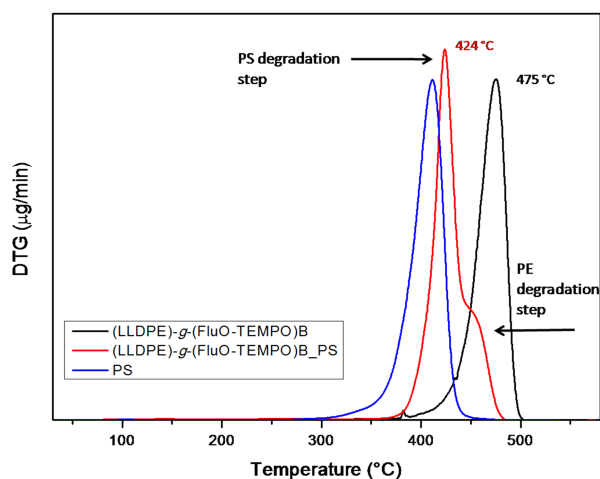
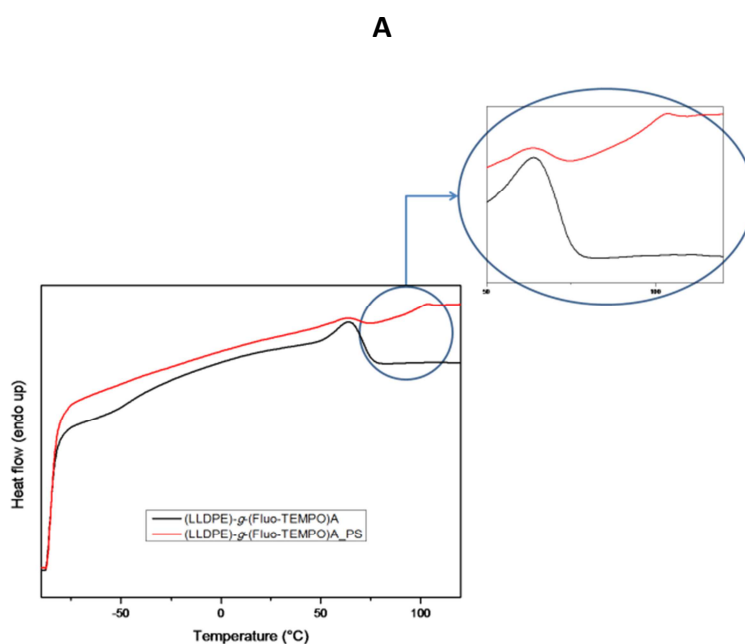


Figure 6.1.14: DTG curves of (LLDPE)-*g*-(Fluo-TEMPO)B (black line), (LLDPE)-*g*-(Fluo-TEMPO)B_PS (red line) and PS (blue line). The analysis carried out under nitrogen flow.

Differential Scanning Calorimetry (DSC) analysis were carried out and the thermogram of each sample was recorded in the second heating run at 10 °C/min to eliminate the thermal history (Figure 6.1.15).



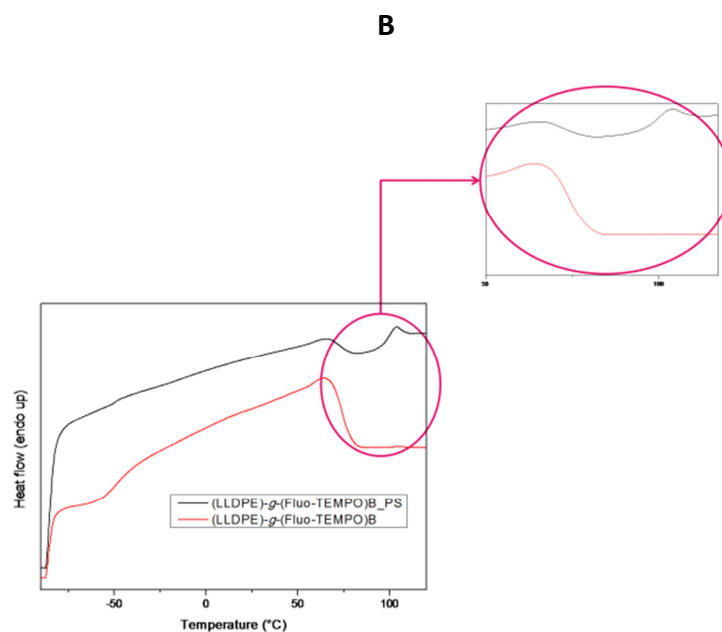


Figure 6.1.16: DSC curves of **A:** (LLDPE)-*g*-(Fluo-TEMPO)B (black line), (LLDPE)-*g*-(Fluo-TEMPO)B_PS (red line) and **B:** (LLDPE)-*g*-(Fluo-TEMPO)A (black line), (LLDPE)-*g*-(Fluo-TEMPO)A_PS (red line).

By comparing the macroinitiators DSC curves before and after the treatment with styrene, appeared the clear presence of a second order transition at around 93 °C which may be related to the PS T_g . These observations further evidenced the successfully PS grafting from the polyolefin matrix.

6.2. Conclusions

In this Chapter macroalkoxyamines obtained through the NRC reaction of AzO-TEMPO, ThiO-TEMPO and Fluo-TEMPO with polyolefin macroradicals, were used as macroinitiators for the synthesis of polyolefin-*g*-polystyrene graft copolymers via “grafting from” technique using styrene or styrene derivatives as (co)monomers.

ATR-FTIR, TGA and DSC analysis fully highlighted the grafting occurrence: in particular the obtained thermograms showed a lower degradation temperature for the polyolefins treated with the comonomer compared to the matrices. This behavior was caused by the breaking of bonds between the polyolefin and the PS brushes. However the TGA curves did not allow quantifying the PS grafted amount, but it can undoubtedly state that the

grafting yield was significantly higher when macroalkoxyamines bearing Fluo-TEMPO were used as matrices. The reason of this lies in different factors: first of all the grafting reaction onto polyolefins functionalized with AzO- and ThiO-TEMPO was carried out with lower amount of comonomer and in presence of solvent which caused a reduction in the polymerization rate and significantly limited the monomer conversion. In addition the same alkoxyamines showed higher thermal stability than (LLDPE)-g-(Fluo-TEMPO) by reducing the availability and the amount of species able to initiate the styrene polymerization, with detriment in copolymer grafting yield.

In conclusion, the obtained functional macroalkoxyamines can be considered as “activated compounds” which can be interestingly used later time as macroinitiators to synthesize polymer materials with tuned/tailored structures and fascinating properties.

Experimental Part

CHAPTER 7

EXPERIMENTAL PART

7.1: Materials

The used materials are grouped in two different tables: in the first all the commercial available nitroxides or materials required for the new ones synthesis; the materials required for the polyolefins modification by means of free radical grafting or by photografting technique; and the materials required for the copolymerization reaction between the modified polyolefins and styrene or styrene derivatives through Nitroxide Mediated Polymerization, are grouped together (Table 7.1.1). In the second table all the polymer matrix used in this project are listed (Table 7.1.2).

Table 7.1.1: Chemicals used

Materials	Formula/ Abbreviations	Characteristics
		Origin
4-Hydroxy-2,2,6,6-tetramethylpiperidine-1-oxyl	HO-TEMPO	Fluka
4-benzoyloxy- 2,2,6,6-tetramethylpiperidine-1-oxyl	BzO-TEMPO	Fluka
4-(phenylazo)benzoyl chloride	-	Sigma Aldrich
triethylamine	Et ₃ N	Sigma Aldrich
4-aminobenzoic acid	-	Sigma Aldrich
tetrafluoroboric acid	HF ₄	Sigma Aldrich
4-aminobenzoic acid	-	Sigma Aldrich
sodium nitrite	NaNO ₂	Sigma Aldrich
2-bromothiophene	-	Sigma Aldrich
tetrahydrofuran	THF	Sigma Aldrich
N,N'-dicyclohexylcarbodiimide*	DCC	Sigma Aldrich

Experimental Part

Ilaria Domenichelli

4-dimethylaminopyridine*	DMAP	Sigma Aldrich
dimethylsulfoxide-d ₆	DMSO-d ₆	Sigma Aldrich
Dioxane	-	Sigma Aldrich
acetonitrile	AcN	Sigma Aldrich
4,4,5,5,6,6,7,7,8,8,9,9,9- Tridecafluorononanoicacid	F	Sigma Aldrich
1-naphtoic acid	NfCOOH	Sigma Aldrich
1-naphtoyl chloride	NfCl	Sigma Aldrich
Dichloromethane*	DCM	Sigma Aldrich
Benzoyl peroxide	BPO	Sigma Aldrich
Chloroform-d	CDCl ₃	Sigma Aldrich
1,4-dinitrobenzene	-	Sigma Aldrich
1,4-dimethoxybenzene	-	Sigma Aldrich
trans-2-[3-(4-tert-butylphenyl)-2-methyl-2- propenylidene]	-	Sigma Aldrich
malononitrile		
Di(tert-butylperoxy-isopropyl)benzene (mixture of isomers)	DTBPIB, Perkadox 14S-FL	Akzo Nobel
4-methoxybenzophenone	MeOBP	Sigma Aldrich
Diethylether	-	Sigma Aldrich
1-vinyl-2-pyrrolidinone	NVP	Sigma Aldrich
Styrene	Sty	Sigma Aldrich
Pentafluoro styrene	F ₅ STy	Sigma Aldrich
4-styrene sulfonate	SS	Sigma Aldrich
Vinylbenzylchloride	VBC	Sigma Aldrich
Acetone	-	Sigma Aldrich
Chloroform	-	Sigma Aldrich
Toluene	-	Sigma Aldrich
1,2,4-trichlorobenzene	-	Sigma Aldrich

Experimental Part

Ilaria Domenichelli

*DCC: was washed with ethyl acetate/dichloromethane (1/9; vol/vol), dried on magnesium sulfate over night, filtered and dried under vacuum; DMAP was recrystallized from toluene; DCM was refluxed over CaH₂ for 4 h and distilled under nitrogen.

**Fluka pre-coated aluminum F254 silica gel 60 sheets were used for TLC analyses. Purifications by flash-chromatography were performed using silica gel Merck 60 (particle size 0.040–0.063 mm). All the reactions were performed under argon by standard syringe, cannula and septa techniques.

Table 7.1.2: Polymer matrix

Material	Abbreviation	Characteristics					
		Origin	M _n (g/mol)	M _w (g/mol)	Dispersity	Density (g/cm ³)	MFR
High density polyethylene	HDPE	Lacqtene 2070MN60 Arkema	21000	86000	4.10	0.96	7g/10min (2.16Kg at 190°C)
Random copolymer ethylene/ α -olefin	EOC	-	50000	102000	2.15	0.87	4.7g/10min (2.16Kg at 190°C)
Poly(butylene succinate)	PBS	Bionolle 1001 Showa High Polymer Co	17700	42180	2.38	-	1.5 g/10min (2.16 kg at 190 °C)
Poly(lactic acid)	PLA	2002D 96% L-lactide NatureWorks	111460	199340	1.79	-	4-8 g/10min (2.16 kg at 190 °C)
Polystyrene- <i>b</i> -poly(ethylene- <i>co</i> -butylene)- <i>b</i> -polystyrene	SEBS	Kraton G1657M, Kraton Polymers	-	-	-	-	22g/10min (5Kg at 230°C)
Linear low density polyethylene (copolymer ethylene- α -olefin)	LLDPE	-	-	-	-	-	-

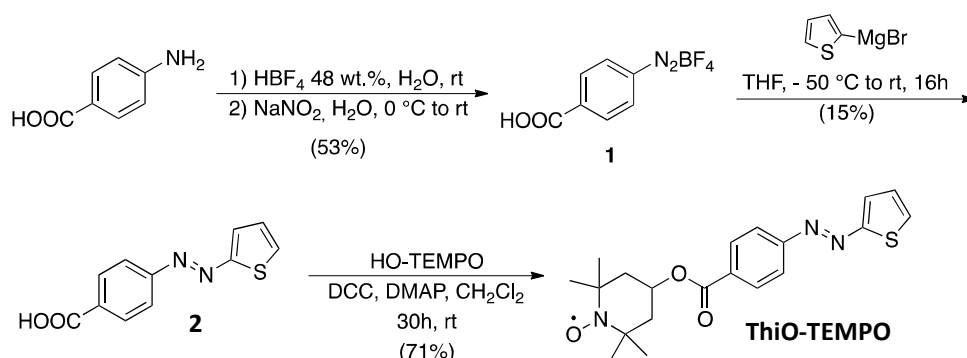
7.2: SYNTHESIS OF NITROXIDES

7.2.1: Synthesis of 4-(phenylazo)benzoyl-2,2,6,6-tetramethylpiperidine-1-oxyl radical (AzO-TEMPO)

A solution of 4-(phenylazo)benzoyl chloride (0.71 g, 2.9×10^{-3} mol), HO-TEMPO (0.5 g, 2.9 mmol) and triethylamine (0.47 mL, 2.9 mmol) in dichloromethane (20 mL) was mixed at room temperature under nitrogen for 24 h. Crude mixture was hydrolyzed with water (50 mL) and extracted with dichloromethane (3x50 mL). AzO-TEMPO was purified by column chromatography by using toluene/ethyl acetate (8/2) as eluting mixture. Yield 80%. Melting point = 130°C^{47} ; MS(Cl): m/z: 381 [M + 1], 380 [M]; FT-IR (KBr): $\nu = 3055, 2970, 2936, 1717, 1468, 1407, 1316, 1279, 1240, 1179, 1112, 865, 776, 691 \text{ cm}^{-1}$. $\text{C}_{22}\text{H}_{26}\text{N}_3\text{O}_3$ Calculated C, 69.45; H, 6.89; N, 11.04. Found: C, 69.40; H, 6.87; N, 11.00.

7.2.2: Synthesis of 4-(2-thienylazo)-benzoyl-2,2,6,6-tetramethylpiperidine-1-oxyl radical (ThiO-TEMPO)

The synthesis of ThiO-TEMPO was carried out as reported in Scheme 7.2.2.1.



Scheme 7.2.2.1: Synthesis of 4-(2-thienylazo)-benzoyl-2,2,6,6-tetramethylpiperidine-1-oxyl radical (ThiO-TEMPO)

Synthesis of *p*-carboxybenzenediazonium tetrafluoroborate (1)¹⁶³

4-Aminobenzoic acid (6.86 g, 50 mmol) was dissolved in a solution of tetrafluoroboric acid (48 wt. % in water, 26.2 mL, 36.58 g, 200 mmol) and water (50 mL). The mixture was stirred at room temperature until the aminobenzoic acid was completely dissolved, and

then cooled at 0 °C (some precipitation of solid occurred). The solution was maintained at 0 °C and a solution of sodium nitrite (3.65 g, 53 mmol) in water (10 mL) was added dropwise within 30 minutes. During the addition it was observed the precipitation of a solid. At the end of the addition the mixture was allowed to warm to room temperature, which caused the complete dissolution of the solid. The reaction mixture was then cooled to 5 °C, and the resulting solid was recovered by filtration, washed with cold diethyl ether and dried in vacuo, giving 1 as a colorless solid (6.25 g, 53 % yield). ¹H-NMR (DMSO-d₆) δ 8.80 (m, J = 7.8 Hz, 2H); 8.45 (m, J = 7.8 Hz, 2H). ¹⁹F-NMR (DMSO-d₆) δ -148.2; -148.3.

Synthesis of 4-(2-thienylazo)-benzoic acid (2)

According to the procedure reported in the literature for the synthesis of 4-(2-thienylazo)-N,N-diethylaniline⁴⁸ to a suspension of magnesium turnings (0.734 g, 30.2 mmol) in tetrahydrofuran (10 mL) was added dropwise a solution of 2-bromothiophene (2.9 mL, 4.89 g, 30 mmol) in tetrahydrofuran (20 mL) at room temperature (an exothermic reaction was observed). After all the magnesium was consumed (3 hours), the resulting solution was added via cannula to a suspension of p-carboxybenzenediazonium tetrafluoroborate (1) (3.54 g, 15 mmol) in a mixture of tetrahydrofuran and dioxane (5/2, 70 mL) cooled at -50 °C. After the addition, the resulting deep red mixture was allowed to warm to room temperature and stirred overnight. The reaction mixture was then quenched with a saturated aqueous sodium carbonate solution and washed with ethyl acetate. The aqueous basic phase was acidified to pH = 5 with acetic acid and extracted with ethyl acetate (4 x 30 mL) and with dichloromethane (2 x 30 mL). The collected organic extracts were dried on anhydrous sodium sulfate, concentrated in vacuum and the residue was purified by flash chromatography on silica gel using a mixture of n-hexane and ethyl acetate (50:50) as eluent, to yield 2 (0.46 g, 15 %) as an orange solid.

MS [m/z]: 232 (86) [M⁺]; 121 (26); 111 (100); 83 (48); 65 (26); 39 (36).

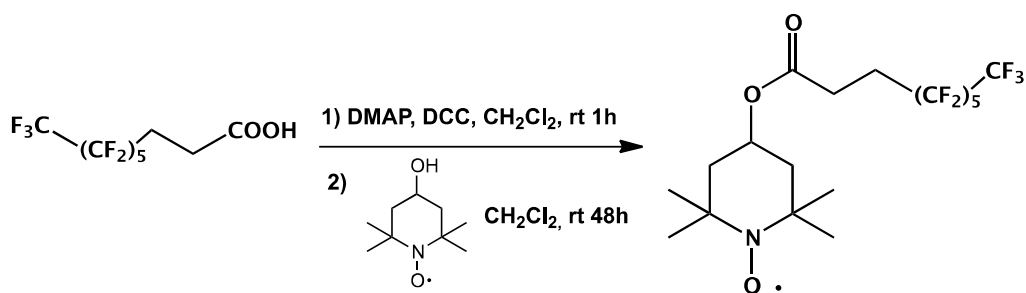
¹H NMR (DMSO- d₆) δ 8.13 (m, J = 8.5 Hz, 2H); 7.92 (dd, J = 3.9 Hz, J = 1.2 Hz, 1H); 7.88 (m, J = 8.5 Hz, 2H); 7.66 (dd, J = 5.2 Hz, J = 1.2 Hz, 1H); 7.25 (dd, J = 5.2 Hz, J = 3.9 Hz, 1H).

Synthesis of 4-(2-thienylazo)-benzoyl-2,2,6,6-tetramethylpiperidine-1-oxyl radical (ThiO-TEMPO)

To a suspension of 2 (0.46 g, 2 mmol) and 4-hydroxy-2,2,6,6-tetramethylpiperidine-1-oxyl (0.35 g, 2 mmol) in dichloromethane (50 mL) was added N,N'-dicyclohexylcarbodiimide (0.49 g, 2.4 mmol) and 4-dimethylaminopyridine (0.29 g, 2.4 mmol). The resulting clear solution was stirred at room temperature for 30 h, during the reaction a precipitate was formed. At the end of the reaction dichloromethane was added and the suspension was filtered on Celite. The crude product was purified by flash chromatography on silica gel using a mixture of toluene and ethyl acetate (85:15) as the eluent, to give TiO-TEMPO as a deep orange solid (0.54 g, 71%). Melting point = 155-158 °C; MS(Cl): m/z: 386 [M] ; FT-IR (KBr): $\nu = 3080, 2970, 2936, 1717, 1468, 1411, 1316, 1279, 1240, 1179, 1112, 865, 776, 711 \text{ cm}^{-1}$. Anal. Calc. for $\text{C}_{20}\text{H}_{24}\text{N}_3\text{SO}_3$: C, 62.15; H, 6.26; N, 10.87; S, 8.30. Found: C, 62.10; H, 6.21; N, 10.82; S, 8.28%.

7.2.3: Synthesis of 2,2,6,6-tetramethylpiperidine-1-oxyl-4-yl 4,4,4,5,5,6,6,7,7,8,8,9,9,9-tridecafluorononanoate (Fluo-TEMPO)

The synthesis of Fluo-TEMPO was carried out as reported in Scheme 7.2.3.1.



Scheme 7.2.3.1: Synthesis of 4-(4,4,4,5,5,6,6,7,7,8,8,9,9,9-tridecafluorononanoate)-2,2,6,6-tetramethylpiperidine-1-oxyl (Fluo-TEMPO)

In a three-necked round bottom flask were introduced 0.718 g (1.83 mmol) of 4,4,4,5,5,6,6,7,7,8,8,9,9,9-tridecafluorononanoic acid and 0.045 g (0.37 mmol) of DMAP in 10 mL of anhydrous dichloromethane, followed by addition of 0.378 g (1.83 mmol) of DCC in 4 mL of dichloromethane. The resulting mixture was stirred under nitrogen atmosphere for 1h. Then, a solution of 0.315 g (1.85 mmol) of HO-TEMPO in 6 mL of anhydrous dichloromethane was added. The reaction mixture was refluxed for 48h at ambient

temperature. The solution was cooled and the precipitate was filtered off. The organic solid was washed with 5% NaHCO₃, 5% HCl and water, each time with 50 mL of solution until neutrality. The organic phase was dried with anhydrous sodium sulfate overnight, and finally evaporated to dryness under vacuum.

The resulting solid was purified by column chromatography by using silica gel as stationary phase and dichloromethane/ethyl acetate (95/5 vol/vol) as eluant. Finally the yield of product is 22 %. m.p. 60–61°C. IR (KBr): $\nu = 2980, 2850, 1740, 1145-984 \text{ cm}^{-1}$. MS (ESI): m/z: 547 [M+1], 532 [M-14]; elemental analysis calc (%) for C₁₈H₂₁F₁₃NO₃ (546): C 39.56, H 3.85, F 45.24, N 2.56

7.2.4: Synthesis of 4-(1-naphthoate)-2,2,6,6-tetramethylpiperidine-1-oxyl (NfO-TEMPO)

The synthesis of NfO-TEMPO was carried out like in a previous paper⁸. To a solution of 4-hydroxy-2,2,6,6-tetramethylpiperidine-1-oxyl (914 mg, 5.3 mmol) in 20 mL of dichloromethane, 0.80 mL of 1-naphthoylchloride (2.65 mmol) and 0.42 mL of triethylamine (2.65 mmol) were added. The resulting mixture has been stirred under inert atmosphere for 24 h. The reaction was hydrolyzed with water (50 mL), the organic phase was extracted twice with water (2 × 50 mL). The dichloromethane phase was dried over anhydrous sodium sulfate then solvent was removed under reduced pressure. The resulting orange solid was purified by column chromatography by using silica gel as stationary phase and dichloromethane as eluant. The NfO-TEMPO was recovered from the second orange band which eluded as a micro-crystalline orange solid (yield 52%). m.p. 99–100 °C (lit. 100–102 °C).

IR (KBr): $\nu = 3052, 2974, 2937, 2863, 1713, 1593, 1577, 1510, 1462, 1377, 1364, 1311, 1278, 1216, 1197, 1180, 1134, 1075, 1030, 1013, 872, 815, 559, 509 \text{ cm}^{-1}$; MS(Cl): m/z: 349 [M + 23], 327 [M + 1], 346 [M]; elemental analysis calc (%) for C₂₀H₂₄NO₃ (326.42): C 73.59, H 7.41, N 4.29; found: C 73.49, H 7.20, N 4.11.

7.3: POLYMERS MODIFICATION THROUGH TEMPO DERIVATIVES

7.3.1: Polyolefins melt functionalization procedure

The melt reactions were carried out in an internal batch mixer (BrabenderPlastographOHG47055) with a chamber of 30 mL. Torque and temperature data were acquired by Brabender Mixing software Win-Mix ver.1.0. Functionalization of HDPE was carried out at 190°C, 50 rpm for 20 min. 20 g of polymer were introduced in the hot brabender and after the melting, 0.145 mol% of ThiO-TEMPO or AzO-TEMPO were added and one minute later 0.043 mol% of DTBPIB in the ThiO and AzO-TEMPO was introduced in the brabender chamber (Table 7.3.1). Functionalized crude samples were cut in small pieces and extracted with boiling acetone for 16 h and further purified by dissolution in hot xylene and precipitation from acetone. Samples were dried to constant weight and analyzed.

Melt functionalization of the random copolymer ethylene/ α -olefin (EOC) was carried out at 170 °C, 50 rpm for 20 min by adopting the same procedure described for the preparation of functionalized HDPE samples. In this case 0.28 mol% of AzO-TEMPO and 0.09 mol% of DTBPIB or 0.17 mol% of Fluo-TEMPO and 0.057 mol% of DTBPIB were used (Table 7.3.1.1). Crude sample was extracted with boiling acetone for 16 h in order to remove all low molecular weight sub-products and it was further purified by dissolution in hot toluene (80 °C) and collected by precipitation of the toluene solution in acetone. The purified sample was dried to constant weight and analyzed.

The functionalization degree (FD) of the functionalized polymers was evaluated by using the FT-IR spectroscopy⁹. Particularly, in the case of functionalized EOC with AzO-TEMPO, the FD was evaluated by using a previously described calibration curve⁹ where the ratio between the area of a peak at 1112 cm⁻¹ (associated to the grafted specie) and that of the methylene rocking of polyethylene at 720 cm⁻¹ was considered. In the case of HDPE, in the spectral region near 700 cm⁻¹ two peaks are present at about 720 cm⁻¹ and 730 cm⁻¹ attributed to the crystalline phase of HDPE. These two peaks are superimposed to a broad band centered ad about 723 cm⁻¹ associated with the amorphous phase of the polymer matrix¹⁶⁴. To evaluate the FD of HDPE functionalized samples (Table 7.3.1.1), total area of all peaks in the region between 700 and 740 cm⁻¹ was considered as representative of the

total amount of methylene groups¹⁶⁵, and the same calibration curve used in the case of EOC was applied.

In the case of EOC functionalized with Fluo-TEMPO the FTIR calibration curve was prepared *ad hoc* (See section 7.5.6)

Table 7.3.1.1: Radical functionalization of polyolefins: feed composition, functionalization degree (FD) and thermal properties

Sample name	Feed composition		Functionalization Degree ¹		Thermal properties	
	X-TEMPO ² (mol%)	Peroxide (mol%)	FD _{FT-IR} ³ (mol%)	FD _{TGA} ⁴ (mol%)	T _{5%} ⁵ (°C)	T _{max} ⁶ (°C)
EOC ⁷	-	-	-	-	440	470
HDPE ⁷	-	-	-	-	456	488
(EOC)-g-(AzO-TEMPO)	0.28	0.09	0.18	0.20	430	475
HDPE-g-(AzO-TEMPO)	0.14	0.04	0.12	0.09	447	486
HDPE-g-(ThiO-TEMPO)	0.14	0.04	0.11	0.08	455	487
(EOC)-g-(Fluo-TEMPO)	0.17	0.057	0.08	0.11	422	472

¹Functionalization Degree (FD): moles of the grafted functional groups with respect to 100 moles of monomer repeating units. ²X-TEMPO: functional TEMPO derivative. ³FD evaluated by FT-IR analysis. ⁴FD evaluated by TGA analysis under nitrogen. ⁵Temperature corresponding to 5% weight loss. ⁶Maximum degradation temperature. ⁷co-EO and HDPE starting polymers.

7.3.2: Polyesters melt functionalization procedure

The PBS functionalization reactions using BPO as a peroxide were performed at 120 °C, 50 rpm and 6 min (6 min was selected as the time of mixing since the half-life of BPO at 120 °C is about 3 min) (Table 7.3.2.1). The functionalization of PBS using DTBPIB as a radical initiator was carried out at 150 °C, 50 rpm and 14 min (14 min was selected as the time of mixing since the half-life of DTBPIB at 150 °C is about 10.6 min) (Table 7.3.2.1). In a typical experiment, 25 g of PBS were introduced in the hot Brabender chamber, the functionalizing agent was added two minutes after the matrix melted and the peroxide was introduced in the Brabender chamber one minute later. In order to remove unreacted reagents and byproducts of the peroxide decomposition, small pieces of PBS

samples were weighed (around 1.5 g), placed into a cellulose extraction thimble, extracted with boiling methanol for 15 h, and finally vacuum dried to constant weight.

The functionalization reaction of PLA, using DTBPIB as a radical initiator, was carried out at 180 °C, 50 rpm and 14 min (Table 7.3.2.2). The half-life of DTBPIB at 180 °C is 0.6 min; thus, it can be reasonably hypothesized that at the end of the mixing all the peroxide was consumed. In a typical experiment, 25 g of PLA were introduced into the hot Brabender chamber, the functionalizing agent was added two minutes after the matrix melted and the peroxide was introduced into the Brabender chamber one minute later. The functionalized PLA sample was purified by dissolution in chloroform at room temperature and collected by precipitation in diethyl ether. The procedure was repeated twice.

Table 7.3.2.1: PBS radical functionalization: feed composition, functionalization degree (FD) and molecular weight

Sample name	Feed composition		Functionalization Degree ^a		Molecular weight and distribution		
	X-TEMPO ^b (mol%)	Peroxide (mol%)	FD _{UV} ^c (mol%)	FD _{NMR} ^d (mol%)	M _n ⁵ (g/mol)	M _w ⁶ (g/mol)	M _w /M _n
PBS ^e	-	-	-	-	17700	42180	2.38
PBS_120	-	-	-	-	16900	42700	2.53
PBS_BPO_120	-	1	-	-	n.d. ^f	n.d. ^f	n.d. ^f
PBS_BT1_BPO_120	0.5	1	0.15	n.d.	15630	35100	2.24
PBS_BT2_BPO_120	1	1	0.24	0.24	15060	34410	2.28
PBS_Nft1_BPO_120	0.5	1	0.26	n.d.	15130	33860	2.24
PBS_Nft2_BPO_120	1	1	0.30	0.29	16980	39910	2.35
PBS_150	-	-	-	-	17420	39470	2.26
PBS_DTBPIB_150	-	1	-	-	n.d. ^f	n.d. ^f	n.d. ^f
PBS_BT2_DTBPIB_150	1	1	0.14	n.d.	15970	39150	2.45

^a Functionalization Degree (FD): moles of the grafted functional groups with respect to 100 moles of monomer repeating units. ^b X-TEMPO: functional TEMPO derivative. ^c FD evaluated by UV-Vis calibration curve. ^d FD evaluated by ¹H-NMR analysis. ^e PBS pristine polymer extracted with boiling MeOH for 15h. ^f Not determined because the sample is partially insoluble in CHCl₃.

Table 7.3.2.2: PLAradical functionalization: feed composition, functionalization degree (FD) and molecular weight

Sample name	Feed composition		Functionalization Degree ^a		Molecular weight and distribution		
	X-TEMPO ^b	Peroxide	FD _{UV} ^c	FD _{NMR} ^d	M _n ⁵	M _w ⁶	M _w /M _n
	(mol%)	(mol%)	(mol%)	(mol%)	(g/mol)	(g/mol)	
PLA	-	-	-	-	111460	199340	1.79
PLA_180	-	-	-	-	108750	184730	1.70
PLA_DTBPBIB_180	-	0.5	-	-	n.d. ^e	n.d. ^e	n.d. ^e
PLA_Nft2_DTBPBIB_180	1	0.5	0.04	0.04	69290	168070	2.43

^a Functionalization Degree (FD): moles of the grafted functional groups with respect to 100 moles of monomer repeating units. ^b X-TEMPO: functional TEMPO derivative. ^c FD evaluated by UV-Vis calibration curve. ^d FD evaluated by ¹H-NMR analysis. ^e Not determined because the sample is partially insoluble in CHCl₃.

7.3.3: Polymer photografting

Method A: This method was applied to functionalize both LLDPE and SEBS. 0.1 mmol of X-TEMPO derivative were dissolved in 1mL of acetone and 2.8×10^{-2} mmol of MeOBP were added to the solution (X-TEMPO : MeOBP = 3.6 mol : 1 mol). In the preparation of EOC functionalized with MeOBP (LLDPE-g-(MeOBP)A) 9×10^{-3} mmol of reactant were used. The resulting mixture was introduced into the reservoir of an airbrush (nozzle diameter: 0.3 mm; cup capacity: 7 mL; air pressure: 1 bar) and sprayed on the LLDPE or SEBS film (dimension about 3 cm x 7 cm, thickness ca. 80 μm). After the evaporation of the solvent (about 3 min under hood) the film was irradiated for 20 minutes. The entire procedure (spray of the acetone solution, evaporation of the solvent and irradiation of the film) was repeated two more times. The irradiated samples were purified by boiling acetone extraction for 5 h, and finally dried. In the case of SEBS only NfO-TEMPO and Fluo-TEMPO were used. The acronym of the samples obtained by this procedure is: (LLDPE or SEBS)-g-(X-TEMPO)A.

The weight percent of grafted X-TEMPO was calculated by the following equation:

$$\text{Percentage of grafted X-TEMPO} = [(W_1 - W_0) / W_0] \times 100,$$

where W_0 is the weight of the starting film and W_1 is the weight of the film after irradiation and purification by acetone extraction.

The grafting of the semipinacol derived from MeOBP, obtained by method A, was confirmed by ATR-FTIR analysis (Figure 4.1.2 in Chapter 4) by the presence of bands at 700 (out of plane bending of the phenyl ring), 1174 (probably C-O stretching), 1250 (asymmetric C-O-C stretching of the MeO group), 1510 and 1604 cm^{-1} (C=C stretching of the aromatic ring)¹⁰⁸.

Method B: It was applied only to LLDPE. Indeed, in the case of SEBS this procedure cannot be applied because of the high melting temperature of the matrix that is not compatible with the thermal stability and volatility of MeOBP and of the X-TEMPO derivatives. In the case of EOC, a pre-reactive mixture was obtained by adding, to the molten matrix, both X-TEMPO and MeOBP. The samples were prepared by using an internal batch mixer (Brabender Plastograph OHG47055) with a chamber of 30 cc. Torque and temperature data were acquired by Brabender Mixing software Win-Mix ver.1.0. The run was performed at 100°C, 50 rpm for 10 min. 20 g of EOC were introduced in the hot Brabender chamber, the functionalizing agent (BzO-TEMPO and NfO-TEMPO 0.30 mol % or in the case of Fluo-TEMPO 0.15 mol %) was added two minutes after the melting of the matrix and the photoinitiator (0.1 mol % in the case of BzO-TEMPO and NfO-TEMPO or 0.05 mol% in the case of Fluo-TEMPO) was introduced in the Brabender chamber 1 min later. Polymer films of these mixtures (dimension about 3 cm x 7 cm, thickness ca. 80 μm) were prepared by compression molding at 110°C and irradiated with the UV-lamp for 20 min. The irradiated samples were purified by boiling acetone extraction for 5 h, and dried. The acronym of the samples obtained by this procedure is: LLDPE-g-(X-TEMPO)B. Films obtained by the two previously described methods were irradiated in the presence of air to avoid the use of specially designed devices.

7.3.4: Photografting of (LLDPE)-g-(PVP), (LLDPE)-g-(NfO-TEMPO) and (LLDPE)-g-(Fluo-TEMPO) according to the two step mechanism

0.056 mmol (11.88 mg) of MeOBP and 1 mL of acetone were introduced into the container of an airbrush, and sprayed on LLDPE film. The film was covered with another LLDPE film to limit the presence of oxygen and irradiated for 20 min. After irradiation, the films were separated, purified at reflux with acetone for 5 hours and dried completely

(LLDPE-g-MeOBP_E). Later 1-vinyl-2-pyrrolidinone (NVP) (32,23 mg, 0.29 mmol) was deposited onto one of the film and the second film was used as a cover, the sample obtained by this method is coded (LLDPE)-g-(PVP). In another run the NVP deposition was conducted on a LLDPE film not previously functionalized with the photoinitiator, the sample obtained by this method is coded LLDPE/NVP. Finally, NfO-TEMPO (97.8 mg, 0.3mmol) or Fluo-TEMPO (163.8 mg, 0.3 mmol) dissolved in 3 mL of acetone was deposited onto one of the LLDPE-g-MeOBP_E grafted film and the second film was used as a cover. All polymer film sandwiches were irradiated for 30 minutes. After irradiation, the two films were separated and purified by boiling acetone extraction for 5 h. Films were dried under vacuum for 24 h to a constant weight and analyzed.

7.4: Radical copolymerization of styrene and styrene derivatives onto the PE-g-X-TEMPO according to the Nitroxide Mediated Polymerization (NMP) technique

METHOD 1: This method was applied to copolymerize (HDPE)-g-(AzO-TEMPO), (HDPE)-g-(ThiO-TEMPO) and (EOC)-g-(AzO-TEMPO) with Styrene (Sty). The copolymerization was performed in a 50 mL flask where the macroinitiator (500 mg,) was dissolved in 10 mL of 1,2,4-trichlorobenzene at 120 °C. Separately Sty ($[Sty]/[X-TEMPO]= 180$) was degassed by N₂ bubbling for 30 min. The monomer was then transferred into the solution of functionalized polyethylene. The reaction was stopped after 48 h and the crude product was washed by extraction via centrifugation in chloroform or acetone for HDPE and EOC samples respectively. The recovered solid was then dried under vacuum at 80 °C overnight.

The same method was used also to copolymerize (EOC)-g-(AzO-TEMPO) with Sty together with some styrene derivatives as Pentafluoro styrene (F₅Sty), Sodium 4-styrene sulfonate (SS) and 4-Vinylbenzylchloride (VBC); in this case the used ratios were: $[Monomers]/[X-TEMPO]= 360$, $[Sty]: [Styrene\ derivatives]= [50]: [50]$.

METHOD 2: The radical copolymerization of (LLDPE)-g-(Fluo-TEMPO)A and (LLDPE)-g-(Fluo-TEMPO)B films (110 and 300 mg respectively) with Sty was performed in a 50 mL flask where the macroinitiators were immersed in 5 mL and 2.5 mL respectively of monomer

([Sty]/[X-TEMPO]= 6900). After degassing them by N₂ bubbling for 30 min, the films were heated, under stirring, at 120 °C for 72 h. Then the crude products were washed by extraction in chloroform in order to separate the polyethylene-g-polystyrene from the ungrafted polystyrene. Then the films were recovered and dried under vacuum at 80 °C overnight.

Table 7.4.1: Experimental conditions for the radical (co)polymerization of functionalized polyolefins with styrene and styrene derivatives.

Sample	monomer A	monomer B	[monomer]/ [X-TEMPO]	T (°C)	Time (h)
(EOC)- <i>g</i> -(AzO-TEMPO)_PS ^a	Sty	-	180	120	48
(HDPE)- <i>g</i> -(AzO-TEMPO)_PS ^a	Sty	-	180	120	48
(HDPE)- <i>g</i> -(ThiO-TEMPO)_PS ^a	Sty	-	180	120	48
(EOC)- <i>g</i> -(AzO-TEMPO)_PS-co-PF ₅ Sty ^a	Sty	F ₅ Sty	360*	120	48
(EOC)- <i>g</i> -(AzO-TEMPO)_PS-co-PSS ^a	Sty	SS	360*	120	48
(EOC)- <i>g</i> -(AzO-TEMPO)_PS-co-PVBC ^a	Sty	VBC	360*	120	48
(LLDPE)- <i>g</i> -(FluO-TEMPO)A_PS ^b	Sty	-	6900	120	72
(LLDPE)- <i>g</i> -(FluO-TEMPO)B_PS ^b	Sty	-	6900	120	72

Conditions ^a: Solvent used = 1,2,4-trichlorobenzene 10 mL; ^b: Bulk reaction, *: [Sty]/[Sty derivatives]= 1/1

7.5: Characterization

7.5.1: Melting point measure

Melting points were recorded on a hot-stage microscope (Reichert Thermovar).

7.5.2: Gas-liquid Chromatography

GLC analysis were performed using two types of capillary columns: an Alltech AT-35 bonded FSOT column (30 m x 0.25 mm i.d.) and an Alltech AT-1 bonded FSOT column (30 m x 0.25 mm i.d.).

7.5.3: Mass Spectroscopy

The mass spectra were acquired on an AB Sciex API 4000 triple quadrupole mass spectrometer equipped with a turbo-V ion spray source, coupled to a Perkin Elmer Series 200 Micro HPLC Pump. The experimental conditions have been as follows: Curtain Gas (Nitrogen, CUR): 10; Gas Sources 1 & 2 (air; GS1 & GS2): 25; GS2 Temperature (TEM): 300 °C; Ionspray Voltage (IS): 5.5 kV; Declustering Potential (DP): 20 V; Entrance Potential (EP): 10 V; Scan Range (Positive ions): 150–800 Th in 0.5 s; EI-MS spectra were measured at 70 eV by GLC/MS.

7.5.4: Nuclear Magnetic Resonance (NMR)

A Bruker AV 400 (400 MHz) equipped with a 5 mm multinuclear probe with reverse detection was used to record the ^1H -NMR spectra. 2048 scans were recorded with an acquisition time of 5 seconds at 32 °C. About 40 mg of each polymer sample were dissolved in 1 mL of chloroform-d (CDCl_3) at room temperature and a known amount of a solution of 1,4-dinitrobenzene (reference compound, RC) or of 1,4-dimethoxybenzene in the case of PLA, in CDCl_3 (6.6×10^{-3} M) was added. The resulting solution was analyzed.

7.5.5: Size Exclusion Chromatography (SEC)

Number average molecular weight (M_n) and weight average molecular weight (M_w) as well as dispersity (M_w/M_n) of the samples were determined using size exclusion chromatography (SEC), Agilent Technologies 1200 Series. The instrument was equipped with an Agilent degasser, an isocratic HPLC pump, an Agilent refractive index (RI) detector, and two PLgel 5 mm MiniMIX-D columns conditioned at 35 °C. Chloroform (CHCl_3) was used as the mobile phase at a flow rate of 0.3 mL min^{-1} . The system was calibrated with polystyrene standards in a range from 500 to $3 \times 10^5 \text{ g mol}^{-1}$. Samples were dissolved in CHCl_3 (2 mg mL^{-1}) and filtered through a 0.20 micron syringe filter before analysis. M_n and M_w were determined using Agilent ChemStation software.

7.5.6: Fourier Transform Infrared Spectroscopy (FTIR) and Fourier Transform Infrared-Attenuated total Reflectance Spectroscopy (FTIR-ATR)

The Fourier transform infrared-attenuated total reflectance (ATR-FTIR) and the transmission FT-IR spectra were recorded at room temperature with a Perkin-Elmer Spectrum Two Spectrometer equipped with the ATR accessory with diamond crystal. ATR-FTIR spectra were acquired in the 4000-650 cm^{-1} region with resolution of 4 cm^{-1} using 16 scans. FT-IR spectra were acquired in the 4000-400 cm^{-1} region with resolution of 4 cm^{-1} using 16 scans. Spectra of polymers were obtained from films prepared by compression molding at 190 °C for HDPE and SEBS and at 110 °C for EOC and LLDPE.

The FT-IR calibration curves used for the determination of the functionalization degree (FD) of (HDPE)-*g*-(AzO-TEMPO), (HDPE)-*g*-(ThiO-TEMPO) (EOC)-*g*-(AzO-TEMPO), and (LLDPE)-*g*-(BzO-TEMPO) sample functionalized by method B were obtained by applying a previously described procedure⁹. Concerning the (EOC)-*g*-(Fluo-TEMPO), (LLDPE)-*g*-(Fluo-TEMPO)B and (LLDPE)-*g*-(NfO-TEMPO)B samples, two calibration curves were prepared *ad hoc*. Known amounts of NfO-TEMPO or Fluo-TEMPO were added to EOC in toluene solutions. The resulting solutions were deposited onto KBr windows and after evaporation of the solvent FT-IR spectra were acquired. In the case of NfO-TEMPO the ratio between the area of the peaks at 1720 cm^{-1} (C=O stretching NfO-TEMPO) and 720 cm^{-1} (CH₂ rocking EOC) was reported as a function of the amount of NfO-TEMPO in the solution (mole of NfO-TEMPO with respect to 100 moles of monomeric repeating unit of EOC). For each concentration 3 spectra were acquired. The linear fitting of the data gives the calibration curve reported in Figure 4.1.12 (Chapter 4). In the case of Fluo-TEMPO the ratio between the peaks at 1145 cm^{-1} (CF₃ stretching) and 720 cm^{-1} (CH₂ rocking of EOC) was considered (See Figure 2.1.12 of Chapter 2 for the calibration curve). To determine the area of the bands of interest, a mathematical deconvolution of the opportune spectral region was performed by using a NLSF method (Non linear Least Squares Fitter) (Origin 7.5 software), by using a Gaussian-shaped bands in the deconvolution⁹. The equations of the calibration were obtained by a linear fitting procedure (Origin 7.5).

7.5.7: Thermogravimetric Analysis (TGA)

Thermo gravimetric analysis (TGA) were carried out by using the instrument Seiko EXSTAR 7200 TGA/DTA. In a typical experiment, the sample (about 10 mg) was placed in an alumina sample pan and the run was carried out at a standard rate of 10°C/min from 30 to 700°C (or 600°C for the macroalkoxyamines grafted with styrene) under nitrogen flow.

7.5.8: Differential Scanning Calorimetry Analysis (DSC)

Differential Scanning Calorimetry (DSC) analysis was carried out using a Perkin-Elmer DSC-4000 differential scanning calorimeter thermal analyzer equipped with a 3 stage cooler able to reach -130°C. Thermal scans were carried out on 10-15 mg samples under nitrogen atmosphere. Previously, the instrument was calibrated by using indium (m.p. 156.6 °C, $\Delta H = 28.5$ J/g) and zinc (m.p. 419.5 °C). HDPE samples were heated from 30 to 180°C then cooled to 30°C and heated again to 180°C at a cooling/heating rate of 10 °C/min. EOC samples were cooled to -60°C, heated to 130°C and cooled to 30°C at a cooling/heating rate of 10°C/min. LLDPE samples were cooled to -90°C, heated to 90°C, cooled to -90° and heated one more time to 120°C at a cooling/heating rate of 10 °C/min.

7.5.9: UV-Visible spectra

UV-Vis absorption spectra were recorded at room temperature with a Perkin-Elmer Lambda 25 UV-Vis Spectrometer. Acetonitrile solution of AzO-TEMPO and ThiO-TEMPO (about 5×10^{-5} M) and films of functionalized polymers were analyzed. HDPE films were prepared by compression moulding, EOC films were prepared by solution casting onto a quartz plate.

LLDPE films were prepared by compression moulding.

PBS solutions were prepared by dissolving 50 mg of each sample in 5 mL of CHCl_3 . A quantitative analysis of the samples was obtained by referring to calibration curves.

Two different UV-Vis calibration curves were developed by measuring the absorbance of CHCl_3 dilute solutions of PBS/BzO-TEMPO and PBS/NfO-TEMPO blends having known composition, and then plotting the absorbance versus the TEMPO-derivative

concentration. In the case of BzO-TEMPO, a PBS solution was obtained by dissolving 108 mg of the polymer in 10 mL of CHCl_3 ; a 2.935×10^{-2} M solution of BzO-TEMPO in CHCl_3 was also prepared. Then, exact volumes of the BzO-TEMPO solution (10 μL , 30 μL , 60 μL , 100 μL , 150 μL , 210 μL , 290 μL , 390 μL , 410 μL , and 550 μL) were added into the PBS solution (10 mL). The UV-Vis absorbance at 282 nm (which is a characteristic absorption band of BzO-TEMPO) of these dilute solutions was recorded and plotted versus the BzO-TEMPO concentration (Figure 7.5.9.1). By a linear fitting of the data it was obtained a curve, which was a straight line in the range of selected concentrations (the absorbance of the calibration samples was < 1). The FD of the PBS-g-(BzO-TEMPO) samples (expressed as the moles of nitroxide moieties per 100 moles of monomeric units of polymer) was determined by measuring the UV-Vis absorbance of sample solutions prepared by dissolving in CHCl_3 a known amount of polymer.

Following the same procedure, the UV-Vis calibration curve for the samples functionalized with NfO-TEMPO was obtained preparing a PBS CHCl_3 solution (by dissolving 115 mg of the polymer in 10 mL of CHCl_3) and a 1.189×10^{-2} M CHCl_3 solution of NfO-TEMPO. Then, exact volumes of the NfO-TEMPO solution (10 μL , 20 μL , 70 μL , 150 μL , and 250 μL) were added into the PBS solution (10 mL). For each blend the absorbance at 298 nm (which is a characteristic absorption band of NfO-TEMPO) versus the NfO-TEMPO concentration was plotted (Figure 7.5.9.2). The linear fitting of the data allowed to obtain the calibration curve, which was used to evaluate the FD of the NfO-TEMPO functionalized PBS samples. For both the calibration curves the absorbance (Abs) of the pure PBS solution at the wavelength of absorption of the chromophore was evaluated. Moreover, the Abs Max of the calibration blends was calculated by considering the value of the absorbance at 282 nm in the case of BzO-TEMPO and at 298 nm in the case of NfO-TEMPO, and subtracting to this value the absorbance at 450 nm (considered as the baseline).

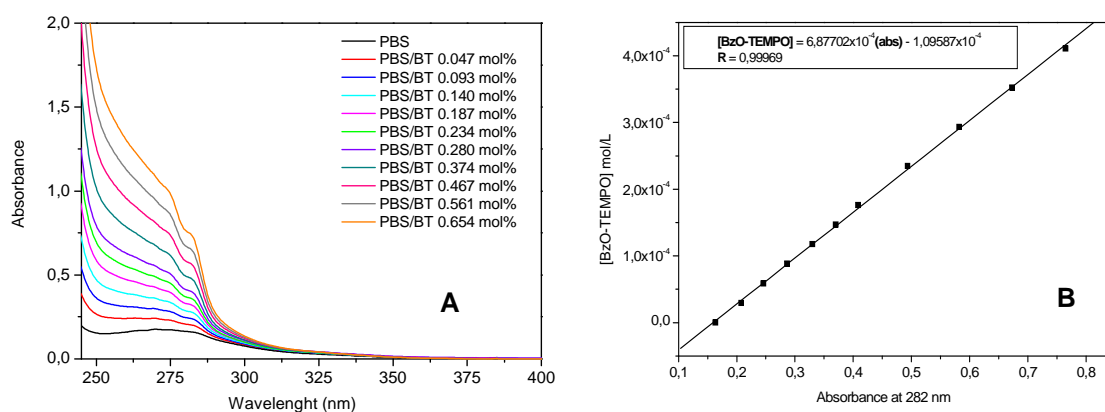


Figure7.5.9.1: (A) UV-Vis spectra of PBS/BzO-TEMPO calibration solutions and (B) UV-Vis calibration curve at 282 nm

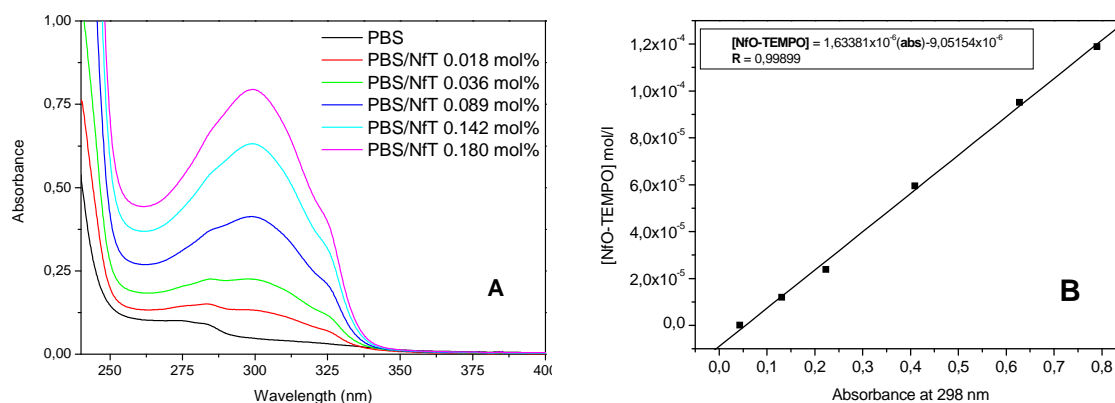


Figure7.5.9.2: (A) UV-Vis spectra of PBS/NfO-TEMPO calibration solutions and (B) UV-Vis calibration curve at 298 nm

7.5.10: Steady-state fluorescence spectra

Fluorescence emission spectra of polymer films were acquired under isotropic excitation with a Perkin Elmer luminescence spectrometer LS55 controlled by FL Winlab software and equipped with the front-surface accessory, excitation wavelength= 300 nm.

7.5.11: Photo-activation of AzO-TEMPO, ThiO-TEMPO and functionalized polymers

Photo-activation of AzO-TEMPO, ThiO-TEMPO and functionalized polymers was carried out with a Black Light equipment from Helios Italquartz Triwood 25/36 system equipped with 2 quartz glass lamps screened at 366 nm (6 Watt each) and with 2 quartz glass lamps screened at 254 nm (6 Watt each).

7.5.12: UV light irradiation for photografting technique

UV-light irradiation on the surface of film obtained by UV technology Honle UVA CUBE400, for 20 min. The lamp used was a high pressure Mercury Lamp with a power of 400 W.

7.5.13: Electron Paramagnetic Resonance (EPR)

X band EPR spectra were obtained by a Varian E112 spectrometer, controlling the temperature with a Varian E257 temperature control unit. The EPR spectrometer was interfaced to an IPC 610/P566C industrial grade Advantech computer by means of a data acquisition system. This consisted of an acquisition board capable of acquiring up to 500 000 12 bit samples per second. The experiments were run by placing a small amount (about 30 mg) of the LLDPE-g-(X-TEMPO) or PBS-BT2-BPO-120 samples into a quartz tube (internal diameter 3 mm) and gradually increasing the temperature.

7.5.14: Static Contact Angle

Static contact angles with water and *n*-hexadecane (θ_w and θ_h) were measured on films by using the sessile drop method with a Camtel FTA200 goniometer at room temperature. The reported values have to be considered as the average of 7 measurements for each sample. Data were recorded 25 seconds after the drop deposition. Static contact angles were then used to determine the surface tension (γ_s) of the polymer films by following the Owens–Wendt–Kaelble approach^{119, 120} and presented in ref¹¹⁸. Briefly, in this method the solid surface tension:

$$\gamma_s = \gamma_s^d + \gamma_s^p \quad (1)$$

combined with the Young's equation yields:

$$\gamma_L(1 + \cos\theta) = 2 \left[(\gamma_s^d \gamma_L^d)^{1/2} + (\gamma_s^p \gamma_L^p)^{1/2} \right] \quad (2)$$

where γ_s^d and γ_s^p are the unknown dispersion and polar components of surface tension of the solid film, respectively.

7.5.15: Polymer films preparation

Polymer films were prepared by compression moulding at 190°C for HDPE and SEBS or 110°C for EOC and LLDPE, under a pressure of about 5 tons by using the Carvel press 3851-0.

7.5.16: Gel content calculation

The amount of toluene insoluble fraction for the LLDPE functionalized films, obtained by using method A and B, was determined by extracting the functionalized films with boiling toluene for 16 h. The insoluble toluene fractions were dried at constant weight under vacuum.

The insoluble toluene fraction was calculated as the following:

$$\text{Insoluble toluene fraction} = \frac{W_2}{W_1} \times 100,$$

where W_1 and W_2 are the weight of the original sample and of the insoluble toluene fraction, respectively.

Conclusions

CHAPTER 8

CONCLUSIONS

In this thesis the Nitroxide Radical Coupling (NRC) reaction between polymers macroradicals and TEMPO derivatives carrying different functionalities, was investigated.

The obtained data allowed undoubtedly stating that:

- ✓ the NRC reaction provided a versatile and convenient route for introducing different functional groups into polymer matrices by limiting the radical-induced side reactions of the polymer substrate;
- ✓ the functionalization can occur both in the bulk and onto the surface of the polymer matrices;
- ✓ the NRC reaction is able to functionalize different substrates: its high efficiency was indeed demonstrated for both polyolefins and polyesters modification;
- ✓ the properties of the functional polymers were affected by the nature of the specific functional TEMPO groups used, and reflected their intrinsic chemical-physical features;
- ✓ the X-TEMPO detaching occurs at high temperatures, thus suggesting the >NO-C bond stability at room temperature;
- ✓ finally the obtained functional polymers may be seen as “activated compounds” which can be interestingly used later time as macroinitiators to synthesize tailored grafted polymer materials bearing peculiar features and characteristics.

Bibliography

CHAPTER 9

BIBLIOGRAPHY

1. D. Yang, C. Feng and J. Hu, *Polymer Chemistry*, 2013, **4**, 2384-2394.
2. B. I. Chaudhary, L. Chopin and J. Klier, *Polymer Engineering & Science*, 2007, **47**, 50-61.
3. D. K. Hyslop and J. S. Parent, *Polymer*, 2013, **54**, 84-89.
4. A. S. Micallef, J. P. Blinco, G. A. George, D. A. Reid, E. Rizzardo, S. H. Thang and S. E. Bottle, *Polymer Degradation and Stability*, 2005, **89**, 427-435.
5. B. S. Sumerlin and A. P. Vogt, *Macromolecules*, 2010, **43**, 1-13.
6. L. S. Boffa and B. M. Novak, *Chemical Reviews*, 2000, **100**, 1479-1494.
7. G. Moad, *Progress in Polymer Science*, 1999, **24**, 81-142.
8. F. Cicogna, S. Coiai, C. Pinzino, F. Ciardelli and E. Passaglia, *Reactive and Functional Polymers*, 2012, **72**, 695-702.
9. F. Cicogna, S. Coiai, E. Passaglia, I. Tucci, L. Ricci, F. Ciardelli and A. Batistini, *Journal of Polymer Science Part a-Polymer Chemistry*, 2011, **49**, 781-795.
10. M. M. Reddy, S. Vivekanandhan, M. Misra, S. K. Bhatia and A. K. Mohanty, *Progress in Polymer Science*, 2013, **38**, 1653-1689.
11. M. K. Georges, R. P. N. Veregin, P. M. Kazmaier and G. K. Hamer, *Macromolecules*, 1993, **26**, 2987-2988.
12. B. Boutevin, Y. Hervaud, A. Boulahna and M. El Asri, *Macromolecules*, 2002, **35**, 6511-6516.
13. M. Mariani, M. Lelli, K. Sparnacci and M. Laus, *Journal of Polymer Science Part A: Polymer Chemistry*, 1999, **37**, 1237-1244.
14. G. Moad, E. Rizzardo and D. H. Solomon, *Polymer Bulletin*, **6**, 589-593.
15. E. Albizzati, *Enciclopedia Treccani-Materiali polimerici, II / RAFFINAZIONE E PETROLCHIMICA*, 759-788.
16. N. K. Boan and M. A. Hillmyer, *Chemical Society Reviews*, 2005, **34**, 267-275.
17. J.-Y. Dong and Y. Hu, *Coordination Chemistry Reviews*, 2006, **250**, 47-65.
18. N. M. G. Franssen, J. N. H. Reek and B. de Bruin, *Chemical Society Reviews*, 2013, **42**, 5809-5832.
19. M. Ouchi, T. Terashima and M. Sawamoto, *Chemical Reviews*, 2009, **109**, 4963-5050.
20. M. Aglietto, R. Bertani, G. Ruggeri, P. Fiordiponti and A. L. Segre, *Macromolecules*, 1989, **22**, 1492-1493.
21. N. G. Gaylord and M. K. Mishra, *Journal of Polymer Science: Polymer Letters Edition*, 1983, **21**, 23-30.
22. N. G. Gaylord, M. Mehta and R. Mehta, *Journal of Applied Polymer Science*, 1987, **33**, 2549-2558.
23. N. G. Gaylord and R. Mehta, *Journal of Polymer Science Part A: Polymer Chemistry*, 1988, **26**, 1189-1198.
24. G. Samay, T. Nagy and J. L. White, *Journal of Applied Polymer Science*, 1995, **56**, 1423-1433.
25. A. Guyot, *Polym. Adv. Technol*, 1996, **7**, 61-66.
26. E. Passaglia, S. Coiai, F. Cicogna and F. Ciardelli, *Polymer International*, 2014, **63**, 12-21.
27. K. E. Russell, *Progress in Polymer Science*, 2002, **27**, 1007-1038.

28. M. A. F. Ciardelli, M. B., E. P. Coltelli, G. Ruggeri, and S. and Coiai, *Modification and Blending of Synthetic and Natural Macromolecules*, Springer Netherlands, 2004.
29. E. Passaglia, S. Coiai, M. Aglietto, G. Ruggeri, M. Rubertà and F. Ciardelli, *Macromolecular Symposia*, 2003, **198**, 147-160.
30. T. Bray, S. Damiris, A. Grace, G. Moad, M. O'Shea, E. Rizzardo and G. van Diepen, *Macromolecular Symposia*, 1998, **129**, 109-118.
31. B. Kouini and A. Serier, *Materials & Design*, 2012, **34**, 313-318.
32. S. K. Chang, I. S. Seo and D. W. Hong, *Journal*, 1994.
33. X. Zhou, Dai, G., Guo, W., Qunfang and Lin, *J. Appl. Polym. Sci*, 2000, **76**, 1359-1365.
34. S. Al-Malaika, *Ed.; Blackie Academic*, 1997, **Chapter 6**.
35. S. Al-Malaika and W. Kong, *Journal of Applied Polymer Science*, 2001, **79**, 1401-1415.
36. S. Coiai, E. Passaglia, M. Aglietto and F. Ciardelli, *Macromolecules*, 2004, **37**, 8414-8423.
37. S. Augier, S. Coiai, T. Gragnoli, E. Passaglia, J.-L. Pradel and J.-J. Flat, *Polymer*, 2006, **47**, 5243-5252.
38. D. Wan, L. Ma, Z. Zhang, H. Xing, L. Wang, Z. Jiang, G. Zhang and T. Tang, *Polymer Degradation and Stability*, 2012, **97**, 40-48.
39. D. Graebing, *Macromolecules*, 2002, **35**, 4602-4610.
40. Z. Zhang, H. Xing, J. Qiu, Z. Jiang, H. Yu, X. Du, Y. Wang, L. Ma and T. Tang, *Polymer*, 2010, **51**, 1593-1598.
41. Z. Zhang, D. Wan, Y. An, F. Liu, H. Xing, L. Wang, Z. Jiang and T. Tang, *Polymer Degradation and Stability*, 2011, **96**, 653-659.
42. X. Drooghaag, D. D. J. Rousseaux, G. R. P. Henry, M. Sclavons, V. Carlier and J. Marchand-Brynaert, *Polymer Degradation and Stability*, 2010, **95**, 342-345.
43. R. Pfaendner, *Comptes Rendus Chimie*, 2006, **9**, 1338-1344.
44. D. D. J. Rousseaux, M. Sclavons, P. Godard and J. Marchand-Brynaert, *Reactive and Functional Polymers*, 2012, **72**, 17-24.
45. J. Kulis, C. A. Bell, A. S. Micallef, Z. Jia and M. J. Monteiro, *Macromolecules*, 2009, **42**, 8218-8227.
46. G. Wang and J. Huang, *Polymer Chemistry*, 2014, **5**, 277-308.
47. S. i. Nakatsuji, M. Fujino, S. Hasegawa, H. Akutsu, J.-i. Yamada and V. S. Gurman, *The Journal of Organic Chemistry*, 2007, **72**, 2021-2029.
48. C. R. Moylan, B. J. McNelis, L. C. Nathan, M. A. Marques, E. L. Hermstad and B. A. Brichler, *The Journal of Organic Chemistry*, 2004, **69**, 8239-8243.
49. G. N. R. A. V. Zemskov, Yu. G. Tuchin, V. V. Karpov, *Journal of Applied Spectroscopy*, 1988, **49**, 1020-1024.
50. U. Georgi, P. Reichenbach, U. Oertel, L. M. Eng and B. Voit, *Reactive and Functional Polymers*, 2012, **72**, 242-251.
51. H. M. D. Bandara and S. C. Burdette, *Chemical Society Reviews*, 2012, **41**, 1809-1825.
52. G. Zimmerman, L.-Y. Chow and U.-J. Paik, *Journal of the American Chemical Society*, 1958, **80**, 3528-3531.
53. A. Yabe, Y. Kawabata, H. Niino, M. Tanaka, A. Ouchi, H. Takahashi, S. Tamura, W. Tagaki, H. Nakahara and K. Fukuda, *Chemistry Letters*, 1988, **17**, 1-4.
54. T. Seki, K. Tanaka and K. Ichimura, *Polym J*, 1998, **30**, 646-652.
55. R. M. Parker, J. C. Gates, H. L. Rogers, P. G. R. Smith and M. C. Grossel, *Journal of Materials Chemistry*, 2010, **20**, 9118-9125.
56. E. Fischer, *The Journal of Physical Chemistry*, 1967, **71**, 3704-3706.
57. G. Gauglitz and S. Hubig, *Journal of Photochemistry*, 1981, **15**, 255-257.
58. H. Rau, *Journal of Photochemistry*, 1984, **26**, 221-225.
59. G. Gauglitz, *Journal of Photochemistry*, 1976, **5**, 41-47.
60. H. Rau, *Photoisomerization of azobenzenes*, 2002.

61. A. Airinei, N. Fifere, M. Homocianu, C. Gaina, V. Gaina and B. C. Simionescu, *International Journal of Molecular Sciences*, 2011, **12**, 6176.
62. M. Maafi and R. G. Brown, *Photochemical & Photobiological Sciences*, 2008, **7**, 1360-1372.
63. L. Calucci, F. Cicogna and C. Forte, *Physical Chemistry Chemical Physics*, 2013, **15**, 15584-15594.
64. G. S. Kumar and D. C. Neckers, *Chemical Reviews*, 1989, **89**, 1915-1925.
65. C. Wang and R. G. Weiss, *Macromolecules*, 2003, **36**, 3833-3840.
66. N. Sarkar, A. Sarkar and S. Sivaram, *Journal of Applied Polymer Science*, 2001, **81**, 2923-2928.
67. W. Gu, A. J. Hill, X. Wang, C. Cui and R. G. Weiss, *Macromolecules*, 2000, **33**, 7801-7811.
68. C. Rosales, L. Márquez, J. González, R. Perera, B. Rojas and M. Vivas, *Polymer Engineering & Science*, 1996, **36**, 2247-2252.
69. P. J. Phillips, *Chemical Reviews*, 1990, **90**, 425-436.
70. N. Wagner and P. Theato, *Polymer*, 2014, **55**, 3436-3453.
71. E. Passaglia, S. Coiai and S. Augier, *Progress in Polymer Science*, 2009, **34**, 911-947.
72. P. Dubois and R. Narayan, *Macromolecular Symposia*, 2003, **198**, 233-244.
73. Y. Nabar, J. M. Raquez, P. Dubois and R. Narayan, *Biomacromolecules*, 2005, **6**, 807-817.
74. W. S. C. Y. J. Phua, Z. A. MohdIshak, *eXPRESSPolym. Lett*, 2013, **7**.
75. D. J. Kim, W. S. Kim, D. H. Lee, K. E. Min, L. S. Park, I. K. Kang, I. R. Jeon and K. H. Seo, *Journal of Applied Polymer Science*, 2001, **81**, 1115-1124.
76. D. J. Kim, H. J. Kang and K. H. Seo, *Journal of Applied Polymer Science*, 2001, **81**, 637-645.
77. G. Li, R. Qi, J. Lu, X. Hu, Y. Luo and P. Jiang, *Journal of Applied Polymer Science*, 2013, **127**, 3586-3594.
78. P. Ma, Z. Ma, W. Dong, Y. Zhang and P. J. Lemstra, *Macromolecular Materials and Engineering*, 2013, **298**, 910-918.
79. D. Carlson, P. Dubois, L. Nie and R. Narayan, *Polymer Engineering & Science*, 1998, **38**, 311-321.
80. D. Carlson, Nie, L., Narayan, R. and Dubois, P, *J. Appl. Polym. Sci.*, 1999, **72**, 477-485.
81. R. Mani, Bhattacharya, M. and Tang, J., *J. Polym. Sci. A Polym. Chem*, 1999, **37**, 1693-1702.
82. S. W. Hwang, S. B. Lee, C. K. Lee, J. Y. Lee, J. K. Shim, S. E. M. Selke, H. Soto-Valdez, L. Matuana, M. Rubino and R. Auras, *Polymer Testing*, 2012, **31**, 333-344.
83. F. Signori, M. Badalassi, S. Bronco and F. Ciardelli, *Polymer*, 2011, **52**, 4656-4663.
84. F. Romani, R. Corrieri, V. Braga and F. Ciardelli, *Polymer*, 2002, **43**, 1115-1131.
85. I. Domenichelli, S. Coiai, F. Cicogna, C. Pinzino and E. Passaglia, *Polymer International*, 2015, **64**, 631-640.
86. M. B. R. Mani, J. Tang, *Journal of Polymer Science Part A: Polymer Chemistry*, 1999, **37**, 9.
87. P. Rizzarelli and S. Carroccio, *Polymer Degradation and Stability*, 2009, **94**, 1825-1838.
88. S. Detyothin, S. E. M. Selke, R. Narayan, M. Rubino and R. Auras, *Polymer Degradation and Stability*, 2013, **98**, 2697-2708.
89. L. N. D. Carlson, R. Narayan, P. Dubois, , *Journal of Applied Polymer Science*, 1999, **72**, 9.
90. D.-Y. Wang, U. Gohs, N.-J. Kang, A. Leuteritz, R. Boldt, U. Wagenknecht and G. Heinrich, *Langmuir*, 2012, **28**, 12601-12608.
91. C. Coenjarts, O. García, L. Llauger, J. Palfreyman, A. L. Vinette and J. C. Scaiano, *Journal of the American Chemical Society*, 2003, **125**, 620-621.
92. J. P. Blinco, D. J. Keddie, T. Wade, P. J. Barker, G. A. George and S. E. Bottle, *Polymer Degradation and Stability*, 2008, **93**, 1613-1618.
93. K. E. Fairfull-Smith, J. P. Blinco, D. J. Keddie, G. A. George and S. E. Bottle, *Macromolecules*, 2008, **41**, 1577-1580.
94. Y. Zhang and J. Yang, *Journal of Materials Chemistry B*, 2013, **1**, 132-148.
95. J. Deng, L. Wang, L. Liu and W. Yang, *Progress in Polymer Science*, 2009, **34**, 156-193.

96. Z. Lin, E. A. Decker and J. M. Goddard, *Journal of Coatings Technology and Research*, 2016, **13**, 395-404.
97. H. Asamoto, Y. Kimura, Y. Ishiguro, H. Minamisawa and K. Yamada, *Journal of Applied Polymer Science*, 2016, **133**, n/a-n/a.
98. S. Schwark and M. Ulbricht, *European Polymer Journal*, 2012, **48**, 1914-1922.
99. B. Yang, X. Duan and J. Huang, *Langmuir*, 2015, **31**, 1120-1126.
100. D. Hafner, L. Ziegler, M. Ichwan, T. Zhang, M. Schneider, M. Schiffmann, C. Thomas, K. Hinrichs, R. Jordan and I. Amin, *Advanced Materials*, 2016, **28**, 1489-1494.
101. A. Vitale, R. Bongiovanni and B. Ameduri, *Chemical Reviews*, 2015, **115**, 8835-8866.
102. K. Kato, E. Uchida, E.-T. Kang, Y. Uyama and Y. Ikada, *Progress in Polymer Science*, 2003, **28**, 209-259.
103. B. Rånby, W. T. Yang and O. Tretinnikov, *Nuclear Instruments and Methods in Physics Research Section B: Beam Interactions with Materials and Atoms*, 1999, **151**, 301-305.
104. W. Yang and B. Rånby, *Journal of Applied Polymer Science*, 1996, **62**, 545-555.
105. A. Bhattacharya and B. N. Misra, *Progress in Polymer Science*, 2004, **29**, 767-814.
106. T. Sun, P. Xu, Q. Liu, J. Xue and W. Xie, *European Polymer Journal*, 2003, **39**, 189-192.
107. H. Ma, R. H. Davis and C. N. Bowman, *Polymer*, 2001, **42**, 8333-8338.
108. P. Castell, M. Wouters, H. Fischer and G. de With, *Journal of Applied Polymer Science*, 2007, **106**, 3348-3358.
109. P. Castell, M. Wouters, G. de With, H. Fischer and F. Huijs, *Journal of Applied Polymer Science*, 2004, **92**, 2341-2350.
110. T. Ohtake, H. Oda, T. Takaoka and M. Nakagawa, *Journal of Photopolymer Science and Technology*, 2009, **22**, 205-211.
111. I. Lukac, C. Kosa and R. G. Weiss, *Photochemical & Photobiological Sciences*, 2009, **8**, 1389-1400.
112. H. Ma, R. H. Davis and C. N. Bowman, *Macromolecules*, 2000, **33**, 331-335.
113. Q. Wu and B. Qu, *Polymer Engineering & Science*, 2001, **41**, 1220-1226.
114. Z. Liqun, G. S. Irwan, T. Kondo and H. Kubota, *European Polymer Journal*, 2000, **36**, 1591-1595.
115. R. A. Ortiz, E. A. R. Salas and N. S. Allen, *Polymer Degradation and Stability*, 1998, **60**, 195-204.
116. C. Della Volpe, D. Maniglio, M. Brugnara, S. Siboni and M. Morra, *Journal of Colloid and Interface Science*, 2004, **271**, 434-453.
117. S. Siboni, C. Della Volpe, D. Maniglio and M. Brugnara, *Journal of Colloid and Interface Science*, 2004, **271**, 454-472.
118. E. Martinelli, G. Galli, D. Cwikel and A. Marmur, *Macromolecular Chemistry and Physics*, 2012, **213**, 1448-1456.
119. D. H. Kaelble, *The Journal of Adhesion*, 1970, **2**, 66-81.
120. D. K. Owens and R. C. Wendt, *Journal of Applied Polymer Science*, 1969, **13**, 1741-1747.
121. M. M. Kitova S., Danev G., *J. Optoelectron. Adv. M.*, 2005, **7**, 249-252.
122. M. Żenkiewicz, *J. Achievements in Materials and Manufacturing Engineering*, 2007, **24**, 9.
123. Y. Ma, L. Liu and W. Yang, *Polymer*, 2011, **52**, 4159-4173.
124. M. H. Gutierrez-Villarreal, M. G. Ulloa-Hinojosa and J. G. Gaona-Lozano, *Journal of Applied Polymer Science*, 2008, **110**, 163-169.
125. Z. Liu, S. Chen and J. Zhang, *Polymer Degradation and Stability*, 2011, **96**, 1961-1972.
126. S. Ganesan, J. Felo, M. Saldana, V. F. Kalasinsky, M. R. Lewin-Smith and J. F. Tomashefski, *Mod Pathol*, 2003, **16**, 286-292.
127. W. M. Moore and M. Ketchum, *Journal of the American Chemical Society*, 1962, **84**, 1368-1371.
128. M. C. H. W. Koch, *Wiley-VCH Verlag GmbH & Co. KGaA.*, 2001.
129. R. O. Jones and O. Gunnarsson, *Reviews of Modern Physics*, 1989, **61**, 689-746.

130. P. Hohenberg and W. Kohn, *Physical Review*, 1964, **136**, B864-B871.
131. G. W. T. M. J. Frisch, H. B. Schlegel, G. E. Scuseria, M. A. Robb, J. R. Cheeseman, G. Scalmani, V. Barone, B. Mennucci, G. A. Petersson, H. Nakatsuji, M. Caricato, X. Li, H. P. Hratchian, A. F. Izmaylov, J. Bloino, G. Zheng, J. L. Sonnenberg, M. Hada, M. Ehara, K. Toyota, R. Fukuda, J. Hasegawa, M. Ishida, T. Nakajima, Y. Honda, O. Kitao, H. Nakai, T. Vreven, J. A. Montgomery, Jr., J. E. Peralta, F. Ogliaro, M. Bearpark, J. J. Heyd, E. Brothers, K. N. Kudin, V. N. Staroverov, R. Kobayashi, J. Normand, K. Raghavachari, A. Rendell, J. C. Burant, S. S. Iyengar, J. Tomasi, M. Cossi, N. Rega, J. M. Millam, M. Klene, J. E. Knox, J. B. Cross, V. Bakken, C. Adamo, J. Jaramillo, R. Gomperts, R. E. Stratmann, O. Yazyev, A. J. Austin, R. Cammi, C. Pomelli, J. W. Ochterski, R. L. Martin, K. Morokuma, V. G. Zakrzewski, G. A. Voth, P. Salvador, J. J. Dannenberg, S. Dapprich, A. D. Daniels, Ö. Farkas, J. B. Foresman, J. V. Ortiz, J. Cioslowski, and D. J. Fox, *Gaussian, Inc., Wallingford CT*, 2009.
132. A. D. Becke, *The Journal of Chemical Physics*, 1993, **98**, 5648-5652.
133. C. Lee, W. Yang and R. G. Parr, *Physical Review B*, 1988, **37**, 785-789.
134. S. H. Vosko, L. Wilk and M. Nusair, *Canadian Journal of Physics*, 1980, **58**, 1200-1211.
135. P. J. Stephens, F. J. Devlin, C. F. Chabalowski and M. J. Frisch, *The Journal of Physical Chemistry*, 1994, **98**, 11623-11627.
136. E. Papajak, H. R. Leverentz, J. Zheng and D. G. Truhlar, *Journal of Chemical Theory and Computation*, 2009, **5**, 1197-1202.
137. T. H. Dunning, *The Journal of Chemical Physics*, 1989, **90**, 1007-1023.
138. L. Goerigk and S. Grimme, *Journal of Chemical Theory and Computation*, 2011, **7**, 291-309.
139. S. Grimme, S. Ehrlich and L. Goerigk, *Journal of Computational Chemistry*, 2011, **32**, 1456-1465.
140. B. Zhao and W. J. Brittain, *Progress in Polymer Science*, 2000, **25**, 677-710.
141. S. Banerjee, T. K. Paira and T. K. Mandal, *Polymer Chemistry*, 2014, **5**, 4153-4167.
142. J. Bonilla-Cruz, E. Saldívar-Guerra, J. R. Torres-Lubián, R. Guerrero-Santos, B. López-Carpy and G. Luna-Bárceñas, *Macromolecular Chemistry and Physics*, 2008, **209**, 2268-2283.
143. M. Abbasian, Namazi, H. and Entezami, A. A, *Polym. Adv. Technol.*, 2004, **15**, 606-611.
144. S. Mohajery, S. Rahmani and A. A. Entezami, *Polym. Adv. Technol.*, 2008, **19**, 1528-1535.
145. E. Saldívar-Guerra, J. Bonilla-Cruz, B. Hernandez-Mireles and G. Ramirez-Manzanares, *Macromol. Symp.*, 2009, **283-284**, 110-119.
146. M. Abbasian, M. Shahparian and S. E. S. Bonab, *Iran. Polym. J.*, 2013, **22**, 209-218.
147. J. Nicolas, Y. Guillaneuf, C. Lefay, D. Bertin, D. Gigmes and B. Charleux, *Progress in Polymer Science*, 2013, **38**, 63-235.
148. G. Moad and E. Rizzardo, *Macromolecules*, 1995, **28**, 8722-8728.
149. J. Ding, C. Chuy and S. Holdcroft, *Advanced Functional Materials*, 2002, **12**, 389-394.
150. A. Narumi, T. Matsuda, H. Kaga, T. Satoh and T. Kakuchi, *Polymer*, 2002, **43**, 4835-4840.
151. D. Hua, W. Deng, J. Tang, J. Cheng and X. Zhu, *Int. J. Biol. Macromol.*, 2008, **43**, 43-47.
152. A. Allı, S. Allı, C. R. Becer and B. Hazer, *European Journal of Lipid Science and Technology*, 2016, **118**, 279-287.
153. J. Nicolas and Y. Guillaneuf, in *Encyclopedia of Polymeric Nanomaterials*, eds. S. Kobayashi and K. Müllen, Springer Berlin Heidelberg, Berlin, Heidelberg, 2015, DOI: 10.1007/978-3-642-29648-2_191, pp. 1133-1148.
154. K. Jankova and S. Hvilsted, *Macromolecules*, 2003, **36**, 1753-1758.
155. H. Herman, R. C. T. Slade and J. R. Varcoe, *Journal of Membrane Science*, 2003, **218**, 147-163.
156. T. Şanal, O. Oruç, T. Öztürk and B. Hazer, *Journal of Polymer Research*, 2015, **22**, 3.
157. S. Brusseau, J. Bellenev, S. Magnet, L. Couvreur and B. Charleux, *Polymer Chemistry*, 2010, **1**, 720-729.
158. G. Zorn, J. E. Baio, T. Weidner, V. Migonney and D. G. Castner, *Langmuir*, 2011, **27**, 13104-13112.

159. F. Liu, B.-K. Zhu and Y.-Y. Xu, *Applied Surface Science*, 2006, **253**, 2096-2101.
160. T. A. Sherazi, S. Ahmad, M. A. Kashmiri, D. S. Kim and M. D. Guiver, *Journal of Membrane Science*, 2009, **333**, 59-67.
161. T. A. Sherazi, T. Rehman, S. A. R. Naqvi, A. J. Shaikh, S. A. Shahzad, G. Abbas, R. Raza and A. Waseem, *Applied Surface Science*, 2015, **359**, 593-601.
162. M. M. Hassan and K. Koyama, *Polymers for Advanced Technologies*, 2015, **26**, 1285-1293.
163. H. McNab and L. C. Monahan, *Journal of the Chemical Society, Perkin Transactions 1*, 1989, DOI: 10.1039/p19890000419, 419-424.
164. H. Hagemann, R. G. Snyder, A. J. Peacock and L. Mandelkern, *Macromolecules*, 1989, **22**, 3600-3606.
165. D. Daoust, S. Bebelman, N. Chaupart, R. Legras, J. Devaux and J. Costa, *Journal of Applied Polymer Science*, 2000, **75**, 96-106.

